

REPUBLIQUE DU CAMEROUN
Paix-Travail-Patrie

UNIVERSITE DE YAOUNDE I

CENTRE DE RECHERCHE ET DE
FORMATION DOCTORALE EN SCIENCES,
TECHNOLOGIES ET GEOSCIENCES

UNITE DE RECHERCHE ET DE
FORMATION DOCTORALE EN
PHYSIQUES ET APPLICATIONS

B.P 812 Yaoundé
Email: crfd_stg@uy1.uninet.cm



REPUBLIC OF CAMEROON
Peace-Work-Fatherland

UNIVERSITY OF YAOUNDE I

POSTGRADUATE SCHOOL OF
SCIENCES, TECHNOLOGY AND
GEOSCIENCES

RESEARCH AND POSTGRADUATE
TRAINING UNIT FOR PHYSICS
AND APPLICATIONS

P.O. Box 812 Yaoundé
Email: crfd_stg@uy1.uninet.cm

LABORATORY OF MECHANICS, MATERIALS AND STRUCTURE
LABORATOIRE DE MECANIQUE, MATERIAUX ET STRUCTURE

WIND SPEED FORECASTING USING NEURAL NETWORKS AND EFFECTS OF FRICTIONAL POWER LOSS IN WIND TURBINES

Thesis submitted in partial fulfillment of the requirements for the degree of
Doctor of Philosophy (Ph.D.) in Physics

Option : Fundamental mechanics and complex systems

By

FOGNO FOTSO Hervice Roméo

Registration Number: 17T5860

Master of Science in Physics

Under the supervision of

DJUIDJE KENMOE Germaine épse ALOYEM

Professor, University of Yaoundé I



Year 2022



DÉPARTEMENT DE PHYSIQUE
DEPARTMENT OF PHYSICS

ATTESTATION DE CORRECTION DE LA THÈSE DE DOCTORAT/Ph.D

Nous, Professeur **NJANDJOCK NOUCK Philippe** et Professeur **WOAFO Paul**, respectivement Examineur et Président du jury de la Thèse de Doctorat/Ph.D de Monsieur **FOGNO FOTSO Hervice Romeo**, Matricule **17T5860**, préparée sous la supervision du Professeur **DJUIDJE KENMOE Germaine**, intitulée : « **Wind speed forecasting using neural networks and effects of frictional power loss in wind turbines** », soutenue le Mardi, **05 Juillet 2022**, en vue de l'obtention du grade de Docteur/Ph.D en Physique, Spécialité **Mécanique, Matériaux et Structures**, attestons que toutes les corrections demandées par le jury de soutenance ont été effectuées.

En foi de quoi, la présente attestation lui est délivrée pour servir et valoir ce que de droit.

Fait à Yaoundé, le 08 Juillet 2022

Examineur

Pr NJANDJOCK NOUCK P.

Le Chef de Département de Physique



Le Chef de Département de Physique
Pr NDJAKA Jean-Marie

Le Président du jury

Pr. WOAFO Paul

Dedications

This work is dedicated to God and to my family:

♣ My dear mother **DJIPE Marie** and my late father **FOTSO Jean Marie** for their love, patience and support;

♣ Mr **TABOUE NOUAYE Flaubert** and Mme **DJUIDJE FOTSO Edith épouse TATBOUE** for their moral and financial support during my school career;

♣ My sisters and brothers **KENGNE Aurelie**, **BAKAM Diane**, **KAMGA Jule**, **FOKAM Simplicie** and **KAUTE Yanik** for all their help and availability;

♣ My darling **AZEBAZE Françoise Laurence** who encourages me to realize my dreams and my child **FOGNO FOTSO Adrien**. May they find here my sincere gratitude and my love for them.

Acknowledgements

I am deeply grateful for the opportunity to have learned from and worked with so many brilliant teachers, collaborators and students. Next, I would like to express my sincere gratitude to:

- My supervisor **Prof. DJUIDJE KENMOE Germaine**, for motivating discussions and great time we had during my dissertation. She gave me the opportunity to work in the Mechanics Lab and showed me the way to postgraduate study. In spite of huge academic and administrative duties, she always found time to discuss with me and answer my queries;
- **Prof. KOFANE Timoléon Crépin** head of the Laboratory of Mechanics, Materials and Structures for his high human qualities, guidance and constant support during this research work;
- The head of Department of Physics **Prof. NDJAKA Jean Marie**, I am very grateful for the quality of his orientations and for his constructive comments;
- **Dr. ALOYEM KAZE Claude Vidal**, for his high human qualities, guidance and constant support during this research work. I am very grateful for the quality of his teaching and for his constructive comments;
- Thank you to my friend **NGONGCHIA MARCELLINUS Chia Nindum** for the correction of the English language in all the work of this thesis;
- The honourable members of the Jury, who agreed to put aside their multitude occupations so as to evaluate this work. I express to them all my greatest respect;
- Thank you to my friends **ZEUFACK Armel, BELA Lionel, NAFACK Blanca, AZE-BAZE Simplicite, MADJIKE Crescence, TANKOU Eric, BABOU Blaise, ATZIAZE Boris, MALIAZE Audrey, KAMGUIA André, KOUAM Nestor and DJOKO Jean Paul**. Their curiosity and their questions have given me many things and the new view of physics;
- **Dr. DJIHA Eric, Dr. TAKOUTSING Cédric, Dr. FOPOUSSI André, Dr. NDY Paul, Dr. KEPNANG PEBEU Fabrice, Dr. WADOP NGOUONGO Yannick**

Joel and PhD students, **ZANGA Dieudonné, TCHIO Didier**. I am very pleased to recognize trade and constructive discussions combined with great moments of sharing at of Mechanics laboratory;

- **Prof. WOAFO Paul, Prof. TCHAWOUA Clément , Prof. ZEKENG Serge Sylvain, Prof. SIEWE SIEWE Martin, Prof. FEWO Serge Ibraïd, Prof. NANA NBENDJO, Prof. BOUETOU BOUETOU Thomas, Prof. FOTSIN Hilair, Prof. TCHINDA Rene, Prof. TCHIOTSOP Daniel, Prof. KENNE Godpromesse, Prof. KENGNE Jacque, Prof. DJOMO Donatien, Prof. TCHUEN Ghislain, Prof. SIMO Elie, Prof. NFAH MBAKA Eustace, Prof. AKUME Daniel, Prof. FOGUE Medard, Prof. MTOPI Blaise, Prof. PELAP Franois, Prof. DIKANDE Alain Moïse, Prof. TCHOFFO Martin, Prof. TALLA Pierre Kisito and Prof. YEMELE David** for their teachings and their visions of the evolution of Science;
- The teaching staff of the Department of Physics, Faculty of Science and University of Yaounde I for their management, I specially express my acknowledgements;
- My late sister **BISSIMO Nadine** for his love and support;
- My nephews and nieces for their love and their deep attachment;
- The rest of my family (uncles, aunts, cousins,...) for their love and availability;
- My fellow graduates of the HTTTC of Bambili for their encouragement;
- I say thank you to all those whose names I certainly forget to mention here.

Contents

Dedications	i
Acknowledgements	ii
Table of Contents	iv
List of Figures	vii
List of tables	x
List of Abbreviations	xi
Abstract	xiii
Résumé	xv
General introduction	1
Chapter I Literature Review	7
I.1 Introduction	7
I.2 State of the art in wind energy	7
I.2.1 Utilization of wind energy	8
I.2.2 Wind energy potential	8
I.2.3 Wind turbines	12
I.2.4 Wind energy problems	17
I.3 Wind speed and power forecasting methods	21
I.3.1 Multi-step-ahead forecasting	21
I.3.2 Wind forecasting time-horizon	22
I.3.3 Wind forecasting methods	22
I.4 Artificial neural networks	27
I.4.1 Artificial neuron	27
I.4.2 Overview on artificial neural network	28
I.4.3 Application of artificial neural networks models for wind energy potential forecasting	32

I.5	Wind turbines power losses	36
I.5.1	Wind turbine efficiency	37
I.5.2	Wind turbine gearboxes technologies	38
I.5.3	Wind turbine gearbox power losses	41
I.5.4	Gearboxes power losses modeling and prediction	46
I.6	Problems statement	48
I.7	Conclusion	49
Chapter II Methodology		51
II.1	Introduction	51
II.2	Models designing for times series forecasting	51
II.2.1	Artificial neural network model designing	51
II.2.2	Neural networks structures and parameters	57
II.2.3	ARIMA model designing	68
II.3	Wind speed forecasting and application for expected wind turbine power output estimation	70
II.3.1	Multi-step wind speed forecasting	71
II.3.2	Expected WTPG estimation	73
II.4	Combined ARIMA neural network for more accurate wind speed fore- casting	74
II.5	Optimal input variables of neural network disposition to enhance the forecasting performance	76
II.5.1	Neural Networks models optimization	76
II.5.2	Neural Networks Models Building	77
II.5.3	Effects of the IVD on neural networks performances investigation	77
II.6	Gearboxes power losses modeling and prediction	78
II.6.1	Related methodology	79
II.6.2	Model definition	79
II.6.3	Neural network prediction model designing	87
II.7	Conclusion	88
Chapter III Results and Discussion		89
III.1	Introduction	89
III.2	Analysis of actual wind data	89
III.3	Wind speed and expected wind turbine power output forecasting	91
III.4	Improving the accuracy of wind speed forecasting with a new combined ARIMA neural network model	98
III.4.1	Data preprocessing and input weather variables forecasting	99
III.4.2	Multi-step wind speed forecasting	101

III.4.3 Applications of proposed forecasting model	106
III.5 Optimal input variables disposition of neural network models	107
III.5.1 IVD and neural networks Performances	108
III.5.2 Neural network models optimization based on input variables dis- positions	111
III.6 Power losses in the wind turbines	118
III.6.1 Actual wind turbine gearbox power losses evaluation	118
III.6.2 Prediction of rolling bearing power loss using BPNN model	122
III.7 Conclusion	123
Bibliography	130
List of Publications	143

List of Figures

Figure 1	Wind power converting process	9
Figure 2	General model of wind turbine power curve [40]	10
Figure 3	Mains components of wind turbines: (a) HAWT and (b) VAWT [38].	13
Figure 4	Three-mass model of the wind turbine	15
Figure 5	Wind forecasting methods	23
Figure 6	Analogy between a biological neuron (a) and artificial neuron (b)[88]	27
Figure 7	Artificial neural networks architectures	29
Figure 8	Artificial neural network for wind speed or power forecasting . .	33
Figure 9	Simplified schematic of WT drivetrains and their gearboxes models: (a) One-stage planetary and two-stage parallel, (b) Two-stage planetary and one-stage parallel and (c) Two-stage planetary (LSS = Low Speed Shaft, ISS = Intermediate Speed Shaft, HSS = High Speed Shaft) [122]	40
Figure 10	Power loss contributions [124]	42
Figure 11	Rolling torque mechanisms: (a) Roller-raceway contact showing bulge due to rolling deformation and (b) Hysteresis loop for elastic material subjected to reversing stresses [128]	44
Figure 12	Ball-raceway contact area of a radial bearing with sliding directions presented [129].	45
Figure 13	Artificial neural network design stages [104]	52
Figure 14	Bapouh location	53
Figure 15	Weather data recording system	54
Figure 16	Bapouh experiment site	54
Figure 17	Back-propagation neural network architecture	58
Figure 18	NARX neural networks architectures based on time series forecasting: (a) open-loop and (b) closed-loop	59
Figure 19	Adaptive Neuro-Fuzzy Inference System [89]	61

Figure 20	Neural networks activation functions: (a) Linear, (b) Log-sigmoid, (c) Tangent-sigmoid and (d) Gaussian	63
Figure 21	Membership functions: (a) trapezoidal and (b) triangular	64
Figure 22	Flowchart of ARIMA model development for time series forecasting	69
Figure 23	Flowchart for wind speed forecasting and application for expected power estimation	72
Figure 24	Multi-step ahead forecasting scheme	72
Figure 25	Flowchart of proposed hybrid wind speed forecasting model . . .	75
Figure 26	Flowchart of effects of neural networks input variables disposition investigation	78
Figure 27	Flowchart of proposed rolling bearing power loss prediction in wind turbine gearbox approach	80
Figure 28	Considered wind turbine Gearbox: (a) two-stage planetary and one-stage parallel [123] and (b) bearings setup.	82
Figure 29	Neural network for power loss prediction flowchart	87
Figure 30	Natural measured wind data: (a) V , (b) Ta , (c) Pa , (d) RH) and WD	90
Figure 31	Comparing wind speed forecasting results from Dataset1: (a) 1-step, (b) 2-step and (c) 3-step	95
Figure 32	Comparing wind speed forecasting results from Dataset2: (a) 1-step, (b) 2-step and (c) 3-step	96
Figure 33	Predicted WTPG from Dataset1 comparison: (a) power, (b) error .	97
Figure 34	Predicted WTPG from Dataset2 comparison: (a) power, (b) error .	98
Figure 35	Concordance between the weather variables. All normalized: (a) and (b). Transformed Ta , Pa , t and RH with normalized V : (b) and (d)	100
Figure 36	Concordance between normalized wind speed and other transformed weather variables	101
Figure 37	BPNN models performances: (a) training and forecasting, (b) RMSE (m/s), (c) MAE (m/s) and (d) MAPE(%)	110
Figure 38	NARXNN models performances: (e) training and forecasting, (f) RMSE (m/s), (g) MAE (m/s) and (i) MAPE(%)	110
Figure 39	Flowchart of proposed BPNN with optimal IVD searching	114
Figure 40	Proposed BPNN optimization by GA with IVD consideration . . .	115
Figure 41	Bar chart showing the forecasting errors from the proposed and comparison models	116

Figure 42	Best fitness values of GA along with neural networks models . . .	117
Figure 43	Bearing power loss at each stage of gearboxes under rated parameters: (a) WT1 and (b) WT2 from Ref [33].	120
Figure 44	Bearing power loss around power curve of WT1	120
Figure 45	Gearbox operating parameters and bearing power loss of WT1 . .	121
Figure 46	Comparing actual and ANN predicted bearing power loss with different oils: (a) MINR, (b) POAR, (c) PAGD	123

List of Tables

Table 1	Time-horizon classification for wind forecasting.	22
Table 2	Parameters of the related gearbox rolling bearings.	81
Table 3	Gear geometric parameters of the gearbox.	81
Table 4	Physical properties of gear oils	82
Table 5	Natural wind data characteristics	90
Table 6	Relationship between the natural variables measured	91
Table 7	Statistical information of the considered wind speed Datasets.	92
Table 8	Forecasting models parameter settings	93
Table 9	Manufacturer’s power curve of E-82 2000 kW WT	93
Table 10	Forecasting results from Dataset1	94
Table 11	Forecasting results from Dataset2	95
Table 12	Normalized and transformed weather variables characteristics	99
Table 13	Relation between the weather variables used as input variables of neural networks models	101
Table 14	Forecasting results from Dataset1 comparison	102
Table 15	Forecasting results from Dataset2 comparison	103
Table 16	Improving percentage of forecasting performance from Dataset1	104
Table 17	Improving percentage of forecasting performance from Dataset2	104
Table 18	DM test results of different models	105
Table 19	Statistical performances of ANNs models	109
Table 20	Relations between the performance criteria	111
Table 21	Forecasting performance evaluation of different models	116
Table 22	Improvement percentages of the proposed models	116
Table 23	Coefficient of friction at 80°C [124]	119
Table 24	Constants of the SKF bearings	119
Table 25	Percentage difference of P_{LV} for different oils	122
Table 26	Prediction performance of bearing power loss	124

List of Abbreviations

AI:	Artificial Intelligence
AMFIS:	Adaptive Neuro Fuzzy Inference System
AGC:	Automatic Generation Control
AN:	Artificial Neuron
ANN:	Artificial Neural Network
AR:	Auto Regression
ARIMA :	AutoRegressive Integrated Moving Average
ARMA :	AutoRegressive Moving Average
BN :	Biological Neuron
BP :	Back-Propagation
BPNN :	Back-Propagation Neural Network
ESS:	Energy Storage System
EMD:	Empirical Mode Decomposition
FBNN :	Feedback Neural Network
FL :	Fuzzy Logic
HAWT :	Horizontal-Axis Wind Turbine
HNN :	Hopfield Neural Network
GA :	Genetic Algorithm
IVD :	Input Variables Disposition
LSTMNN :	Long Short Term Memory Neural Network
MA :	Moving Average
ML :	Machine Learning
MAE :	Mean Absolute Error
MAPE :	Mean Absolute Percentage Error
MOBA :	Objective Bat Algorithm
MMIA :	Moyen Mobile Intégrée Autogressif
NARXNN :	Nonlinear AutoRegressive with eXogenous input Neural Network
NWP :	Numerical Weather Prediction
PSO :	Particle Swarm Optimization
SDE :	Stochastic Differential Equations
SLPNN :	Single-Layer Perceptron Neural Network

SSA :	Singular Spectral Analysis
SVM :	Support Vector Machine
TDNN :	Time Delay Neural Network
TSA :	Time Series Analysis
TSF :	Time Series Forecasting
RBNN :	Radial Basis Function Neural Network
RMSE :	Root Mean Square Error
RNA :	Réseau de Neurones Artificiels
RNN :	Recurrent Neural Network
rpm :	Revolutions Per Minute
VAWT :	Vertical-Axis Wind Turbine
VMD :	Variational Mode Decomposition
WT :	Wind Turbine
WTG :	Wind Turbine Gearbox
WTPC :	Wind Turbine Power Curve
WTPG :	Wind Turbine Power Generation

Abstract

This study consists of wind potential forecasting based on artificial neural networks (ANN) in order to quantify the available energy and to allow an optimal management of the transition between different sources of energy. It also enabled the quantification of power losses of the wind turbine gearbox that can improve its performance and therefore the power generation. Five ANN architectures with the wind data collected at Bapouh in Cameroon from 19th November 2016 to 31st December 2017 after every 10 minutes at a height of 70 meters are used for application. The autoregressive integrated moving average (ARIMA) model is used as the main comparison model.

Firstly, we analyze the performance of the six mostly used forecasting models for multi-step ahead wind speed forecasting. The best obtained results are used to estimate the expected electrical power generation by E-82 2000 kW wind turbine. These results showed that the non-linear autoregressive exogenous neural network (NARXNN) and ARIMA models provide better performance than the other models. It was shown that the adaptive neuro-fuzzy inference system (ANFIS) model is the worst model compared to the others for multi-step ahead wind speed forecasting. The best forecasting performances are obtained at 1-step ahead, while the worst are obtained at 3-step ahead. Also, it has been shown that the prediction accuracy of the expected wind turbine power generation depends closely on the wind speed forecasting accuracy.

Subsequently, due to the unstable character of the relationships between the weather variables dependent on the wind speed, a novel hybrid model combining ANN and ARIMA models is proposed to improve the performance of the wind speed forecasting obtained from the previous traditional ANN models. This proposed hybrid model is based on the improvement of the relationship between two weather variables. Thus, a new approach to transform actual data before using them for ANN training is proposed. The experimental results indicate that the proposed data transformation strategy is appropriate in strengthening the relationship between two variables and decrease the seasonal variation. Moreover, in terms of forecasting accuracy, the proposed hybrid model outperforms other comparable models.

Also, we analyse the influence of the ANN input variables disposition (IVD) on its training and forecasting performances. The obtained results for a static model and a dynamic model of ANN showed that their performances change differently with their

IVD. This proves that it is necessary to include the optimal IVD in ANN optimization. Thus, a new approach to ANN optimization is proposed by introducing the IVD into back-propagation algorithm used for ANN training. This approach is validated on three traditional ANN models. The obtained results reveal that each proposed model is superior to its traditional model in terms of wind speed forecasting accuracy.

Finally, due to the complexity of setting up a model for predicting mechanical losses in the wind turbines, the SKF model associated with the ANN is proposed for real-time power losses in the rolling bearings of the wind turbine gearbox modeling and prediction. The SKF model is used to determine the historical values of power losses. The back-propagation neural network (BPNN) model is used for the historical values modeling and predicting the desired values. The achieved results revealed that the bearing power loss is highly influenced by the wind turbine operating parameters, capacity, and oil. The difference between actual and neural network predicted bearing power loss values under real-time operating parameters showed the effectiveness of the proposed approach.

Keywords: wind speed, wind power, wind turbine, gearbox, bearing, artificial neural networks, time series, forecasting, power loss, optimization

Résumé

Cette étude s'inscrit dans le cadre de la prédiction du potentiel d'énergie éolienne à base des réseaux de neurones artificiels (RNA) dans le but de quantifier l'énergie disponible et de permettre une gestion optimale de la transition entre plusieurs sources d'énergies. Elle s'inscrit également dans la quantification des pertes de puissance de la boîte de vitesse de la turbine éolienne pouvant permettre d'améliorer son rendement et donc la quantité d'énergie générée. Tout au long de ces travaux, nous avons utilisé cinq architectures de RNA avec les données du vent collectées dans la localité de Bapouh au Cameroun du 19 Novembre 2016 au 31 Décembre 2017 après chaque 10 minutes et à la hauteur de 70 mètres. Le modèle moyen mobile intégré autorégressif (MMIA) est utilisé comme principal modèle de comparaison des RNA.

Dans un premier temps, nous procédons à l'analyse de la performance des six modèles de prédiction les plus utilisés pour la prédiction à plusieurs étapes de la vitesse du vent. Les meilleurs résultats obtenus sont appliqués à l'estimation de la puissance électrique escomptée de la turbine éolienne E-82 2000 kW. Ces résultats ont montré que le modèle non-linéaire autorégressif avec entrée exogène (NARX) et le modèle MMIA fournissent de meilleures performances comparés aux autres modèles. Par contre, le système à inférence neuro-floue adaptatif (SINFA) fournit de mauvaises performances de prédiction. La comparaison des étapes de prédiction a permis de montrer que l'anticipation à 1-étape est meilleure, tandis que celle à 3-étapes produit de mauvais résultats comparés aux autres étapes. Également, il est montré que la précision de prédiction de la puissance électrique de la turbine éolienne dépend étroitement de la précision de prédiction de la vitesse du vent.

Par la suite, dû au caractère instable des relations entre les autres variables météorologiques et la vitesse du vent, un nouveau modèle hybride combinant le RNA et le MMIA est proposé pour améliorer la performance de prédiction des modèles traditionnels précédents. Ce nouveau modèle hybride est basé sur l'amélioration de la relation entre deux variables météorologiques. Ainsi, une nouvelle approche de transformation de données actuelles avant leurs utilisation pour l'entraînement du RNA est proposée. Les résultats expérimentaux indiquent que cette stratégie proposée est appropriée pour renforcer les relations entre deux variables et diminuer les variations saisonnières. De plus, en terme de précision de prédiction, le modèle hybride proposé surpasse les modèles de com-

paraison.

Également, nous analysons l'influence de la disposition des variables d'entrées du RNA sur sa performance d'entraînement et de prédiction. Les résultats obtenus pour un modèle statique et un modèle dynamique de RNA ont montré que leurs performances changent de manière différente avec la disposition des variables en entrées. Ceci indique qu'il est important d'inclure la disposition optimale des variables d'entrées dans l'optimisation des RNA. Ainsi, une nouvelle approche d'optimisation des RNA est proposée en introduisant l'investigation de la disposition des variables d'entrées dans l'algorithme de rétro-propagation. Cette approche est validée sur trois modèles traditionnels de RNA. Les résultats obtenus révèlent que chaque modèle proposé est plus performant par rapport à son modèle traditionnel en terme de précision de prédiction de la vitesse du vent.

Enfin, vu la complexité de la mise sur pied d'un moyen d'évaluation des pertes mécaniques dans la turbine éolienne, le modèle SKF associé au RNA est proposé pour la modélisation et la prédiction des pertes de puissance dans les roulements de la boîte à vitesse en temps réel. Le modèle SKF est utilisé pour déterminer les valeurs actuelles des pertes de puissance. Le RNA à rétro-propagation est utilisé pour la modélisation de ces valeurs actuelles et la prédiction des valeurs désirées. Les résultats obtenus pour les turbines éoliennes de 2.0 MW et 2.5 MW avec trois types de lubrifiant ont montré que ces pertes sont fortement influencées par les paramètres de fonctionnement, la capacité de la turbine éolienne et le type de lubrifiant. La différence entre les valeurs calculées et les valeurs prédites par le RNA en fonction des paramètres de fonctionnement en temps réel de la turbine éolienne a permis de montrer l'efficacité de cette approche proposée.

Mots clés: vitesse du vent, puissance éolienne, turbine éolienne, boîte de vitesse, roulement, réseaux de neurones artificiels, prédiction, série temporelle, perte de puissance, optimisation

General Introduction

Cameroon is a developing country in Central Africa with a very low supply of electrical energy compared to demand. Moreover, the demand for electricity is growing rapidly as a result of industrialization and population growth worldwide. In 2015, one in every four persons had access to electricity in Sub Saharan Africa countries [1]. The backbone of the development of every economy, both in the developed and developing countries over the world, is energy [2]. The main sources of electricity generation are from hydropower and a very little fraction from thermal power in Cameroon [2]. Hydropower is not only insufficient but also imposes the centralization of the energy production unit, which leads to additional transportation costs and energy losses during the transportation from the production plant to the consumer. The production of electrical energy from thermal sources is very expensive because of the high cost of fuel. In addition, fossil fuels cause problems such as the pollution and global warming. They are the major cause of these environmental nuisances which are at the center of any human activities. Thus, to achieve its economic emergence projected in 2035, Cameroon must increase its production capacity in electrical energy. The most appropriate and promising solution is to use renewable energies such as wind energy [3]. According to Asan Vernyuy Wirba et al. [4], the development of new renewable energy sources such as wind energy is required for Cameroon electrification.

Wind energy is the use of wind to provide mechanical power through Wind Turbines (WTs) to turn generators for electrical power generation. Wind is a clean, free, and readily available renewable energy source over the world. Each day, around the world, WTs are capturing the wind's power and converting it to electricity. Wind Turbine Power Generation (WTPG) plays an increasingly important role in the way we

power our world, in a clean, sustainable manner [5]. WTPG is proportional to wind speed cubed. However, given the dependence of WTPG to the characteristics of fluctuation, nonlinearity, randomness and uncertainty of wind speed, wind energy generation is nearly unpredictable and is one of the most intermittent sources of renewable energy [6]. Also, it varies from site to site and from height to height. Because of this intermittent character, WTPG is only inserted in a limited way into the electrical grids. Thus, it is necessary to use in addition other energy production sources, with main difficulty the management of the dispatch between these two energy types. Therefore, accurate short-term WTPG forecasting in order to quantify available energy and to allow the optimal transition between intermittent and conventional energies sources is particularly useful for the integration and scheduling of wind power [7, 8]. Since wind speed forecasting provides an important reference for WTPG, it is necessary to improve the wind speed forecasting accuracy [9]. Also, accurate short-term wind speed is critical to the operation of wind turbines so that dynamic controls can be accomplished to increase the energy conversion efficiency and reduce the risk of overloading. According to Krishnaveny R. Nair et al. [10], in order to increase the penetration of energy from wind, every producer has to predict their power production. For this reason, modeling of the wind speed and WTPG through Time Series Forecasting (TSF) methods is becoming widespread.

Many wind speed and WTPG forecasting methods are been developed in the literature. They can be classified into the physical method, statistical method and hybrid method [11-13]. Physical method uses a physical and meteorological variables, including numerical weather prediction (NWP) and environmental temperature for wind speed prediction. It usually requires solving complex mathematical equations and do not appraise for short-term forecasting [14]. The statistical method includes Time Series Analysis (TSA) method, stochastic method, and Artificial Intelligence (AI) method. TSA method employs models such as AutoRegressive Integrated Moving Average (ARIMA) model which uses mathematical statistics to construct the relationships from historical wind data pursuing for unknown values forecasting. More accurate forecasting results are achieved from the TSA method compared to the physical method. But, they are

suitable for linear time series and cannot capture the nonlinear patterns of wind very well [15]. Stochastic method uses the mathematical models of stochastic equations to reproduce the wind behavior [16]. The AI method is based on the historical weather data sample process by learning the relationships between wind and other weather variables for desired values forecasting [17]. The AI method with artificial neural networks (ANNs) models, have been widely used and shown to have the ability in robust pattern modeling and nonlinear wind forecasting compared with other forecasting models [18]. It has easy implementation and combination with others in a different way compared with other existing forecasting tools. Erasmo Cadenas et al. [19] compared the ARIMA model and recurrent nonlinear autoregressive with exogenous input artificial neural network (NARXNN) model for wind speed forecasting. The achieved results showed that the NARXNN forecasts well the wind speed than the ARIMA model. The hybrid or combined method (model) is combining different methods [9, 20]. The combined models have been shown to forecast wind accurately than single models [21]. These hybrid models are mainly based on a single ANN model, so the objective is to optimize its parameters (exogenous and endogenous) using another forecasting model (ARIMA, fuzzy logic, ANN, etc...) or algorithm (ensemble empirical mode decomposition, singular spectrum analysis, evolutionary algorithm, generic algorithm, etc...) [22]. An accurate TSF requires an optimal ANN model based. Also, the forecasting step plays an important role in terms of forecasting accuracy. Therefore, the multi-step forecasting ahead is required to find the more accurate models. But most of the previous works are done with a specific forecasting step and model. The commonly used WTPG forecasting model is based on Wind Turbine Power Curve (WTPC) modeling model and wind speed forecasting model. It allows to forecast both wind speed and WTPG [23].

Nowadays, several efforts have been made in the development and applications of ANN models, mainly oriented toward the improvement of their optimization-based TSF. These existing optimization approaches are based on optimal parameters and minimum model structure of ANNs [24, 25]. Piazza et al. [26] combined Genetic Algorithm (GA) and Optimal Brain Surgeon (OBS) strategy to determine the optimal NARXNN

model to forecast wind speed and solar radiation. The optimization techniques of developed neural networks were based on optimal hidden neurons, biases, and weights determination. The time-series input variables represent an external parameter of an ANN model. They are commonly collected at a different order of magnitude and relations with the target variable. Great publications have shown the adequate input variables as one of the most important parameters for an optimal ANN and accurate TSF [27]. They influence the forecasting accuracy through the number of nodes, the length and the relation between them, and each of them and target [28]. Sovann et al. [29] proposed a method to determine the input variables for the ANN model; Autocorrelation, partial autocorrelation, and cross-correlation are used to measure the correlated input variables with target variable to increase the accuracy of Multilayer Perceptron neural networks (MLPNN) architecture based on electrical load demand prediction. Yaci et al. [30] studied the effect of reduced inputs of ANNs on the predictive performance of the solar energy system. The results of study show that the degree of MLPNN predicting model accuracy would gradually decrease with reduced input variables number. However, the optimal ANNs architectures have not been analyzed regarding their input variables disposition adequacy in TSF accuracy. Furthermore, wind speed and WTPG forecasting are not an easy task because they are affected by many parameters such as air temperature, atmospheric pressure, relative humidity, and wind direction. The ANN models process by capturing the natural relationships between those weather variables and wind speed. A forecasting model based on ANN will be more accurate as much as the relationship between each variable used as input and the target variable is important. For the wind, these relationships are intermittent over time as environmental changes are even almost non-existent in some cases. In this manuscript, we investigate the mostly used of existing traditional wind speed forecasting models with application for hybrid WTPG prediction. In order to improve and ensure the wind speed forecasting accuracy everywhere and every moment, a combined statistical model is proposed. It is a novel hybrid ANN and ARIMA model to forecast wind speed with weather relationships improved. We also investigate the effect of IVD of ANNs architectures in order to

determine their optimal models pursuing to the horizontal TSF.

The electrical generators of WTs require a very high drive speed, while the turbine blades rotate at the wind speed, which is very low. Thus, to accommodate the rotational speed of the main rotor blades to the needs of the generator, a multiplying gearbox is inserted between the hub and the electrical generator [31]. The generated power by WTs already exceeds 5.0 MW. This means that the power to be handled by the gearboxes increases [31]. The gearboxes are subjected to inevitable frictional power losses during operation, which greatly depends on the amount of WTPG [32]. The reduction of these power losses will increase the gearbox efficiency. Even a small efficiency increase can save energy useful for several additional households [33]. Studies about the gearboxes power losses have subsequently attracted the attention of several researchers and have been the subject of several scientific works. Load-dependent gear and rolling bearing are main sources of power loss in gearbox [34]. It is very difficult to develop a simple and general formulation to evaluate these power losses in wind turbine gearbox (WTG) [35]. The calculations based on existing analytical models remain complex and robust, and require the experimental parameters according to the systems for effective power loss prediction. The power curve shows that a WT transmits the power in nonlinear region and the rated region. Most of the WTs operate in the nonlinear region, because the rated speed is reached very rarely. Due to WT working conditions under variable load and its operating environment, it is imperative to predict the power loss in the gearbox under real-time operating conditions. Previous works have limited their studies on rated operating parameters with fixed rotational speed [33]. In this manuscript, the rolling bearing power loss in the gearbox for 2.0 MW and 2.5 MW WTs under real-time operating conditions is predicted by using an SKF model and ANN model.

The outline of this thesis is as follows. *Chapter I* provides the basic concepts required to understand wind energy conversion and utilization. Wind forecasting approaches and ANN fundamentals are presented. We further present the design of WTG and power losses. In *chapter II*, the methodology used is developed, where the application context, forecasting models evaluation criteria, ANN models and ARIMA model for

PhD thesis of FOGNO FOTSO H.R. Laboratory of Mechanics, Materials and Structures

TSF developing scheme, and rolling bearing power loss modelling model are described in details. In the last chapter, we present direct results obtained with the historical wind data used for the applications. All the proposed forecasting models are analysed in comparison to the traditional models. A new ANN structures optimization approach based on IVD are proposed and analysed. Also, a study of the influences of WTs capacity, gearbox oils and WTs operating conditions on rolling bearing power loss are shown. The thesis ends with a conclusion and outlook for future investigations.

LITERATURE REVIEW

I.1 Introduction

Renewable energy is useful energy that is collected from renewable resources, which are naturally replenished on a human timescale. Renewable energy sources includes hydropower, wind power, solar energy, wave energy, bioenergy, and geothermal energy. They are clean and free sources of energy. They have the advantage of being available in unlimited quantities. Their use permits both energy production and respect for the environment. Unfortunately, these renewable sources of electricity are, for the most part intermittent production. Therefore, accurate power generation forecasting is required for their integration. In this chapter, a state of the art is done for wind energy potential and its forecasting approaches. Also, the wind energy conversion systems face power losses mainly due to friction which reduce the amount of electrical energy produced. The state of the art on the models of wind turbine gearboxes and the origin of power losses in them is given in this chapter.

I.2 State of the art in wind energy

The wind energy is a renewable energy from kinetic energy in the wind. It is the movement of air, which results from temperature differences in different places. It is one of the most plentiful and widely available natural resources available on our planet. The kinetic energy in wind captured by WTs is converted into mechanical energy, which can be used in many applications [5]. For centuries, mankind has harvested the power of the wind for applications such as maritime and agriculture. Today, several technologies are developed to contribute to the solution to produce electrical energy and drinking water

based on wind energy. For instance, Marc Parent in 2008, developed a WT which can generate power and drinking water from humid air by condensation [36]. This device can supply electricity and water in every part of the world such as rural communities in arid countries.

I.2.1 Utilization of wind energy

The use of wind energy can be traced back thousands of years to many ancient civilizations. But following the invention of the electric generator, engineers began harnessing wind energy to produce electricity. Wind energy succeeded in the United Kingdom and the United States in 1887-1888. However, modern wind power is said to have started in Denmark, where a modern WT for electric generation started operation in 1897. Wind power is nowadays considered to be one of the most important kinds of clean energy used to save fossil energy and reduce greenhouse gases emission. According to Amir Ghaderi et al. [37], the world total Wind Turbine Power Generation (WTPG) capacity has doubled every three years since 2000, reaching an installed capacity of 197 GW in 2010 and 369 GW in 2014 [38]. According to a report published by the IFC in 2020, the African continent alone has over 59000 GW of technical wind resource potential. In 2020, 821 MW of new wind power capacity was installed in Africa, with 515 MW in South Africa. Which taps into 0.01% of its wind power potential. Until 2021, no wind power system had been installed in Cameroon.

I.2.2 Wind energy potential

The main wind energy potential are wind power, WTPG and wind characteristics.

I.2.2.1 Wind power

Wind power defines the power available in wind which can be captured by WT. Kinetic energy exists whenever an object of a given mass is in motion with a translational or rotational speed. This available power in wind P_w can be expressed as given in Equation

(1) [38],

$$P_w = \frac{1}{2}\rho AV^3, \quad (1)$$

where ρ is the air density, A is the swept area of blades and V is the wind speed.

I.2.2.2 Wind turbine power generation

The process employed by the WTs for wind power conversion into another power such as mechanical power and electrical power follows the steps described into Figure 1.

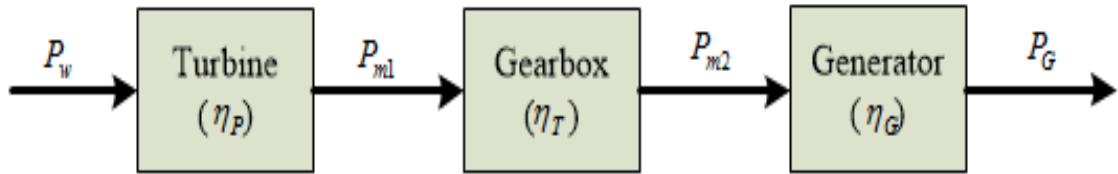


Figure 1: Wind power converting process

The turbine converts the wind power into mechanical power P_{m1} with an efficiency η_P (or power capacity, C_P); Gearbox transmits P_{m1} to another mechanical power P_{m2} with efficiency η_T ; while the electrical generator converts P_{m2} into electrical power P_G with an efficiency η_G . The powers at each step of the conversion process are given as,

$$P_{m1} = \frac{1}{2}\eta_P \cdot \rho \cdot A \cdot V^3, \quad (2)$$

$$P_{m2} = \frac{1}{2}\eta_P \cdot \eta_T \cdot \rho \cdot A \cdot V^3, \quad (3)$$

$$P_G = \frac{1}{2}\eta_P \cdot \eta_T \cdot \eta_G \cdot \rho \cdot A \cdot V^3. \quad (4)$$

Equation (4) reveals that in order to obtain a higher WTPG, a higher wind speed is required, a longer length of blades for gaining a larger swept area, and a higher air density. Because the wind power output is proportional to the cubic of the wind speed. Also, the WTPG is highly influenced by the efficiencies of the WT.

The electrical power that can be generated by a controlled WT by conversion of the available wind P_w is usually represented by its wind power curve [39]. The Wind Turbine Power Curve (WTPC) establishes the relationship between the wind speed and the

WTPG [40]. Every modern WT has one power curve which is calibrated and provided by its manufacturer [41]. It can be determined from the field measurements. The typical power curve of a pitch controlled WT can be presented as shown in Figure 2.

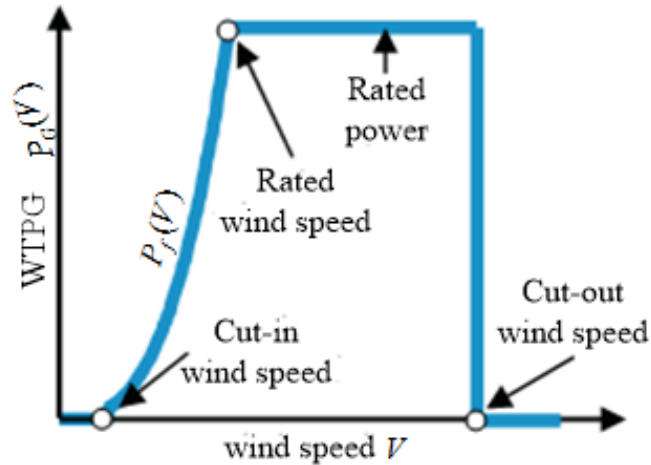


Figure 2: General model of wind turbine power curve [40]

As shown in Figure 2, the WT starts to produce usable power at a low wind speed, defined as the *cut-in speed*. The power output increases continuously with the increase of the wind speed until reaching a saturated point, at which the power output reaches its maximum value, defined as the *rated power* output. Correspondingly, the speed at this point is defined as the *rated speed*. At the rated speed, more increase in the wind speed will not increase the power output due to the activation of the power control. When the wind speed becomes too large to the extent that it can potentially damage the WT, it needs to shut down immediately to avoid damaging the WT. This wind speed is defined as the *cut-out speed*. Thus, the *cut-in* and *cut-out* speeds have defined the operating limits of WT [41-43].

1.2.2.3 Wind characteristics

Wind is a weather variable which varies with the geographical locations, time of day, season, and height above the earth's surface, weather, and local landforms. The understanding of the wind characteristics will help to make-decision for the wind energy

project such as optimize WT design, develop wind measuring techniques, select wind farm sites, and WTPG estimation. Wind is mainly characterized by its speed and its direction [44].

i Wind direction

The wind direction is defined as the direction from which the wind blows, e.g. the north wind comes from the North and blows to the South. However, if the wind direction is represented by an arrow, the arrowhead points to the direction to which the wind blows. Statistical data of wind directions over a long period of time is very important in the site selection of wind farm and the layout of WTs in the wind farm. The wind rose diagram is a useful tool of analyzing wind data that are related to wind directions at a particular location over a specific time period (year, season, month, week, etc.) [44].

ii Wind speed

Wind speed or wind flow speed, is an atmospheric quantity caused by air moving from high to low pressure, due to changes in temperature. It is a higher random variable which varies in both time and space, determined by many factors such as geographic and weather conditions. Therefore, the wind speed is characterized by an unpredictability and a variability [13]. As seen in subsection I.2.2.2, it is one of the most critical wind energy characteristics; since the WTPG is proportional to the cubic power of the wind speed, its small variation in wind speed can result in a large change in electrical power. The wind speed is now commonly measured with an anemometer. However, due to the fact that it is a random parameter, measured its data are also dealt with using statistical methods such as Weibull distribution. The variation in wind speed at a particular site is described using the Weibull distribution function [45]. The Weibull distribution function illustrates the probability of different wind speeds occurring at the site during a period of time [7, 46]. D. Afungchui and C.E. Aban [47], employed the Weibull distribution function to analyse the wind regimes for energy estimation in Bamenda, of the North West Region of Cameroon. For a further comprehensive review of the Weibull distribu-

tion and its application for wind potential study, the interested reader is referred to the work presented in Refs [48-51].

I.2.3 Wind turbines

WT is an energy-converting machine driven by the wind, its role is to capture and to convert the power available in the wind to another power. A modern WT converts the wind power into mechanical power and in turn into electrical power as shown in Figure 1. In this thesis we consider the modern WTs.

I.2.3.1 Wind turbine classification

WTs exist with different topologies and design features. They can be mainly classified according to the turbine generator configuration, airflow path relatively to the turbine rotor and turbine capacity [52].

i Horizontal-axis and vertical-axis wind turbines

When considering the configuration of the rotating axis of rotor blades, modern WTs can be classified into the horizontal-axis and vertical-axis turbines. Horizontal-Axis Wind Turbines (HAWT) are the WTs in which the rotating shaft is mounted parallel to the wind flow/ground (see Figure 3(a)). They have two types of rotors: up-wind and down-wind. The majority HAWT being used today are upwind turbines, in which the wind rotors face the wind. However, a yaw mechanism is needed to align the turbine with the prevailing wind. The main advantage of upwind designs is to avoid the distortion of the flow field as the wind passes through the wind tower and nacelle. For a downwind turbine, wind blows first through the nacelle and tower and then the rotor blades. This configuration enables the rotor blades to be made more flexible without considering tower strike. However, because of the influence of the distorted unstable wakes behind the tower and nacelle, the WTPG from a downwind turbine fluctuates greatly [38, 45].

Vertical-axis wind turbines (VAWT) are the WTs in which the axis of rotation is verti-

cal to the wind flow/ground (see Figure 3(b)). They are independent of wind direction and thus no yaw control is needed. Since their main components can be set up on the ground, it greatly simplifies the wind tower design and construction, and consequently reduces the turbine cost. However, the VAWT must use an external energy source to rotate the blades during initialization. Because the axis of the WT is supported only on one end at the ground, its maximum practical height is thus limited. Due to the lower wind power efficiency, vertical-axis wind turbines today make up only a small percentage of WTs [38].

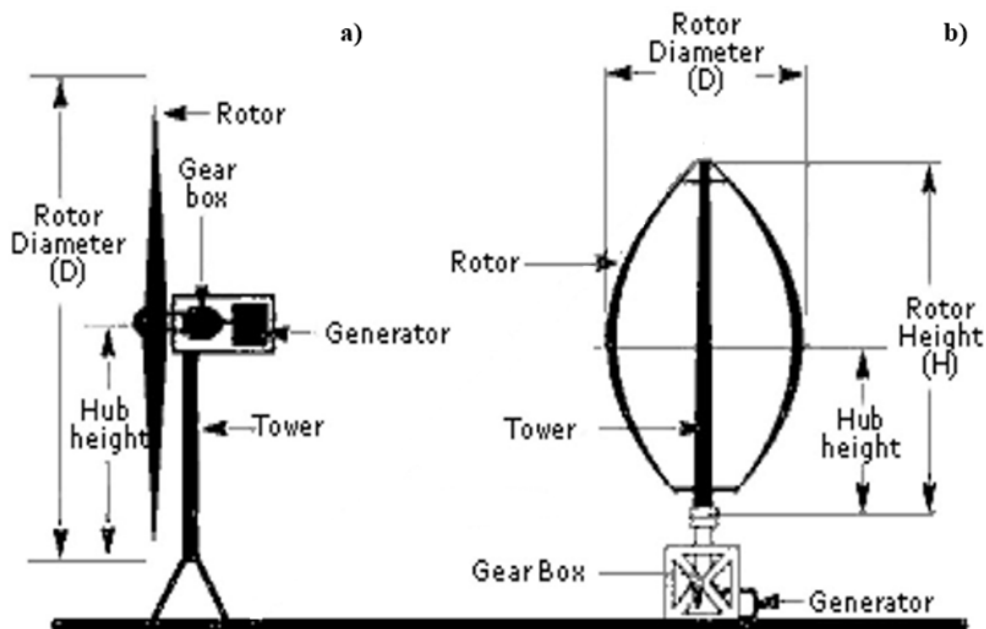


Figure 3: Mains components of wind turbines: (a) HAWT and (b) VAWT [38].

ii Wind turbine capacity

The capacity of a WT defines the rated power that it can generate. Therefore, WTs can be divided into a number of broad categories in view of their rated power: small, medium, large, and ultra-large. Small WTs usually refer to the turbines with the output power less than 100 kW; medium wind turbines have the capacity range from 100 kW to 1 MW; The capacity of large WTs is up to 10 MW; while ultra-large WTs are referred to WTs with the capacity more than 10 MW [45].

I.2.3.2 Wind turbine description

Despite the different appearances of HAWT and VAWT, the basic mechanics of the two systems are very similar. As shown in Figure 3, the main components of classic WTs are the following [38]:

- **Blades:** Lifts and rotates when wind is blown over them, causing the rotor to spin;
- **Gearbox:** It constitutes the transmission system and helps to convert the low-speed shaft to the high-speed shaft, increasing the rotational speeds required by generators to produce electricity;
- **Tower:** Made from tubular steel, concrete, or steel lattice. Supports the structure of the turbine. Because wind speed increases with height, taller towers enable turbines to capture more energy and generate more electricity;
- **Generator:** Converts the mechanical energy from gearbox into electrical energy; it is usually an off-the-shelf induction generator;
- **Rotor:** Blades and hub together form the rotor;
- **Nacelle:** Sits atop the tower, housing most turbine components inside. Some nacelles are large enough for a helicopter to land on.

Most of the modern WTs are HAWT, they integrate other component such as :

- **Anemometer:** Measures the wind speed and transmits its data to the controller;
- **Brake:** Stops the rotor mechanically, electrically, or hydraulically, in emergencies;
- **Controller:** Starts up the machine at cut-in wind speed and shuts off the machine at cut-out wind speed;
- **Pitch:** Turns (or pitches) blades out of the wind to control the rotor speed, and to keep the rotor from turning in winds that are too high or too low to produce electricity;

- **Wind vane:** Measures wind direction and communicates with the yaw drive to orient the turbine properly with respect to the wind;
- **Yaw drive:** Orients upwind turbines to keep them facing the wind when the direction changes. Downwind turbines don't require a yaw drive because the wind manually blows the rotor away from it;
- **Yaw motor:** Powers the yaw drive.

I.2.3.3 Wind turbine modeling

The wind turbine is usually presented by modeling the mechanical part by the three-mass, two-mass or one-mass model. What is modeled is the torque transmission, i.e. the behavior of the power train.

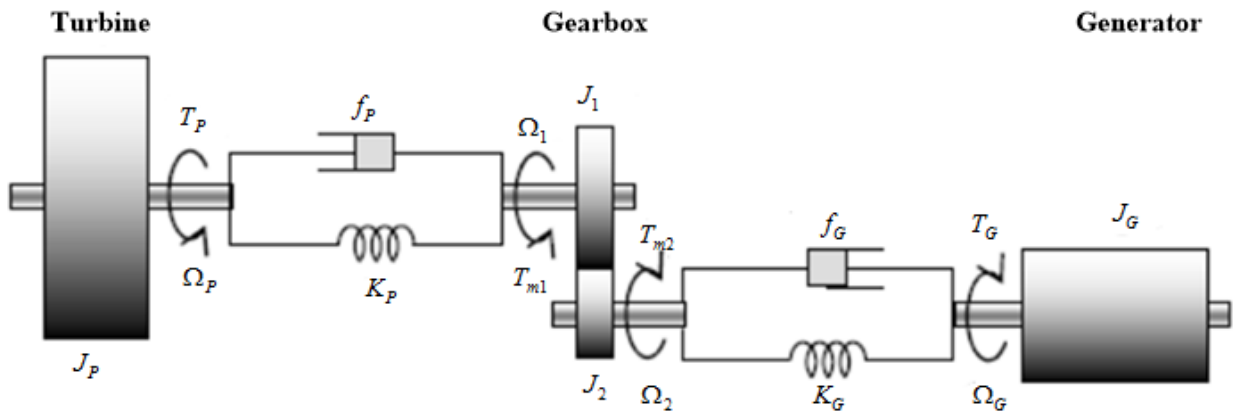


Figure 4: Three-mass model of the wind turbine

The equivalent three-mass model of the wind turbine power train is shown in Figure 4. The masses correspond to a large mass for the wind turbine rotor, a mass for the gearbox and a mass for the generator respectively. Taking into account the elasticity and friction coefficients for the two shafts, the dynamic equations of motion of the system are given by

$$J_P \frac{d\Omega_P}{dt} = T_P - f_P \Omega_P - K_P (\theta_P - \theta_1), \quad (5)$$

$$J_1 \frac{d\Omega_1}{dt} = T_{m1} - f_P \Omega_1 - K_P (\theta_1 - \theta_P), \quad (6)$$

$$J_2 \frac{d\Omega_2}{dt} = T_{m2} - f_G \Omega_2 - K_G (\theta_2 - \theta_G), \quad (7)$$

$$J_G \frac{d\Omega_G}{dt} = -T_G - f_G \Omega_G + K_G (\theta_2 - \theta_G), \quad (8)$$

with

$$\frac{d\theta_P}{dt} = \Omega_P, \quad \frac{d\theta_1}{dt} = \Omega_1, \quad \frac{d\theta_2}{dt} = \Omega_2, \quad \frac{d\theta_G}{dt} = \Omega_G, \quad (9)$$

where J_1 , J_2 , J_P and J_G are respectively the moment of inertia of the slow shaft, of the fast shaft, of the turbine and of the generator, Ω_1 , Ω_2 , Ω_P and Ω_G are respectively the mechanical speed at the input of the gearbox, at the output of the gearbox, of the turbine and of the generator, K_P and K_G are the elasticity of the slow and fast shafts and f_P and f_G are the coefficients of friction of the slow and fast shafts.

Doubly fed induction generator is commonly used in WT. It is composed by a stator and a rotor, both have three sinusoidally distributed windings, corresponding to three phases, displaced by 120 degree. A three-winding transformer gives different voltage levels for stator and rotor side. The voltage relations on rotor and stator sides are obtained by Kirchhoff's and Faraday's law are given in equations (10) and (11),

$$\begin{bmatrix} v_{as} \\ v_{bs} \\ v_{cs} \end{bmatrix} = R_s \begin{bmatrix} i_{as} \\ i_{bs} \\ i_{cs} \end{bmatrix} + \frac{d}{dt} \begin{bmatrix} \phi_{as} \\ \phi_{bs} \\ \phi_{cs} \end{bmatrix}, \quad (10)$$

$$\begin{bmatrix} v_{ar} \\ v_{br} \\ v_{cr} \end{bmatrix} = R_r \begin{bmatrix} i_{ar} \\ i_{br} \\ i_{cr} \end{bmatrix} + \frac{d}{dt} \begin{bmatrix} \phi_{ar} \\ \phi_{br} \\ \phi_{cr} \end{bmatrix}. \quad (11)$$

The subscripts r and s denote rotor and stator quantities, respectively. The subscripts a , b and c are used for phases a , b and c quantities, respectively. The symbols v and i are for voltages and currents and ϕ represents flux linkages. R_s and R_r are the stator and rotor winding resistances.

I.2.4 Wind energy problems

I.2.4.1 Intermittency

Intermittent power refers to an electrical power that is not continuously available due to external factors that cannot be controlled, produced by energy generating sources that vary in their conditions on a fairly short time scale [53]. As shown in section I.2.2, wind speed is a stochastic weather variable; i.e. it varies unpredictably hour-to-hour and in space. Since the WTPG is directly related to the cubic of the wind speed, a small variation in wind speed induces a large variation in WTPG. Also, some features of power systems such as voltage and frequency might be affected. Therefore, wind energy is highly intermittent and non-dispatchable energy source. In other words, WTPG is not always available when needed and cannot be scheduled and controlled. As a result, large scale WTPG penetration will lead to impacts on power system operational security and stability and subsequently, higher costs. The WTPG intermittency is the biggest challenge to the implementation of wind power as the major power source [53, 54]. These impacts reduce the operators' motivation to integrate WTPG into the power systems [55]. The entire modern power system is built around meeting electricity load demand when it is needed. Demand varies hugely hour to hour, and fluctuates on a seasonal basis as well. Often times demand can fluctuate unpredictably and forecasting exactly how much power will be needed hour to hour is challenging.

i Impact on system reserves

Reserves are needed to balance the differences between power generation and electrical load demand in power systems. The intermittent nature of WTPG imposes new uncertainty on the system that operators have to cope with. Furthermore, variations in WTPG and electricity load demand are usually antithetical, especially during the peak load hours. More reserves are required to cover sudden increases in load demand and decreases in WTPG. The intermittence of wind energy therefore results in higher reserve

capacities. Therefore, reserve requirements increase with increasing intermittent WTPG penetration level [53].

ii Impact on power system reliability

Power system reliability is comprised of two fundamental aspects: system adequacy and system security. 1) System adequacy is used to evaluate the ability of system to meet the load demand. It is usually quantified as the surplus available generation capacity during peak load hours expressed as a percentage of peak load. This percentage should be adequate to ensure a reliable power supply (range between 15% and 25%). Variable sources can meet peak load demand if their fluctuations are positively correlated with load demand. However, the correlation between intermittent WTPG and load demand is usually negative, a phenomenon known as anti-peak regulation. Furthermore, due to its intermittent nature, the WTPG is not always available when it needed. Thus, high WTPG penetration has a significant impact on system adequacy. Then, system reliability is gradually decreased with increasing intermittent WTPG. 2) System security quantifies the risk associated with energy deficit on the security of power system infrastructures. The power system risk index increases with increasing intermittency of the power penetration. Furthermore, integrating WTPG into power systems affects the performance of Automatic Generation Control (AGC). Because AGC performance may deteriorate due to WTPG intermittency. Therefore, system security deteriorates with large-scale WTPG integration [56].

iii Impact on costs

With increasing wind energy integration, more reserve capacities are required to cope with WTPG intermittency, resulting in higher reserve service costs. Furthermore, traditional power plants have to be operated more flexibly to balance the variability in residual demand, which leads to an increase in operating costs. Thus, total balancing costs are increased due to WTPG intermittency. The balancing costs will increase as the intermittent WTPG penetration level increases [54].

I.2.4.2 Wind power intermittency's mitigation

Despite the intermittency of WTPG and its impacts, the capacity of installed wind power is growing and constitutes one of more promising green source of energy all over the world [20, 57]. This is because the intermittency of wind power can be predicted, managed and mitigated by technology [54]. These technological solutions include energy storage, optimal geographic distribution of wind farms, reasonable layout of wind turbines, and high-accuracy wind speed and WTPG forecasting methods.

i Geographic distribution of wind farms

The spatial distributions of wind resources are diversified and uneven. It is generally thought that the wind lacking from one site can be partially accommodated by the wind in other sites. This means that WTPG in different regions are complementary [53]. In other words, aggregating geographically dispersed wind farms or wind turbines can mitigate WTPG intermittency. But this technique is used less because the satisfaction is limited. Also, it generates an additional cost for the transport as well as power losses in line during the transport from one site to another. Furthermore, it promotes the centralization of energy production units.

ii Mitigation solutions based on energy storage

WTPG cannot meet the load demands because of the intermittency. Energy storage systems (ESSs) provide an option to tackle this problem. The excess WTPG is stored in ESSs in different forms during off-peak load periods [58]. While during peak load periods, the energy stored in ESSs can be released to supply electricity. The effects of ESSs include output smoothing, time shifting, frequency regulation, alleviate transmission congestion, oscillation damping, reserve application, emergency power supply, and changing the load demand. ESSs can efficiently mitigate wind power intermittency due to these effects. But it is limited by the bulk and the high cost of the ESS and the adverse effects of the intermittency of the charge over its lifetime.

iii Mitigation solutions based on wind speed and wind power forecasting

Another solution that can make it possible to cope with the intermittent nature of WTPG and ensure large-scale penetration into the electric grid while at the same time preserving the security of the latter and a quality of supply is the parallel use of other sources of energy. The main difficulty for this solution is the optimal management of the rocking. The flip-flops with great flexibility are needed to handle the variations. Thus, the electric grid manager will need to have tools for predicting WTPG. Their predictions will make it possible to predict the energy reserves which will take over to preserve the security of the system and allow better integration [59]. Therefore, the intermittency can be better mitigated with high accuracy of WTPG behavior forecasting. It has several benefits for the promotion of wind energy, among which we can have:

- Accurate WTPG forecasting is an important basis for power grid planning, which helps grid dispatch organization to make plans and promote real-time balance of system power [60]. At the same time, it is advantageous for grid distributors to timely adjust the adverse effects of the operation of grid-connected wind farms to avoid large-scale power failure accidents;
- Accurate WTPG forecasting can improve the competitiveness of wind power in the electricity market and lay the groundwork for wind power participation in tenders for power generation. The randomness of intermittent wind power weakens the competitiveness of the wind power market. Therefore, efficient WTPG forecasting will reduce the uncontrollability of wind power production and improve its competitiveness in the market;
- Accurate WTPG can not only guarantee the safe operation of the power grid, but also help the wind farm to formulate scientific control strategies, greatly reduce the rotating reserve capacity and hence reduce the overall cost of wind power generation.

Since power generated is a function of wind speed, as much as the accurate power forecasting is important as demonstrated above, the accurate wind speed forecasting is more important. Besides the fact that an accurate wind speed forecasting will induce an accurate WTPG prediction, forecasted wind speed values can be also utilized for wind energy potential assessment [61, 62], wind farms designing [63], wind turbine control and performance prediction [64].

The high accurate WTPG or wind speed forecasting model development is one of the biggest challenges for the development of wind energy source. Thus, several forecasting methods have been reported in the literature over the past few years. They will be presented in detail in the next section.

I.3 Wind speed and power forecasting methods

Because of its importance for the integration of WTPG, the development of methods for the accurate wind behaviour forecasting has received much attention from researchers. Therefore, several methods have been proposed based on the multi-step forecasting approach and forecasting horizons. In this section, different methods will be detailed.

I.3.1 Multi-step-ahead forecasting

Multi-step forecasting is the task of predicting a sequence of values in a time series. It consists of applying a predictive model step-by-step and using the predicted value of the current time step to determine its value in the next time step. A time series is a succession of observations (or measurements) during the time representing a phenomenon. In other words, a time series is a sequence of observations in which each observation $y(t)$ is recorded at a particular timestamp t [65].

I.3.2 Wind forecasting time-horizon

From the point of view of the electric grid operator, the needs in terms of wind potential forecasting and intermittent resources in general are very varied. We can distinguish them according to the time-horizon considered: the resource that will be available on the following days ($d+1$, $d+2$ and $d+3$), the next day in hourly steps ($h+24$), in 1 hour ($h+1$), and in 5 minutes ($m+5$). These different horizons make it possible to understand the different aspects of forecasting: the very short-term, short-term, medium-term and long-term [12, 66]. Table 1 presents the specific time-horizon in view of the operation of electricity systems. The applications of specific time-horizon in electricity systems are consequentially different. Thus, in order to better manage the balance between electricity production and consumption, the very short term and short forecasting (a few minutes to a few hours) of the energy produced by wind farms is crucial.

Table 1: Time-horizon classification for wind forecasting.

Time-horizon	Range	Applications
Very-short-term	Few minutes to one hour ahead	Electricity market clearing, real-time grid operations, regulation actions
Short-term	One hour to several hours ahead	Economic load dispatch planning, load reasonable decisions, operational security in electricity market
Medium-term	Several hours to one week ahead	Unit commitment decisions, reserve requirement decisions, generator online
Long-term	One week to one year or more ahead	Maintenance planning, operation management, optimal operating cost, feasibility study for design of the wind farm

I.3.3 Wind forecasting methods

To handle wind speed and WTPG forecasting, many methods by modeling time series have been proposed in the literature. These methods can be divided into three categories [13], involving physical method, statistical method and hybrid method as shown in Figure 5.

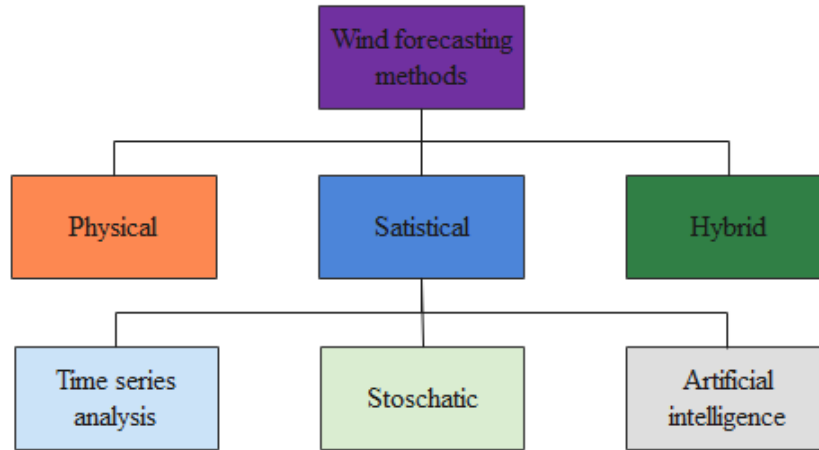


Figure 5: Wind forecasting methods

I.3.3.1 Physical method

Physical method use parameterizations based on a detailed physical description of the atmosphere [67]. With the physical method, the wind speed at the WT hub height is predicted according to the Numerical Weather Prediction (NWP) data and then the WTPG is calculated based on the WTPC. It is independent of the measured historical data and can be used for both the newly built and the operating wind farms [68]. NWP models are commonly developed by solving the incompressible fluid (Equation (12)) and Navier-Stokes (Equation (13)) equations. Solving these equations is very complex, then NWP are rendered on supercomputers as they need lots of computations. Customarily, NWP are run 1 or 2 times a day due to the difficulty to gain information in short-time and the associated high costs. This limits its usefulness from medium to long-term forecasts (> 6 h ahead). These give most accurate predictions when weather conditions are stable [69, 70].

$$\nabla \cdot u = 0, \quad (12)$$

$$\frac{\partial u}{\partial t} + u \cdot \nabla u = -\frac{1}{\rho} \nabla p + \nu \nabla^2 u \quad (13)$$

where u is the fluid velocity vector, p is the fluid pressure, ρ is the fluid density, ν is the kinematic viscosity, and ∇^2 is the Laplacian operator.

I.3.3.2 Statistical method

Statistical method aims at finding the relationship of the historical wind measured data. In other words, the statistical method is based on training with measured data and uses difference between the predicted and the actual values in the immediate past to tune model parameters. It is easy to model, inexpensive, and provides timely forecasting [71]. The statistical methods perform well for short-time periods, but carry the disadvantage that the prediction error increases as the prediction time increases [72]. Sub-classification of this method includes: *Time-series analysis method*, *stochastic method*, and *artificial intelligence method*.

i Time series analysis method

Time series analysis (TSA) method consists of analyzing time series data in order to extract meaningful statistics and other characteristics of the data. It uses models such as Auto-Regressive Moving Average (ARMA) [73], Auto-Regressive Integrated Moving Average (ARIMA) [21], Bayesian [74], grey predictor [75] and exponential smoothing [76] to detect changes in the evolution of a time series from before to after some intervention which may affect the underlying variable. The more accurate forecasting results are achieved from TSA models comparing with physical models [15]. But, they are suitable for linear time series and cannot capture the nonlinear patterns of wind very well. ARIMA model is the most popular type in the TSA method to predict future values of wind speed or power, because they are robust, as well as easy to understand and implement. The ARIMA model can best characterize nonlinear data than other TSA models.

The general ARIMA model is known as ARIMA(p, d, q) [19], where p represents the order of the autoregression (AR) of the model, d represents the degree of differencing to make the model stationary and q order of the moving average (MA) aspect of the model. It is defined for the y time series as,

$$y_t = \sum_{k=1}^p \phi_k y_{t-k} + \sum_{j=1}^q \theta_j \varepsilon_{t-j} + \varepsilon_t, \quad (14)$$

where ϕ_k is the k -th autoregressive parameter, θ_j is the j -th moving average parameter and ε_t is the error term at time t . In this thesis, the ARIMA model will use mainly as a benchmark model to perform a comparison with other models.

ii Stochastic method

Stochastic method uses the mathematical models of stochastic equations to reproduce the wind speed or power behavior [77, 78]. They are based on wind historical data of a specific location to estimate its probability distributions. In comparing with the physical models, the stochastic models have the potential to be used for various applications where wind speed or WTPG are stochastic inputs [16]. Stochastic differential equations (SDEs) are widely used to model stochastic phenomena in wind engineering [79]. It is suitable for short-term and long term wind forecasting. The interested reader can find theoretical background on SDEs and stochastic method in Refs [8, 80-82].

iii Artificial intelligence method

Artificial Intelligence (AI) method is the recent statistical method which consists of use models based on historical data sample to learn the relationships between wind speed or power and other depending weather variables such as air temperature, relative humidity, atmospheric pressure, wind direction, and solar radiation. Various AI models for wind speed or WTPG forecasting have been developed including Artificial Neural Network (ANN) [15], Fuzzy Logic (FL) [83], and Support Vector Machine (SVM) [84]. AI forecasting models predict more accurately than traditional statistical TSA models.

The ANN models can represent a complex nonlinear relationship and extract the dependence between variables through the training process. They are the widely used time series forecasting model and have been shown to have the ability in robust pattern modelling and nonlinear wind speed and power forecasting compared with other models [85]. Thus, ANN based method is an appropriate model to apply into the problem to forecast the wind speed or power, but selecting the type of ANN model for the best performance hinges on data sources. Various types of ANN have been developed. They

will detail in the next section.

I.3.3.3 Hybrid method

A *Hybrid method* or *combined method* is a combination of several methods [21]. The objective of hybrid models is to benefit from the advantages of each method and obtain a globally optimal forecasting performance. Since the information contained in the individual forecasting method is limited, hybrid method can maximize the available information, integrate individual model informations and make the best use of the advantages of multiple forecasting methods thus improving the prediction accuracy [66].

Many types of hybrid models were utilized to predict wind speed or power. The types of combinations can be: combination of physical and AI methods, combination of TSA and AI methods, combination of statistical and combination of alternative AI models. Lorenzo Donadio et al. [86] coupled NWP and ANN models for wind power forecasting for complex sites in the Jura mountains in Switzerland. One year of weather research and forecasting model simulations were run to obtain data that were overlapped with the archived data from the wind farm in order to train the neural network for desired wind power values forecasting. Krishnaveny R. Nair et al. [10] compared single ANN models, ARIMA model, and hybrid ARIMA-ANN model for wind speed forecasting. To succeed in the hybrid ARIMA-ANN model, the forecasting variable is decomposed into linear and nonlinear parts. Huaiwu Peng et al. [23] presented a hybrid method to forecast WTPG based on ANN and WTPC. An ANN model is developed for wind speed forecasting employed to estimate the unknown power by using fitted power curve. This approach is the most promising and the most used for the short-term WTPG forecasting, because it is simple and its major stake lies in the development of an accurate wind speed forecasting model. More accurate wind speed forecasting models are achieved from hybrid ANN models. They will be detailed in the next section.

I.4 Artificial neural networks

A neural network or ANN is a type of Machine Learning (ML), which consist of an ensemble of simple neurons operating in parallel. It's a mathematical model that tries to simulate the structure and functionalities of biological neural networks [87]. ML is a subfield of AI (technology which enables a machine to simulate human behavior), which enables machines to learn from past data or experiences without being explicitly programmed.

I.4.1 Artificial neuron

An Artificial Neuron (AN) is a simple mathematical model (function) inspired by biological nervous systems. It is a basic building block of every ANN. Its design and functionalities are derived from observation of a Biological Neuron (BN) which is the basic building block of biological neural networks (systems) and includes the brain, spinal cord and peripheral ganglia [87,88]. A schematic diagram of a typical analogy between the BN and the mathematical model of an AN architecture is shown in Figure 6.

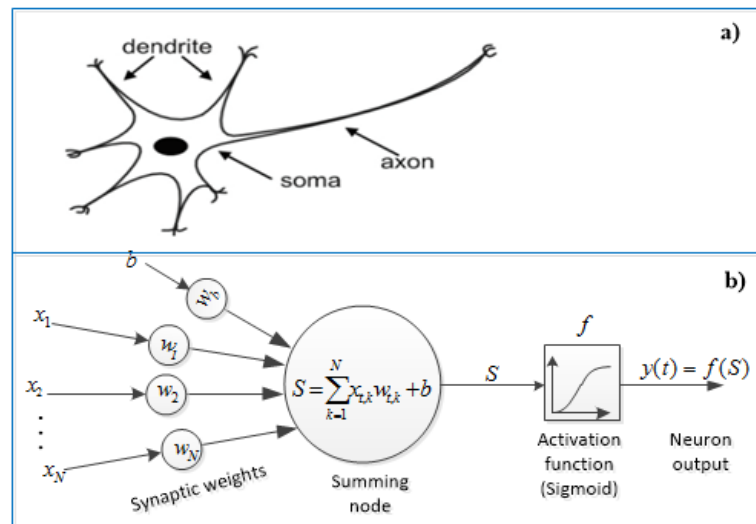


Figure 6: Analogy between a biological neuron (a) and artificial neuron (b)[88]

In case of BN information comes into the neuron via dendrite, soma processes the information and passes it on via axon. In case of AN the information comes into the body

of an AN via inputs that are weighted (each input can be individually multiplied with a weight). The body of an AN then sums the weighted inputs, bias and processes the sum with a transfer function. At the end an AN passes the processed information via output(s) [88]. Benefit of AN model simplicity can be seen in its mathematical description below,

$$y(t) = f \left(\sum_{k=1}^N w_k(t) \cdot x_k(t) - b \right), \quad (15)$$

where $x_k(t)$ and $w_k(t)$ are the input value and weight value respectively, b is the bias and f the transfer function. $y(t)$ is output value at time t ; k represents an input variable which goes from 1 to N .

As seen from a model of an AN and its Equation (15) the major unknown variables of our model is its transfer function and weights. Transfer function defines the properties of artificial neuron and can be: *Step function, linear function and non-linear function (hyperbolic tangent sigmoid, logistic sigmoid and gaussian)*.

I.4.2 Overview on artificial neural network

When combining two or more ANs we are getting an ANN. If single AN has almost no usefulness in solving real-life problems the ANNs have it. In fact ANNs are capable of solving complex real-life problems by processing information in their basic building blocks (AN) in a non-linear, distributed, parallel and local way. As in nature, the network function is determined largely by the connections between neurons. ANNs process by experience; knowledge is acquired by the ANN through a learning process. It learns from the historical events by adjusting the values of the connections (synaptic weights) between the nodes (neurons and input variables). The synaptic weights represent the strength of connections of neurons among themselves as well as between neurons and input variables of the network. The synaptic weights are used to store the knowledge [88].

The manner in which individual ANs are interconnected is called topology, architec-

ture or type of artificial ANNs. The commonest type of ANN consists of three groups, or layers: an *input layer* is connected to *hidden layer(s)*, which is connected to *output layer(s)*. The activity of the input layer represents the raw information that is fed into the network. The activity of each hidden layer is determined by the activities of the input layer and the weights on the connections between the input and the hidden layers. The behavior of the output layer depends on the activity of the hidden layers and the weights between the hidden and output units [87,89].

I.4.2.1 artificial neural network structures

The fact that interconnection can be done in numerous ways results in numerous possible topologies that are divided into two basic classes as shown in Figure 7 [89]: *static artificial neural network* and *dynamic artificial neural network*.

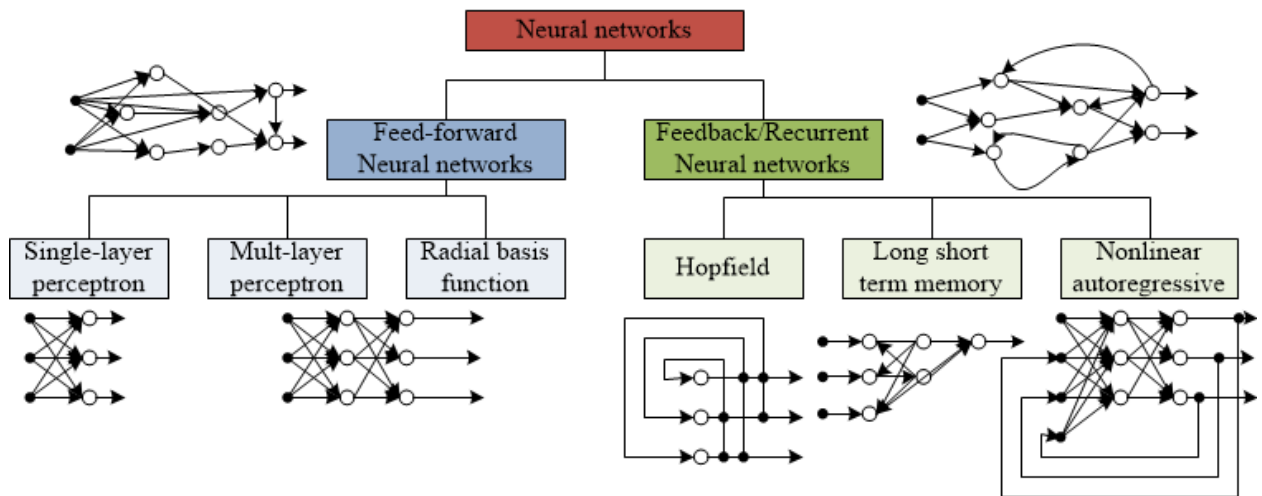


Figure 7: Artificial neural networks architectures

i Feed-forward artificial neural networks

The static ANN or Feed Forward Neural Networks (FFNN) allow signals to travel one way only; from input to output. There is no feedback (loops) i.e. the output of any layer does not affect that same layer. They tend to be straight forward networks that associate inputs with outputs [90]. FFNN includes the Single-Layer Perceptron neural networks (SLPNN), the Multi-Layer Perceptron neural networks (MLPNN) and Radial

Basis Function neural networks (RBFNN). The SLPNN was among the first and simplest learning machines that are trainable. It consists of the class of two-layer feed forward networks, whose first-layer has fixed function with fixed connection weights from the inputs, and whose connection weights linking this first layer to the second layer of outputs are learnable. The MLPNN and RBFNN are organized in several layers within which information flows from the input layer to the output layer. They have one or more layers hidden between input layer and output layer. MLPNN however is highly nonlinear in its parameters compared to RBF neural network, which has linear parameters [91].

ii Feed-forward artificial neural networks

The dynamic ANN or Feedback Neural Networks (FBNN) or Recurrent Neural Networks (RNN) allows signals traveling in both directions by introducing loops in the network. This creates an internal state of the network which allows it to exhibit dynamic temporal behaviour. RNN can use their internal memory to process any sequence of inputs. As RNN we mainly have Hopfield neural network (HNN), Nonlinear Auto-Regression with exogenous input Neural Network (NARXNN) and Long Short Term Memory neural network (LSTMNN). A HNN is a type of recurrent artificial neural network that is used to store one or more stable target vectors. These stable vectors can be viewed as memories that the network recalls when provided with similar vectors that act as a cue to the network memory. These binary units only take two different values for their states that are determined by whether or not the units' input exceeds their threshold [92]. A NARXNN can be defined as a feed forward Time Delay Neural Network (TDNN). It also called input-output mapping neural network consisting of a FFNN that takes as input a window of past independent inputs (exogenous inputs) and past outputs (endogenous inputs) and determines the current output. Unlike a conventional RNN which has local feedback loops, the NARXNN have a limited feedback coming only by the output neuron rather than the hidden states (global loops) [93]. Nevertheless, it has been demonstrated that it is as much computationally powerful as a fully

connected RNN. LSTMNN is built from long short term memory blocks that are capable of remembering value for any length of time. This is achieved with gates that determine when the input is significant enough remembering it, when continue to remembering or forgetting it, and when to output the value [94, 95].

I.4.2.2 Artificial neural networks learning

An ANN is trained by changing the weights and biases of the connections between nodes. These weights can be randomly chosen or individually chosen. Usually, a computer program randomly generates values for connection weights. Then, the network is given an input, and it is allowed to process the information through its nodes to produce an output. There are three major learning paradigms; *supervised learning*, *unsupervised learning* and *reinforcement learning*. Usually they can be employed by any given type of ANN architecture. Each learning paradigm has many training algorithms [88]. An ANN training algorithm is chosen mainly according to the ANN generating performance and training conversion rate.

i Supervised learning

Supervised learning is a machine learning technique that sets parameters of an ANN from training data. The task of the learning ANN is to set the value of its parameters for any valid input value after having seen the output value. The training data consist of pairs of input and desired output values that are traditionally represented in data vectors [96]. Supervised learning uses Back-Propagation (BP) training algorithms such Gradient Descent, Conjugate Gradient and Levenberg-Marquardt. Levenberg-Marquardt algorithm is faster and has better performance than the other BP algorithms [97].

ii Unsupervised learning

Unsupervised learning is a machine learning technique that sets parameters of an ANN based on given data and a cost function which is to be minimized. Cost function can be any function and it is determined by the task formulation. Unsupervised learning is

PhD thesis of FOGNO FOTSO H.R. Laboratory of Mechanics, Materials and Structures

mostly used in applications that fall within the domain of estimation problems such as statistical modelling, compression, filtering, blind source separation and clustering. In unsupervised learning we seek to determine how the data is organized. It differs from supervised learning and reinforcement learning in that the artificial neural network is given only unlabelled examples. One common form of unsupervised learning is clustering where we try to categorize data in different clusters by their similarity. The Self-organizing maps are the most commonly use unsupervised learning algorithms among others such as *K*-Means, *K*-Medoids and Hierarchical clustering [96, 97].

iii Reinforcement learning

Reinforcement learning is a machine learning technique which consists of using experience gained through interacting with the world and evaluative feedback to improve a system's ability to make behavioral decisions. It has been called the artificial intelligence problem in a microcosm because learning algorithms must act autonomously to perform well and achieve their goals. One popular algorithm is the upper confidence bound [98].

I.4.3 Application of artificial neural networks models for wind energy potential forecasting

Nowadays, ANNs models represent the most used wind speed and WTPG forecasting tools because of its robustness, its ability to model stochastic variables and its different optimization techniques. They are more accurate than other traditional forecasting models. The supervised learning algorithms are the mostly used approaches, since the historical measurement of weather data and wind speed or WTPG data are available. When historical WTPG data are no available (e.g. WT not operating in this site), a hybrid method is employed which consists of using an ANN model to forecast the unknown wind speed values and its application for corresponding WTPG estimation by using another approach such wind turbine power curve modeling. Whether for the wind speed forecasting, power or both, single models and hybrid models of ANN are

used. Generally the network has several inputs and one output. As shown in Figure 8, the principle consists in using the past values of weather variables (air temperature, relative humidity, atmospheric pressure, wind direction, time, etc) naturally influencing the wind speed or the power as input variables and the past values of the wind speed or power as the output variable to train the network. The actual input variables are introduced into the trained ANN model to forecast the desired wind speed or WTPG values. The forecasting performance depends on the network training performance. The training performance of ANN depends on its endogenous (number of nodes, weights, transfer functions, etc) and exogenous parameters (relationship between the input variables and target variables, number of input variables, training set, testing set, etc).

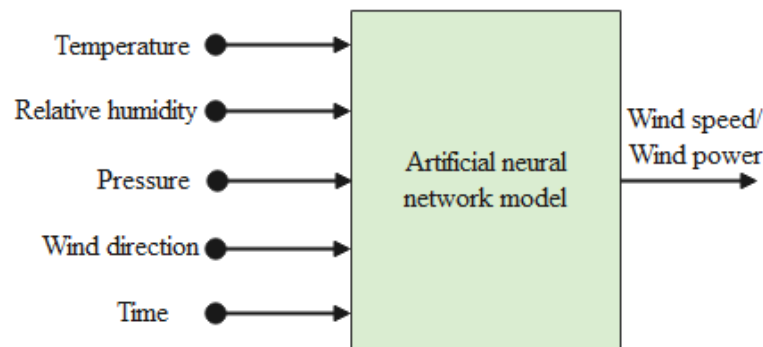


Figure 8: Artificial neural network for wind speed or power forecasting

I.4.3.1 Single models

Single models refer to traditional ANN models trained with traditional algorithms. Different single models have been studied for wind speed and power forecasting at different sites and wind farm in several countries by many researchers [99, 100]. Erasmo Cadenas et al. [101] used NARXNN model for one step wind speed forecasting in La Mata, Oaxaca, Mexico by using data from meteorological system. Erasmo Cadenas and Wilfrido Rivera [102], used MLPNN model for short-term wind speed forecasting in La Venta, Oaxaca, Mexico. Cristian-Dragos Dumitru and Adrian Gligor [103], presented a FFNN model for daily average wind energy forecasting in Romania. Anirudh S. Shekhawat [104], applied NARXNN model for predicting power output of WTs based on historical

measured values in ELIA-A Belgium.

I.4.3.2 Models optimization

Hybrid or combined model refers to a single ANN model combined with one or more other models (ANN or not) or with one or more other algorithms in order to optimize its performance. Generally, hybrid ANN models are qualified as optimized models when they are associated with an algorithm other than the traditional one. The Hybrid models have been widely used for the prediction of wind speed and power. They have been proven to be more efficient than the individual models in terms of forecasting performance [14, 17]. ANN model optimization consists of optimal topology selection, endogenous and exogenous parameters designing.

i Artificial neural networks optimization based on endogenous parameters

It is mainly based on the optimization of the synaptic weights of the network for given values of other intrinsic parameters such as the number of hidden layers, the number of neurons in each hidden layer, the activation functions and training parameters. Generally these other parameters are kept according to the forecasting performance of the model after several tests. Apart from the number of neurons in the hidden layer of a three-layer network which can be determined using Kolmogorov's theorem [105], there is no rule for determining these parameters. There are algorithms for optimizing the synaptic weights of ANNs such as Genetic Algorithm (GA) [106], Multi-Objective Bat Algorithm (MOBA) [107] and particle swarm optimization (PSO). Piazza et al. [108] combined GA and Optimal Brain Surgeon (OBS) strategy to determine the optimal NARXNN structure to forecast wind speed and solar radiation. Jianzhou Wang et al. [109] presented a study of a combined model based on MOBA for multi-step ahead wind speed forecasting. The proposed model consists of four ANNs models with optimum weight coefficients based on MOBA. E. Pratheepraj et al. [110] presented a very short term WTPG forecasting using hybrid PSO-ANN. PSO is used to optimize the weights of MLPNN model.

ii Artificial neural networks optimization based on exogenous parameters

It refers to optimal input variables selection and data pre-processing. The time series input variables represent an external parameter of an ANN model. They are commonly collected at different order of magnitude and relations with the target variable. Many publications have shown the adequate input variables as one of the most important parameters for an optimal ANN and accurate time series forecasting [111]. They influence the forecasting accuracy through the number of node, the length and the relation between them, and each of them and target. Thus, several works have been done in order to orient the best selection of the input variables of the ANNs. Wei et al. [28] presented a general approach to determine the input variables of ANNs models for time series forecasting. The proposed approach was based on autocorrelation criterion used to measure the degree of correlation between the neighboring time series data used as input variables of FFNN. Furthermore, Sovann et al. [29] proposed a method to determine the input variables for the ANN model; Autocorrelation, partial autocorrelation, and cross correlation were used to measure the correlated input variables with target variable to increase the accuracy of MLPNN model based on electrical load demand prediction. Yaïci et al. [30] studied the effect of reduced inputs of ANNs on the predictive performance of the solar energy system. The results of the study show that, the degree of FFNN model predicting model accuracy would gradually decrease with reduced input variables number.

For ANNs models optimization, data pre-processing consists of decomposing each input and output time series signals into several components. Because the traditional single ANNs models cannot fully characterize the fluctuating characteristics of wind speed and power, another solution consist of associating with the ANN model a signal decomposition model such as Variational Mode Decomposition (VMD) [112], Empirical Mode Decomposition (EMD) [113] and Singular Spectral Analysis (SSA) [114] to tackle this problem. Shouxiang Wang et al. [115] presented a hybrid ensemble EMD, GA and MLPNN applied for short-term wind speed forecasting. Gang ZHANG et al.

[116] developed in association with MLPNN model and ARIMA model for wind power forecasting.

iii Combined forecasting models

An ANN model can be combined with another forecasting model (which is not generally an ANN model) to constitute a hybrid model in order to benefit from the advantages of each model. The most used ANN-based combined models for wind speed and power forecasting are Adaptive Neuro Fuzzy Inference System (ANFIS) and ARIMA-ANN. 1) ANFIS model is a type of AI able to combine a fuzzy system's ability to model a reasoning process and to handle uncertainty, with the learning ability and adaptivity of an ANN. ANN in ANFIS adjusts parameters of membership function in the fuzzy logic. It is very widely used for the wind potential forecasting. Shahaboddin Shamsirband et al. [117] developed an ANFIS model for short-term wind speed forecasting in Serbia. Sinvaldo Rodrigues Moreno and Leandro dos Santos Coelho [118], proposed a combination of SSA and ANFIS models for multi-step wind speed forecasting. 2) Hybrid ARIMA-ANN model combines ARIMA model and ANN model. Usually a decomposition technique is used to decompose the wind speed (or wind power) time series signal into nonlinear part and linear part. An ANN model is used for the nonlinear part modelling to forecast the desired corresponding values. While the ARIMA model is used for the modelling and prediction of the corresponding values desired in the linear part. At the end, a reconstruction of the predicted values of the two models is made. Jian Jiao [119], used hybrid ARIMA and MLPNN model for wind speed forecasting. Compared with ARIMA model and ANN model, the hybrid model forecasts better wind speed.

I.5 Wind turbines power losses

As shown in Figure 3, the gearbox is the main mechanical part of a WT. This gearbox, like all mechanical systems, faces friction which induces power losses. These power losses affect its efficiency and consequently the electrical power generation.

I.5.1 Wind turbine efficiency

WT efficiency is the amount of kinetic energy in the wind that is converted to electrical power. It can also be defined as the ratio between the electrical energy generated and the kinetic energy captured by the blades of the WT from the wind. The blades of WT rotate at very low speeds, typically 20 revolutions per minute (rpm), which are not suitable for conventional power generation using an electrical generator. The generators used require a very high drive speed, of the order of 1000 rpm. This constraint is solved by using a multiplying gearbox between the hub and the electrical generator. By considering the efficiency of each of these sub-components of the WT, i.e. the rotor, the gearbox, and the electric generator, its overall efficiency is expressed as follows,

$$\eta_{global} = \eta_P \times \eta_T \times \eta_G. \quad (16)$$

The efficiency of the gearbox is highly influenced by friction losses. It is expressed in Equation (17) as follows,

$$\eta_T = \frac{P_{m1}}{P_{m1} - P_V}, \quad (17)$$

where P_V represents the overall power losses in the gearbox. Efficiency is a major requirement of a WT gearbox [120]. Furthermore, the gearbox is one of the components in WTs most prone to cause complications. The costs for maintenance and replacement of gearboxes, along with the costs caused by production losses due to non-functioning gearboxes, constitute a large share of the expenses of operating wind power plants. The rapid growth in wind power needs fast improvements in technology, so in order to make wind energy competitive with other power sources in the near future, enhancements on gearbox efficiency, availability, reliability and lifetime are required [31].

I.5.2 Wind turbine gearboxes technologies

I.5.2.1 Wind turbine gearboxes definition

Mechanical power from the rotation of the WT rotor is transferred to the generator rotor through the main shaft, the gearbox, and high-speed shaft. Wind Turbine Gearbox (WTG) is an integral part of the drivetrain in large-scale WT systems which consists of a large number of moving mechanical components. The components of the WTG are in contact with each other, which creates enormous friction during operation. Lubricating oil is used in the WTG to reduce this friction. Small WT may turn at speeds of the order of hundreds of revolutions per minute and may not require a gearbox. In these cases, known as direct drive, electric generators with a sufficiently high number of poles may be directly coupled to the rotor. In large-scale WT systems, the gearbox is coupled to the rotor through the low-speed shaft and is connected to the generator through the high-speed shaft. It is the convention in gearbox design to distinguish between the rotor side and the generator side. The basic function of the gearbox is to transmit mechanical power from the rotor shaft side, running at low speeds, to the generator side, running at higher speeds [121].

In WT, the gearbox is speed-increasing, where the defining parameter is the gearbox speed ratio, i . The speed ratio relates the input speed on the rotor side, n_{in} , to the output speed on the generator side, n_{out} ,

$$i = \frac{n_{out}}{n_{in}}. \quad (18)$$

The WTG receives power on the rotor side, P_{m1} , and delivers power on the generator side, P_{m2} . The gearbox will experience power loss, P_V , as heat is generated due to friction between parts with relative motion (shaft seals, gears, bearings, etc) and viscous losses (lubrication system). Conservation of energy will apply to give,

$$P_{m2} = P_{m1} + P_V. \quad (19)$$

However, the WT transmitted power is usually related to the power from the rotor by the gearbox efficiency which is mainly affected by gear loss and oil churning loss, as defined in Equation (17). The transmitted power can be expressed as,

$$P_{m1} = \eta_T \cdot P_{m2}. \quad (20)$$

The electrical power generated by the WT can be expressed as,

$$P_G = \eta_G \cdot \eta_T \cdot P_{m1}. \quad (21)$$

From Equation (21), η_G is fixed (generally around 80%) and the power received at the input of the gearbox is directly proportional to the power captured by the blades of the turbine. Therefore, the power generated (P_G) by the WT is mainly influenced by the losses of the gearbox.

1.5.2.2 Wind turbine gearbox designs

Majority of gearbox designs in modern WTs have very similar configurations, therefore they experience similar friction modes. Depending on the required output speed to be fed into the generator, the commonly used WTG configurations are classified as either bevel designs, where gears are perpendicular to each other, or spur designs, where two gears rotate parallel to each other. They include one planetary gear stage followed by two parallel gear stages (see Figure 9(a)) or two planetary gear stages followed by one parallel gear stage (see Figure 9(b)). Another design configuration includes only two planetary gear stages (see Figure 9(c)). In all gearbox design configurations, the ring gear does not rotate and is fixed on the gearbox casing [122].

Parallel gears consist of a meshing pinion and gear. Parallel arrangements can be simple, or compounded with other parallel gear sets to obtain high gear ratios. The conventional way to describe such a gear is double increaser or triple increaser. Parallel gears can use, helical or double helical elements. A planetary or epicyclic gear has multiple gear meshes and bearings, and has greater mean time to repair and exposure

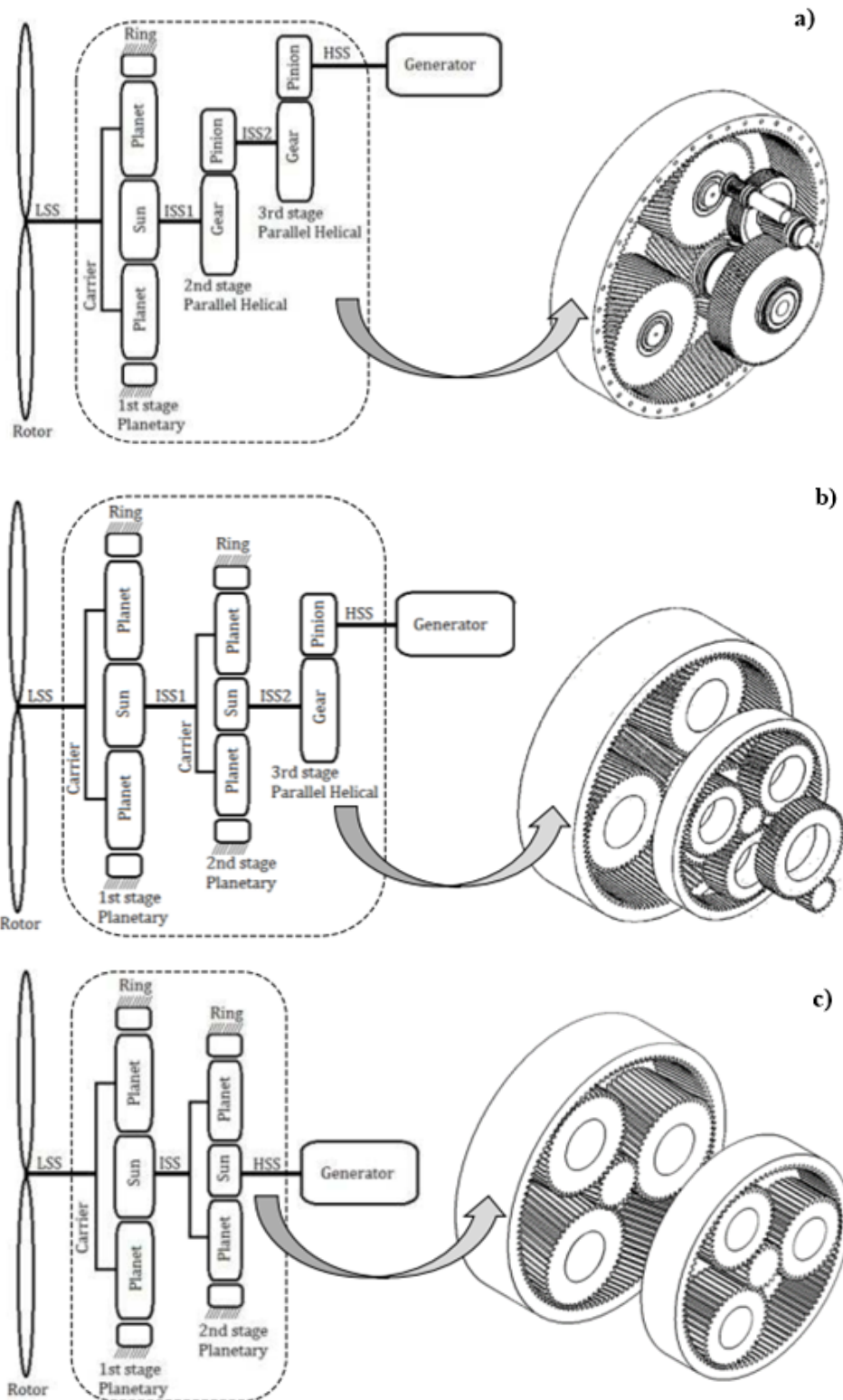


Figure 9: Simplified schematic of WT drivetrains and their gearboxes models: (a) One-stage planetary and two-stage parallel, (b) Two-stage planetary and one-stage parallel and (c) Two-stage planetary (LSS = Low Speed Shaft, ISS = Intermediate Speed Shaft, HSS = High Speed Shaft) [122]

to lower reliability than parallel shaft gears owing to its larger number of component parts. In this arrangement, multiple outer gears, planets, revolve around a single center gear, the sun. In order to achieve a change in the rpm, an outer ring or annulus is required. Planetary gearing systems exhibit higher power densities than parallel axis gears, and are able to offer a multitude of gearing options, and a large change in rpm within a small volume. The disadvantages of planetary gearing systems include the need for highly-complex designs, the general inaccessibility of vital components, and high loads on the shaft bearings [123]. The most used gearbox in WT consists of three stages with planetary gear for each of the first two stages and helical gear for the output stage [124].

I.5.3 Wind turbine gearbox power losses

This section is dedicated to a review of the different power loss mechanisms and models present in a gearbox.

I.5.3.1 Gearbox power loss model

Predicting the power loss in a gearbox has always been a daunting task. Infinite combinations of rolling bearings, gears, seals, casing geometries, oil formulations and operating conditions can be used, resulting in a large number of variables influencing power loss of a gearbox and hence very difficult to model it. However, the power loss models for gearboxes should always be a focus for tribologists and engineers, because of the increasing importance of improving efficiency and reducing fuel emissions. Alternatively, gearbox testing can be used to measure the power loss of a gearbox, but such option is time demanding, quite expensive and in some cases the technical aspects are very difficult to overcome.

It is currently accepted that the different power loss mechanisms acting in a gearbox are those presented in Figure 10. These mechanisms are divided in load dependent and load independent.

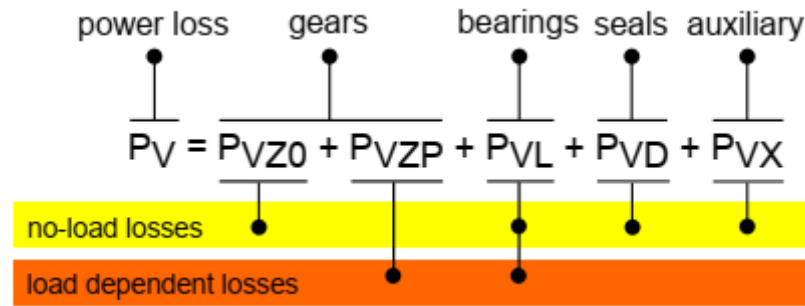


Figure 10: Power loss contributions [124]

The load dependent losses are directly influenced by the applied load torque while the load independent mechanisms depend mainly on the rotational speed, gearbox geometry and oil physical properties, the density and the viscosity. The load dependent losses are due to gears (P_{VZP}) and rolling bearings (P_{VL}). The load independent or no-load losses are due to seals (P_{VD}) as well as rolling bearings (P_{VL}) and gears (P_{VZ0}).

Under the nominal torques and rotational speeds, in an automotive or industrial gearbox, the load dependent gear losses are the main source of energy dissipation followed by the rolling bearing losses. The load independent losses usually have less influence, but may have a large influence when the speed is very high and dip lubrication is used.

1.5.3.2 Gear losses

i Load independent gear losses

Depending on input power and rotational speed, lubricant characteristics, and gearbox design, the no-load gear power losses (or spin power losses) usually are a very important source of energy dissipation. Spin power losses are directly related to the type of lubrication method used. Dip lubrication is often used in low to medium speed automotive gearbox or industrial transmission. When the operating gear speeds are relatively high, jet lubrication is preferred [125].

Under dip lubrication the total spin power losses are divided in two categories: losses due to the interaction between the rotating gears with the fluid and losses due

to interaction of the gear at the gear mesh interface. The interaction of the rotating gears can be both with air (windage) or oil (churning). The most relevant losses in the gear mesh interface are the squeezing and pocketing [126]. When jet-oil lubrication is used, the power loss is attributed to windage caused by the rotation of the gears in air/oil-air mixture environments. The losses due to squeezing of compressible air/oil-air mixture on the meshing gears and the drag power losses due to air drag along the teeth and sides of rotating gears are the usual focus on the literature [125].

ii Load dependent gear losses

The contact between meshing teeth, which constitutes the most important source of power loss in a gear transmission system, occurs mainly in cases when the velocity is not very high. This is the case in many current applications, such as vehicle gearboxes and industrial transmissions, as in the case of wind turbine gearboxes. The sliding losses are the most important source of load dependent gear losses. However, it should be remarked that gears can produce rolling losses that are also dependent on the load applied. In almost every case the rolling losses are neglected, since an involute gear which is perfectly shaped and has low tooth flexibility has no rolling losses [127].

1.5.3.3 Rolling bearing losses

Rolling bearing losses are divided into rolling, sliding and drag losses.

i Rolling friction losses

The rolling friction losses in a rolling bearing are identified in literature by the following effects: deformation and elastic hysteresis. 1) The solids in contact in a rolling bearing, usually balls or rollers, are under normal loads to the contact surface. These normal loads cause a deformation at each contact. Because of the deformation and due to the rolling motion of the elements over the raceway, which require a tangential load to overcome rolling resistance, the raceway material is squeezed up to form a bulge in the forward portion of the contact as shown in Figure 11(a). A depression is subsequently

formed in the rear of the contact area. Thus, an additional tangential load is required to overcome the resisting force of the bulge. A depression is subsequently formed in the rear of the contact area. Thus, an additional tangential load is required to overcome the resisting force of the bulge. 2) A rolling element under compressive load travels over a raceway, the material in the forward portion of the contact in the direction of rolling undergoes compression while the material in the rear of the contact is relieved of stress. It is possible to recognize that as load increases, as presented in Figure 11(b). The area between the curves in the Figure 12(b) is called hysteresis loop, and it represents an energy loss [128].

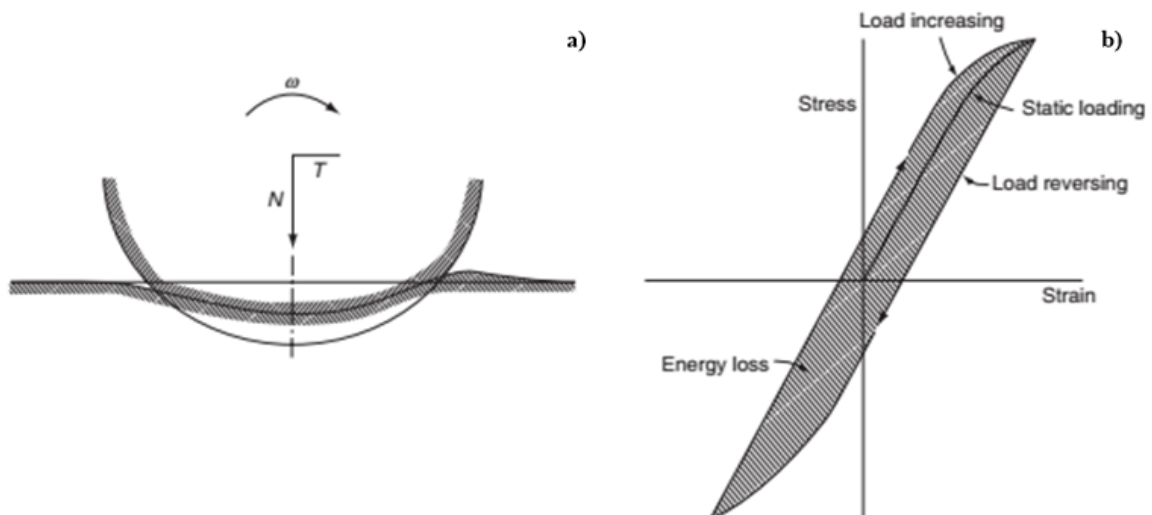


Figure 11: Rolling torque mechanisms: (a) Roller-raceway contact showing bulge due to rolling deformation and (b) Hysteresis loop for elastic material subjected to reversing stresses [128]

ii Sliding friction losses

Sliding is the major source of friction in a rolling bearing, mainly at low speed. The sliding friction occurs due to microslip and sliding due to rolling motion. If a rolling bearing operates without misalignment under moderate speed, then the total slip of one surface over another would not occur. However, depending on the elastic properties of the contacting bodies and the coefficient of friction between the contacting surfaces, microslip could occur and energy is lost.

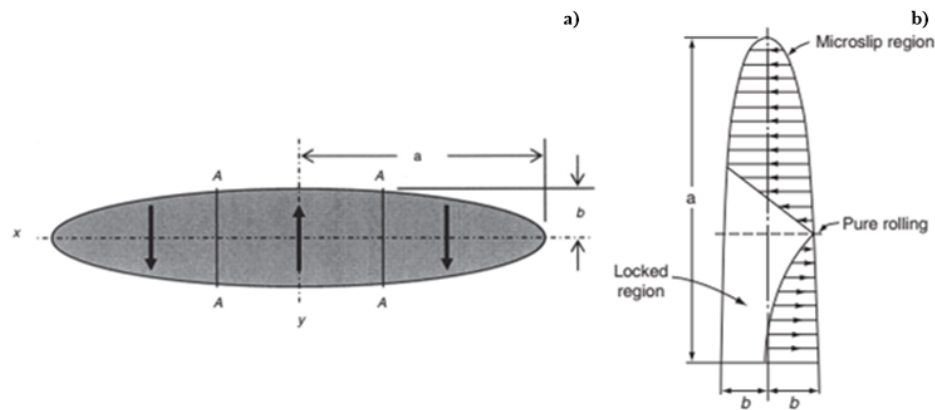


Figure 12: Ball-raceway contact area of a radial bearing with sliding directions presented [129].

A rolling bearing under simple radial load, pure rolling can only occur in points contained in two lines designated "A" as presented in Figure 12(a). At all other points along the contact, sliding must occur in a direction parallel to rolling motion. Outside the lines "A", sliding occurs in one direction; between points "A" sliding occurs in the opposite direction. It assumes that the coefficient of friction is not sufficiently great to cause the possibility of a locked region as presented in Figure 12(b). In the case of lubricated bearings this never happens because the coefficient of friction is not very high [129].

1.5.3.4 Drag friction

As stated by the theory [130], the lubricant builds up a film between the raceway and the rolling elements. Usually, from the oil provided to cool and lubricate the contact, only a small portion is used to build up the fluid film. The excess of oil acts as a friction force contrary to the rotational speed of the rolling elements. The power loss due to drag friction is dependent on the viscosity of the lubricant and on the speed.

1.5.3.5 Rolling bearing seals friction

Seals are used to prevent the bearing from being contaminated with moisture, corrosive media or any other material. The seal also retains the lubricant in the housing. The

contact between the rubber of the seal and the shaft generates friction and must be considered as a source of power loss. The loss due to seals friction is mainly dependent on the rotational speed [131].

I.5.3.6 Shaft seal losses

Seals power losses are due to friction in the contact zone. They were discussed in the rolling bearing losses section, since they are one of the possible contributions to the total power loss of a rolling bearing. However, the use of seals in the shafts is very usual in gearboxes and should be considered in the total power loss. The friction has been the scope of many researchers but the problem of seal losses is not very well understood yet. The contact zone is very small and the microscopic phenomena is difficult to parameterize [132].

I.5.3.7 Auxiliary losses

The auxiliary losses take into account other dissipative sources that are not generated by gears, bearings or the sealing elements.

I.5.4 Gearboxes power losses modeling and prediction

While the main focus of researchers and engineers on WT applications is mainly the gearbox reliability, the energetic efficiency of such large machines should not be disregarded [33]. WTGs handle several megawatt of power and even a small efficiency increase in the gearbox can save energy useful for several more households. The generated power by WTs already exceeds 5.0 MW [131]. The power loss reduction has a direct influence on lubrication quality, increased efficiency, i.e. lower heat dissipation and lower oil operating temperature. If the efficiency of a 1 MW wind turbine gearbox is increased by 1%, approximately 10 kW of additional power would be available in only one machine. The 1 MW wind turbines are very rare nowadays, since the current output power is in some cases above 5 MW [33]. Lowering the operating temperature

minimizes oil oxidation and degradation, which has a large impact on the lubrication quality and consequently on the surface protection against failures. Hohn et al. [133] showed that reducing the oil temperature also reduces the risk of failure. Even in the case of gearboxes without failure problems overtime, the oil change will be less frequent contributing to the reduction of the maintenance costs, related to the cost of fresh oil, but also to the cost of replacing it in a WT.

In order to increase gearbox efficiency it is important to quantify the power losses. That is why studies on the gearboxes power loss have attracted the attention of several researchers and have been the subject of several publications [134, 135]. Ohlendorf's model [136] is currently used to predict the average gear mesh losses, a constant and average coefficient of friction along the path of contact is assumed. Several models are currently used to predict the power loss of rolling bearings. Some models are validated by a large number of experimental results, as the ones presented by the major rolling bearing manufacturers in the world, such as SKF [137], NTN [138], and NSK [139]. Carlos M.C.G. Fernandes et al. [140] studied the influence of gear loss factor on the power loss prediction. Different gear loss formulations proposed in the literature were compared and it was shown that only few were able to yield satisfactory correlations with experimental results. To contribute to rolling bearing prediction, Carlos M.C.G. Fernandes et al. [124] calibrated SKF model for rolling bearing torque loss modeling using the experimental results for ball bearings and roller bearings lubricated with several WT gear oils under different formulations. Based on the model presented in [124], Carlos MCG Fernandes et al. [33] predicted the power loss for a 2.5 MW WT gearbox by using numerical simulations based on analytical model. This prediction is carried out under rated operating conditions involving input rotational speed, input torque and transmitted power.

I.6 Problems statement

The choice of an ANN structure for building a wind speed or power forecasting model is highly influenced by the quality of the data available, i.e. the site. Furthermore, no extensive study has been done using different ANN models for wind speed and power forecasting in Cameroon. The work carried out in other countries was limited to precise models with a specific forecasting step in specific sites. No comparative study of models for multi-step wind speed or power forecasting at the same site has been presented. Therefore, in order to provide a guide in the decision-making process for future wind energy projects in Cameroon and to suggest a better model and forecasting step, this thesis investigates the most used ANN models in multi-step wind speed forecasting and its application for wind turbine power output prediction in Bapouh, Cameroon. The multi-step forecasting involves 1-step, 2-step, and 3-step ahead, validated on five ANN models and ARIMA model.

The optimization techniques of ANNs models based on accurate time series forecasting presented in the literature have been limited to optimal input nodes, hidden nodes and weight, learning paradigm and so on, regardless of the input variables disposition. Thus, an investigation of the optimal disposition of the input variables of the ANNs for accurate wind speed forecasting will be presented in the next chapter of this thesis. Furthermore, wind speed or power forecasting is not an easy task because it is affected by many parameters such as air temperature, atmospheric pressure, relative humidity, and wind direction over time. The ANN models process by capturing the natural relationships between those weather variables and wind speed. A forecasting model based on ANN model will be more accurate as much as the relationship between each weather variable used as input and the wind speed (or power) is important. These relationships are intermittent over time as environmental changes and even almost non-existent in some cases. Thus, to ensure the accurate wind speed or power forecasting everywhere and at every moment, a combined ARIMA model and ANN model based on weather

variables relationships improving will presented the next chapter.

It is very difficult to develop a simple and general formulation to evaluate those power losses in WTG [35]. The calculations based on existing analytical models remain complex and robust, and require experimental parameters according to the systems for effective power loss prediction. Wind speed is one of the most critical characteristics in wind power generation. It varies with both time and space, and influenced by many factors such as geographic and weather conditions. The stochastic nature of WT operating wind speed induces the transmitted power intermittent. Most of the WTs operate in the nonlinear region, because the rated speed is reached very rarely. Due to WT working conditions under variable load and its operating environment, it is imperative to predict the power loss in gearbox under real-time operating conditions. The previous works have limited their studies on rated operating parameters with fixed rotational speed. Therefore, the rolling bearing power loss in gearbox forecasting for modern WTs under real-time operating condition approach will be developed in the next chapter.

I.7 Conclusion

From the review presented in this chapter, it emerges that the power generated by wind energy conversion systems is very intermittent due to the stochastic nature of wind speed. Despite this intermittency, the development of wind energy has its place, it will suffice to integrate it correctly into an energy mix. This is why this energy source is today, one of the most promising among renewable energy sources. This integration of wind energy requires an accurate power forecasting model. Recent works have shown that artificial neural network models are better tools for predicting wind speed and power. Thus, several models have been developed for wind speed and power forecasting in different cities. Most of these models are hybrid (more accurate than single models), i.e. they use neural network optimization techniques or combined forecasting models. But they limited to the optimal neural network parameters selection. The wind turbine gearbox causes power losses which are mainly due to friction. These losses have

a great influence on the efficiency of the turbine, so their reduction would increase the efficiency of the system. Improvement in efficiency involves controlling these losses, which depend on the operating conditions of the wind turbine. Thus, in the next chapter of this thesis, we will explore the methodology for multi-step wind speed forecasting using several neural network models employed for wind power prediction in Bapouh, Cameroon. A new approach to optimizing the performance of neural networks for times series forecasting based on the input variables disposition will be presented. The modeling and prediction of the power losses in the rolling bearing of the gearboxes in real time by combining the SKF model and the neural network will be given with its validation at Bapouh.

METHODOLOGY

II.1 Introduction

In this chapter we present the site of our study. The models designing for TSF and the forecasting models evaluation criteria are presented. Each proposed wind speed and WTPG model scheme is elaborated. The related WTG is detailed. At the end, the SKF model for rolling bearing power loss modelling is elaborated.

II.2 Models designing for times series forecasting

In this thesis, ANN models and ARIMA are used for time series forecasting. Therefore, in order to considerably validate our proposals, five ANN models are used in our studies. ARIMA model is mainly employed as benchmark model. All these models and their designing process are presented in this section.

II.2.1 Artificial neural network model designing

All the predictions proposed in this thesis are based on the use of time series of measured historical data. Thus, supervised learning is employed for the ANN models. In order to solve a given problem of supervised learning various steps have to be considered. In the first step we have to determine the type of training examples. In the second step we need to gather a training data set that satisfactory describes a given problem. In the third step we need to describe gathered training data set in form understandable to a chosen ANN. In the fourth step we do the learning and after the learning we can test the performance of learned ANN with the test (validation) data set. Test data set consist of

data that has not been introduced to ANN while learning. Figure 13 describes the work flow for the general neural network design process.

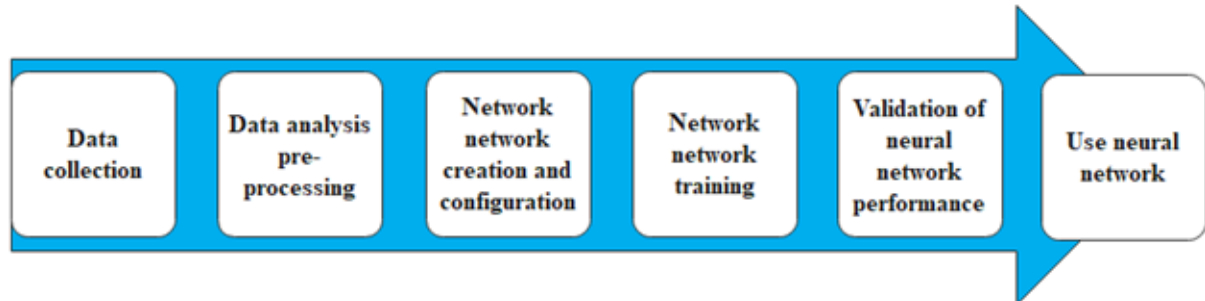


Figure 13: Artificial neural network design stages [104]

II.2.1.1 Data collection

Data collection consists of historical time series data collection. The objective of this step is to collect sufficient quantity of data required to build a representative database, which will be used for learning and testing (forecasting) the neural network. It includes interested variable and dependent variables. Therefore the study context such as the wind farm and the type of data play an important role. This is why it is important to investigate the performance of neural network models in the study of wind power and wind turbine in Cameroon. Until 2021, no wind energy farm had been constructed in Cameroon. Therefore, historical data for wind turbine power generation and power losses in wind turbine gearboxes are not available. But, many systems are installed in many places in the country to collect weather data which can be used to evaluate and analyze the renewable energy potential in each locality before further energy conversion systems installation. Such systems are installed in Eseka in the Center Region and in Bapouh in the West Region. The system installed at Eseka provides data of air temperature, atmospheric pressure, relative humidity and solar irradiation. These data are adequate for the study of the solar energy potential. While the system installed at Bapouh provides data of air temperature, atmospheric pressure, relative humidity, wind direction and wind speed. The data provided at Bapouh are favorable for the study of wind energy potential.

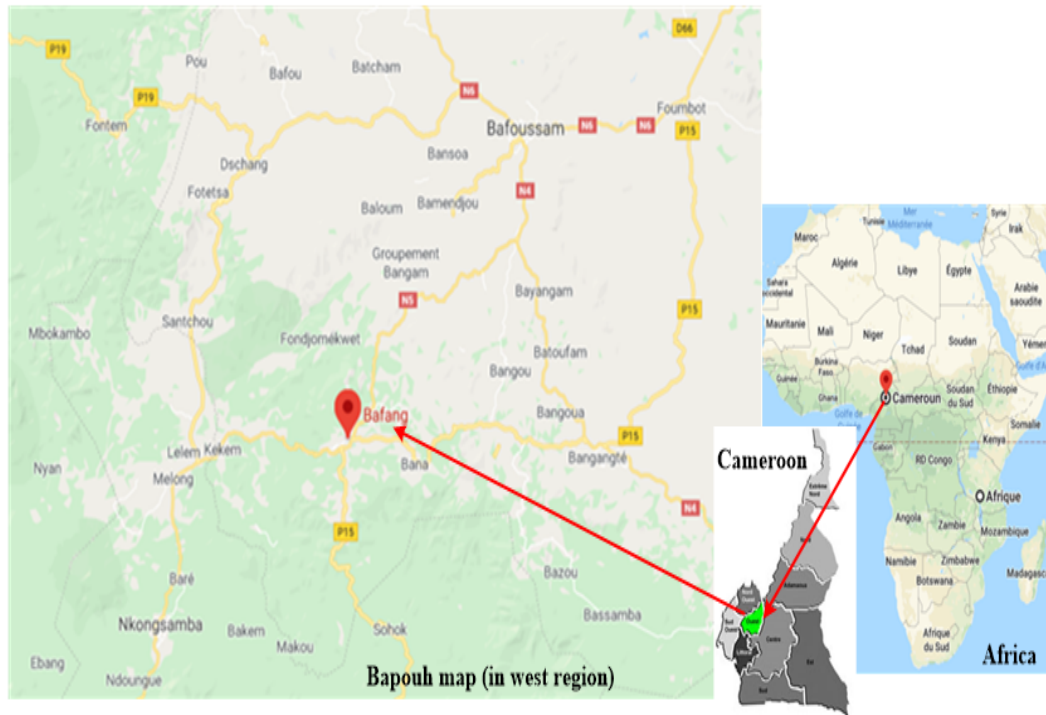


Figure 14: Bapouh location

With the aim to support decision-making for future wind energy exploitation in Cameroon, for all our applications in this thesis, we used the weather data provided by the system installed at Bapouh. Bapouh is a village located near the Town of Bafang, in the Western Region of Cameroon as shown in Figure 14. The geographical coordinates of the site are N 05o09'35.52" and E 10o19'21.90 ". The data collection system consists of a meteorological sensor reading and stored in the SymphonyPlus3 data logger installed in January 2016. The configuration of the measuring system as well as the characteristics of the different components is shown in Figure 15. Figure 16 shows the experiment site of Bapouh.

The weather data including average wind speed (V), air Temperature (T_a), Relative Humidity (RH), and atmospheric Pressure (P_a) were recorded at an interval of 10 minutes from 20th November 2016 to 31st January 2017. The height of measurement is 70 meters and the scanning frequency is 144 times per day from 00:00 to 24:00, with 10512 samples for 73 days. Before using them for neural network-based prediction, these data are analyzed and preprocessed.

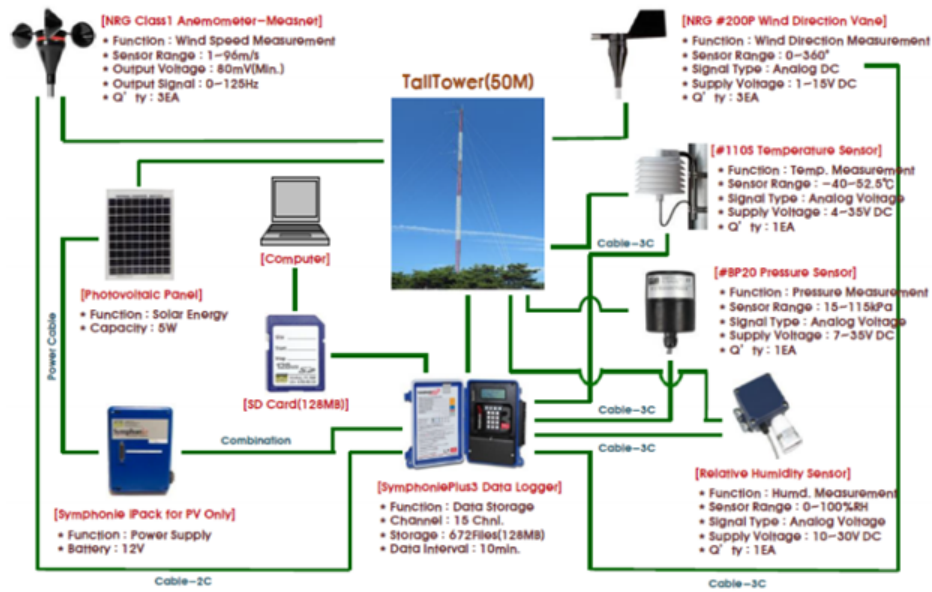


Figure 15: Weather data recording system



Figure 16: Bapouh experiment site

II.2.1.2 Data analysis and preprocessing

The selection of the variables to be used at the inputs of the neural network is done through the analysis of the correlation strength between the input variables and between each input variable and the target variable. According to Wei et al.[28], the input variables of an ANN need to have high strength correlation between each of them and the target variable, but should not be correlated. Therefore, the objective is to select input variables with a weak relationship between them and strong relationships between each of them and the output variable. In our studies, the relationships between the variables are measured by using the *Spearman rank correlation* to determine the correlation coefficient. The Spearman correlation or correlation coefficient between two variables, $x(t)$ and $y(t)$ with the size of the sample T is defined by,

$$R^2 = \frac{\sum_{t=1}^T [(x(t) - \bar{x})(y(t) - \bar{y})]}{\sqrt{\sum_{t=1}^T (x(t) - \bar{x})^2 \cdot \sum_{t=1}^T (y(t) - \bar{y})^2}}, \quad (22)$$

where \bar{x} and \bar{y} are the mean values both variables respectively. The value of R^2 is between [-1 1]. The sign of R^2 indicates the direction of the relationship while its value indicates the degree of correlation. The sign of R^2 indicates the direction of the relationship while its value indicates the degree of correlation. The closer the absolute value of R^2 to 1, the stronger the correlation. The correlation is bad when the absolute value of R^2 is close to 0. Standard deviation (Sd) is employed to measure the dispersion of the dataset of each variables. A volatile dataset has a high Sd , while the deviation of a stable blue-chip dataset is usually rather low. Sd of a variable $x(t)$ is calculated as given in Equation (23),

$$Sd = \sqrt{\frac{\sum_{t=1}^T (x(t) - \bar{x})^2}{T}}. \quad (23)$$

The input and target variables of the prediction tools have been collected at difference unity. Data preprocessing consist to transform them in order to minimize noise and

so that the ANN model can learn relevant patterns. This normalization must take into account the amplitudes accepted by the neural network through the activation functions used. Some time series data transformation are defined in [141]. Therefore, in this thesis, every used variables are normalized between 0 and 1 using Equation (24) before the training process of ANN models. At the end of the forecasting process, the natural values of the forecasting variables are achieved by transforming its normalized values using Equation (25) given as following,

$$y(t)_N = \frac{y(t) - y_{\min}}{y_{\max} - y_{\min}}, \quad (24)$$

$$\hat{y}(t)_d = \hat{y}(t)_N(y_{\max} - y_{\min}) + y_{\min}, \quad (25)$$

where $y(t)$, $y(t)_N$, $\hat{y}(t)_N$ and $\hat{y}(t)_d$ are natural, normalized, predicted, and renormalized variable respectively, at a given time t ; y_{\max} and y_{\min} are respectively the maximum and minimum value of the natural measured variables. Variables selection and data preprocessing help to select the appropriate neural network architecture for model building.

II.2.1.3 Neural network creation and configuration

This step consists of ANN model building. It must start with the choice of the neural network architecture. In this thesis, despite the weaknesses of the different architectures as presented in the previous chapter, we investigated the performance of five types of neural networks in our applications for time series forecasting, i.e. three simple models involving BPNN, NARXNN and RBFNN, and two hybrid models involving GABPNN and ANFIS.

After the choice of the structure, the intrinsic configuration of the network comes into play. This mainly consists in making a compromise between the complexity of the network by reducing the number of hidden layers and the number of neurons for each layer, and its performance. However, a two-layer ANN with a sigmoid activation function in the first layer (hidden layer) and a linear function in the output layer can approximate any interest function with arbitrary accuracy, provided that there are enough

neurons in the hidden layer. We have thus opted for the two-layer ANN models (i.e. with a hidden layer) with the sigmoid function in the hidden layer and the linear function in the output layer. For the output layer, the number of neurons is determined by the number of outputs to approximate, i.e. to predict. For our applications, it will be a question of predicting a single variable, either the wind speed or the power loss in the gearbox of the wind turbine. The case is not so easy for the number of neurons in the hidden layers. The number of adjustable weight is one of the fundamental factors of the success of an application. Indeed, with a limited number of neurons (too small), the network will not perform well on learning, and with a number of weights too large the network may have poor generalization properties (overlearning). Usually the best model (based on prediction performance) is obtained after trying different numbers of neurons in the hidden layer. But this approach is very time consuming. Kolmogorov [105] proposed a theorem to determine for a two layer network the number of neurons in the hidden layer as,

$$H = 2N + 1, \quad (26)$$

where H is the number of hidden node and N is the number of input node.

II.2.2 Neural networks structures and parameters

II.2.2.1 Back-Propagation neural network

The Back-Propagation neural network (BPNN), is an MLPNN architecture based on a gradient descent or BP method that minimizes the sum of the squared errors between the output values and the actual values [142]. The process of the BP algorithm is divided into two phases, updating and learning. Figure 17 illustrates the architecture of a MLPNN with one hidden layer, yellow, intended to the time series forecasting.

From Figure 17, the input layer (black), is made of N nodes $[x_1(t), x_2(t), \dots, x_N(t)]$, constituting the number of past data used as input variables of ANN, the hidden layer

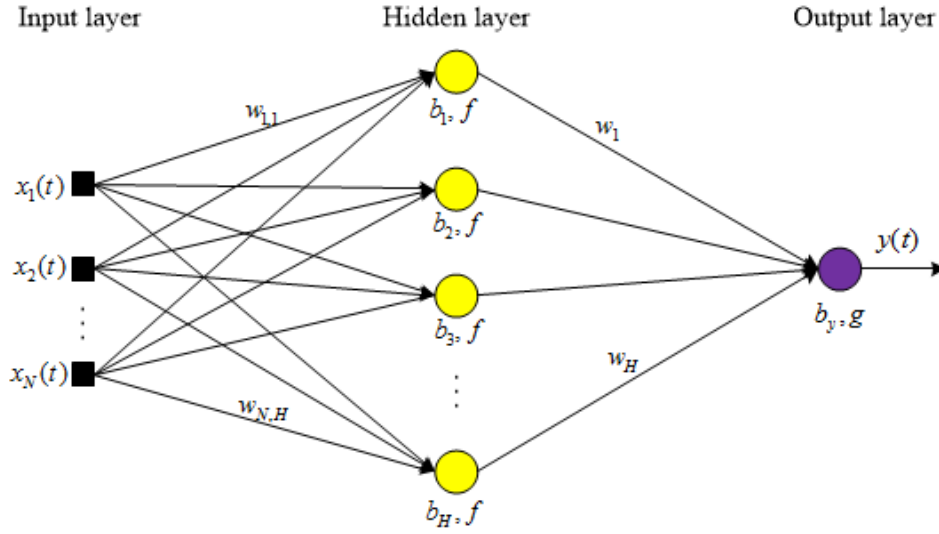


Figure 17: Back-propagation neural network architecture

has H nodes (yellow) and output layer have only one node (purple) constructing the forecasting variable. The output of the hidden layer is calculated as follows,

$$h_j(t) = f \left(\sum_k^N w_{k,i} \cdot x_k(t) - b_j \right), \quad (27)$$

$$k = 1, 2, \dots, N, j = 1, 2, \dots, H,$$

where $h_j(t)$ is the output of the j node of the hidden layer at a time step t , $w_{k,j}$ is the connection parameter (synaptic weight) between the k node of the input layer and the j node of the hidden layer, b_j is bias of the j node of the hidden layer and f is the activation function used in each node of the hidden layer. The evaluation of the forecasting variable at the output layer is expressed as follows,

$$y(t) = g \left(\sum_j^H w_{j,y} \cdot h_j(t) - b_y \right), \quad (28)$$

where $y(t)$ is the forecasting variable at a time step t at the output layer, $w_{j,y}$ is the synaptic weight which connects the j node of the hidden layer and the alone node of the output layer, b and g are the bias and activation function respectively, of the output node.

Then, the forecasting variable from the developed MLPNN is finally designed as,

$$y(t) = g \left[\sum_j^H w_{j,y} \cdot f \left(\sum_k^N w_{k,j} \cdot x_k(t) - b_H \right) - b_y \right]. \quad (29)$$

II.2.2.2 NARXNN

The Nonlinear Autoregressive with exogenous inputs Neural Networks (NARXNN) is a dynamic driven RNN with global feedback coming only from the output layer rather than by the hidden states. It consists of an MLPNN which takes as inputs a window of past independent (exogenous inputs) and past outputs (endogenous inputs), and determines the current output. So, only the output of NARXNN is fed back to the MLPNN. NARXNN architecture exists in open-loop and closed-loop [26]. Figure 18 presents the NARXNN architectures based on the time series forecasting.

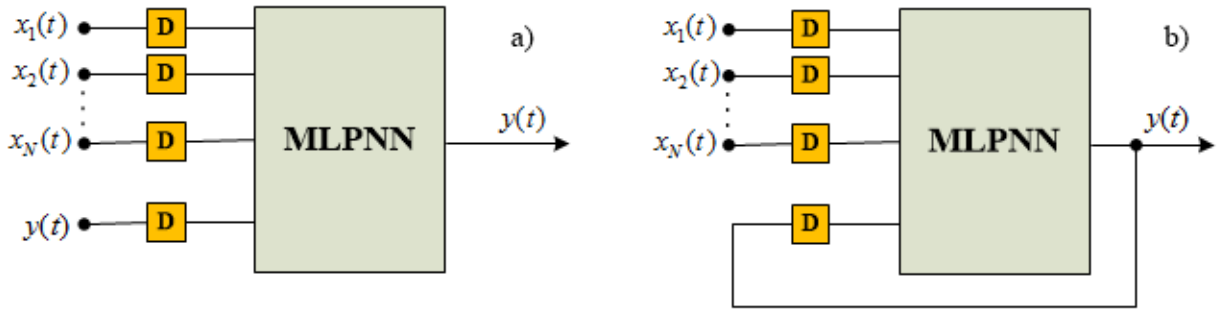


Figure 18: NARX neural networks architectures based on time series forecasting: (a) open-loop and (b) closed-loop

NARXNN is designed as a class of discrete-time nonlinear systems and can be expressed mathematically as follow,

$$\begin{aligned} y(t) &= \Gamma [y(t); x_1(t); x_2(t); \dots x_N(t)], \\ &= \Gamma [y(t-1), y(t-2), \dots, y(t-u_y); x_1(t), x_1(t-1), \dots, x_1(t-u_{x_1}); \\ &\quad x_2(t), x_2(t-1), \dots, x_2(t-u_{x_2}); \dots; x_N(t), x_N(t-1), \dots, x_N(t-u_{x_N})], \end{aligned} \quad (30)$$

where $y(t)$ is the current output, endogenous input, and $x_1(t), x_2(t), x_N(t)$ are the exogenous inputs at a time step t , D is the time delay line, Γ is an unknown mapping nonlinear function, and $u_y \geq 1, u_{x_1} = u_{x_2} = \dots = u_{x_N} \geq 1, u_y \geq u_{x_N}$ are the inputs and output

memory orders [19, 142].

II.2.2.3 Radial basis function neural network

The Radial Basis Function (RBF) neural network is a type of FFNN that uses radial basis functions as activation function introduced. It has typically three layers: an input layer, a hidden layer with a non-linear RBF activation function and a linear output layer. There are no weights between the input hidden layers. Its output layer is given by the following linear regression Equation (31),

$$y(t) = \sum_{k=1}^H f_k(x) \cdot w_k + b, \quad (31)$$

where $f_k(x)$ is the activation function of the k -th hidden node, w_k is weight between k -th hidden node and output node, H is the number of hidden node, b is the biased weight of the output. The typical radial function is the Gaussian which in the case of a scalar input. Then the activation function at the k -th hidden node is expressed as follow,

$$f_k(x) = \exp \left(-\frac{\sum_{k=1}^N (x_k - \mu_k)^2}{2\sigma_k^2} \right), \quad (32)$$

where x_k is the k -th input sample, μ_k is the mean value of the k -th hidden unit representing the center vector, σ_k^2 is the variance of the k -th hidden unit denoting the width of the RBF kernel function, and N is the number of input node [143].

II.2.2.4 Generic Algorithm Back Propagation neural network

Generic Algorithm Back Propagation neural network (GABPNN) is a combining ANN and GA model; which consist to train the BPNN by using GA. The weight of ANN is used as a population of GA by making the string and GA evaluate the fitness. Then, applying GA to ANN mainly plays two roles. One is to optimize neural network structure, the other is apply GA update the weights of neural network, this is, use GA to replace

some of the traditional back propagation algorithms in GABPNN [115, 144].

II.2.2.5 Adaptive Neuro-Fuzzy Inference System

Adaptive Neuro-Fuzzy Inference System (ANFIS) is a hybrid framework that is obtained by combining the concepts of FL and neural network into a unified platform. The model has a fuzzy inference system in the form of an adaptive network for system identification and a predictive tool that maps a given input space to its corresponding output space based on a representative training data set. The ANFIS inference system relies on both fuzzified human knowledge (human knowledge modelled in the form of fuzzy "if-then" rules) and a set of input-output data pairs (patterns) to accomplish the process of input-output mapping. Figure 19 shows the architecture of ANFIS model for 2 inputs, $x_1(t)$ and $x_2(t)$ and one output $y(t)$. The functions of each layer are described below,

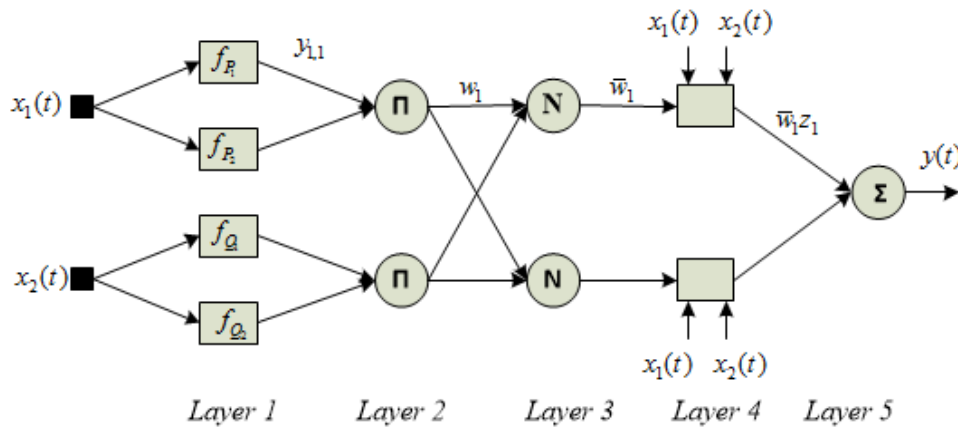


Figure 19: Adaptive Neuro-Fuzzy Inference System [89]

The *first layer* is the input layer. It maps the crisp inputs using membership functions, f (i.e., gaussian, triangular, triopzoidal). The value of membership grade varies between 0 and 1. Each node of this layer stores the parameters to define a bell-shaped membership function as given by,

$$y_{1,k}(t) = f_{p_k}(x_1), \quad (33)$$

$$y_{1,j}(t) = f_{Q_{j-2}}(x_2), \quad (34)$$

where $k = 1, 2$ and $j = 3, 4$; $x_1(t)$ and $x_2(t)$ are the inputs; P_j or Q_j are the linguistic label. In the *second layer* each node of this layer performs connective operation "AND" within the rule antecedent to determine the corresponding firing strength, w_k . The node function of this layer can be written as follows [145],

$$y_{2,k}(t) = f_{P_k}(x_1) * f_{Q_k}(x_2) = w_k. \quad (35)$$

In the *third layer*, the nodes perform a normalization process to produce the normalized firing strength,

$$y_{3,k}(t) = \frac{w_k}{\sum w_k} = \bar{w}_k. \quad (36)$$

The *fourth layer* deals with the consequent part of the fuzzy rule. The node of this layer is adaptive with output,

$$y_{4,k}(t) = \bar{w}_k z_k, \quad (37)$$

where $z_k = \alpha_k + \beta_k x_1(t) + \gamma_k x_2(t)$; α , β and γ are constant parameters.

In the *fifth layer*, the final output is the weighted average of all rule outputs. It is computed as,

$$y_5(t) = \sum_{k=1}^2 \bar{w}_k (\alpha_k + \beta_k x_1(t) + \gamma_k x_2(t)) = y(t). \quad (38)$$

II.2.2.6 Activation functions

i FFNN activation functions

The activation functions used in FFNN are linear, Log-sigmoid and Tangent-sigmoid, expressed by Equations (39), (40) and (41), respectively. Their shapes are shown in figures 20(a), 20(b) and 20(c) respectively,

$$f(t) = t, \quad (39)$$

$$f(t) = \frac{1}{1 + \exp(-t)}, \quad (40)$$

$$f(t) = \frac{1 - \exp(-t)}{1 + \exp(t)}. \quad (41)$$

ii Radial basis functions

The radial basis function used in RBFNN is the Gaussian function. It is defined by its mean value μ and standard deviation $\sigma > 0$, as expressed in Equation (32). Its appearance is given in Figure 20(d).

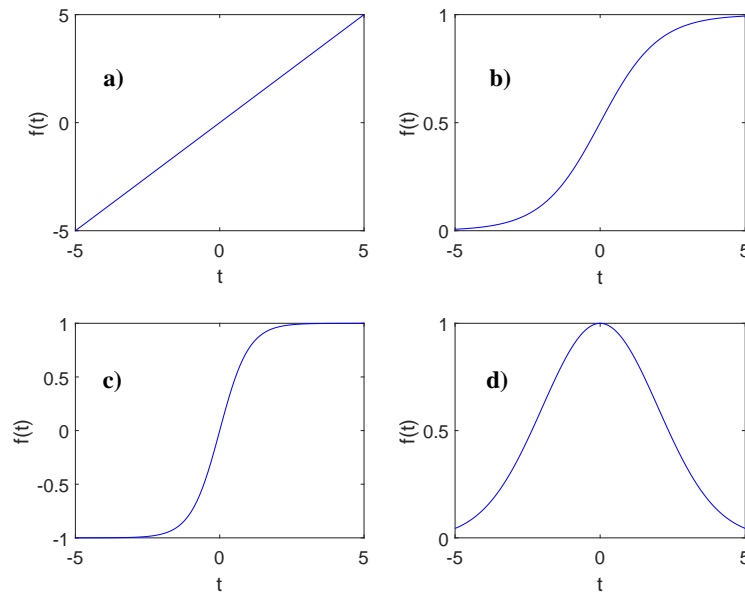


Figure 20: Neural networks activation functions: (a) Linear, (b) Log-sigmoid, (c) Tangent-sigmoid and (d) Gaussian

iii Membership functions

The typical membership functions used in AMFIS are Gaussian, Triangular, and Trapezoidal. The trapezoidal function is defined by its lower limit a and its upper limit d , and the lower and upper limits of its nucleus, b and c respectively, as shown in Equation (42) and Figure 21(a). While the triangular function is defined by its lower limit a , its upper

limit c , and the modal value b , such that $a < b < c$. We call the value $c - b$ margin when it is equal to the value $b - a$, as shown in Equation (43) and Figure 21(b).

$$f(t) = \begin{cases} 0, & t \leq a \\ \frac{t-a}{b-a}, & a \leq t \leq b \\ 1, & b \leq t \leq c \\ \frac{d-t}{d-c}, & c \leq t \leq d \\ 0, & d \leq t \end{cases} \quad (42)$$

$$f(t) = \begin{cases} 0, & t \leq a \\ \frac{t-a}{b-a}, & a \leq t \leq b \\ \frac{c-t}{c-b}, & b \leq t \leq c \\ 0, & c \leq t \end{cases} \quad (43)$$

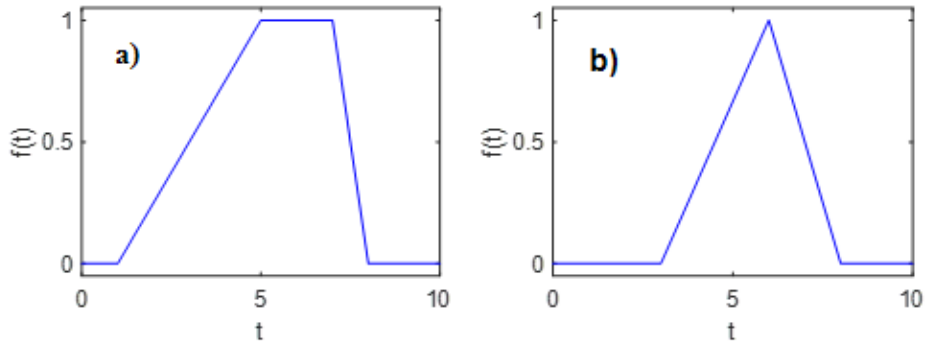


Figure 21: Membership functions: (a) trapezoidal and (b) triangular

For our applications, all developed ANN models have two layers. The tangent hyperbolic function is used in hidden nodes of BPNN and NARXNN models, and Gaussian is used as membership function of ANFIS model. For NARXNN model, the open-loop architecture is used in the training process and closed-loop architecture is used in forecasting step.

II.2.2.7 Neural networks training

Once the neural network architecture is chosen and configured, it must be trained. The training involves in calculating the optimal weights of the different links using the learning algorithm. Before starting with the training, the historical data is divided into three datasets. One dataset (training set; a set of samples used for learning, that is to fit the parameters of the ANN model) is built to perform the training, the other dataset (validation set; a set of samples used to tune the parameters of a ANN model, for example to choose the number of hidden nodes) to validate the training and last one (testing set; a set of samples used only to assess the forecasting performance) to test the trained neural network and determine its performance. The validation set and testing set must each represent no more than 25% of the total samples. Testing set consist of data that has not been introduced to ANN while learning. Generally, training set and validation set are grouped at the beginning and the set is called training set. The learning process consists in initializing the synaptic weights which are then iteratively modified. The input data is presented to the network several times and each time the weights are updated. With supervised learning, we used the BP algorithm, especially the Levenberg-Marquardt (LM) algorithm. The LM algorithm is the most used because it gives better results in terms of training convergence rate and generalization performance. The latter seeks to minimize a cost function that is a measure of the difference between the actual responses of the network and its desired responses.

The learning procedure is controlled by a cross-validation technique based on the training set and validation set. The cross-validation technique in learning is a method for estimating the reliability of a model. Suppose we have a statistical model with one or more unknown parameters, and a training set on which we can train the model. The training process optimizes the parameters of the model so that it matches the data as closely as possible. If we then take an independent validation sample, from the same training data, it will usually turn out that the model does not perform as well during the validation as during the training: this is called overlearning. So cross-validation is a

way to predict the efficiency of an ANN model.

II.2.2.8 Evaluation of the neural networks performance

It consists in testing the forecasting performance of the trained ANN model. Once the training of the network is completed, the testing set is used to estimate its generalization quality. If the obtained performance is not satisfactory, either change the architecture of the network, or modify the training set, or further optimize the model. There are many indicators to evaluate the performance of the ANN. In this thesis, to evaluate the forecasting ability of the models, the traditional evaluation criterion are employed to evaluate the forecasting accuracy. Furthermore, Diebold-Mariano (DM) test is used to evaluate the significance level of accuracy of the proposed models over the comparison models.

i Traditional forecasting accuracy criteria

Three traditional error criteria are used in the forecasting experiments to measure the average spread, the average bias and the percentage of the error of the forecasting models, including the Root Mean Square Error (RMSE), the Mean Absolute Error (MAE) and the Mean Absolute Percentage Error (MAPE), respectively. They are expressed as,

$$RMSE = \sqrt{\frac{1}{T} \sum_{t=1}^N (y(t) - \hat{y}(t))^2}, \quad (44)$$

$$MAE = \frac{1}{T} \sum_{t=1}^N |y(t) - \hat{y}(t)|, \quad (45)$$

$$MAPE = \frac{1}{T} \sum_{t=1}^N \left| \frac{y(t) - \hat{y}(t)}{y(t)} \right| \times 100, \quad (46)$$

where $y(t)$ and $\hat{y}(t)$ are the measured and predicted wind speed values respectively at the time step t and T is the total number of the forecasting time steps. The forecasting model is better as its RMSE, MAE, and MAPE values are lowest. To compare the forecasting performance of the two different models, the improvement percentage of three

error criteria are evaluated as follow,

$$IP = \left| \frac{Error_1 - Error_2}{Error_2} \right| \times 100, \quad (47)$$

where subscript 1 indicates a proposed model, and the subscript 2 indicates a comparison model.

ii Diebold-Mariano test

The traditional forecast evaluation criteria have limitations in application to some degree [146]. To further analyze the forecasting performance, the significant differences of forecasting accuracy from two different models are evaluated by using Diebold-Mariano (DM) test. DM is a hypothesis test which can be used to quantify the level of confidence of the difference between two forecasting models [15, 147]. It is defined as follows:

let the observed value be defined by,

$$y(t), t = 1, \dots, T + k, \quad (48)$$

and

$$\hat{y}(t)^{(1)}, t = 1, \dots, T + k, \quad (49)$$

$$\hat{y}(t)^{(2)}, t = 1, \dots, T + k, \quad (50)$$

defines the forecasting values from two competing models. The forecasting errors of the two models are

$$\varepsilon(t + h)^{(1)} = y(t + h) - \hat{y}(t + h)^{(1)}, h = 1, \dots, k, \quad (51)$$

$$\varepsilon(t + h)^{(2)} = y(t + h) - \hat{y}(t + h)^{(2)}, h = 1, \dots, k. \quad (52)$$

The precision of each forecasting model is measured by a proper loss function $L(\varepsilon(t + h)^{(j)})$, $j = 1, 2$. Two popular loss functions involve the square error loss defined by,

$$L(\varepsilon(t+h)^{(j)}) = (\varepsilon(t+h))^2, \quad (53)$$

and the absolute deviation loss defined by,

$$L(\varepsilon(t+h)^{(j)}) = |\varepsilon(t+h)^{(j)}|. \quad (54)$$

The Diebold-Mariano test statistic can be defined as,

$$DM = \frac{\frac{1}{T} \sum_{t=1}^T (L(\varepsilon(t+h)^{(1)}) - L(\varepsilon(t+h)^{(2)}))}{\sqrt{S^2/k}}, \quad (55)$$

where S^2 is an estimator of the variance of $d = L(\varepsilon(t+h)^{(1)}) - L(\varepsilon(t+h)^{(2)})$ [15].

To determine whether one model is more accurate than another, we test the equal accuracy hypothesis. The null hypothesis is defined by,

$$H_0 : L(\varepsilon(t+h)^{(1)}) - L(\varepsilon(t+h)^{(2)}) = 0, \forall t. \quad (56)$$

The null hypothesis is that the two forecasting models have the same accuracy. The alternative hypothesis is that the two forecasting models have different levels of accuracy. The DM test statistics converge to a standard normal distribution, the null hypothesis at 10% level of significance is rejected if $|DM| \leq 1.96$. If $2.8 \leq |DM| > 1.96$ the null hypothesis is rejected at the 5% significance level, and is rejected at 1% when $|DM| > 2.8$ [15, 146-148].

II.2.3 ARIMA model designing

The ARIMA model is based only on the time series of historical data of the desired variable. An ARIMA(p, d, q) model is developed for time series prediction by identifying its optimal parameters. The procedure is described by the flowchart given in Figure 22. The data are divided into training set and testing set, as in the previous case with the neural network.

1) We start by identifying the given training set series in order to make it stationary

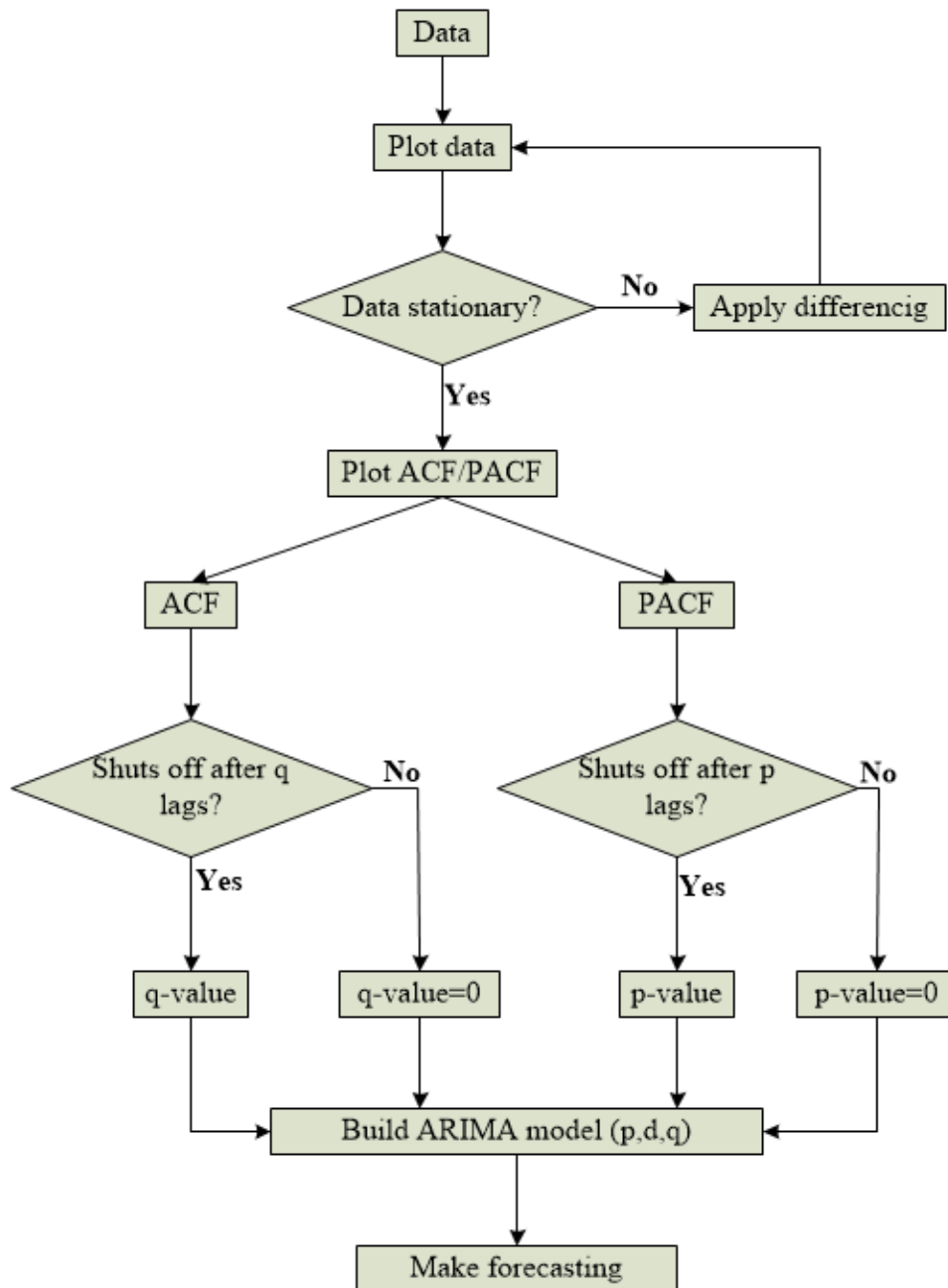


Figure 22: Flowchart of ARIMA model development for time series forecasting

(in case it was not stationary before). A stationary time series is one whose properties do not depend on the time at which the series is observed. Thus, time series with trends, or with seasonality, are not stationary; the trend and seasonality will affect the value of the time series at different times. On the other hand, a white noise series is stationary; it does not matter when you observe it, it should look much the same at any point in time. A stationary time series will have no predictable patterns in the long-term.

Differencing helps to stabilize the mean of a time series by removing changes in the level of a time series, and therefore eliminating (or reducing) trend and seasonality. The Autocorrelation (ACF) plot is useful for identifying non-stationary time series. For a stationary time series, the ACF will drop to zero relatively quickly, while the ACF of a non-stationary data decreases slowly. 2) After having the stationary data series, we have to identify the parameters of the model. In order to determine the order of the p (AR) and q (MA) components, a time series basic diagnostics chart is built with the ACF and partial autocorrelation functions (PACF). PACF should cut off after p lags. ACF should cut off after q lags. 3) After the model is built, it is tested for prediction and its performance is evaluated by comparing the result obtained with the testing set.

In this thesis, all the experiments are operated in MATLAB R2018a on Windows 7 with 2.27 GHz Intel Core i3-6700HQ CPU, 64-bit and 2 GB RAM using developed code. The first application presented in the next section investigates ANN and ARIMA models for wind speed and power forecasting.

The tangent hyperbolic sigmoid and linear functions are used as activation functions of each hidden node and output node, respectively. The NARXNN models are trained using its open-loop architecture and multi-step forecasting is carried out with its closed-loop architecture. Several delays have been tried and the better results from NARXNN models had been achieved with four delays per variable, $D = 4$. Before the training process of neural network models, the data sets are brought within the same order of magnitude. Thus, every data has been normalized between 0 and 1.

II.3 Wind speed forecasting and application for expected wind turbine power output estimation

In order to suggest the better models and forecasting step, this section investigates the mostly used existing wind speed forecasting models and its application for expected wind turbine power output prediction. The schematic illustration of the fol-

lowed methodology is depicted in Figure 23. It consists of three main stages. The historical wind data are collected in *stage (I)*. In *stage (II)*, the statistical method is used to forecast the wind speed patterns. To find the best way of wind speed forecasting, the mostly used statistical prediction tools are investigated on different step ahead forecasting. Therefore, four AI models and ARIMA model are developed for multi-step ahead wind speed forecasting. There are the single ANN models, BPNN, RBFNN, and NARXNN and the hybrid models, GABPNN and ANFIS. Each model is developed and trained using historical wind data pursuing for desired wind speed values forecasting. *Stage (III)* consists of using the physical method for estimating the WTPG. Firstly, the characteristics of the related wind turbine are determined. And, its power curve is modeled and used with the previously predicted wind speed values to estimate the corresponding expected WTPG.

II.3.1 Multi-step wind speed forecasting

The multi-step ahead applied here involves 1-step, 2-step, and 3-step ahead forecasting as given in Figure 24. With the 1-step ahead forecasting, the forecasting value $\hat{y}(T+1)$ is achieved only through the past observation values $\{y(1), y(2), \dots, y(T-1), y(T)\}$, with T the total number of wind speed training samples. In the 2-step ahead forecasting, the forecasting value $\hat{y}(T+2)$ is achieved by using the past values $\{y(1), y(2), \dots, y(T-1), y(T)\}$ and the previously forecasting value $\hat{y}(T+1)$. While the forecasting value $\hat{y}(T+3)$ in 3-step ahead is obtained based on the historical $\{y(1), y(2), \dots, y(T-1), y(T)\}$ and the two previously forecasting values $\hat{y}(T+1)$ and $\hat{y}(T+2)$ [148].

Two Datasets; Dataset1 and Dataset2 are constituted from two months of real data measured from 1st to 30th December 2016 and from 1st to 30th January 2017, respectively. Each Dataset has 4320 data points, these observations are split into two subsets, which are training set and testing set. Time (t), air temperature (Ta), atmospheric pressure (Pa) and relative humidity (RH) are employed as input variables of neural network models, while wind speed is used as target variable. The number of hidden nodes of ANN models

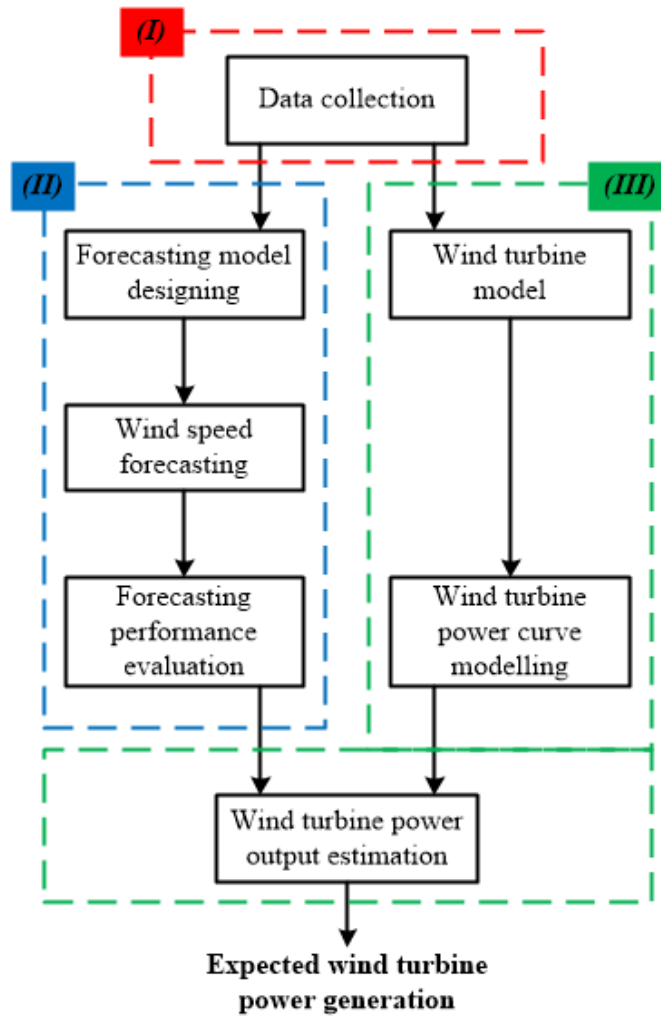


Figure 23: Flowchart for wind speed forecasting and application for expected power estimation

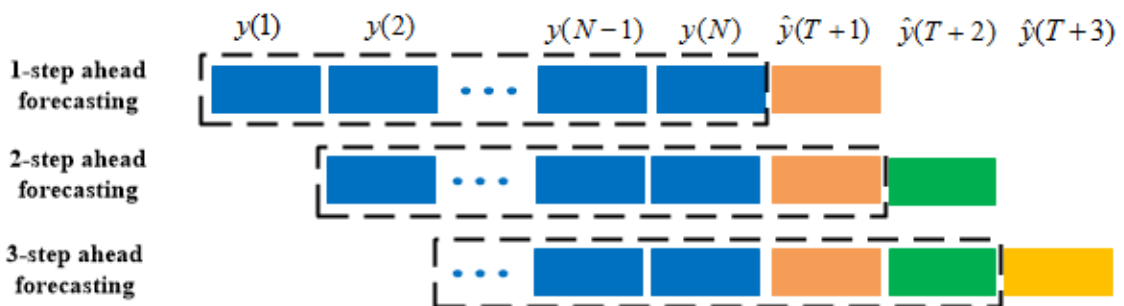


Figure 24: Multi-step ahead forecasting scheme

is determined such defined in Equation (26) Thus, with four selected input variables we have used nine hidden neuron for each ANN model with a linear output node.

II.3.2 Expected WTPG estimation

The electrical power that can be generated by the wind turbine by conversion of the previous available wind power is usually represented by its WTPC [39]. The WTPC establishes the relationship between the wind speed and the power generation of a wind turbine [40] as shown in Figure 2. Each wind turbine has one power curve which is calibrated and provided by its manufacturer's [41]. Therefore, WTPC is one of the most important tools commonly used to forecast the WTPG under given wind conditions of a wind farm [41, 42]. The typical power curve of a pitch controlled wind turbine can be mathematically modeled as shown in Equation (57),

$$P_G(V) = \begin{cases} 0, & V < V_{ci} \\ P_f(V), & V_{ci} \leq V < V_r \\ P_r, & V_r \leq V < V_{co} \\ 0, & V_{co} < V \end{cases}, \quad (57)$$

where $P_G(V)$ is the WTPG at a given wind speed V , $P_f(V)$ is the nonlinear part of WTPG, P_r is the *rated power*, V_{ci} is the *cut-in speed*, V_r is the *rated speed*, and V_{co} is the *cut-out speed*. The nonlinear part $P_f(V)$ of a controlled WT can be represented mathematically by using: *Polynomial power curve*, *exponential power curve*, *cubic power curve*, *approximate cubic power curve* or *general power curve* model [41-43].

For our study, according to the wind characteristics, the wind turbine model E-82 2000 kW of ENERCON manufacturer, have been chosen for application. The general model developed in [40], is used for the nonlinear part of WTPC modeling as shown in Equation (58),

$$P_f(V) = P_r \left(\frac{V^a - V_{ci}^a}{V_r^a - V_{ci}^a} \right), \quad (58)$$

with a being the order of power output curve, and its value for this work is 1.26 obtained by fitting the manufacturer's WTPC of the interested WT.

II.4 Combined ARIMA neural network for more accurate wind speed forecasting

A forecasting model based on ANN model will be more accurate as much as the relationship between each weather variable used as input and the wind speed is important. Given the random nature of wind speed, these relationships are intermittent over time as environmental changes and even almost non-existent in some cases. Thus, this section presents a novel combined statistical model to ensure accurate wind speed forecasting everywhere and at every moment. To achieve the most accurate wind speed forecasting, the proposed hybrid forecasting model combines ANN and ARIMA models.

The proposed wind speed forecasting model involves improving the relationship between the weather variables used as input variables and the wind speed used as output variables respectively of neural network models pursuing to get more accurate desired wind speed forecasting values. As shown in Figure 25, it is carried out in nine steps (in two stages) sequentially from step 1 (*stage I*) to step 9. The historical data samples of the weather variables are collected in step 1 and are subdivided into the training set and testing set in the second step. These input and target weather variables of the prediction tools are transformed (or normalized) during the data preprocessing step. Traditionally, Equation (26) permits the normalization of the data between 0 and 1. Therefore, in the proposed forecasting model, Equation (26) is used to normalize the training target variable (wind speed) in step 4, before the training process of the neural network model. Before it, to normalize the training input variables of the neural network models by increasing the relationship between each of them and the wind speed variable, we have proposed a novel form of time series data normalization given in Equation (59) to transform them in step 3. Therefore, the expression of the Equation (59) allows each input variable to fit the target variable by normalizing it between 0 and 1.

$$x(t)_N = \frac{x(t) \cdot y(t) - x_{\min} \cdot y_{\min}}{x_{\max} \cdot y_{\max} - x_{\min} \cdot y_{\min}}, \quad (59)$$

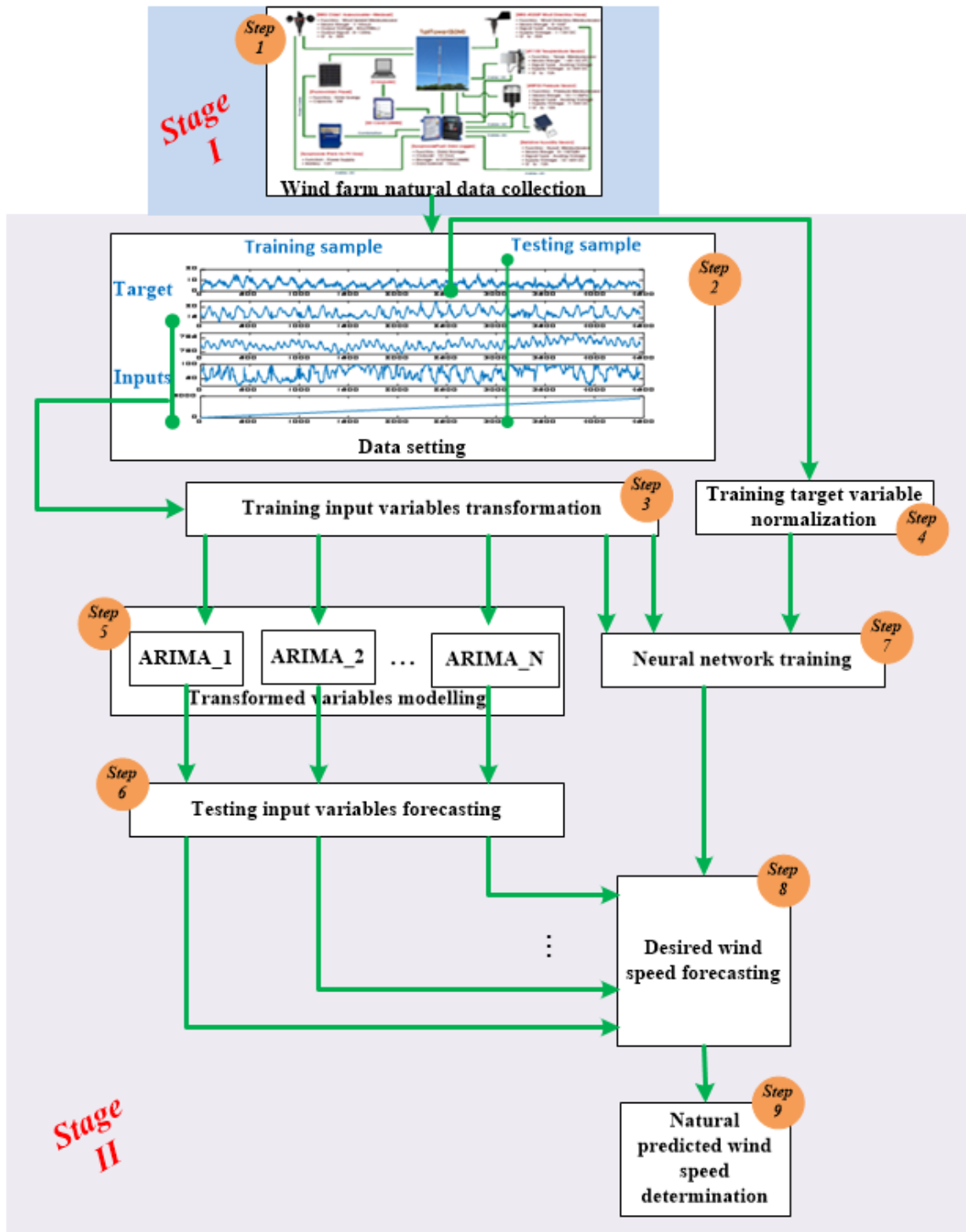


Figure 25: Flowchart of proposed hybrid wind speed forecasting model

where $y(t)$ and $x(t)$ denote respectively the natural measured wind speed variable and weather variable, and $x(t)_N$ denotes a transformed weather variable used as input variable of ANN model.

An optimal ARIMA model is developed for each transformed input variable mod-
PhD thesis of FOGNO FOTSO H.R. Laboratory of Mechanics, Materials and Structures

eling (step 5) and is used to forecast (step 6) the testing input data. The ANN model is trained by using the transformed input variables and normalized target variable in step 7. By using the predicted testing input variables from ARIMA model, the trained ANN model is used to forecast the unknown wind speed values in step 8. At the end of the forecasting process, the natural values of the forecasting wind speed variable are gotten in step 9 by transforming the normalized forecasting values using Equation (25). The ARIMA model is built following the procedure given in Figure 25.

To evaluate the reliability of this proposed wind speed forecasting model, we had applied it in BPNN, RBFNN, NARXNN, ANFIS and GABPNN for multi-step ahead (1-step, 2-step and 3-step). The ARIMA model is employed as the benchmark model.

II.5 Optimal input variables of neural network disposition to enhance the forecasting performance

The optimal ANN models have not been analyzed regarding their Input Variables Disposition (IVD) adequacy in TSF accuracy. Therefore, this section aims at investigating the effect of IVD of BPNN and NARXNN in order to determine their optimal models pursuing for wind speed forecasting.

II.5.1 Neural Networks models optimization

Whatever ANN architecture, choosing an appropriate parameter is crucial to building an efficient forecasting model. In order to estimate the optimal BPNN and NARXNN architectures developed in the previous Subsection II.2.2 based on IVD investigation tested on more wind speed forecasting accuracy, the optimization methods presented in the literature by various authors were applied in each parameter of the networks. The method of autocorrelation was used to select the optimal input variables of neural networks. Therefore, the Spearman's rank correlation method was applied to determine the relation between past variables (see Table 1). After correlation determination,

a maximum of four weather variables were chosen to be used as input variables of both neural networks, provide that the forecasting performance of ANN models increases as the number of input nodes increases. Therefore, the past-selected input variables such as Ta , Pa , RH , and V are the target of both ANNs. Also, the time step t is used as the input variable of both ANNs architectures.

II.5.2 Neural Networks Models Building

We have chosen four variables to use as input variables of optimized BPNN and NARXNN models, aimed to better the accurate TSF. To study the influence of the IVD of each developed ANN on the training and TSF performances, we had used the mathematical formula of arrangement to determine the number of possible disposition of the chosen input variables. Thus, the way input variables were disposed defines the neural networks model. It can be expressed by Equation (60),

$$M_o = N! \quad (60)$$

where M_o is the possible number of ANNs models. Therefore, using the four chosen input variables, each of the developed ANN models had 24 models, $M_o = 24$ which were trained and tested to forecast one day-ahead of wind speed.

II.5.3 Effects of the IVD on neural networks performances investigation

Figure 26 indicates the steps followed to evaluate the influence of the IVD on both neural networks models performance. All the developed ANNs models used the same common parameters.

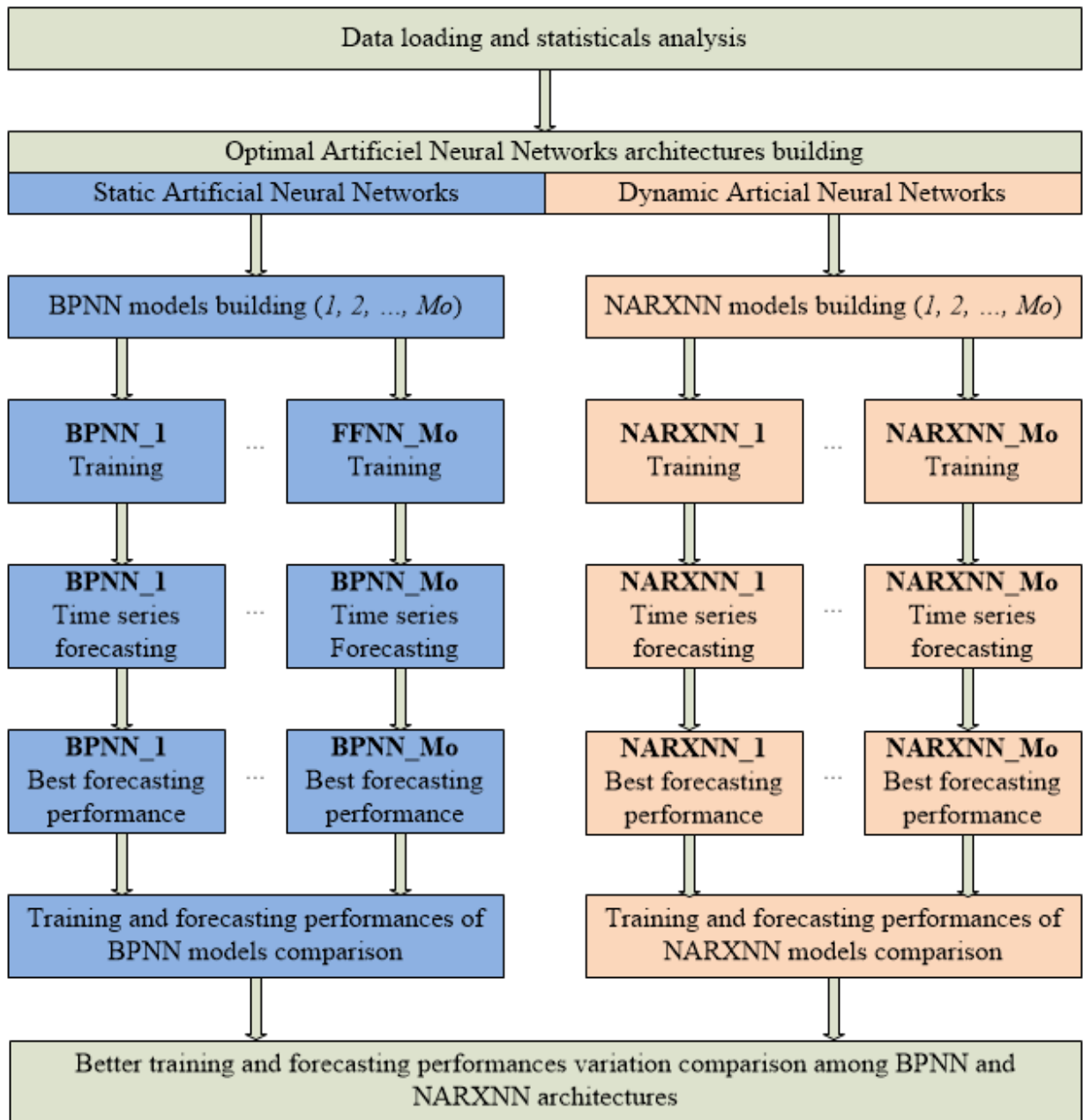


Figure 26: Flowchart of effects of neural networks input variables disposition investigation

II.6 Gearboxes power losses modeling and prediction

This section aims to predict the rolling bearing power loss in the gearbox for a modern WT under real-time operating conditions by using an ANN model. The related gearbox has three stages, including two planetary and one parallel gear. Due to lack of a historical dataset of experimental data, the bearing power loss model was developed by

using the previous experimental calibrated analytical model. The relations between the real-time wind speed, gearbox load and rotational speed are established. Based on calibrated analytical models, calculations were carried out to determine the actual bearing power loss data. BPNN model is developed for actual values of power loss modeling, to predict the unknown values. This proposed approach is validated for 2.0 MW and 2.5 MW WTs.

II.6.1 Related methodology

Figure 27 shows the flowchart of the proposed rolling bearing power loss in wind turbine gearbox under real-time operating conditions prediction scheme. It consists of two main phases, the experimental stage (*I*) and modeling and prediction stage (*II*). The experimental stage consists of collecting wind data for actual WT operating parameters and bearing power loss calculation. The actual bearing power loss data in the gearbox are estimated by using the calibrated SKF model with actual WT operating conditions. Stage (*II*) consists of designing and training of an ANN model using the actual data of bearing power loss and WT operating parameters for predicting the desired bearing power loss values.

II.6.2 Model definition

II.6.2.1 Gearbox description

The considered gearbox model in this study is presented in Ref [33]. It consists of three stages gear configurations with planetary gear at stage 1 (low-speed stage) and stage 2 (intermediate speed stage), and a helical gear at stage 3 (high-speed stage) as shown in Figure 28(a). The planetary gears have a fixed ring, the Low Speed Shaft (LSS) of the first stage would be connected to the rotor hub to receive the input speed and torque, while its sun gear would be connected to the first Intermediate Speed Shaft (ISS1) of the carrier of second stage. The torque from the sun of the second stage would be transferred in the third stage through the second Intermediate Speed Shaft (ISS2). The High Speed Shaft

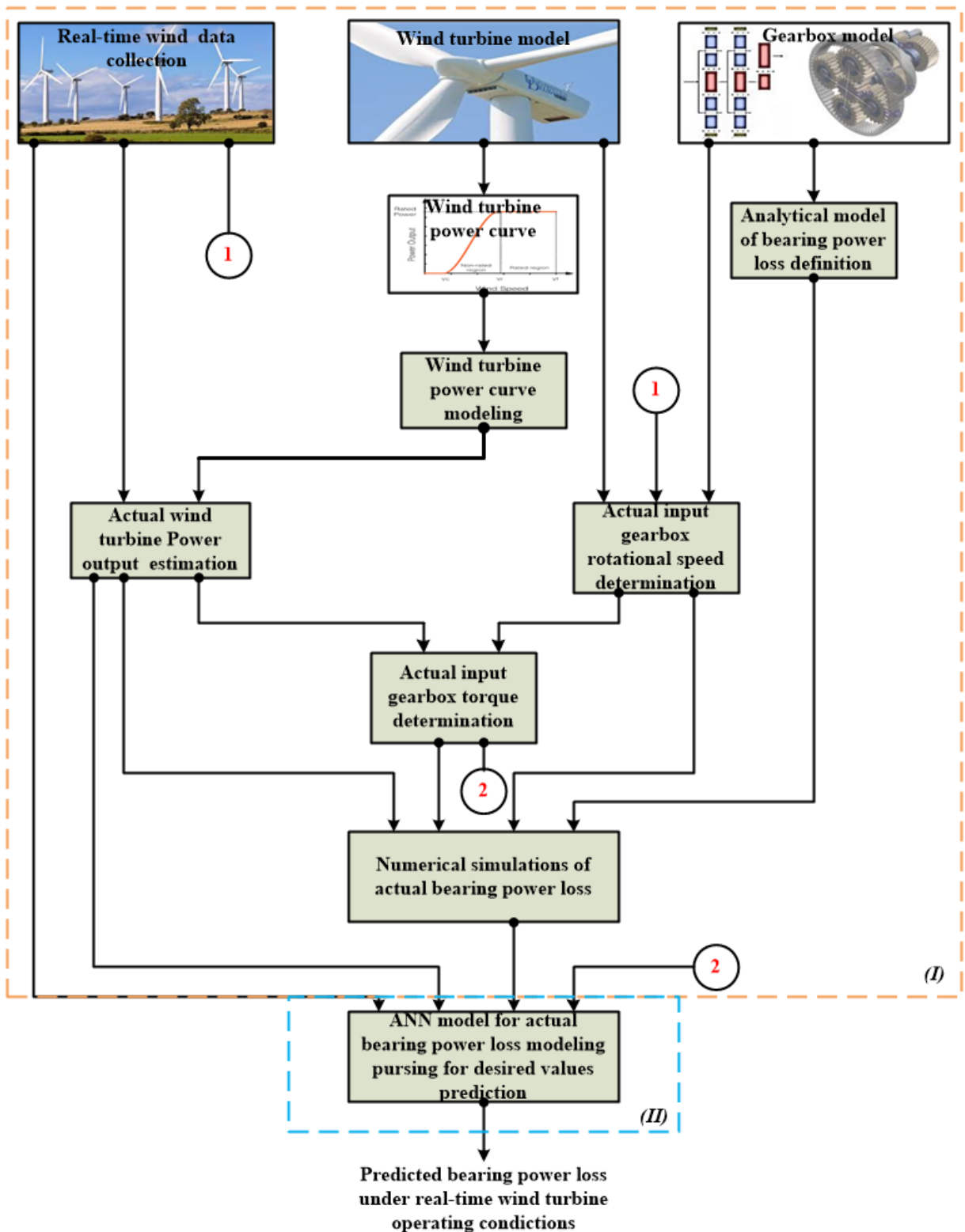


Figure 27: Flowchart of proposed rolling bearing power loss prediction in wind turbine gearbox approach

(HSS) would make the gearbox output torque available to the electrical generator. The total transmission ratio of gearbox is 102. Figure 2(b) shows the gearbox bearings setup. The parameters of rolling bearings that supported the shafts are listed in Table 2. The basic properties for the gears in the gearbox are shown in Table 3. Where Z is the gear number of teeth, i is the gear ratio, β is the gear helix angle in degree, α is gear pressure angle in degree, and m_g is the gear module in mm .

Three fully formulated ISO VG 320 gear oils are been considered; mineral (MINR), polyalpholephin (PAOR), and polyalkylene glycol (PAGD) oils. Their physical properties are displayed in Table 4. Where ρ is the oil density in g/cm^3 , α_t is the thermal expansion coefficient and VI is the viscosity index. chemical structure such as infrared spectra which helps in identifying some of the characteristic peaks of the investigated WT gear oils are shown in Refs [124] and [149].

Table 2: Parameters of the related gearbox rolling bearings.

Stage	Type	Reference	Location	Number	d(mm)	D(mm)	B(mm)
Stage1	CRB	SKF NU 20/800 ECMA	Carrier	1	800	1150	200
	CRB	SKF NU 1080 MA	Carrier	1	400	600	90
	CRB	SKF NNUD 6056 ECMAS/P53	Planets	3	280	420	250
Stage2	CRB	SKF NU 244 ECMA	Carrier	1	200	400	65
	CRB	SKF NU 1060 MA	Carrier	1	300	460	74
	CRB	SKF NNCF 4930 CV	Planets	3	150	210	60
Stage3	CRB	SKF NU 1060 MA	Wheel	1	300	460	74
	TRB	SKF 32960	Wheel	2	300	420	76
	CRB	SKF NU 1036 ML	Pinion	1	180	280	46
	CRB	SKF NU 20/800 ECMA	Pinion	1	180	320	52
	CRB	SKF NU 20/800 ECMA	Pinion	1	180	280	46

Table 3: Gear geometric parameters of the gearbox.

Parameter	Stage1			Stage2			Stage3	
	Sun	Planet	Ring	Sun	Planet	Ring	Pinion	Wheel
Z	21	31	-96	23	38	-103	117	35
i	5.587			5.464			3.343	
β	20			20			20	
α	10			10			10	
m_g	12			9			7	

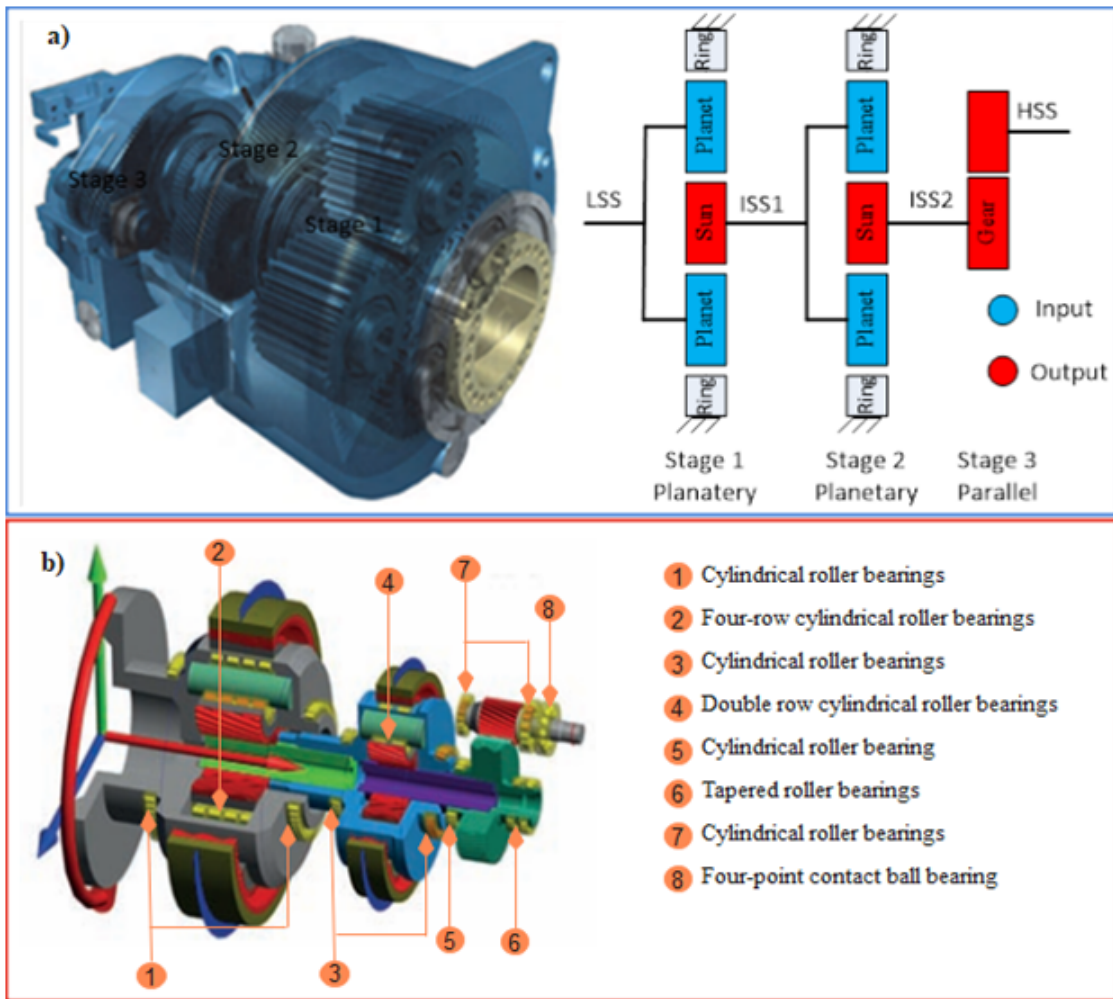


Figure 28: Considered wind turbine Gearbox: (a) two-stage planetary and one-stage parallel [123] and (b) bearings setup.

Table 4: Physical properties of gear oils

Parameter	Unit	MINR	PAOR	PAGD
ρ at 15C	g/m^3	0.902	0.859	1.059
$\alpha_t \times 10^{-4}$		5.8	5.5	7.1
v at 40C	cSt	319.22	313.52	290.26
v at 70C	cSt	65.81	84.99	102.33
v at 100C	cSt	22.33	33.33	51.06
VI		85	153	252

II.6.2.2 Bearing power loss model

SKF model [137] was used for analytical bearing power loss formulation. The power loss is expressed through the torque loss. Therefore, the total bearing friction torque T_t

accounts for rolling frictional torque T_{rr} , sliding frictional torque T_{sl} , viscous drag T_{drag} , and the seal torque loss T_{seal} as given in Equation (61),

$$T_t = T_{rr} + T_{sl} + T_{drag} + T_{seal}. \quad (61)$$

The seal loss (T_{seal}) was disregarded in this study, because we assumed that the system does not have seal. The rolling torque is defined by Equation (62) as follow,

$$T_{rr} = \phi_{ish} \cdot \phi_{rs} \cdot [G_{rr} (n \cdot v)^{0.6}], \quad (62)$$

where ϕ_{ish} defines the inlet shear heating given in Equation (63), while ϕ_{rs} given in Equation (64), defines the replenishment/starvation reduction factor, both for rolling element raceway contact,

$$\phi_{ish} = \frac{1}{1 + 1.84 \times 10^{-9} \cdot (n \cdot d_m)^{1.28} \cdot v^{0.64}}, \quad (63)$$

$$\phi_{rs} = \frac{1}{e^{K_{rs} \cdot v \cdot n \cdot (d+D) \cdot \sqrt{K_Z/2 \cdot (D-d)}}}, \quad (64)$$

with n the rotational speed in rpm , v the kinematic viscosity in mm^2/s of the lubricant at the operating temperature, d_m the bearing mean diameter in mm , K_{rs} the replenishment/starvation constant for oil lubrication, geometric factor of related bearing, D and d are the bearing outside and bearing bore in mm , respectively. The bearing load constant G_{rr} represents the influence of applied load and geometrical parameters on the rolling friction torque. Then, it is defined according to the bearing type, as given in Equations (65) and (66) for Cylindrical Roller Bearing (CRB) and Tapered Roller Bearing (TRB), and Equation (67) for Contact Ball Bearing (CBB), respectively,

$$G_{rr} = R_1 \cdot d_m^{2.41} \cdot F_a^{0.31}, \quad (65)$$

$$G_{rr} = R_1 \cdot d_m^{2.38} (F_r + R_2 \cdot Y \cdot F_a)^{0.31}, \quad (66)$$

$$G_{rr} = R_1 \cdot d_m^{1.97} (F_r + F_{Mg} + R_2 \cdot F_a)^{0.54}, \quad (67)$$

with

$$F_{Mg} = R_3 \cdot d_m^4 \cdot n^2, \quad (68)$$

where F_a and F_r represent the axial and radial load in *Newton* respectively, while Y is the axial load factor. R_1 , R_2 and R_3 are the geometric constants for rolling frictional moments, where their values depend on bearing series. Both loads, F_r and F_a are always considered as positive.

The sliding torque is expressed by Equation (69) as,

$$T_{sl} = G_{sl} \cdot \mu_{sl}, \quad (69)$$

where G_{sl} is the sliding friction parameter, which represents the bearing load's influence on the sliding resistance. It is defined according to the bearing type as shown in Equations (70) and (71) for CRB, TRB and CBB respectively. It is expressed for CBB in Equation (72),

$$G_{sl} = S_1 \cdot d_m^{0.9} \cdot F_a + S_2 \cdot d_m \cdot F_r, \quad (70)$$

$$G_{sl} = S_1 \cdot d_m^{0.82} (F_r + S_2 \cdot Y \cdot F_a), \quad (71)$$

$$G_{sl} = S_1 \cdot d_m^{0.26} \left((F_r + F_{Gg})^{4/3} + S_2 \cdot F_a^{4/3} \right), \quad (72)$$

with

$$F_{Gg} = S_3 \cdot d_m^4 \cdot n^2, \quad (73)$$

where S_1 , S_2 , and S_3 are the geometric constants, depending on bearing series.

The global coefficient of friction, μ_{sl} permits the study of the effect of lubrication on sliding friction of the rolling bearing. It strongly depends on the lubrication regime and is defined as given in Equation (74),

$$\mu_{sl} = \phi_{bl} \cdot \mu_{bl} + (1 - \phi_{bl}) \cdot \mu_{EHL}, \quad (74)$$

where μ_{bl} and μ_{EHL} are the boundary film coefficient of friction and the full film friction coefficient respectively. Their recommended values are $\mu_{bl} = 0.15$ and $\mu_{EHL} = 0.05$ for mineral oils and $\mu_{EHL} = 0.04$ for synthetic oils. The weighting factor, ϕ_{bl} materializes the influence of asperity contact and lubricant shearing mechanisms. It is expressed as given in Equation (75),

$$\phi_{bl} = \frac{1}{e^{2.6 \times 10^{-8} (n \cdot v)^{1.4} \cdot d_m}}. \quad (75)$$

The bearing drag losses are defined for ball bearings and roller bearings by equations (76) and (77), respectively,

$$T_{drag} = 0.4 V_M \cdot K_{ball} \cdot d_m^5 \cdot n^2 + 1.093 \times 10^{-7} n^2 \cdot d_m^3 \left(\frac{n \cdot d_m^2 \cdot f_t}{v} \right)^{-1,379} R_s, \quad (76)$$

$$T_{drag} = 4 V_M \cdot K_{roll} \cdot C_w \cdot B \cdot d_m^4 \cdot n^2 + 1.093 \times 10^{-7} n^2 \cdot d_m^3 \left(\frac{n \cdot d_m^2 \cdot f_t}{v} \right)^{-1,379} \cdot R_s, \quad (77)$$

with

$$K_{ball} = \frac{i_{rw} \cdot K_Z (d + D)}{d - D} \times 10^{-12}, \quad (78)$$

and

$$K_{roll} = \frac{K_L \cdot K_Z (d + D)}{d - D} \times 10^{-12}, \quad (79)$$

where i_{rw} is the number of ball rows. The C_w factor is given by equation (80),

$$C_w = 2.789 \times 10^{-10} l_D^3 - 2.786 \times 10^{-4} l_D^2 + 0.0195 l_D + 0.6439, \quad (80)$$

with

$$l_D = \frac{5.K_L.B}{d_m}, \quad (81)$$

$$f(t) = \begin{cases} \sin(0.5t), & \text{if } 0 \leq t \leq \pi \\ 1, & \text{if } \pi \leq t \leq 2\pi \end{cases}, \quad (82)$$

$$R_S = 0.36d_m^2 (t - \sin t) f_A, \quad (83)$$

were

$$t = 2 \cos^{-1} \left(\frac{0.6d_m - H}{0.6d_m} \right), \quad (84)$$

and

$$f_A = \frac{0,005.K_Z.(D + d)}{D - d}. \quad (85)$$

The total bearing power loss (P_{LV} in kW) in WTG was calculated using equation (83) as follow [34],

$$P_{LV} = \frac{n.T_t}{9550}. \quad (86)$$

II.6.2.3 Wind turbine and application context

The transmitted power of a WT significantly varies with wind speed. Hence, every controlled WT has a unique power performance curve which aids in generating power prediction without the technical details of the components of the WT generating system. In order to investigate the power loss in the WT gearbox under real conditions, ENERCON 2.0 MW (E-82 2000 kW) WT was chosen as the application.

In order to predict the bearing power loss under real conditions, Equations (58) and (??) were used to estimate WT transmitted power. The input gearbox rotational speed and torque at LSS were determined using Equations (86) and (87), respectively [150],

$$n = \frac{60 \times TSR}{2\pi \cdot R} V, \quad (87)$$

$$T_{in} = \frac{9550 \times P_G}{n}, \quad (88)$$

where TSR is the tip speed ratio [151], which depends on the number of blades and R is the rotor radius in m . TSR was considered to be equal to 6 for three blades. The Willis formula expressed in Equation (89) was used to determine the different transmission ratios in gearbox stages as follows,

$$n_p \cdot Z_p = n_c \cdot (Z_p + Z_s) - n_s \cdot Z_s, \quad (89)$$

where n_p , n_c and n_s are the planet, carrier and sun rotational speeds respectively; while Z_p and Z_s are the planet and sun number of teeth respectively.

II.6.3 Neural network prediction model designing

BPNN model was built for bearing power loss modeling and prediction by using the gearbox operating parameters as input variables and P_{VL} as output variable, as shown in Figure 29. The gearbox operating parameters include V , P_G , T_{in} and t . Wind data for four days was used for validation. Their values range from $2.15m/s$ to $11.2m/s$. Three days (from 28th to 30th January 2017) of actual power loss data were used to train the ANN model for predicting the unknown values of the fourth day (31st January 2017).

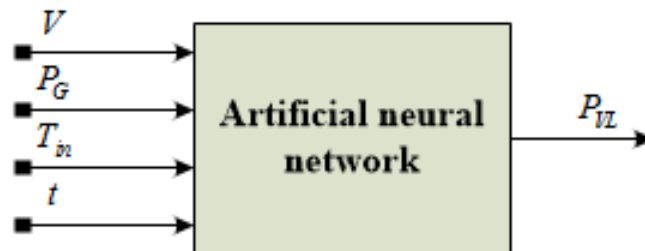


Figure 29: Neural network for power loss prediction flowchart

II.7 Conclusion

In this chapter, we have described the general approach in developing an ANN model for time series forecasting. Three single and two hybrid ANN models used in this thesis have been presented. The ARIMA model and its development principle have also been presented. These models were used for multi-step forecasting of wind energy potential and rolling bearing power losses of the wind turbine gearbox using weather data collected at Bapouh in Cameroon. Two new approaches for optimizing the performance of ANN models for accurate wind speed forecasting have also been presented. The SKF model used for modelling these power losses has been described including the gearbox model considered. The next chapter deals with the results and discussions.

RESULTS AND DISCUSSION

III.1 Introduction

In this chapter, results are presented followed by discussions. We analyze the natural wind data collected in the first section. The second section presents the comparison of ANN models for wind speed forecasting and its application for expected power estimation. The third section studies the improvement of the relationship between the meteorological variables for the optimization of the ANN performance for wind speed forecasting. The effects of the input variables disposition of the ANNs on their performance for wind speed forecasting are studied in the fourth section. The fifth section analyzes the modeling and prediction of power losses in the rolling bearing gearbox of the WT in real time. The last section of the chapter is reserved for conclusion.

III.2 Analysis of actual wind data

This section presents the statistical analysis of the meteorological variable data collected for a period of 73-days, from 20th November 2016 to 31st January 2017 in Bapouh, Cameroon. As mentioned in the previous chapter, these variables included average V (m/s), Pa (mb), RH ($\%$), Ta ($^{\circ}C$) and WD ($^{\circ}$) collected at an interval of 10 minutes from 00h:00 to 23h:50 each day. The objective was to select the wind potential dependent variables (wind speed) to be used in the applications in this thesis. Figures 30 shows the plots of these different variables. These curves show random variables.

Table 5 gives the characteristics of each of the variables, i.e. the number of observations, the maximum value (Max), the minimum value (Min), the mean value ($Mean$) and the standard deviation (Sd). We had a total of 10573 observations for each variable. V

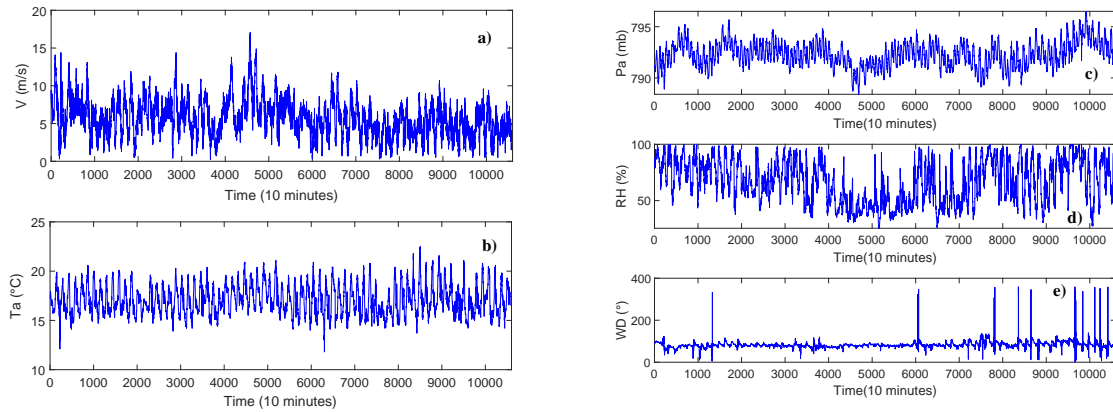


Figure 30: Natural measured wind data: (a) V , (b) Ta , (c) Pa , (d) RH and WD

varies from 0.2 m/s to 17.1 m/s, with a mean of 5.7396 m/s. This large gap between the average and maximum value of V reflects a huge variation. The Sd value of the wind speed of 2.4214 is considerable compared to that of Ta and Pa . This confirms the dispersion of these samples. Thus, V at this site is very intermittent compared to Ta and Pa . In addition, the values of V are low with an average value much lower than the nominal value (of the order of 13 m/s) of V required by controlled WT to provide a constant power. Therefore, the WTs will operate in the non-linear zone at this site, and thus provide intermittent electrical power at a cubic degree of V . Hence the need to develop an efficient forecasting model of the wind power generation for its integration.

Table 5: Natural wind data characteristics

Variable	Observations	Mean	Max	Min	Sd
V (m/s)	10573	5.73	17.1000	0.20	2.42
Ta (°C)	10573	17.11	22.50	11.80	1.52
Pa (mb)	10573	792.29	796.50	788.40	1.23
RH (%)	10573	67.17	100.20	25.40	19.28
WD (°)	10573	82.77	359	0	17.90

To assist in the selection of variables influencing wind speed for the development of ANN-based forecasting models, Table 6 gives the results of the correlation coefficients used to measure the relationships between the different variables collected. The most important relationship for the development of an efficient forecasting model is the relationship between each dependent variable (Ta , Pa , RH and WD) and V . The results in

PhD thesis of FOGNO FOTSO H.R. Laboratory of Mechanics, Materials and Structures

Table 6: Relationship between the natural variables measured

	Ta	Pa	RH	WD
V	0.11	-0.12	-0.42	-0.17
Ta	1	0.20	-0.61	-0.20
Pa		1	-0.057	-0.05
RH			1	0.24
WD				1

Table 6 show a very weak relationship, i.e., 0.1135, -0.1220, -0.4229, and -0.1757 between V and Ta , Pa , RH , and WD respectively. These low values of the correlation coefficient between V and other variables do not bode well for the effectiveness of the forecasting model. Thus it is necessary to find ways of optimization through the optimal section of the variables that will be used as inputs to the ANN. Ta and Pa will be used mainly for their low Sd values. Also, despite the high value of the Sd of RH as presented in Table 5, it has a considerable relationship with V , which is why it will be used for the development of ANN models. On the other hand, WD has a very weak relationship with V and a very high Sd , which is why it will not be used. Thus, the three selected variables, i.e. Ta , Pa and RH will be used as input variables for the investigation of the performance of ANN models for wind speed forecasting in the following section.

III.3 Wind speed and expected wind turbine power output forecasting

This section investigates six wind speed forecasting models for hybrid method, combining statistical method and physical method to predict WTPG. Thus, the BPNN, NARXNN, RBFNN, GABPNN, ANFIS and ARIMA models are used for multi-step wind speed forecasting. The predicted wind speed values are then used for the estimation of the expected WTPG based on manufacturer's WTPC modeling. Two Datasets from the collected data are constituted for applications. These Datasets, which are Dataset1 and Dataset2 are made up of two months of real measured wind speed data from 1st to 30th

December 2016 and from 1st to 30th January 2017, respectively. Each Dataset has 4320 points, which are split into two subsets, which are the training set and testing set. The characteristics of the wind speed in both Datasets are given in Table 7.

Table 7: Statistical information of the considered wind speed Datasets.

Datasets	Samples	Numbers	Characteristics			
			Mean(m/s)	Max(m/s)	Min(m/s)	Sd(m/s)
Dataset1	Observations	4320	8.52	20.80	1	3.01
	Training	4176	8.56	20.80	1	3.04
	Testing	144	7.31	11.00	3.30	1.59
Dataset2	Observations	4320	6.69	16.80	1	2.54
	Training	4176	6.70	16.80	1	2.56
	Testing	144	6.24	10.10	2.50	1.67

From the Table 7, the large gap between the minimum and maximum wind speed values of both Datasets show the very fluctuation of wind speed amplitude and frequency between series. Moreover, the *Sd* of the wind speed observations for Dataset1 and Dataset2 is 3.01 m/s and 2.54 m/s respectively, which demonstrate significant fluctuations of the wind speed of these Datasets. Since, the wind speed varies with time (t), therefore, it is used as an input variable for the ANN models. Thus, Ta , Pa , RH and t are used as input variables while V is used as target variable of ANN models. Also, the relationships (R^2) between the natural V and each other weather variables are evaluated. The results presented in Table 6 show that the relationship between V and the other variables is weak. As shown in Table 7, the testing samples represent the data of the 30th day and the training samples the remains of the days of both Datasets. The applied multi-step ahead wind speed forecasting in this study consists of 1-step, 2-step and 3-step as shown in the previous chapter. In order to minimize the impact of relationships between the input variables on the neural networks forecasting performance, they are arranged so as avoid the high strength relation between the neighboring variables. Therefore, we disposed of the input variables of neural networks models in both Datasets as $Pa-Ta-RH-T$. The forecasting models are developed according to the parameters giving in Table 8.

Table 8: Forecasting models parameter settings

Indexes	Parameters	Values	Indexes	Parameters	Values
BPNN	Maximum iterations	1000	RBFFNN	Spread	0.5
	Validation check	1000		Maximum number of training	1000
NARXNN	Maximum iterations	1000	GA	Training requirement precision	0.00002
	Validation check	1000		Maximum generations	200
	Delay	04		Fitness limit	10^{-5}
ANFIS	Number of MF	02			
	Maximum epochs	1000			

According to the application wind characteristics, the wind turbine model E-82 2000 kW of ENERCON manufacturer, is chosen for application. Its power curve is shown in Table 9.

Table 9: Manufacturer's power curve of E-82 2000 kW WT

Wind speed (m/s)	Output power (kW)	Wind speed (m/s)	Output power (kW)	Wind speed (m/s)	Output power (kW)
1	0	10	1 580	19	2 050
2	3	11	1 810	20	2 050
3	25	12	1 980	21	2 050
4	82	13	2 050	22	2 050
5	174	14	2 050	23	2 050
6	321	15	2 050	24	2 050
7	532	16	2 050	25	2 050
8	815	17	2 050		
9	1 180	18	2 050		

Table 10 and Table 11 present the multi-step forecasting results from the Dataset1 and Dataset2 respectively, using MAPE, MAE and RMSE error criteria. From these tables, it can obviously be seen that the MAPE, MAE and MSE values show that the performance are different depending on the forecasting step, Datasets and forecasting models:

- Based on the forecasting models, the ARIMA models perform the wind speed forecasting in all steps and Datasets than neural networks models. The average forecasting errors, RMSE, MAE and MAPE from ARIMA models are 1.1938, 1.04

and 15.0837, respectively in Dataset1. Their values in Datasets2 are 1.25, 0.98, and 17.21, respectively. The NARXNN models are the best among the neural networks models for all forecasting steps and in both Datasets. The ANFIS models presents the worst wind speed multi-step ahead forecasting performances;

- Based on the forecasting steps, 1-step ahead forecasting globally presents the better results in both Datasets. The average 1-step ahead forecasting errors, RMSE, MAE and MAPE are 1.46, 1.16 and 17.27 in Dataset1 and 1.53, 1.18 and 20.11 in Dataset2, respectively. The 3-step ahead forecasting has the worst performance in both Datasets. The average RMSE, MAE and MAPE for 3-step ahead forecasting are 1.60, 1.30 and 19.77 in Dataset1 and 1.5606, 1.2210 and 20.5793 in Dataset2, respectively;
- Globally, NARXNN models under 1-step ahead forecasting have the better wind speed forecasting performance amongst the other AI models from both Datasets. While a better wind speed forecasting performance from ARIMA models for both Datasets is achieved under 2-step ahead forecasting.

Table 10: Forecasting results from Dataset1

Models	1-step			2-step			3-step		
	RMSE	MAE	MAPE (%)	RMSE	MAE	MAPE (%)	RMSE	MAE	MAPE (%)
BPNN	1.61	1.27	17.78	1.52	1.24	18.37	1.48	1.21	19.18
AMFIS	2.37	1.88	26.28	2.43	1.95	28.23	2.35	1.89	27.40
NARXNN	0.97	0.73	11.94	1.16	0.84	15.22	1.35	1.04	15.26
RBNN	1.31	1.04	17.34	1.43	1.18	18.36	1.43	1.18	18.36
GABNN	1.25	1.01	15.38	1.60	1.30	21.44	1.69	1.44	22.95
ARIMA	1.23	1.03	14.90	1.26	1.01	14.86	1.31	1.07	15.47

Figures 31 and 32 plot the comparison between actual and forecasting wind speed values versus time in Dataset1 and Dataset2, respectively. Based on the proximity of the curves of the predicted values to those of the measured values, we can confirm

Table 11: Forecasting results from Dataset2

Models	1-step			2-step			3-step		
	RMSE	MAE	MAPE (%)	RMSE	MAE	MAPE (%)	RMSE	MAE	MAPE (%)
BPNN	1.74	1.33	21.33	1.62	1.25	21.12	1.62	1.26	21.15
AMFIS	2.34	1.58	24.69	3.10	2.30	37.02	2.41	1.66	25.86
NARXNN	1.03	1.03	17.33	1.48	1.23	19.20	1.47	1.22	19.51
RBFNN	1.36	1.17	20.83	1.32	1.12	21.21	1.33	1.15	20.72
GABPNN	1.19	1.00	18.96	1.55	1.31	23.70	1.20	1.02	18.99
ARIMA	1.24	0.98	17.50	1.22	0.98	16.92	1.30	1.00	17.21

that NARXNN models under 1-step ahead forecasting and ARIMA models under 2-step ahead forecasting perform well the wind speed forecasting in both Datasets.

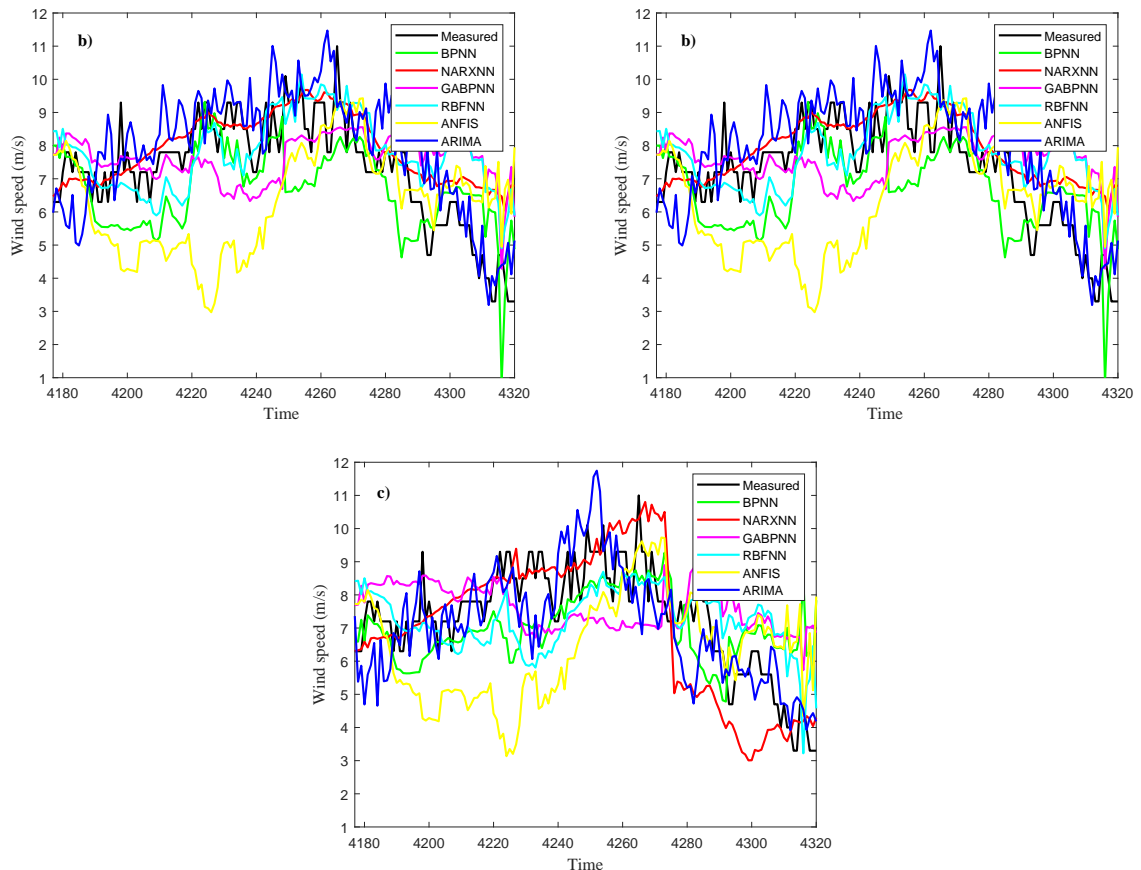


Figure 31: Comparing wind speed forecasting results from Dataset1: (a) 1-step, (b) 2-step and (c) 3-step

By using the WTPC modeling, each better result of predicted wind speed achieved

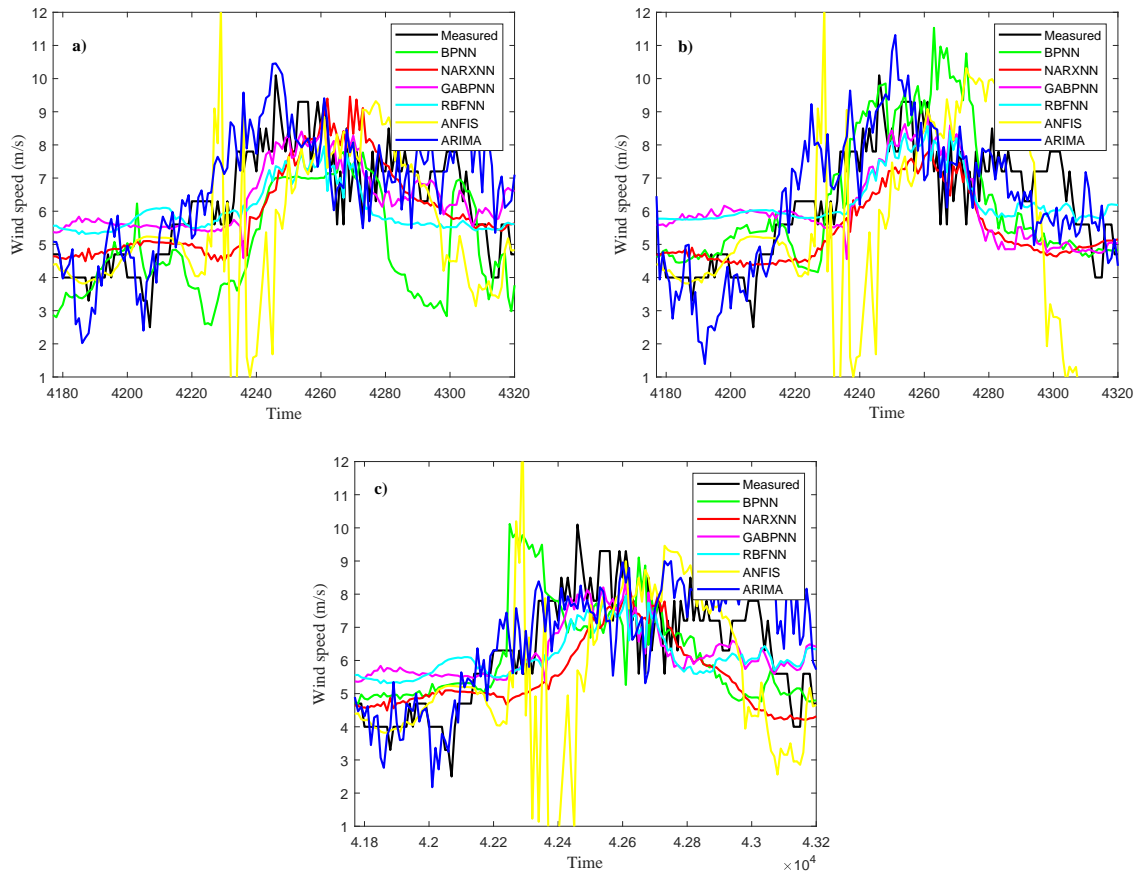


Figure 32: Comparing wind speed forecasting results from Dataset2: (a) 1-step, (b) 2-step and (c) 3-step

from neural networks models and from ARIMA models are applied for 24 hours expected WTPG from E-82 2000 kW wind turbine prediction in both Datasets. Then, the results from NARXNN models under 1-step ahead forecasting and from ARIMA models under 2-step ahead forecasting are employed. The measured wind speed data are used to estimate the actual WTPG values, which are used to compare the predicted values from hybrid models. Figures 33 and 34 give the WTPG comparisons, between the actual values (P_m) and predicted values from hybrid NARXNN models (P_{NARXNN}) and hybrid ARIMA models (P_{ARIMA}) for Dataset1 and Dataset2 respectively. Figures 33(a) and 34(a) show a plot of the P_m , P_{NARXNN} and P_{ARIMA} versus time for Dataset1 and Dataset2 respectively. From Figure 33(a) it can be observed that P_{NARXNN} follows the form of P_m more than P_{ARIMA} ; while P_{ARIMA} follows the form of P_m more than P_{NARXNN} in Figure 34(a). Figures 33(b) and 34(b) draw the difference between P_m and P_{NARXNN} on

the one hand, and between P_m and P_{ARIMA} on the other hand versus time for Dataset1 and Dataset2, respectively. These are the absolute values of errors $P_m - P_{NARXNN}$ and $P_m - P_{ARIMA}$. From Figure 33(b), $P_m - P_{NARXNN}$ is ranges from 0.28 kW to 567 kW; while $P_m - P_{ARIMA}$ is ranges from 1.7 kW to 822 kW. From figure 34(b), $P_m - P_{NARXNN}$ is ranges from 0.99 kW to 707 kW; while $P_m - P_{ARIMA}$ is ranges from 1.3 kW to 783 kW. The average values of $P_m - P_{NARXNN}$ and $P_m - P_{ARIMA}$ are 132 kW and 197 kW in Dataset1 and 175 kW and 165 kW in Dataset2. From the previous results, it is clear that the wind speed forecasting accuracy is crucial for effective WTPG prediction. The hybrid method based on 1-step ahead wind speed forecasting using NARXNN model and WTPC modeling have been shown to be more efficient for WTPG prediction.

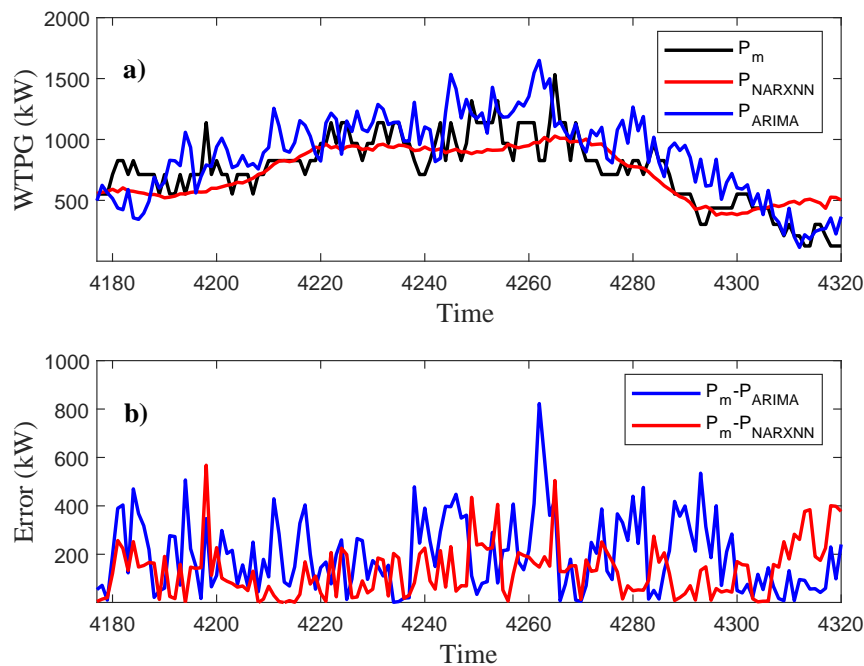


Figure 33: Predicted WTPG from Dataset1 comparison: (a) power, (b) error

The results obtained here prove that the accuracy of the WTPG prediction depends closely on the accuracy of the wind speed forecasting. Therefore in our next studies, we will focus on the development of accurate wind speed forecasting models. This study also enabled us to compare the traditional models used for wind speed forecasting under three steps ahead. Although some models stood out in terms of their forecasting

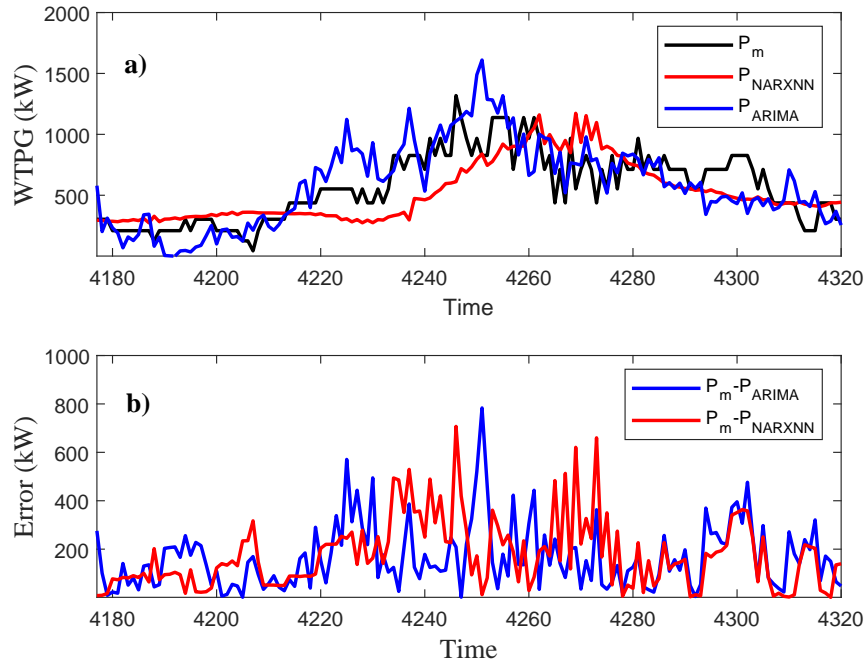


Figure 34: Predicted WTPG from Dataset2 comparison: (a) power, (b) error

performance compared to others, the results remain just acceptable. Thus, there is a need to improve the forecasting performance of these models. In order to improve and ensure the accuracy of wind speed forecasting at any site and time, the next section will examine the feasibility of the new hybrid wind speed forecasting model based on the improvement of the relationship between the meteorological variables used.

III.4 Improving the accuracy of wind speed forecasting with a new combined ARIMA neural network model

To improve the forecasting performance of the ANN models of the previous section, this section analyzes their coupling with the ARIMA model. The training data set used as input variables of the ANN models are transformed in order to normalize them between 0 and 1 and to improve the relationship between each of them and the output variable (V). V is normalized between 0 and 1. The testing data set is predicted for each input variable using ARIMA models. The first subsection analyzes the transformation and

forecasting of the input variables. The second subsection discusses the results of forecasting the desired values of V . The third subsection discusses some applications of this hybrid model.

III.4.1 Data preprocessing and input weather variables forecasting

The relations between wind speed and other weather variables are shown in Table 12 for both Datasets. From the results of Table 12 it can be observed that the values of R^2 between the natural wind speed and the other natural weather variables are too weak in both Datasets. It can also be seen that the relationships between the normalized wind speed and the transformed weather variables are greatly improved in comparison with that obtained with natural data in both Datasets, both on strength (absolute values of R^2) and on the sense (signs of R^2). The results of Sd are also presented in Table 12, it is employed to evaluate the dispersion degree of series of the natural and transformed weather variables. Thus, it is clear that the Sd of all transformed weather variables is improved for both Datasets comparing with the same normalized variables. This means that the degree of linearity of these variables is improved.

Table 12: Normalized and transformed weather variables characteristics

Variables	Dataset1				Dataset2			
	Normalized		Transformed		Normalized		Transformed	
	R^2	Sd	R^2	Sd	R^2	Sd	R^2	Sd
Ta	0.25	0.19	0.97	0.13	0.39	0.15	0.96	0.13
t	0.07	0.15	0.57	0.15	-0.13	0.17	0.39	0.16
RH	-0.47	0.23	0.63	0.08	-0.53	0.26	0.55	0.08
Pa	-0.12	0.28	0.99	0.14	0.17	0.28	0.99	0.13

In addition to elucidating the relationships between the weather variables, Figure 35 shows a plot of the transformed and normalized data versus time for all the recorded weather variables. The very strong non-compliance between the normalized pace of wind speed and those of other weather variables can be observed in Figure 35(a) and Figure 35(c). This shows more the disparity between the natural weather variables of

both Datasets. Figure 35(b) and Figure 35(d) show that the transformed variables try to copy the pace of the normalized wind speed over time. In Figure 35(b) and Figure 35(d) the curves of pressure are confused with that of wind speed in both cases, reflecting high strength of correction coefficient achieved in Table 12.

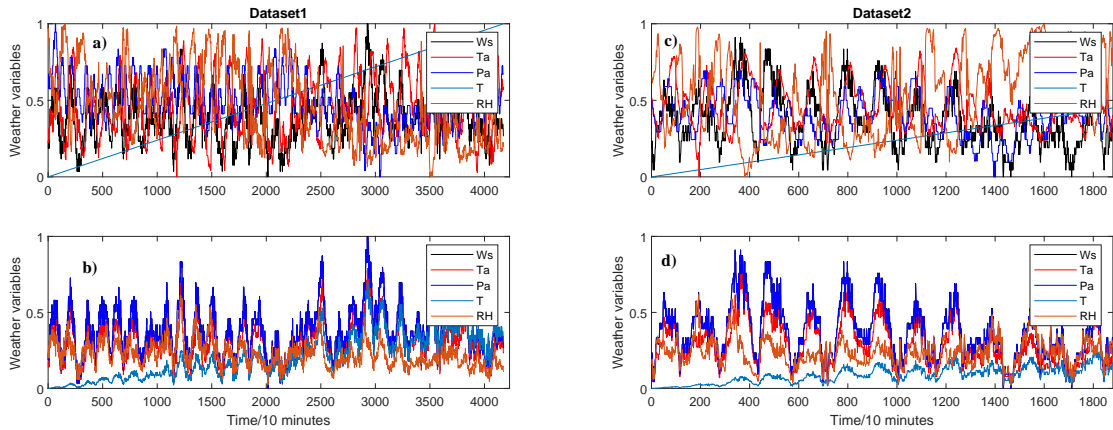


Figure 35: Concordance between the weather variables. All normalized: (a) and (b). Transformed Ta , Pa , t and RH with normalized V : (b) and (d)

Furthermore, how the relationships between the actual normalized V variable and each actual transformed other weather variables, the scatter plots are visualized as shown in Figure 36. The advantages of the scatter plot between the desired variable versus dependent variable allow to see the direction, forms, strength, and outliers of their relations. It can be observed in Figure 36 that the disparity between normalized variables is considered in each case. However, it can be confirmed that all the transformed variables have a positive dependency on the actual normalized wind speed. It is thus clear that all the actual transformed have shown a strong linear dependency with the actual wind speed. Therefore, we can affirm that the proposed data preprocessing formula adequately evaluates the data normalization while improving the degree of dependency between two variables and decreases the degree of nonlinearity of the second variable. This dependency between the variables which will be used as input and the target variable respectively of the neural networks models is crucial for their performance because it will help them to better learn and convergence. Also, the weak nonlinearity of the transformed variables is a main requirement for ARIMA model modeling.

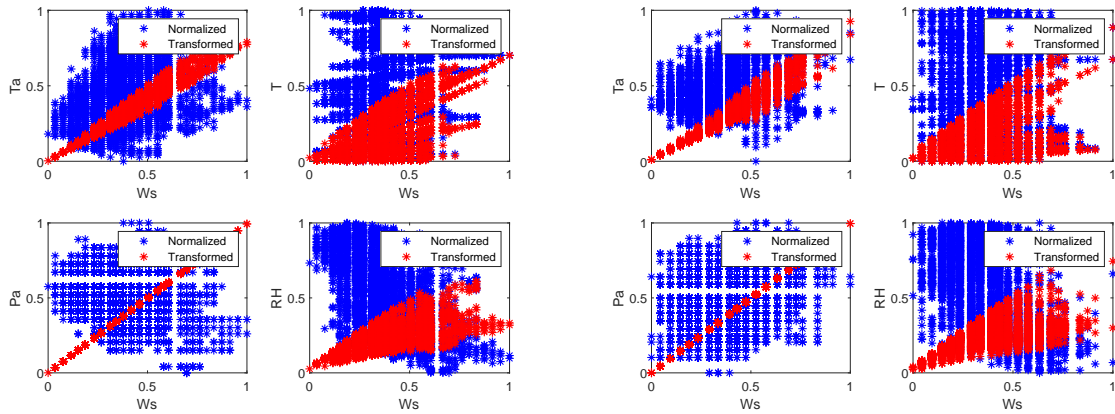


Figure 36: Concordance between normalized wind speed and other transformed weather variables

As shown in Figure 22, based on autocorrelation function and partial autocorrelation function, an optimal ARIMA model is developed for each transformed weather variable modeling and pursuing to forecast the desired values. Multi-step forecasting is applied for each variable involving 1-step, 2-step and 3-step ahead in both Datasets.

III.4.2 Multi-step wind speed forecasting

The transformation of weather variables used as input of neural networks models increases the relationship between them as shown in Table 13. We disposed the input variables of ANN models in both Datasets as shown in Section III.3.

Table 13: Relation between the weather variables used as input variables of neural networks models

		Transformed							
		Dataset1				Dataset2			
		Pa	Ta	T	RH	Pa	Ta	T	RH
Natural	Pa		0.97	0.56	0.63		0.96	0.32	0.58
	Ta	0.05		0.52	0.57	0.30		0.33	0.44
	T	-0.38	0.16		0.59	0.39	0.07		0.34
	RH	0.15	-0.59	-0.57		-0.22	-0.65	0.07	

III.4.2.1 First experiment: Models evaluation based on traditional criteria

Table 14 and Table 15 present the multi-step forecasting results from Dataset1 and Dataset2 respectively, using MAPE, MAE and RMSE error criteria. From these Table 14 and Table 15, it can be obviously seen that the MAPE, MAE and RMSE values indicate that the performance varies according to the forecasting step, Datasets, and forecasting model. Also, it can be seen that the proposed hybrid models, CBPNN, CNARXNN, CANFIS, CRBFNN and CGABPNN give the most forecasting performance among other models used in the comparison. Moreover, according to Athraa Ali Kadhem et al. [152], by considering MAPE criterion, each proposed model has a high forecasting accuracy from both Datasets in all forecasting steps, which is not the case for any traditional model and benchmark model.

Table 14: Forecasting results from Dataset1 comparison

Models	1-step			2-step			3-step		
	RMSE	MAE	MAPE (%)	RMSE	MAE	MAPE (%)	RMSE	MAE	MAPE (%)
BPNN	1.61	1.27	17.78	1.52	1.24	18.37	1.48	1.21	19.18
AMFIS	2.37	1.88	26.28	2.43	1.95	28.23	2.35	1.89	27.40
NARXNN	0.97	0.73	11.94	1.16	0.84	15.22	1.35	1.04	15.26
RBFNN	1.31	1.04	17.34	1.43	1.18	18.36	1.43	1.18	18.36
GABPNN	1.25	1.01	15.38	1.60	1.30	21.44	1.69	1.44	22.95
ARIMA	1.23	1.03	14.90	1.26	1.01	14.86	1.31	1.07	15.47
CBPNN	0.82	0.64	9.29	0.75	0.58	8.27	0.68	0.55	8.13
CAMFIS	0.83	0.64	9.31	0.76	0.59	8.44	0.69	0.55	8.15
CNARXNN	0.77	0.59	8.99	0.85	0.66	9.37	0.82	0.64	9.11
CRBFNN	0.83	0.64	9.35	0.76	0.60	8.46	0.68	0.55	8.13
CGABPNN	0.82	0.64	9.57	0.81	0.65	9.26	0.84	0.65	9.76

The percentage of improvement of each combined model versus its based neural network traditional model and ARIMA model is evaluated and presented in Table 16 and Table 17 for Dataset1 and Dataset2 respectively. Thus, Table 16 and Table 17 show that the forecasting errors are most improved in each combined model amongst the single and benchmark models, for the three forecasting steps:

Table 15: Forecasting results from Dataset2 comparison

Models	1-step			2-step			3-step		
	RMSE	MAE	MAPE (%)	RMSE	MAE	MAPE (%)	RMSE	MAE	MAPE (%)
BPNN	1.74	1.33	21.33	1.62	1.25	21.12	1.62	1.26	21.15
AMFIS	2.34	1.58	24.69	3.10	2.30	37.02	2.41	1.66	25.86
NARXNN	1.03	1.03	17.33	1.48	1.23	19.20	1.47	1.22	19.51
RBFNN	1.36	1.17	20.83	1.32	1.12	21.21	1.33	1.15	20.72
GABPNN	1.19	1.00	18.96	1.55	1.31	23.70	1.20	1.02	18.99
ARIMA	1.24	0.98	17.50	1.22	0.98	16.92	1.30	1.00	17.21
CBPNN	0.85	0.65	9.53	0.86	0.66	9.76	0.81	0.65	9.09
CAMFIS	0.86	0.65	9.95	0.83	0.65	9.55	0.82	0.65	9.24
CNARXNN	0.82	0.65	9.64	0.83	0.65	9.74	0.87	0.67	9.95
CRBFNN	0.81	0.65	9.26	0.82	0.65	9.58	0.80	0.65	9.00
CGABPNN	0.87	0.66	9.98	0.87	0.66	9.99	0.85	0.65	9.56

- From Dataset1, the percentage of improvement of forecasting errors amongst the corresponding traditional model ranges from about 20.27%, 18.64%, and 24.69% to 70.66%, 70.64%, and 70.24% for RMSE, MAE and MAPE respectively. Comparing with the ARIMA models they are improved from 32.64%, 34.67%, 36.93% to 47.69%, 48.27%, and 47.47% for RMSE, MAE, and MAPE respectively;
- From Dataset2, the improvements of forecasting errors among the respective traditional model are greatest from about 18.80%, 35.49%, 44.36% to 73.15%, 71.67%, 74.98%, for RMSE, MAE, and MAPE respectively. Comparing with the ARIMA models, they are improved from about 28.85%, 32.41% and 38.23% to 38.23%, 35.50%, and 47.68% for RMSE, MAE, and MAPE respectively.

III.4.2.2 Second experiment: Models evaluation based on DM test

The results of absolute values of DM test of each proposed forecasting model among the based neural network traditional model are given in Table 18, for each forecasting step of both Datasets. The average of absolute values of the DM test of the proposed forecasting models among the ARIMA model is calculated for each forecasting step. Also,

Table 16: Improving percentage of forecasting performance from Dataset1

Models		1-step			2-step			3-step		
Proposed	Comparisons	P_{RMSE}	P_{MAE}	P_{MAPE}	P_{RMSE}	P_{MAE}	P_{MAPE}	P_{RMSE}	P_{MAE}	P_{MAPE}
CBPNN	BPNN	48.82	49.69	47.76	50.72	52.69	54.94	46.67	44.55	49.40
	ARIMA	32.89	37.73	37.68	40.81	42.14	44.29	47.69	48.27	47.47
CANFIS	ANFIS	64.79	65.82	64.57	68.46	69.29	70.08	70.66	70.64	70.24
	ARIMA	32.29	37.46	37.55	39.33	41.15	43.17	47.47	48.20	47.32
CNARXNN	NARXNN	20.27	18.64	24.69	26.85	65.91	38.43	61.23	47.84	56.48
	ARIMA	37.02	42.34	39.67	32.64	34.67	36.93	37.52	40.19	41.12
CRBFNN	RBFNN	37.28	46.12	48.56	56.62	60.51	63.66	56.51	59.04	61.88
	ARIMA	32.29	37.28	50.44	39.29	40.96	43.02	47.73	48.30	47.44
CGABPNN	GABPNN	34.61	36.44	37.78	49.10	49.42	56.78	48.58	41.07	44.96
	ARIMA	33.30	37.36	35.80	35.38	35.36	37.64	47.81	38.89	36.89

Table 17: Improving percentage of forecasting performance from Dataset2

Models		1-step			2-step			3-step		
Proposed	Comparisons	P_{RMSE}	P_{MAE}	P_{MAPE}	P_{RMSE}	P_{MAE}	P_{MAPE}	P_{RMSE}	P_{MAE}	P_{MAPE}
CBPNN	BPNN	51.22	50.67	55.29	46.69	47.09	53.76	50.00	48.29	57.01
	ARIMA	31.30	33.12	45.52	29.22	32.21	42.29	37.96	34.98	47.18
CANFIS	ANFIS	62.98	58.60	59.68	73.15	71.67	74.18	66.00	60.63	64.25
	ARIMA	30.02	33.02	43.13	31.69	33.43	43.53	37.15	34.86	46.27
CNARXNN	NARXNN	19.80	36.49	44.36	43.60	47.24	49.25	44.49	40.51	48.97
	ARIMA	33.26	33.12	44.90	31.48	33.74	42.42	33.08	32.29	42.13
CRBFNN	RBFNN	39.37	44.21	54.80	37.56	41.52	54.80	39.32	43.31	56.53
	ARIMA	33.26	33.12	45.21	32.48	32.82	43.34	38.23	35.03	47.65
CGABPNN	GABPNN	26.80	34.00	47.31	43.59	49.65	57.83	29.63	36.11	49.65
	ARIMA	29.80	32.72	42.93	28.25	32.41	40.95	35.04	34.88	44.42

Table 18 shows the average of absolute values of the DM test of forecasting steps. It can be observed that the forecasting errors of proposed models comparing with the based neural networks models and benchmark model are at least rejected at 10% significance level for all the forecasting steps and Datasets. Moreover, it can be seen that the smallest value of the mean DM test from the three forecasting steps in Table 18 is 2.01, which is larger than the critical value of the 5% significance level. This result means that the proposed forecasting models are significantly superior to the other compared models.

Table 18: DM test results of different models

Models	DM test							
	Dataset1				Dataset2			
	1-step	2-step	3-step	Mean	1-step	2-step	3-step	Mean
BPNN	5.18***	4.50***	3.34***	4.34***	11.69***	0.97*	1.02*	4.56***
ANFIS	4.26***	4.41***	5.19***	4.57***	3.86***	3.31***	2.38**	3.18***
NARXNN	2.12**	9.29***	2.67***	5.51***	3.86***	12.61***	5.65***	7.37***
RBFNN	4.83***	5.55***	1.06*	3.81***	4.30***	2.98***	3.48***	3.58***
GABPNN	3.05***	1.17*	1.82**	2.01**	1.11*	6.17***	3.71***	3.66***
ARIMA	6.94***	10.54***	2.09***	6.52***	3.93***	1.08*	4.22***	2.99***

*, ** and *** denote the significance level at 10%, 5% and 1% respectively

III.4.2.3 Discussions on the proposed wind speed forecasting model

The experiments results of the five combined ARIMA-ANN models are proposed based on three single and two collaborative neural networks models for 1-step, 2-step, and 3-step 24-hours ahead wind speed forecasting from two different Datasets. Considering the ANN model as the main forecasting tool, the input variables of the training set are transformed by trying to fit the shape of wind speed by using a proposed formula.

- To verify the effectiveness of characteristics and relationships improvement of transformed weather variables by using the proposed approach, R^2 and Sd are employed. The achieved results from both Datasets show that every transformed weather variable has the data normalized between 0 and 1, the same direction of variation with wind speed, a very large improvement in the Sd and a decrease in the value of Sd . This revealed that all the transformed weather variables have a strong linear dependency with the actual wind speed and the degree of linearity is improved. Therefore, the proposed data transformation approach is effective to normalize, to improve the data characteristics and the relationships between them;
- The ARIMA models have more ability for wind speed dependent transformed weather variables modeling to forecast the unknown values. Since the degree of nonlinearity of these variables is reduced in comparison to that of natural values

for both Datasets, this implies that accurate multistep forecasting is guaranteed for any transformed weather variables using the proposed approach, regardless of its unpredictable initial characteristic;

- Based on five ANN structures, five combined models (CBPNN, CANFIS, CNARXNN, CRBFNN, and CGABPNN) are developed to forecast wind speed trend by using the forecasting values of transformed weather variables as input variables. The achieved results from the two Datasets show that all the proposed models have a high forecasting accuracy, with the RMSE, MAE, and MAPE error evaluation criteria smaller than that of the comparison and benchmark models. The percentage of improvement as shown in Table 16 and Table 17 ranges from about 19% to 73%, 18% to 71%, and 24% to 74% for RMSE, MAE, and MAPE respectively for both Datasets and all forecasting steps. The results presented in Table 18 show high DM test values with very few rejected at 10% significance level and majority rejected at 1% for all the forecasting steps. Based on the above analysis, the proposed forecasting model has superior performance in wind speed forecasting among all comparison models.

III.4.3 Applications of proposed forecasting model

We found that by using the transformed data as input variables, all the neural networks models typically converge much faster and generate better-forecasting performance than the others which used the traditional data normalization. Thus, the proposed hybrid wind speed forecasting method has not only superior forecasting ability but also several real applications, as shown below:

1. The successful of the proposed weather variables transformation enables the application of the combined model anywhere and under all conditions regardless the meteorological and environmental conditions for accurate wind speed forecasting. Therefore, the unpredictable character of weather variables will not affect the performance of the forecasting model event over time and wind farm conditions;

2. Accurate wind speed forecasting induces an accurate WTPG forecasting. Therefore, by using the power curve of a wind turbine, the power output values are estimated proportionally to the forecasting wind speed values without worrying about other wind farm characteristics. An accurate WTPG is crucial for electrify grid planning, which helps to plan and promote real-time balance of system power. Also, it allows to timely adjust the adverse effects of wind farm operation avoid large scale power failure accidents, thus reducing the uncontrollable nature of electricity production and improving its penetration. In addition, effective WTPG forecasting will help to construct control strategies, greatly reduce the rotating reserve capacity, and thus reduce the overall cost of wind energy production;
3. Wind speed forecasting may also be used in the management of solar power, wave power, and hydropower;
4. Traditionally, WTPG forecasting approaches based on ANN models use the actual wind speed dependent weather variables to forecast the desired values but the proposed hybrid wind speed forecasting in this study can be carried out without actual dependent weather variables, since these actual variables are predicted individually through the ARIMA model. Therefore, this presents a real step forward for the real-time application of WTPG forecasting.

III.5 Optimal input variables disposition of neural network models

Despite the fact that the hybrid models analysed in the previous section produced high wind speed forecasting performance, the study of the effect of the disposition of the input variables of the ANN models is necessary to further optimize them. Thus, this section discusses the optimal disposition of input variables for BPNN, NARXNN and GABPNN. ANFIS is used as the benchmark model. The entire wind database (i.e. 73

PhD thesis of FOGNO FOTSO H.R. Laboratory of Mechanics, Materials and Structures

days for 10573 samples) is used for application. The data for the first 72 days are used to train the ANN models for the prediction of the V of the 73rd day. The input variables of the ANN models Ta , Pa , RH and t . The experimental parameters of developed forecasting models given in Table 8 have been used.

III.5.1 IVD and neural networks Performances

After both neural networks architectures setting and models are constructed in order to investigate the influence of IVD on forecasting accuracy, the sought of best training and forecasting performance of each model is required. Thus, 10 simulations for each of them with 10430 datasets are done. Three months were used in the training process and tested to forecast the short-term wind speed. The best performances of these simulations are considered for each of the developed neural networks models. Table 19 lists the different IVD, training, TrPerform, and forecasting performances of each of the models for BPNN and NARXNN architecture, respectively.

According to the results presented in Table 19, all the models of both ANNs structures have different performances. In other words, the training and forecasting performances are varying according to the ANNs models. The difference between the minimum and maximum value of a performance criterion is evaluated in percentage using Equation (48). For the BPNN architecture, the training performance, TrPerform, varies from 0.0772 to 0.0819, 5.73%; the forecasting errors RMSE, MAE, and MAPE vary from 1.2934 to 1.9017, 31.98%, from 1.0183 to 1.6215, 37.20% and from 18.4749 to 20.9336, 11.74%, respectively. For the NARXNN architecture, the training performance, TrPerform, varies from 0.0289 to 0.0297, 2.69%; the forecasting errors RMSE, MAE, and MAPE vary from 1.0106 to 1.4272, 29.19%, from 0.8227 to 1.074, 23.39%, and from 14.1664 to 18.6297, 23.95%, respectively. These significant differences between each better and worse performance criterion indicate the high influence of the input variables disposition upon training and forecasting performances of neural networks models. Meanwhile, among both neural networks, the BPNN structure has the more significant difference between the performance criteria. Therefore, we can conclude that the BPNN is more sensible to IVD than recurrent neural networks. Figure 37 shows the training and forecasting performances versus models of BPNN structure. Also, Figure 38 shows the training and forecasting performances versus models of NARXNN structure.

The fluctuations of performances of both developed ANNs architectures according

Table 19: Statistical performances of ANNs models

Models		BPNN				NARXNN			
No	disposition	TrPerform	RMSE	MAE	MAPE	TrPerform	RMSE	MAE	MAPE
1	Ta-Pa-RH-t	0.0791	1.9017	1.6215	20.095	0.0294	1.113	0.883	16.4035
2	Ta-Pa-t-RH	0.0803	1.3936	1.0975	20.185	0.0291	1.0973	0.859	16.1747
3	Ta-t-Pa-RH	0.0785	1.4431	1.1681	20.934	0.0297	1.2409	0.963	16.7212
4	Ta-t-RH-Pa	0.0791	1.395	1.1116	20.64	0.0294	1.2684	0.971	16.7102
5	Ta-RH-t-Pa	0.0789	1.4144	1.0663	18.651	0.0293	1.4272	1.074	18.6297
6	Ta-RH-Pa-t	0.0792	1.4026	1.0857	19.498	0.029	1.1854	0.917	17.3096
7	Pa-Ta-RH-t	0.0782	1.4697	1.2028	20.893	0.0293	1.1796	0.949	18.1993
8	Pa-Ta-t-RH	0.0788	1.4917	1.1592	19.115	0.0292	1.23	0.961	16.764
9	Pa-t-RH-Ta	0.0772	1.3431	1.0619	19.349	0.0293	1.1973	0.946	17.4748
10	Pa-RH-t-Ta	0.0787	1.326	1.0773	19.767	0.0295	1.1973	0.946	17.4748
11	Pa-RH-Ta-t	0.0794	1.2934	1.0183	19.626	0.0291	1.1305	0.906	16.7442
12	Pa-t-Ta-RH	0.0796	1.5071	1.0987	19.259	0.0295	1.0449	0.843	15.205
13	RH-Pa-t-Ta	0.0798	1.3811	1.0525	18.485	0.0294	1.0685	0.852	16.01
14	RH-Pa-Ta-t	0.0781	1.3726	1.0856	19.422	0.0292	1.1088	0.885	15.9322
15	RH-t-Pa-Ta	0.0819	1.3763	1.0549	19.138	0.0289	1.1074	0.878	15.1771
16	RH-Ta-Pa-t	0.0796	1.4609	1.1652	20.494	0.029	1.199	0.938	16.4563
17	RH-t-Ta-Pa	0.0819	1.3763	1.0549	19.138	0.0293	1.0387	0.824	14.1664
18	RH-Ta-t-Pa	0.0787	1.4118	1.1257	20.119	0.0289	1.3709	1.039	17.4982
19	t-RH-Pa-Ta	0.0786	1.3433	1.0892	20.382	0.0293	1.0106	0.823	15.4901
20	t-Pa-RH-Ta	0.0797	1.3584	1.0463	18.577	0.0292	1.1174	0.904	16.7915
21	t-RH-Ta-Pa	0.0781	1.3128	1.0657	19.772	0.0293	1.2105	0.977	16.8154
22	t-Ta-RH-Pa	0.0799	1.4297	1.1122	19.148	0.0293	1.0846	0.88	16.525
23	t-Ta-Pa-RH	0.08	1.3492	1.0258	18.475	0.0292	1.0378	0.823	14.9924
24	t-Pa-Ta-RH	0.0781	1.3489	1.0777	19.255	0.0292	1.0332	0.829	15.1903

to their models can be clearly observed in Figures 37 and 38. They clarify the influence of IVD upon static and dynamic neural networks models. Thus, the optimal IVD is required to build the optimal neural networks models based on more accurate TSF.

According to Table 19 and Figures 37 and 38, the first four most accurate forecasting models of the BPNN and NARXNN structure are models 5, 20, 13, 23 and 12, 17, 15, 23, respectively. According to HUANG Wei et al. [28], the input variables of an ANN need to have a high strength correlation between each of them and the target variable, but should not be correlated. Based on the results presented in Tables 6 and 19, this is confirmed by model 5 and 13 of the BPNN structure, but not for any NARXNN models. Therefore, based on the above experiments, it can be concluded that:

- NARXNN structure obtains the most accurate results than BPNN structure;
- The way that the input variables disposition influences the neural networks performance varies according to their architectures;

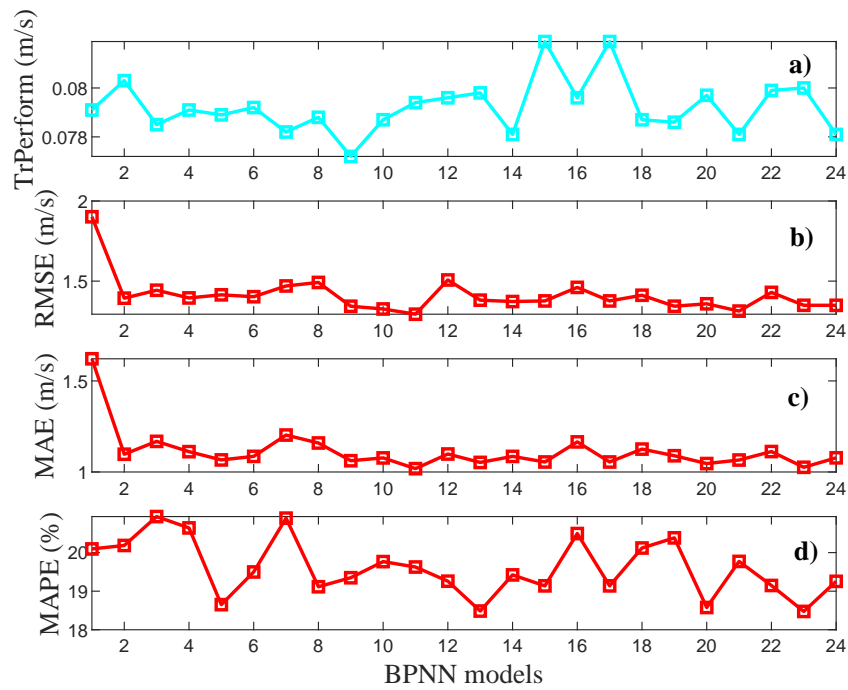


Figure 37: BPNN models performances: (a) training and forecasting, (b) RMSE (m/s), (c) MAE (m/s) and (d) MAPE(%)

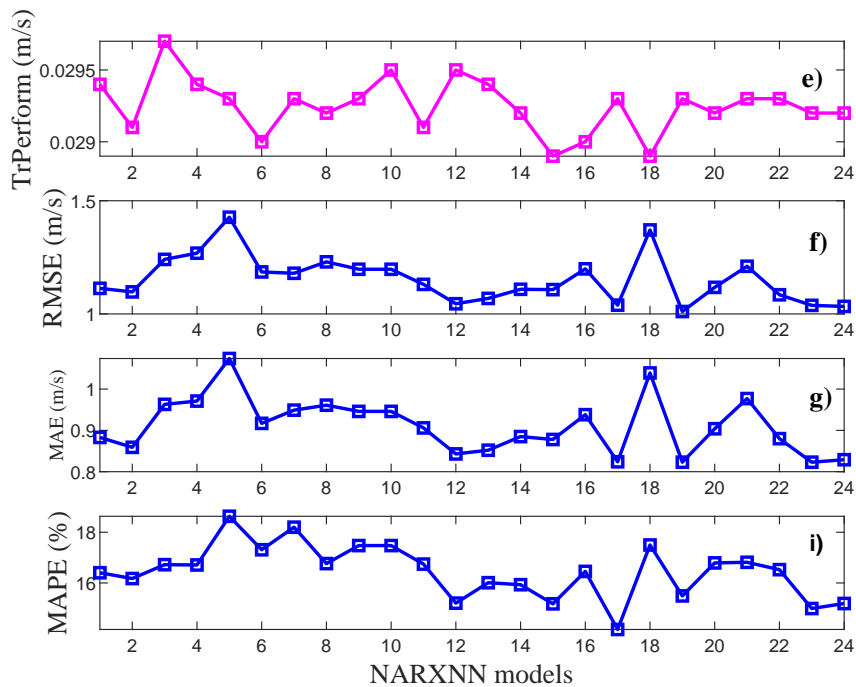


Figure 38: NARXNN models performances: (e) training and forecasting, (f) RMSE (m/s), (g) MAE (m/s) and (i) MAPE(%)

- There is a small possibility of having an optimal BPNN model by arranging its

input variables in such a way as to avoid the strength correlation between two neighboring input variables.

We can also see a real similarity in the variations of graphs 37(b), 37(c) and 37(d). This similarity is more considerable between graphs 38(f), 38(g) and 38(i). These similarities confirm the stability of the match of IVD with forecasting performances of the neural networks models. But these similarities are smaller between the training graph, 37(a) and the forecasting graphs, 37(b), 37(c) and 37(d). Event between 38(e) and 38(f), 38(g) and 38(i). Thus, this lack of concordance between the training performances and those of forecasting reflect the fact that some IVD are subjected to overlearning or overfitting, e.g., models 12 and 18 of NARXNN and model 7 of BPNN. To further illustrate this, Table 19 shows the coefficients of correlation between the performances criteria from the two ANNs architectures.

The most remarkable observation in these results from Table 20 is the smaller relations between training and forecasting errors criteria. They also argue that there are strong relations between the forecasting errors from NARXNN models than BPNN. Therefore, we can conclude that the forecasting performance of NARXNN is less sensitive than that of BPNN to overlearning or overfitting that some IVD may cause.

Table 20: Relations between the performance criteria

ANN		TrPrform	RMSE	MAE	MAPE	ANN
BPNN	TrPrform		-0.0651	-0.0317	0.0276	NARXNN
	RMSE	0.0073		0.9860	0.798	
	MAE	0.1369	0.9526		0.8450	
	MAPE	-0.3116	0.222	0.3989		

III.5.2 Neural network models optimization based on input variables dispositions

The results presented in the previous subsection showed that the IVD influences the static structure and the dynamic structure of ANN in different ways. Therefore, this subsection examines a general method for optimizing the two ANN structures using the IVD.

III.5.2.1 Proposed optimization approach

The goal of the proposed approach is to find the optimal IVD for a more optimal ANN solution. The ANNs are trained with modified Back-Propagation (BP) algorithm by introducing the IVD consideration. The traditional BP algorithm is used to update the

ANNs weights with a random initial IVD. The IVD is permuted and the ANN is re-trained to obtain an optimal solution. Figure 39 shows the flowchart of the proposed modified BPNN training algorithm. The proposed modified BPNN has three main stages: Stage (I) is the traditional BPNN training algorithm. It consists of a feed-forward pass, which take an input variable to express the corresponding output through the synaptic weights, and a feedback pass which updates the neural network weights. At the end of this training process, the ANN is validated in stage (II) by simulating its ability to generalize the desired output. Stage (II) prevents the overlearning and helps in finding the optimal model. Stage (III) is the added feedback pass, which enables the retraining of the neural network (back to stage (I)) for each IVD until a better solution is obtained.

The modified BPNN is proposed for improving TSF accuracy for 1 day ahead wind speed. The detail of the modified BPNN based on TSF is presented in **Algorithm**. As in the training process, the retraining process is controlled through the validation performances, e_s , and the number of retraining iteration, $T_{max} > Mo$.

The proposed modified BPNN is able to be used in combining model as the traditional BPNN. Then, this proposed optimization approach is evaluated in combining GABPNN. Here, the GA was used to find the optimal weights of neural networks in the feedback pass of stage (I). This for different possible IVD until an optimal solution is obtained. Figure 40 shows the whole process of BPNN optimization by GA and IVD consideration.

III.5.2.2 Proposed forecasting models evaluation

This subsection describes the experiments conducted to examine the performance of the proposed ANN optimization approach, which is based on IVD pursuing to enhance TSF accuracy. The proposed forecasting models are then based on this proposed optimization approach. Therefore, the BPNN, NARXNN, and GABPNN models are proposed. To perform the evaluation of the forecasting ability of these proposed models ANFIS is used as the benchmark model. All models are developed using the parameters given in Table 8.

To ensure that the final results are reliable and independent of the initial random weight and bias values of the proposed models, each developed model is repeated 10 times. It had been shown in the previous subsection III.5.1 that the IVD influence the training and forecasting performances of neural networks. Therefore, we will take the better forecasting models of BPNN and NARXNN from Table 19 as comparison models of the proposed models, i.e., models 20 and 17, respectively. Equation (47) is used to describe the improvement percentage of the proposed models over the comparison models.

Algorithm: Proposed neural networks based forecasting approach**Objective:**

Minimise the forecasting errors through the optimal input variables of neural network disposition

Inputs :

X - Input variable

X_{tr} - Training input variable

X_s - Validation input variable

X_t - Testing input variable

Outputs :

Y - Forecasting variable

Y_{tr} - Training target variable

Y_s - Validation target variable

Parameters :

N - Number of input variables

E_{smin} - Minimum validation neural network performances

T_{max} - Maximum retraining iteration

-
1. $X = [x_1, x_2, \dots, x_N]$
 2. Set target into Y_{tr} and Y_s
 3. **for** $i = 1$ to $N!$ **do**
 4. $X_i = \text{permute}(X_i)$
 5. Set X_i into X_{tr} , X_s and X_t
 6. Set neural network architecture and parameters
 7. **for** $j=1$ to T_{max} **do**
 8. Randomly initialize neural network weights and biases
 9. Train neural network model
 10. $S_i^j = \text{Simulate}(\text{neural network}, X_{s_i}^k)$
 11. $E_{s_i}^j = \text{errors}(S_i^j, Y_s)$
 12. **if** $E_{s_i}^j < E_{smin}$ **then**
 13. **break**
 14. **end if**
 15. **end for**
 16. **for** $k = 1$ to $\text{length}(X_t)$ **do**
 17. $O_i^k = \text{predict}(\text{neural network}, X_{t_i}^k)$
 18. **end for**
 19. $E_{f_i} = \text{errors}(O_i^k, Y_f)$
 20. **if** $E_{f_i} < E_{f_{i-1}}$ **then**
 21. $E_f = E_{f_i}$
 22. $Y = O_i^k$
 23. **else**
 24. $E_f = E_{f_{i-1}}$
 25. $Y = O_i^{k-1}$
 26. **end if**
 27. **end for**
 28. **return** E_f
 29. **return** Y
-

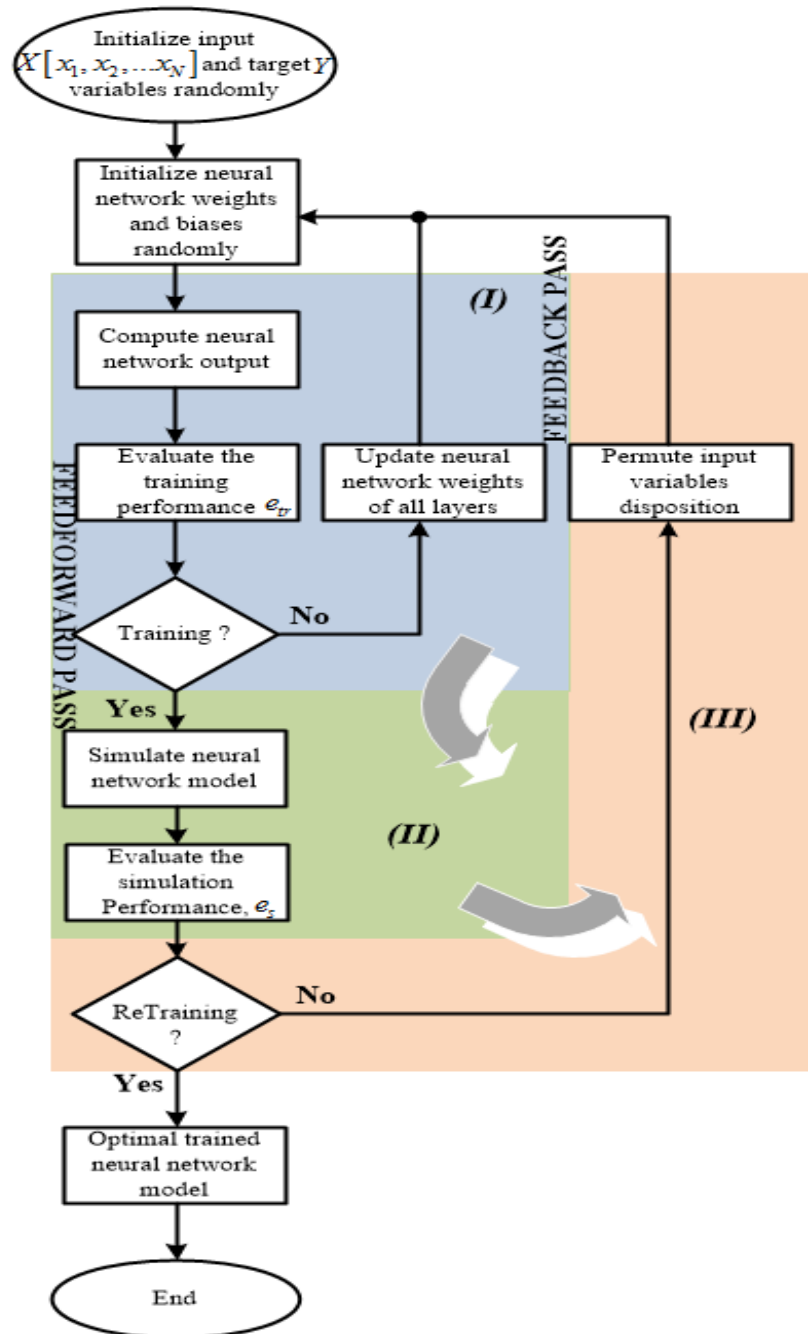


Figure 39: Flowchart of proposed BPNN with optimal IVD searching

The forecasting performance results of the proposed models and the comparing models of the case study are presented in Table 21. According to Table 21 the GABPNN model forecasts better than the ANFIS model. Meanwhile, the proposed NARXNN model performs well the TSF than the proposed BPNN and GABPNN models, while ANFIS is the worse one. The results of forecasting performances from the different proposed and comparing models are shown in Figure 41. Table 22 gives the performances of forecasting improvement of the proposed models over the comparison models.

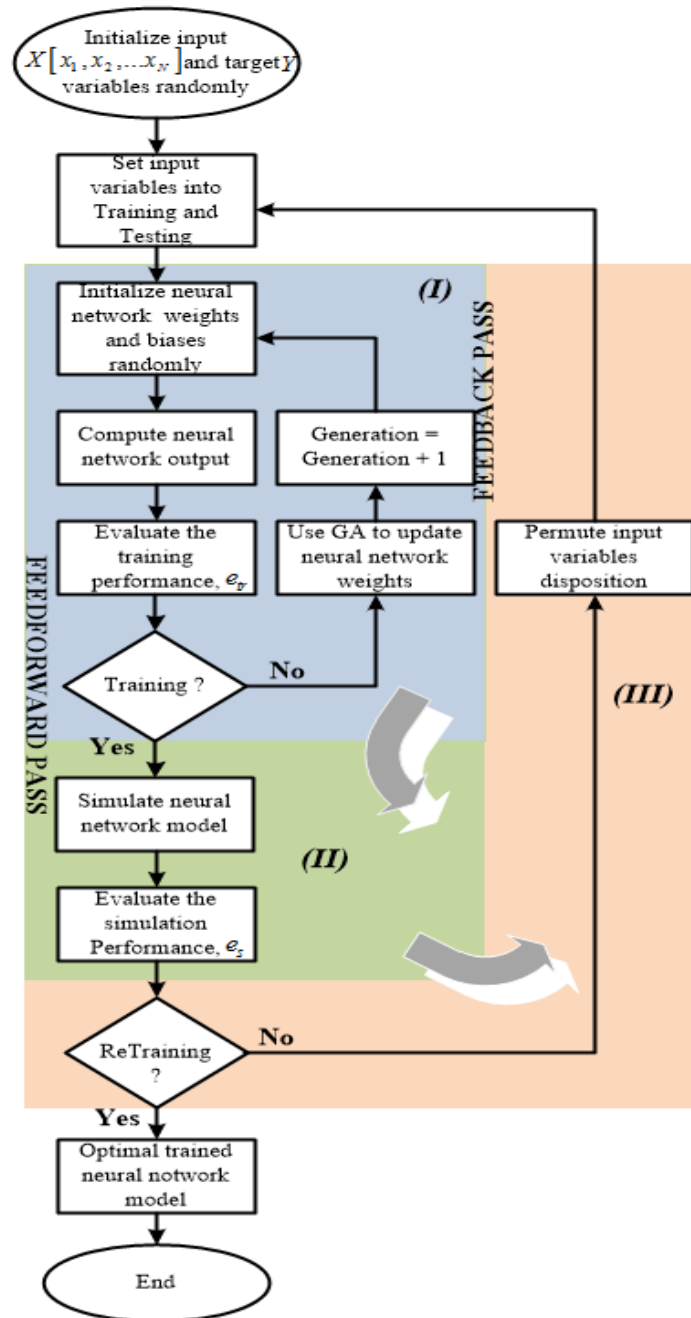


Figure 40: Proposed BPNN optimization by GA with IVD consideration

By observing Table 22, it can be seen that the proposed FFNN (BPNN) model leads to a more accurate forecasting performance than the old BPNN model with a considerable difference, by up to 10% for every performance criteria. This shows the effectiveness of proposed BPNN model to perform TSF. Meanwhile, the proposed NARXNN model is being neutralized with the old model, but it obtains the most accurate results among all developed models. It is important to note that this comparison NAXNN model is built with optimal IVD as shown in subsection III.5.1. Thus, the proposed NAXNN model

Table 21: Forecasting performance evaluation of different models

Models	RMSE	MAE	MAPE(%)
ANFIS	1.3456	1.0814	19.6528
GABPNN	1.2115	1.0231	18.3718
Proposed NARXNN	1.0289	0.8037	14.2817
Proposed BPNN	1.1617	0.9009	15.8855
Proposed GABPNN	1.2753	0.9901	16.5621

Table 22: Improvement percentages of the proposed models

Models	BPNN	NARXNN	GABPNN	ANFIS
RMSE Proposed NARXNN	21.62%	0.940%	15.07%	23.53%
Proposed BPNN	11.50%	-11.84%	4.110%	13.66%
Proposed GABPNN	2.85%	-16.91%	-5.260%	5.220%
MAE Proposed NARXNN	24.58%	2.220%	21.44%	25.67%
Proposed BPNN	15.46%	-9.590%	11.94%	16.69%
Proposed GABPNN	7.090%	-20.45%	3.220%	8.440%
MAPE Proposed NARXNN	23.12%	-0.800%	22.26%	27.32%
Proposed BPNN	14.48%	-12.13%	13.53%	19.16%
Proposed GABPNN	10.84%	-22.77%	9.850%	15.72%

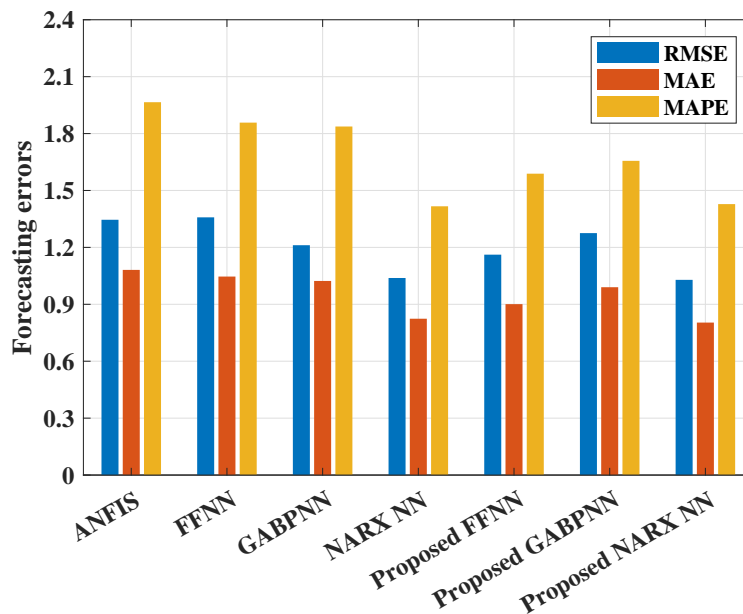


Figure 41: Bar chart showing the forecasting errors from the proposed and comparison models

can always work as a good forecasting model than the old model which is generally built with random IVD. The results presented in Table 22 show that the combining pro-

posed model, GABPNN is a more accurate model than its old comparison model. The sensitivity of the GABPNN to the arrangement of input variables is shown in Figure 42, which presents the fluctuation of best fitness values according to the neural networks models.

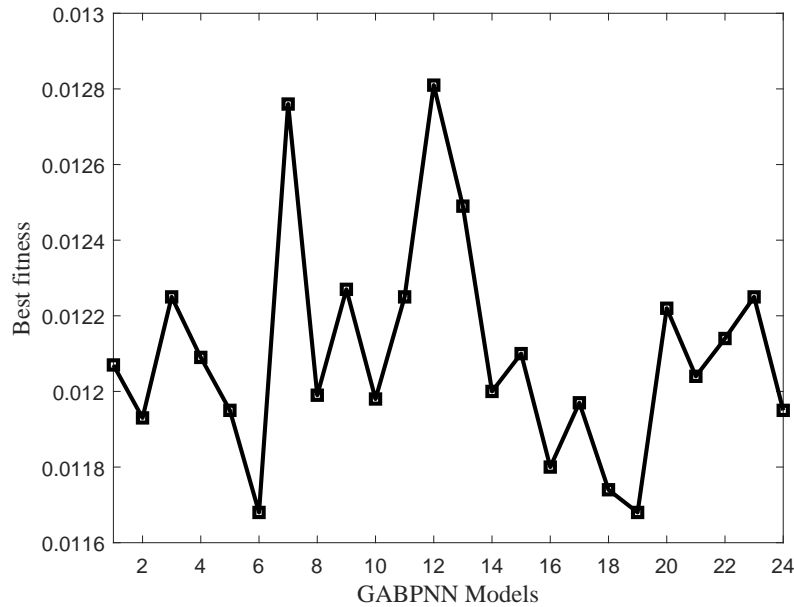


Figure 42: Best fitness values of GA along with neural networks models

The research results of the proposed strategy to improve the TSF performance of ANNs show that the tested models for 24 hours-head wind speed forecasting have the following features:

- Each proposed model always achieves more accurate value than old one. This shows the effectiveness of the proposed neural networks optimization approach to improve the multi-step head TSF accuracy;
- Among all the proposed models, BPNN model is the most improved one with the highest improvement percentage values, by up to 10%. Thus, IVD is very important for static neural networks forecasting performances improvement than dynamic neural networks;
- By using the worse neural networks models of Table 19 as comparison models, we will see that the difference between them and the proposed models will be more considerable.

The presented experiments confirm the competitive forecasting performance of the proposed neural networks models and therefore, show that it will be important to take

into consideration the IVD for the optimization of neural networks models. But it was complex to test step-by-step every possible IVD of neural networks aimed to find the optimal one. Thus, the key advantages of the proposed neural networks training and optimization approach are:

1. It is possible to test all the possible IVD and the search of the optimal disposition is included in the neural networks training algorithm. Thus, the approach does not require any predisposition of the input variables and relations between them analysis stage;
2. The complexity of the approach in terms of computation and speed is much less than the step-by-step method used to find the optimal IVD, hence facilitates the real-time application of the proposed neural networks optimization approach;
3. The forecasting performance is better than that obtained by using other methods to search the optimal IVD such as step-by-step finding and no correlated input variable methods;
4. Possibility to be combined with other techniques to build the hybrid TSF models.

III.6 Power losses in the wind turbines

III.6.1 Actual wind turbine gearbox power losses evaluation

The calculations are carried out using the experimental calibrated parameters of the bearing power loss model presented in chapter II. The usual operating temperature of the gearbox ranges between 60°C and 80°C. Carlos MCG Fernandes et al. [33] showed that the difference between the power loss at 60°C and 80°C is very weak. Therefore, the bearing power loss is predicted at 80°C in this thesis. The calibrated coefficients of friction μ_{bl} and μ_{EHD} in Ref [124], at the operating temperature of 80°C for $3262.5 < n.d_m < 52200$ for Thrust Ball Bearing (TBB) and RTB as given in Table 23 are used. Table 24 gives the SKF bearings constants used in the calculations, $K_{rs} = 3 \times 10^{-8}$.

In order to validate the effectiveness of the developed model and calculations, the power loss of 2.5 MW WT with two planetary and one helical gearbox under rated rotational speed and transmitted power reported in Ref [33] is used as the benchmark (see Figure 43).

Figures 43(a) and 43(b) show the bearing power loss at different stages of gearboxes at rated parameters of 2.0 MW (WT1) and 2.5 MW (WT2) WTs, respectively. As mentioned previously, the bearing power loss results shown in Figure 43(b) were presented

Table 23: Coefficient of friction at 80°C [124]

Oil	Parameter	Bearing type	
		TBB	RTB
MINR	μ_{bl}	0.058	0.035
	μ_{EHD}	0.056	0.018
PAOR	μ_{bl}	0.049	0.039
	μ_{EHD}	0.044	0.010
PAGD	μ_{bl}	0.054	0.025
	μ_{EHD}	0.044	0.010

in Ref [33], and are used in this work as comparison and validation model. The calculations are done for three oil formulations, MINR, PAOR and PAGD. The input rotational speed of the gearboxes is 20 rpm, and the transmitted power is 2.0 MW and 2.5 MW for WT1 and WT2, respectively. From Figure 43, it can be observed that the power loss is very low in the first stage, while stage 3 constitutes the main source of bearing power loss in both gearboxes. The total losses for WT1 are 39 kW, 40 kW and 43 kW with MINR, POAR and PAGD oil, respectively. The total losses for WT2 are 43 kW, 44 kW and 47 kW with MINR, POAR and PAGD oil, respectively. The above results show that, by using MINR oil in the place of PAGD, it is possible to save 4 kW in both WTs, which increases the gearboxes efficiency. These are consistent with the results of other researchers [33].

Table 24: Constants of the SKF bearings

Reference	K_L	K_Z	S_1	S_2	S_3	R_1	R_2	R_3
NU 20/800 ECMA	0.65	5.1	0.16	0.0015	-	1.23×10^{-6}	-	-
NU 1080 MA	0.65	5.1	0.16	0.0015	-	1.23×10^{-6}	-	-
NNUD 6056 EC-MAS/P53	0.7	6.2	0.16	0.0015	-	1.23×10^{-6}	-	-
NU 244 ECMA	0.65	5.1	0.16	0.0015	-	1.23×10^{-6}	-	-
NU 1060 MA	0.65	5.1	0.16	0.0015	-	1.23×10^{-6}	-	-
NNCF 4930 CV	0.7	6.2	0.16	0.0015	-	1.23×10^{-6}	-	-
NU 1036 ML	0.65	5.1	0.16	0.0015	-	1.23×10^{-6}	-	-
NU 236 ECMA	0.65	5.1	0.16	0.0015	-	1.23×10^{-6}	-	-
SKF 32960	0.7	6	0.009	2	-	1.23×10^{-6}	10.9	-
NSK QJ1036	-	3.1	1.2×10^{-2}	0.9	1.4×10^{-12}	4.78×10^{-6}	2.42	1.40×10^{-12}

Figure 44 shows the P_{LV} for each considered oil and 1.5% of P_G for WT1 power curve. The results presented in Figure 44 are used to predict the P_{LV} around the WT1 power curve. Therefore, it can be observed that the P_{LV} increases as the P_G and V increase in

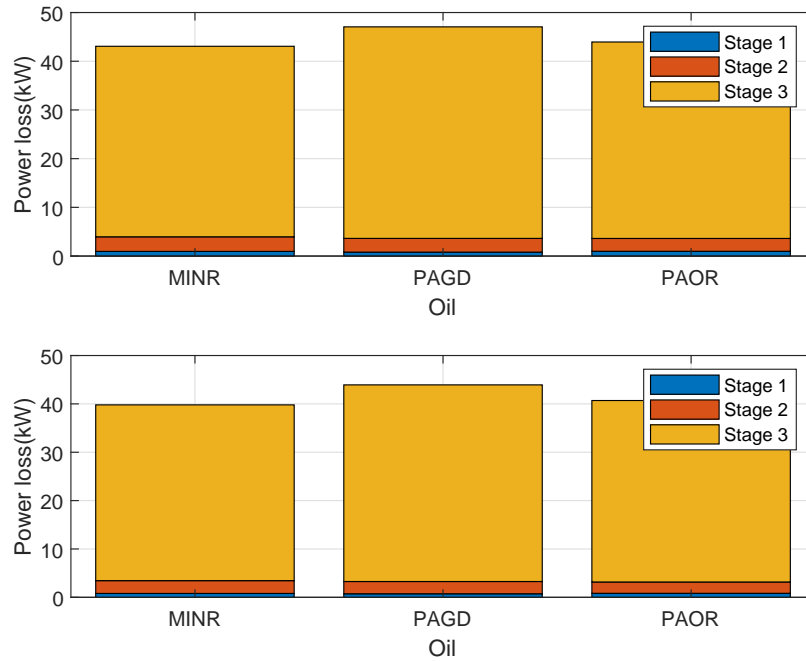


Figure 43: Bearing power loss at each stage of gearboxes under rated parameters: (a) WT1 and (b) WT2 from Ref [33].

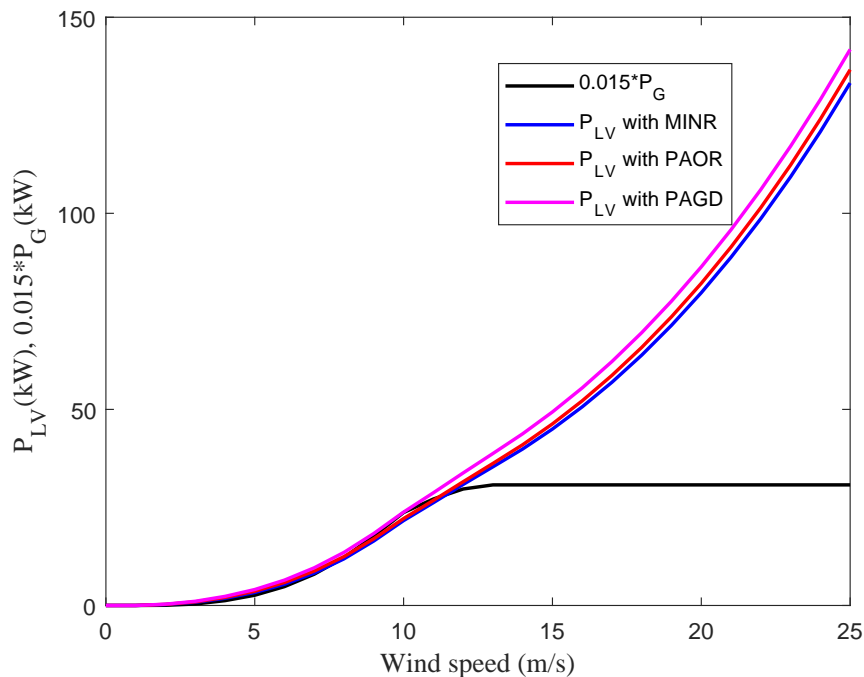


Figure 44: Bearing power loss around power curve of WT1

the nonlinear part of the power curve. In the rated zone, despite the fact that the P_G remains constant, the P_{LV} increases with increasing V . For instance, with MINR oil, the

power loss is 35 kW at 13 m/s and 133 kW at 25m/s. To ensure the safety of the gearbox, its input rotational speed must be stopped at a certain value of V .

The results presented in Figures 43 and 44 show that the P_{LV} greatly depends on V and P_G . To experiment the P_{LV} under actual operation conditions, the experiment's actual wind speed data presented in Figure 45(a) is used to estimate the P_G, T_{in} and then P_{LV} as given in Figures 45(b), 45(c) and 45(d) respectively. P_{LV} is calculated for three days at intervals of 10 minutes. We observe that V, P_G, T_{in} and P_{LV} all have the same shape over time, which reflects strong relationships between them. This relationship introduced by V through P_G , confirms the dependence of P_{LV} on V and P_G .

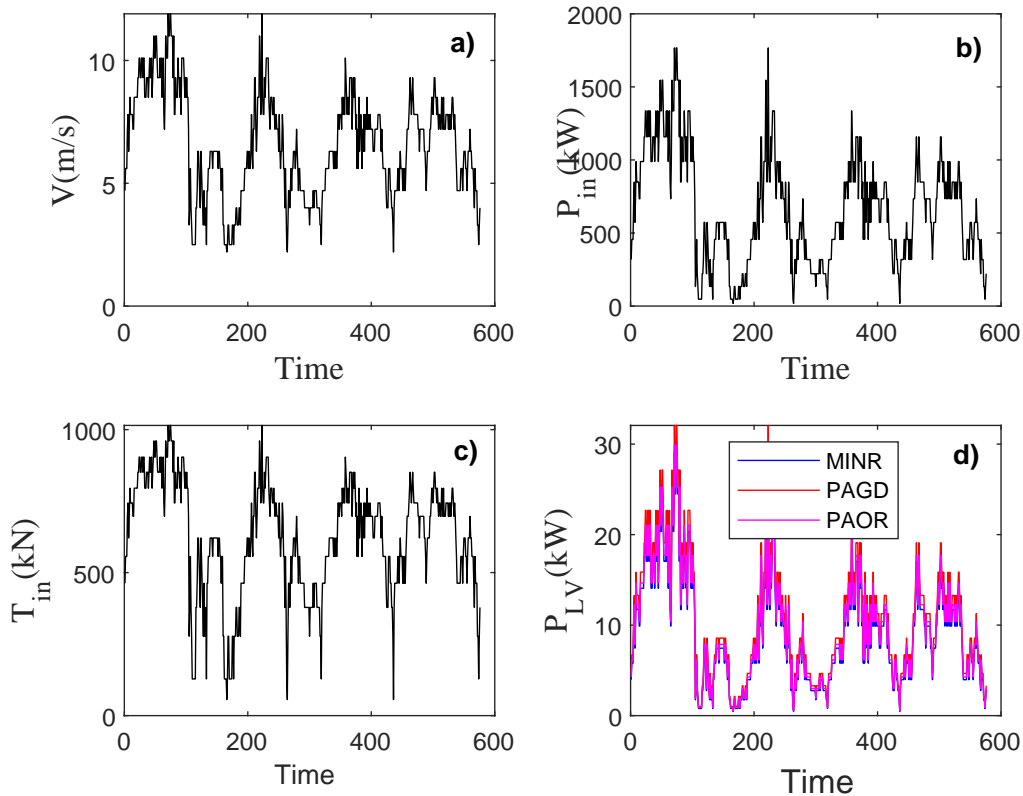


Figure 45: Gearbox operating parameters and bearing power loss of WT1

From Figures 45, V ranges from 2.2 m/s to 11.9 m/s, P_G ranges from 18 kW to 1766.7 kW, and P_{LV} range from 0.46 kW to 29 kW for MINR oil, from 0.53 kW to 30 kW for PAOR oil, from 0.62 kW to 32 kW for PAGD oil. Therefore, the influence of lubricant type is observed in real-time operation. We also confirmed that the WT associated with this study's experimental data only operates in the nonlinear zone of the power curve. The intermittent nature of the WT operating environment, such as wind speed, causes the bearing power loss to vary over time. This means that the gearbox efficiency will be intermittent as wind speed of WT operation over time.

To further investigate the influence of oil and WTs capacity on P_{LV} , Equation (47) is used to assess the percentage difference (IP_{VL}) of one result of P_{LV} over another.

Table 25: Percentage difference of P_{LV} for different oils

Oil	WT1				WT2			
	Rated		WTPC		Actual		Rated	
	POAR	PAGD	POAR	PAGD	POAR	PAGD	POAR	PAGD
MINR	2.32%	9.3%	2.79%	7.67%	4.16%	12.63%	2.25%	10.25%
POAR	-	6.81%	-	4.75%	-	8.13%	-	7.69%

The percentage difference of the P_{LV} of WT1 compared to WT2 is 10.25%, 10%, and 9.3% for MINR, POAR, and PAGD oils, respectively. Thus, the above results show that P_{LV} is more significant in WT1 than in WT2 at the same gearbox input rotational speed. It is clear that the bearing power loss depends also on WT capacity. Also, it can be seen that IP_{VL} between WT1 and WT2 is more significant when MINR oil is used compared to POAR and PAGD oils. Table 25 displays the IP_{VL} for different oils. The MINR is taken as reference oil. At the rated parameters, it can be seen from Table 25 that PAGD oil produces high bearing P_{LV} in the gearbox in comparison with MINR and POAR oils, with the IP_{VL} equal to 9.3% and 6.81% in WT1, and 10.25% and 7.69% in WT2. Compared to POAR oil, MINR oil produces IP_{VL} , the IP_{VL} in this case is 2.32% and 2.25% in WT1 and WT2, respectively. The mean values of IP_{VL} under WTPC and real operating conditions for different oils are also presented in Table 25 for WT1. It can be observed that under both WTPC and real WT operating conditions, the P_{LV} is lower when using MINR oil and POAR oil than when PAGD oil is used. Comparing MINR oil to PAGD, IP_{VL} are 7.67% and 12.63% under power curve and actual WT operating conditions, respectively. Also, MINR oil reduces the P_{LV} by 2.79% and 4.16% compared to POAR oil. Comparing POAR oil to PAGD oil under power curve and real-time WT operating conditions, P_{LV} is reduced by 2.79% and 4.16%, respectively. Therefore, MINR oil produces less P_{LV} than MINR oil and PAGD oil regardless of the exogenous conditions in which the WT operates.

III.6.2 Prediction of rolling bearing power loss using BPNN model

To avoid complex and robust calculations in the future, we used the BPNN model and historical bearing power loss values to predict the desired values under real operating conditions. BPNN model is developed using the parameters defined in Table 8. The previous calculated power loss values are used as actual values to validate the proposed neural network model. Thus, data for 3 days, providing a total of 672 samples, is selected

to train the ANN model by using t , P_G , T_{in} and V as input variables and P_{LV} as target variable. The following 144 samples from one day of WT operating parameters, t , P_G , T_{in} , and V , were fed into a trained neural network model to predict the corresponding P_{LV} samples. Figures 46(a), 46(b), and 46(c) show the prediction results after comparison between the actual and predicted P_{LV} for MINR, PAOR, and PAGD oils, respectively. The approximations of the curves of the actual and predicted values of P_{LV} reflect a high prediction efficiency for all three cases.

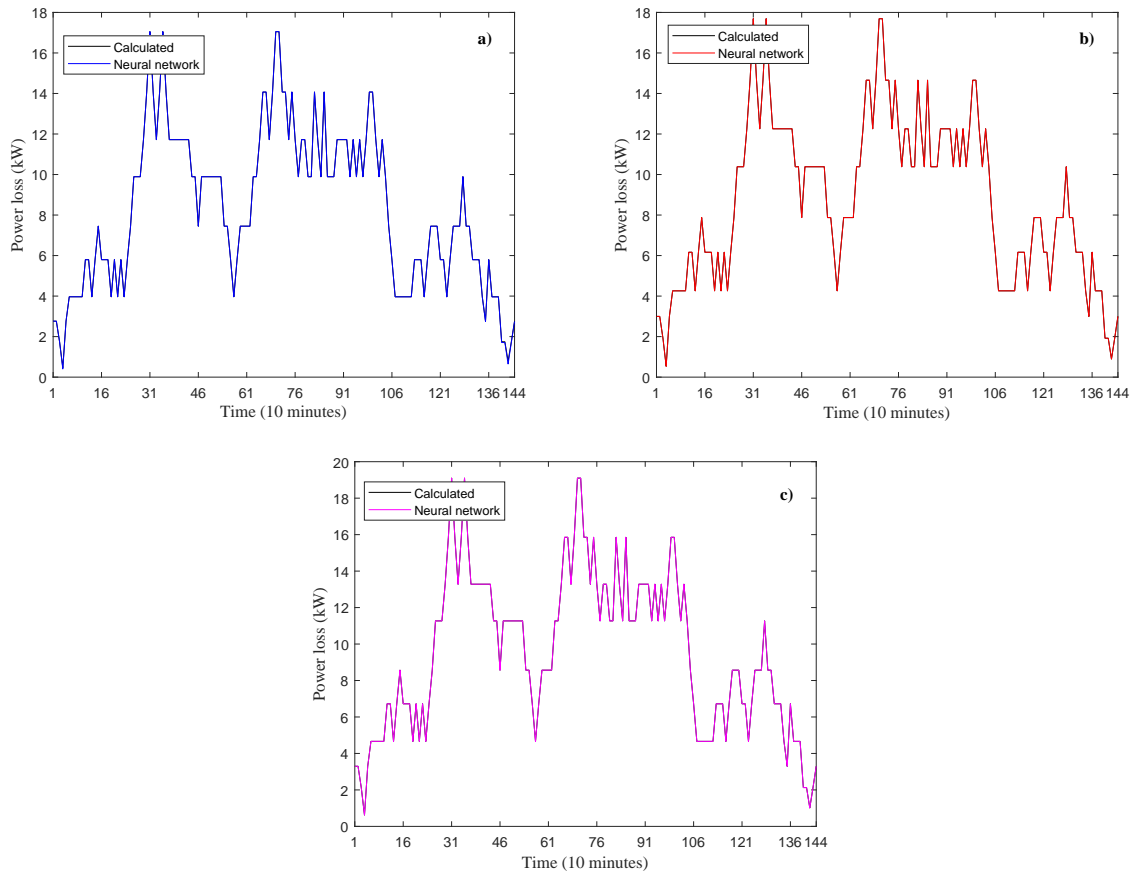


Figure 46: Comparing actual and ANN predicted bearing power loss with different oils: (a) MINR, (b) POAR, (c) PAGD

Furthermore, Table 26 shows the statistical performance of the ANN prediction results of each gearbox oil. From Table 26, RMSE and MAE are below 0.02 kW, and MAPE are below 0.3% for all oil formations. These very low values of RMSE, MAE and MAPE reflect a very high prediction performance of bearing power loss based on BPNN.

III.7 Conclusion

This chapter details the results and discussion on the wind potential and rolling bearing power loss in WTG modelling and prediction. We used the wind data collected at

Table 26: Prediction performance of bearing power loss

	MINR	PAOR	PAGD
RMSE (kW)	0.0142	9.1717e-04	4.4080e-04
MAE (kW)	0.0040	6.7458e-04	2.3080e-04
MAPE (%)	0.2921	0.0201	0.0088

Bapouh in Cameroon for our different applications in this thesis. Thus, we compared six traditional prediction models most used in the literature for the wind speed forecasting with application of the expected wind turbine power. The results obtained showed that the NARXNN and ARIMA models perform better in wind speed forecasting compared to the BPNN, GABPNN and ANFIS models. These results also showed that the 1-step ahead is better for wind speed forecasting, while the 3-step is the worst. Results obtained also show that the effectiveness of WTPG prediction is closely dependent on the wind speed forecasting accuracy. To improve the performance of ANN models used we studied their combined with ARIMA with improvement the relationship between each variable used in their input and the wind speed. This new proposed approach allowed us to improve the forecasting results to more than 35% on average. Also, the results obtained from the different possible disposition of the input variables of the ANNs showed their considerable influence on their performances. Therefore, a new optimization approach for ANNs was analyzed and the results obtained proved its effectiveness. We also analyzed the combination of the calibrated SKF model and ANN for modeling and real-time prediction based on the current operating conditions of the WT. Results show that an increase in the WT capacity induces an increase in bearing power losses and vice versa. The high rotational speed of stage 3 of the WT gearbox causes significant bearing power losses at this level. Bearing power losses are less significant in stage 1 and 2 because of their low rotational speed. The bearing power losses are more significant when PAGD oil is used compared to MINR and PAOR oils regardless of the WT operating conditions. The bearing power loss is less significant when MINR oil is used compared to PAOR oil. The BPNN performs very well the real-time bearing power loss prediction by generating a very high performance.

General conclusion

Summary and contributions

In order to provide a guide in the decision-making process on future wind farm development projects in Cameroon and to develop a better model for predicting wind speed and wind turbine power generation, we first studied the wind energy potential through the development and examination of forecasting models based mainly on artificial neural network architectures. Due to the intermittent nature of wind speed, an accurate wind power forecasting model is imperative for its integration into the electrical grid. It will allow to manage the system of the dispatch between the supply by the different energy sources and the demand. Lastly, we examined the effect of friction on the electrical power generated by the wind turbine through the modelling and prediction of power losses in the rolling bearings of the gearbox. This can be used to control and improve the efficiency of the wind turbine.

Chapter I provided a brief background on wind power, its potential, its intermittent nature and its effect, and the electrical energy conversion system. The wind turbines and their composition are presented. From literature, it was revealed that one of the solutions to increase the competitiveness of wind energy is to use it in addition other energy productions with the difficulty of optimal management of the dispatch between these two energy types. Therefore, time series prediction techniques are developed to predict the wind speed and the power generation. The neural network models, which are the best tools used in these prediction techniques are detailed. It was also revealed that the gearbox of the wind turbine is the main seat of friction in the system. This friction induces power losses that decrease the efficiency of the system, and consequently the electrical power generation. The different configurations of gearboxes and the sources of power losses are presented in this chapter. The bearings and gears are the main sources of power loss in the wind turbine gearboxes.

In chapter II, we presented and described the methods and elements that were used in this thesis; the study context and the data used. The procedures for developing BPNN, NARXNN, RBFNN, GABPNN and ANFIS models for multi-step ahead wind speed forecasting were also presented. The multi-step forecasting used involves 1-step, 2-step and 3-step ahead. The procedure for setting up the ARIMA model is also de-

tailed. The ARIMA model is used as the benchmark model in this thesis, i.e. a model for comparison of neural network models. Supervised learning based on the Levenberg Marquerth back-propagation algorithm is used for neural network training. The modelling of the power curve of the modern wind turbine E-82 2000 kW of the manufacturer EMERCOM is proposed as an application for the estimation of the expected wind power in all our applications in this thesis. To improve the forecasting performance of ANN models, two new approaches are proposed. The first one is a combination of ANN and ARIMA models based on the improvement of the relationships between each variable used at the input of the ANN and the wind speed. Thus, a new technique of data pre-processing allowing to transform them by normalizing between 0 and 1 and increasing the strength of relationships between them is proposed. The transformed data are used for ANN models training and ARIMA model is used for modelling and predicting the ANN testing data set. The second consists of investigating the disposition of the input variables of the ANN models on their performances. The wind turbine gearbox model consisting of two planetary gears and one parallel gear is developed as an application for modelling and prediction of power losses in bearings. Thus, the SKF calibrated model is developed for modelling and determining the historical values of these power losses. The BPNN model is used mainly based on these historical values and the actual operating conditions of the wind turbine to predict the desired values of power losses.

Chapter III is reserved for the presentation of results obtained. These are the forecasting results obtained from the different forecasting models based mainly on statistical criteria, allowing to evaluate their performance. The results of the power losses in the rolling bearings of the wind turbine gearbox obtained by analytical calculations are also presented. The main results obtained in this thesis can be summarized as follows.

The results of the investigation of six models for the multi-step ahead wind speed forecasting at Bapouh in Cameroon, validated with two Datasets, showed that the NARX-NN models and ARIMA models perform better than other models. The ANFIS models are the worst wind speed forecasting models. It was also shown that the 1-step ahead is better for wind speed forecasting, while the 3-step is the worst in both Datasets. The achieved WTPG prediction are revealed that its result is good as well as the wind speed forecasting result is accurate. This proves that accurate wind speed forecasting is crucial for WTPG prediction.

The series of results obtained from the proposed new hybrid ANN-ARIMA model revealed the effectiveness of the proposed approach for data transformation improving the relationships between two weather variables. The Standard Deviation results show that the transformed data has a low level of dispersion compared to real series. This facilitated the high forecasting of actual values of each transformed weather variable. This transformation has been shown ideal to facilitate the neural network model learning and

unknown wind speed values forecasting. Thus, results of RMSE, MAE, and MAPE employed to evaluate the forecasting accuracy have shown the higher superiority of all the proposed models among the comparison models with a percentage improvement up to 77%, 76%, and 74% respectively. Meanwhile, the experimental results of the Diebold-Mariano test employed to evaluate the significance level of forecasting accuracy of each combined model among the based neural network and benchmark models proved the ability of the proposed hybrid wind speed forecasting model. Based on reported experiments, it can be concluded that the proposed hybrid wind speed forecasting model is a promising model with high accuracy. This implies that the proposed forecasting models can be used at all times and in all situations, regardless of the weather variables characteristics, especially that of the wind speed. We have also seen that the proposed hybrid model is ideal for real-time WTPG applications.

The investigation carries out on BPNN and NARXNN models to forecast 24 hours ahead wind speed have shown that their training and forecasting performances vary according to their input variables disposition. Thus, optimal forecasting requires an optimal input variables disposition of ANN based. A new ANN training approach has been proposed; introducing the optimal input variables disposition into Back-Propagation algorithm. This proposed approach has been applied to develop the neural networks forecasting models including combining model using generic algorithm. The results of the case study reveal the effectiveness of the proposed approach to improve accuracy of time series wind speed forecasting, in which every proposed model improves the performance of its old model. The average percentage improvement of each proposed model over its traditional model is 23.1%, 13.81%, and 6.92% for BPNN, NARXNN and GABPNN, respectively.

Form the proposed bearing power loss under real-time WT operating conditions estimation, the calculations results at the rated parameters have shown that the bearing power loss is higher for 2.5 MW WT than for 2.0 MW WT with a percentage difference of 10.25%, 10%, and 9.3% for MINR, POAR and PAGD oils, respectively. In both WTs, the main source of power loss is stage 3 (greater than 30 kW). Stage 1 has the lowest power loss (less than 1 kW). The bearing loss in stage 2 is slightly greater than that of stage 1. The achieved results under power curve characteristics of 2.0 MW WT showed that the power loss varies with the variation of the wind speed and the transmitted power in the nonlinear region. While in the rated zone, the power loss increases with the wind speed despite the constant transmitted power. The real wind speed recorded in Bapouh is employed for real-time rolling bearing power loss calculation. The results after four days for 2.0 MW WT showed that the random nature of wind speed makes bearing power loss intermittent. At rated power curve and real-time 2.0 MW WT operating parameters, the bearing power losses are on average reduced by 9.86% when MINR oil is used

and by 5.56% when PAOR oil is used compared to PAGD oil. They are reduced by 3.09% when MINR oil is used compared to PAOR oil. The back-propagation neural network is built for three days bearing power loss modelling for predicting desired one day ahead values by using the real wind speed, input torque, transmitted power and time step as exogenous input variables. The achieved results of RMSE, MAE, and MAPE employed to compare the calculated and the ANN predicted bearing power loss values are 0.0142, 0.0040 and 0.2921 for MINR oil, 9.1717e-04, 6.7458e-04 and 0.0201 for PAOR, 4.4080e-04, 2.3080e-04 and 0.0088 for PAGD oil, respectively. Therefore, the following conclusions are made:

- The increase in the WT capacity induces an increase in bearing power losses and vice versa.
- The high rotational speed of stage 3 of WT gearbox causes significant bearing power losses at this level. Bearing power losses are less significant in stage 1 and 2 because of their low rotational speed.
- The bearing power losses are more significant when PAGD oil is used compared to when MINR and PAOR oils are used regardless of the WT operating conditions. The bearing power loss is less significant when MINR oil is used compared to when PAOR oil is used.
- The back-propagation neural network performs very well the real-time bearing power loss prediction by generating a very high performance.

Open problems and future directions

Many interesting results have been obtained in this thesis. However numerous aspects related to this rapidly developing topic remain unresolved, and they may be subjected to future investigations:

♠ The best wind speed forecasting performance obtained in this thesis is on average 9% (considering the MAPE criterion) of the proposed hybrid ANN-ARIMA model. This performance could be improved by combining the ANN model optimization method based on the arrangement of input variables (proposed in this thesis) with this hybrid ANN-ARIMA model. Furthermore, the combination of these two approaches proposed could be more accurate for time series forecasting if used together with a multi-objective algorithm such as bat algorithm, evolutionary algorithm, and firefly algorithm. Adding a signal decomposition technique such as empirical mode decomposition and singular spectrum analysis to this resulting model could be more beneficial for improving its forecasting accuracy.

♠ It has been shown in this thesis that the gears and bearings are the two main sources of power losses in the wind turbine gearbox. But we are limited to the evaluation in real time of those in the bearings. It would also be interesting to evaluate the power losses in the gears which could be used for the real time prediction of the efficiency of the gearbox and thus the efficiency of the wind turbine. The operating temperature of the gearbox is considered constant in this study, it would also be interesting to investigate the influence of friction on this temperature in real time. Also, so far the ratio of the gear rotational speed is considered constant in the evaluation of the power losses in the wind turbine gearbox despite the friction. It would therefore be important to evaluate the influence of friction on this rotational speed ratio.

Bibliography

- [1] Lucas, P.L., Dagnachew, A.G., Hof, A.F.: Towards universal electricity access in Sub-Saharan Africa. PBL Netherlands Environmental Assessment Agency (2017).
- [2] Veeyee, K.F., Divine, N., Dorin, B., Nkeng, B., Elambo, G.: Potentials of sustainable electricity production from sawdust by small scale wood transformation units: a case study in Cameroon. *Int. J. Energy Environ. Eng.* **12**, 101-114 (2021).
- [3] Afungchui D. and Aban C.E.: Analysis of wind regimes for energy estimation in Bamenda, of the North West Region of Cameroon, based on the Weibull distribution. *Revue des Energies Renouvelables.* **17**, 137-147 (2014).
- [4] Vernyuy, A., Abubakar, A., Muhammad-sukki, F., Karim, E.: Renewable energy potentials in Cameroon: Prospects and challenges. *Renew. Energy.* **76**, 560-565 (2015).
- [5] Tong W.: Chapter 1. Fundamentals of wind energy. *WIT Transactions on State of the Art in Science and Engineering*, **44**, 1-46 (2009).
- [6] Xiang, L., Li J., Hu, A., Zhang Y.: Deterministic and probabilistic multi-step forecasting for short-term wind speed based on secondary decomposition and a deep learning method. *Energy Convers. Manag.* **220**, 1-12 (2020).
- [7] Kadhem, A.A., Wahab, N.I.A., Aris I., Jasni J. and Abdalla A.N.: Advanced wind speed prediction model based on a combination of Weibull distribution and an artificial neural network. *Energies.* **10**, 1-17 (2017).
- [8] Olsson, M., Perninge, M., Sder L.: Modeling real-time balancing power demands in wind power systems using stochastic differential equations. *Electric Power Systems Research.* **80**, 966-974 (2010).
- [9] Zhang, G., Liu, D.: Causal convolutional gated recurrent unit network with multiple decomposition methods for short-term wind speed forecasting. *Energy Convers. Manag.* **226**, 1-15 (2020).

- [10] Nair, K.R.: Forecasting of wind speed using ANN, ARIMA and hybrid models. Proc. International Conference on Intelligent Computing, Instrumentation and Control Technologies, Kerala, India 6-7 July (2017).
- [11] Yan, X., LiuY., Xu, Y., Jia, M.: Multistep forecasting for diurnal wind speed based on hybrid deep learning model with improved singular spectrum decomposition. *Energy Convers. Manag.* **225**, 1-22 (2020).
- [12] Soman, S.S., Zareipour, H., Member, S., Malik, O., Fellow, L.: A review of wind power and wind speed forecasting methods with different time horizons. Proc. North American Power Symposium, Arlington, TX, USA 26-28 September (2010).
- [13] Lei, M., Shiyan, L., Chuanwen, J., Hongling, L., Yan, Z.: A review on the forecasting of wind speed and generated power. *Renew. Sustain. Energy Rev.* **13**, 915-920 (2009).
- [14] Chitsazan, M.A., Sami Fadali, M., Trzynadlowski, A.M.: Wind speed and wind direction forecasting using echo state network with nonlinear functions. *Renew. Energy.* **131**, 879-889 (2019).
- [15] Zhang, W., Qu, Z., Zhang, K., Mao, W., Ma, Y., Fan, X.: A combined model based on CEEMDAN and modified flower pollination algorithm for wind speed forecasting. *Energy Convers. Manag.* **136**, 439-451 (2017).
- [16] Loukatou, A., Howell, S., Johnson, P., Duck, P.: Stochastic wind speed modelling for estimation of expected wind power output. *Appl. Energy.* **228**, 1328-1340 (2018).
- [17] Wang, J., Dong, Y., Zhang, K., Guo, Z.: A numerical model based on prior distribution fuzzy inference and neural networks. *Renew. Energy.* **112**, 486-497 (2017).
- [18] Fazelpour, F., Tarashkar, N., Rosen, M.A.: Short-term wind speed forecasting using artificial neural networks for Tehran, Iran. *Int. J. Energy Environ. Eng.* **7**, 377390 (2016).
- [19] Cadenas, E., Rivera, W., Campos-amezcua, R., Heard, C.: Wind speed prediction using a univariate ARIMA model and a multivariate NARX model. *Energies.* **109**, 1-15 (2016).
- [20] Samadianfard, S., Hashemi, S., Kargar, K., Izadyar, M.: Wind speed prediction using a hybrid model of the multi-layer perceptron and whale optimization algorithm. *Energy Rep.* **6**, 1147-1159 (2020).

- [21] Wang, J., Hu, J.: A robust combination approach for short-term wind speed forecasting and analysis e Combination of the ARIMA (Autoregressive Integrated Moving Average), ELM (Extreme Learning Machine), SVM (Support Vector Machine) and LSSVM (Least Square SVM) forecasts using a GPR (Gaussian Process Regression) model. *Energy*. **93**, 41-56 (2015).
- [22] Shen, Y., Wang, X., Chen, J.: Wind power forecasting using multi-objective evolutionary algorithms for wavelet neural network-optimized prediction intervals. *Appl. Sci.* **8**, 1-13 (2018).
- [23] Peng, H., Liu, F., Yang, X.: A hybrid strategy of short term wind power prediction. *Renew. Energy*. **50**, 590-595 (2013).
- [24] Loghmanian, S.M.R., Jamaluddin, H., Ahmad, R., Yusof, R., Khalid, M.: Structure optimization of neural network for dynamic system modeling using multi-objective genetic algorithm. *Neural Comput. Appl.* **21**, 1281-1295 (2012).
- [25] Li, Z., Best, M.: Optimization of the input layer structure for feed-forward narx neural networks. *Int. J. Electr. Comput. Energ. Electron. Commun. Eng.* **9**, 673-678 (2015).
- [26] Piazza, A. Di, Carmela, M., Piazza, D., Vitale, G.: Solar and wind forecasting by NARX neural networks. *Renew. Energy Environ. Sustain.* **39**, 1-5 (2016).
- [27] Crone, S.F., Kourentzes, N.: Input-variable specification for neural networks - an analysis of forecasting low and high time series frequency. *Proc. International Joint Conference on Neural Networks, Atlanta, GA, USA 14-19 June* (2009).
- [28] Wei, H., Yoshiteru, N., Shouyang, W.: A general approach based on autocorrelation to determine input variables of neural networks for time series forecasting. *J. Syst. Sci. Complex.* **17**, 297-305 (2004).
- [29] Sovann, N., Nallagownden, P., Baharudin, Z.: A method to determine the input variable for the neural network model of the electrical system. *Proc. 5th International Conference on Intelligent and Advanced Systems, Kuala Lumpur, Malaysia 3-5 June* (2014).
- [30] Yaïci, W.: Simulation study on the effect of reduced inputs of artificial neural networks on the predictive performance of the solar energy system. *Sustainability*. **9**, 1-14 (2017).
- [31] Fernandes, C.M.C.G., Blazquez, L., Martins, R.C., Seabra, J.H.O.: Energy efficiency tests in a full scale wind turbine gearbox. *Tribology Int.* **101**, 375-382 (2016).

- [32] Nutakor, C., Klodowski, A., Sopanen, J., Mikkola, A., Pedrero, J.I.: Planetary gear sets power loss modeling: application to wind turbines. *Tribology Int.* **105**, 42-54 (2016).
- [33] Fernandes, C.M.C.G., Hammami, M.: Power loss prediction : Application to a 2.5 MW wind turbine gearbox. *J. eng. Tribol.* **0**, 1-13 (2015).
- [34] Fernandes, C.M.C.G., Marques, P.M.T., Martins, R.C., Seabra, J.H.O.: Gearbox power loss. Part III: Application to a parallel axis and a planetary gearbox. *Tribology Int.* **88**, 317-326 (2015).
- [35] Fernandes, C.M.C.G., Marques, P.M.T., Martins, R.C., Seabra, J.H.O.: Gearbox power loss. Part II: Friction losses in gears. *Tribology Int.* **88**, 309-316 (2015).
- [36] El-ghonemy, A.M.K.: Fresh water production from / by atmospheric air for arid regions , using solar energy: Review. *Renew. Sustain. Energy Rev.* **16**, 6384-6422 (2012).
- [37] Ghaderi, A., Sanandaji, B.M., Ghaderi, F.: Deep Forecast: Deep Learning-based Spatio-Temporal Forecasting. *Proc. 34th International Conference on Machine Learning*, Sydney, Australia 6-11 August (2017).
- [38] Technology Briefs : Wind Power. Energy Technology Systems Analysis Programme Irena and International Renewable Energy Agency (2016).
- [39] Di, E., Cidra, J., Carrillo, C., Montan, A.F.O.: Review of power curve modelling for wind turbines. *Renew. Sustain. Energy Rev.* **21**, 572-581 (2013).
- [40] Teyabeen, A.A., Jwaid, A.E.: Power curve modelling for wind turbines. *Proc. 19th International Conference on Modelling and Simulation*, Cambridge, UK 5-7 April (2017).
- [41] Lydia, M., Kumar, S.S., Selvakumar, A.I., Prem, G.E.: A comprehensive review on wind turbine power curve modeling techniques. *Renew. Sustain. Energy Rev.* **30**, 452-460 (2014).
- [42] Bandi, M.M., Apt, J.: Variability of the wind turbine power curve. *Appl. Sci.* **6**, 1-9 (2016).
- [43] Pelletier, F., Masson, C., Tahan, A.: Wind turbine power curve modelling using artificial neural network. *Renew. Energy.* **89**, 207-214 (2016).

- [44] Chitsazan, M.A., Fadali, M.S., Trzynadlowski, A.M.: Wind speed and wind direction forecasting using echo state network with nonlinear functions. Proc. American Control Conference, Seattle, WA, USA 24-26 May (2017).
- [45] Kidmo, D.K., Danwe, R., Doka, S.Y., Djongyang, N.: Statistical analysis of wind speed distribution based on six Weibull methods for wind power evaluation in Garoua, Cameroon. *Revue des Energies Renouvelables*. **18**, 105-125 (2015).
- [46] Jiang, Y., Yuan, X., Cheng, X., Peng, X.: Wind potential assessment using the Weibull model at the Inner Mongolia of China. *Energy Explor. Exploit.* **24**, 211-221 (2006).
- [47] Afungchui, D., Aban, C.E.: Analysis of wind regimes for energy estimation in Bamenda, of the North West Region of Cameroon, based on the Weibull distribution. *Revue des Energies Renouvelables*. **17**, 137-147 (2014).
- [48] Mahmood, F.H., Resen, A.K., Khamees, A.B.: Wind characteristic analysis based on Deibull distribution of Al-Salman site, Iraq. *Energy Rep.* **6**, 79-87 (2020).
- [49] Kaoga, D.K., Raidandi, D., Djongyang, N., Doka S.Y.: Comparison of five numerical methods for estimating Weibull parameters for wind energy applications in the district of Kousseri, Cameroon. *Asian Journal of Natural and Applied Sciences*, **3**, 72-87 (2014).
- [50] Badawi, A.S.A., Hasbullaha, N.F., Yusoff, S.H., Khan, S., Hashim, A., Zyoud, A., Elamassie, M.: Weibull probability distribution of wind speed for Gaza Strip for 10 years. *Appl. Mech. Mater.* **892**, 284-291 (2019).
- [51] Dokur, E., Kurban, M.: Wind speed potential analysis Based on Weibull Distribution. *J. Electr. Comput. Eng.* **3**, 231-235 (2015).
- [52] Takase, M., Kipkoech R., Essandoh P.K.: A comprehensive review of energy scenario and sustainable energy in Kenya. *Fuel Communications*. **7**, 1-19 (2021).
- [53] George, S.O., George, H.B., Ph, D., Nguyen, S. V, Ph, D.: Effect of wind intermittency on the electric grid: Mitigating the risk of energy Deficits. (2007).
- [54] Ren, G., Liu, J., Wan, J., Guo, Y., Yu, D.: Overview of wind power intermittency: Impacts, measurements, and mitigation solutions. *Appl. Energy*. **204**, 47-65 (2017).
- [55] Ren, G., Wan, J., Liu, J., Yu, D., Wan, J., Liu, J., Yu, D.: Analysis of wind power intermittency based on historical wind power data. *Energy*. **150**, 482-492 (2018).

- [56] Rahimi, E., Rabiee, A., Aghaei, J., Muttaqi, K.M., Esmael, A.: On the management of wind power intermittency. *Renew. Sustain. Energy Rev.* **28**, 643-653 (2013).
- [57] Qin, S., Liu, F., Wang, J., Song, Y.: Interval forecasts of a novelty hybrid model for wind speeds. *Energy Rep.* **1**, 8-16 (2015).
- [58] Fathima, A.H., Palanisamy, K.: Energy storage systems for energy management in distributed generation systems. (2016).
- [59] Hao, Y., Tian, C.: A novel two-stage forecasting model based on error factor and ensemble method for multi-step wind power forecasting. *Appl. Energy.* **238**, 368-383 (2019).
- [60] Tesfaye, A.: Short-term wind power forecasting using artificial neural networks for resource scheduling in microgrids. *Int. J. Appl. Sci. Eng.* **5**, 144-151 (2016).
- [61] Didane, D.H., Rosly, N., Zulkafli, M.F., Shamsudin, S.S.: Evaluation of wind energy potential as a power generation source in Chad. *Int. J. Rotating Mach.* **2017**, 1-11 (2017).
- [62] Arreyndip, N.A., Joseph, E., David, A.: Wind energy potential assessment of Cameroon's coastal regions for the installation of an onshore wind farm. *Heliyon.* **2**, 1-11 (2016).
- [63] Brahmi, N., Charfi, S., Chaabene, M.: Wind potential assessment for an efficient wind farm sizing. *Wind Eng.* **41**, 1-17 (2017).
- [64] Narayana, M., Putrus, G., Jovanovic, M., Leung, P.S.: Predictive control of wind turbines by considering wind speed forecasting techniques. *Proc. 44th International Universities Power Engineering Conference*, Iasgow, UK 1-4 September (2009).
- [65] Cheng, H., Tan, P., Gao, J., Scripps, J.: Multistep-ahead time series prediction. (2006).
- [66] Chang, W.: A literature Review of Wind Forecasting Methods. *J. Power Energy Eng.* **2**, 161-168 (2014).
- [67] Lange, M., Focken, U.: Physical approach to short-term wind power prediction. *Renewable and Green Energy.* **6**, 1-214 (2006).
- [68] Li, L., Liu, Y.Q., Yang, Y.P., Han, S., Wang, Y.M.: A physical approach of the short-term wind power prediction based on CFD pre-calculated flow fields. *J. Hydrodyn.* **25**, 5661 (2013).

- [69] Alonzo, B., Plougonven, R., Mougeot, M., Fischer, A.: From Numerical Weather Prediction outputs to accurate local surface wind speed: statistical modeling and forecasts. *Renewable Energy: Forecasting and Risk Management*. **11**, 23-44 (2017).
- [70] Hai, Z., Xiang, Z., Lawan, S.M., Azlan, W., Abidin, W.Z., Abubakar, U., Datasets, D.D., Near, P.S.: Multi-step ahead method for wind speed prediction correction based on numerical weather prediction and historical measurement data. *J. Phys. Conf. Ser.* **926**, 180-191 (2018).
- [71] Pearre, N.S., Swan, L.G.: Statistical approach for improved wind speed forecasting for wind power production. *Sustain. Energy Technol. Assessments*. **27**, 180-191 (2018).
- [72] Salfate, I., Lépez-caraballo, C.H., Sabn-sanjulin, C., Lazzs, J.A., Vega, P., Cuturrufo, F., Marn, J.: 24-hours wind speed forecasting and wind power generation in La Serena (Chile). *Wind Eng.* **42**, 1-17 (2018).
- [73] Tian, Z., Wang, G., Ren, Y.: Short-term wind speed forecasting based on autoregressive moving average with echo state network compensation. *Wind Eng.* **44**, 152-167 (2020).
- [74] Bracale, A., De Falco, P.: An advanced bayesian method for short-term probabilistic forecasting of the generation of wind power. *Energies*. **8**, 10293-10314 (2015).
- [75] Salama, M.M.A.: Grey Predictor for wind energy conversion systems output power prediction. *IEEE Trans. Power Syst.* **21**, 1450-1452 (2006).
- [76] Cadenas, E., Jaramillo, O.A., Rivera, W.: Analysis and forecasting of wind velocity in Chetumal, Quintana Roo, using the single exponential smoothing method. *Renew. Energy*. **35**, 925-930 (2010).
- [77] Verdejo, H., Awerkin, A., Saavedra, E., Kliemann, W., Vargas, L.: Stochastic modeling to represent wind power generation and demand in electric power system based on real data. *Appl. Energy*. **173**, 283-295 (2016).
- [78] Bivona, S., Bonanno, G., Burlon, R., Gurrera, D., Leone, C.: Stochastic models for wind speed forecasting. *Energy Convers. Manag.* **52**, 1157-1165 (2011).
- [79] Zárata-miano, R., Anghel, M., Milano, F.: Continuous wind speed models based on stochastic differential equations. *Appl. Energy*. **104**, 42-49 (2013).
- [80] Kloppenborg, J.: Probabilistic forecasts of wind power generation by stochastic differential equation models. *Proc. 59th World Statistics Congress, Hong Kong 25-30 August* (2013).

- [81] Mangalova, E., Shesterneva, O.: K-nearest neighbors for GEFCom2014 probabilistic wind power forecasting. *Int. J. Forecast.* **32**, 1067-1073 (2016).
- [82] Iversen, E.B., Morales, J.M., Moller, J.K., Madsen, H.: Short-term probabilistic forecasting of wind speed using stochastic differential equations. *Int. J. Forecast.* **32**, 981-990 (2016).
- [83] Damousis, I.G., Alexiadis, M.C., Theocharis, J.B., Dokopoulos, P.S.: A fuzzy model for wind speed prediction and power generation in wind parks using spatial correlation. *IEEE Trans. Energy Convers.* **19**, 352-361 (2004).
- [84] Mohandes, M.A., Halawani, T.O., Rehman, S., Hussain, A.A.: Support vector machines for wind speed prediction. *Renew. Energy.* **29**, 939-947 (2004).
- [85] Aoife, M., Paul, G., Eamon, J.: Current methods and advances in forecasting of wind power generation. *Renew. Energy.* **37**, 1-8 (2012).
- [86] Donadio, L., Fang, J., Port-Agel, F.: Numerical weather prediction and artificial neural network coupling for wind energy forecast. *Energies.* **14**, 1-16 (2021).
- [87] Kalogirou, S.A., Arzu, S.: Artificial intelligence techniques in solar energy applications. *Handbook of Research on Solar Energy Systems and Technologies.* (2013).
- [88] Krenker, A., Beter, J., Kos, A.: Introduction to the artificial neural networks. (2016).
- [89] Awodele, O., Jegede, O.: Neural networks and its application in engineering. *Proc. Informing Science and IT Education Conference, Macon, GA, USA 9-11 July* (2009).
- [90] Sazli, M.H.: A brief review of feed-forward neural networks. *Commun. Fac. Sci. Univ. Ankara.* **50**, 11-17 (2006).
- [91] Jasim Saud, L., Kudair Abass, Z.: A Comparison between multi-layer perceptron and radial basis function networks in detecting humans based on object shape. *J. Pure Appl. Sci.* **31**, 210-221 (2018).
- [92] Bharitkar, S., Mendel, J.M.: The hysteretic Hopfield neural network. *IEEE Trans. Neural Networks.* **11**, 879-888 (2000).
- [93] Boussaada, Z., Curea, O., Remaci, A., Camblong, H., Bellaaj, N.M.: Daily direct solar radiation. *Energies.* **11**, 1-21 (2018).
- [94] Sherstinsky, A.: Fundamentals of recurrent neural network and long short-term memory network. *Phys. D.* **404**, 1-28 (2020).

- [95] Le, X.H., Ho, H.V., Lee, G., Jung, S.: Application of long short-term memory network for flood forecasting. *Water*. **11**, 1-19 (2019).
- [96] Uddin, S., Khan, A., Hossain, M.E., Moni, M.A.: Comparing different supervised machine learning algorithms for disease prediction. *BMC Med. Inform. Decis. Mak.* **19**, 1-16 (2019).
- [97] Ki, O., Uncuo, E.: Comparison of three back-propagation training algorithms for two case studies. *Indian J. Eng. Mater. Sci.* **12**, 434-442 (2005).
- [98] Littman, M.L.: Reinforcement learning improves behaviour from evaluative feedback. *Nature*. **521**, 445-451 (2015).
- [99] Kumar, N., Kaur, G.: Wind speed prediction using neural network. *Int. J. Adv. Ind. Eng.* **608**, 36-41 (2017).
- [100] Singh, V.: Application of artificial neural networks for predicting generated wind power. *Int. J. Adv. Comput. Sci. Appl.* **7**, 250-253 (2016).
- [101] Cadenas, E., Rivera, W., Campos-Amezcu, R., Cadenas, R.: Wind speed forecasting using the NARX model, case: La Mata, Oaxaca, México. *Neural Comput. Appl.* **27**, 2417-2428 (2016).
- [102] Cadenas, E., Rivera, W.: Short term wind speed forecasting in La Venta, Oaxaca, using artificial neural networks. *Renew. Energy*. **34**, 274-278 (2009).
- [103] Dumitru, C.D., Gligor, A.: Daily average wind energy forecasting using artificial neural networks. *Procedia Eng.* **181**, 829-836 (2017).
- [104] Shekhawat, A.S.: Wind power forecasting using artificial neural networks *Int. J. Eng. Res.* **3**, 1-12 (2014).
- [105] Kurková, V.: Kolmogorov's theorem and multilayer neural networks. *Neural Networks*. **5**, 501-506 (1992).
- [106] Katoch, S., Chauhan, S.S., Kumar, V.: A review on genetic algorithm: past, present, and future. *Multimed. Tools. Appl.* **80**, 1-36 (2021).
- [107] Yang, X.S.: Bat algorithm for multi-objective optimisation. *Int. J. Bio-Inspired Comput.* **3**, 267-274 (2011).
- [108] Di Piazza, A., Di Piazza, M.C., Vitale, G.: Solar and wind forecasting by NARX neural networks. *Renew. Energy Environ. Sustain.* **39**, 1-5 (2016).

- [109] Wang, J., Heng, J., Xiao, L., Wang, C.: Research and application of a combined model based on multi-objective optimization for multi-step ahead wind speed forecasting. *Energy*. **125**, 591-613 (2017).
- [110] Pratheepraj, E., Abraham, A., Deepa, S.N., Yuvaraj, V.: Very short term wind power forecasting using PSO-neural network hybrid system. *Commun. Comput. Inf. Sci.* **192**, 503-511 (2011).
- [111] Crone, S.F., Kourentzes, N.: Input-variable specification for neural networks, an analysis of forecasting low and high time series frequency. *Proc. International Joint Conference on Neural Networks, Atlanta, GA, USA 14-19 June* (2009).
- [112] Dragomiretskiy, K., Zosso, D.: Variational mode decomposition. *IEEE Trans. Signal Process.* **62**, 531-544 (2014).
- [113] Ge, H., Chen, G., Yu, H., Chen, H., An, F.: Theoretical analysis of empirical mode decomposition. *Symmetry*. **10**, 1-18 (2018).
- [114] Hosseini, H.: Singular Spectrum Analysis: Methodology and comparison. *J. Data Sci.* **5**, 239-257 (2007).
- [115] Wang, S., Zhang, N., Wu, L., Wang, Y.: Wind speed forecasting based on the hybrid ensemble empirical mode decomposition and GA-BP neural network method. *Renew. Energy*. **94**, 629-636 (2016).
- [116] Zhang, G., Liu, H., Zhang, J., Yan, Y., Zhang, L., Wu, C., Hua, X., Wang, Y.: Wind power prediction based on variational mode decomposition multi-frequency combinations. *J. Mod. Power Syst. Clean Energy*. **7**, 281-288 (2019).
- [117] Badrul, N., Mat, L., Shamshirband, S., Petkovic, D.: Sensorless estimation of wind speed by adaptive neuro-fuzzy methodology. *Int. J. Electr. Power Energy Syst.* **62**, 490-495 (2014).
- [118] Moreno, S.R., dos Santos Coelho, L.: Wind speed forecasting approach based on singular spectrum analysis and adaptive neuro fuzzy inference system. *Renew. Energy*. **126**, 736-754 (2018).
- [119] Jian, J.: A hybrid forecasting method for wind speed. *Proc. 2nd International Conference on Electronic Information Technology and Computer Engineering, Shanghai University of Engineering Science, China 12 October* (2018).
- [120] Goncalves, D.E.P., Fernandes, C.M.C.G., Martins, R.C., Seabra, J.H.O.: Torque loss in a gearbox lubricated with wind turbine gear oils. *Lubr. Sci.* **25**, 297-311 (2013).

- [121] McFadden, S., Basu, B.: Wind turbine gearbox design with drivetrain dynamic analysis. **22**, 137-158 (2016).
- [122] Dynamic, S., Al-hamadani, H., An, T., King, M., Long, H.: System dynamic modelling of three different wind turbine gearbox designs under transient loading conditions. *Int. J. Precis. Eng. Manuf.* **18**, 1659-1668 (2017).
- [123] Ragheb, A.M., Ragheb, M.: Wind turbine gearbox technologies. Proc. 1st International Nuclear and Renewable Energy Conference, Mman, Jordan 21-24 March (2010).
- [124] Fernandes, C.M.C.G., Marques, P.M.T., Martins, R.C., Seabra, J.H.O.: Gearbox power loss. Part I: Losses in rolling bearings. *Tribology Int.* **88**, 1-11 (2015).
- [125] Seetharaman, S., Kahraman, A.: Load-independent spin power losses of a spur gear pair: Model formulation. *J. Tribol.* **131**, 1-11 (2009).
- [126] Diab, Y., Ville, F., Velex, P., Chagnenet, C.: Windage losses in high speed gears-preliminary experimental and theoretical results. *J. Mech. Des. Trans.* **126**, 903-908 (2004).
- [127] Jurkschat, T., Lohner, T., Stahl, K.: Improved calculation of load-dependent gear losses by consideration of so far disregarded influences. *Proc. Inst. Mech. Eng. Part J. J. Eng. Tribol.* **233**, 509-519 (2019).
- [128] Balan, M.R.D., Stamate, V.C., Houpert, L., Olaru, D.N.: The influence of the lubricant viscosity on the rolling friction torque. *Tribol. Int.* **72**, 1-12 (2014).
- [129] Harris, T.A., Anderson, W.J.: Rolling Bearing Analysis. *J. Lubr. Technol.* **89**, 521-521 (1967).
- [130] Stokes, D.C.L.: On the theory of lubrication. *Proceedings of the Royal Society of London.* **197**, 191-203 (1886)
- [131] Fernandes, C.M.C.G.: Power loss in rolling bearings and gears lubricated with wind turbine gear oils. PhD thesis, Universidade Do Porto. (2015).
- [132] Anderson, W.J., Ludwig, L.P.: Bearing and seal technology. (2002).
- [133] Höhn, B.R., Michaelis, K.: Influence of oil temperature on gear failures. *Tribol. Int.* **37**, 103-109 (2004).
- [134] Marques, P.M.T., Fernandes, C.M.C.G., Martins, R.C., Seabra, J.H.O.: Tribology International Power losses at low speed in a gearbox lubricated with wind turbine gear oils with special focus on churning losses. *Tribology Int.* **62**, 186-197 (2013).

- [135] Michaelis, K., Michael, B.H., Hinterstoier, M.: Influence factors on gearbox power loss. *Ind. Lubr. Tribol.* **63**, 46-55 (2011).
- [136] Schlegel, C., Hösl, A., Diel, S.: Detailed loss modelling of vehicle gearboxes. *Proc. 7th Conference, Como, Italy 20-22 September (2009)*.
- [137] Edinger, T., Edinger, T.: *General Catalogue*. (1975).
- [138] N.T.N.: *Rolling Bearings Handbook*.
- [139] NSK: *Technical Repor CAT. No. E728g*. (2013).
- [140] Fernandes, C.M.C.G., Marques, P.M.T., Martins, R.C.: Influence of gear loss factor on the power loss prediction. *echanisms and Machine Science.* **24**, 81-88 (2014).
- [141] Kugiumtzis, D., Tsimpiris, A., Connectivity, B.: Measures of analysis of time Series (MATS): A MATLAB toolkit for computation of multiple measures on time series data Bases. *J. Stat. Softw.* **33**, 1-25 (2010).
- [142] Fana, F., Wanga, J., Gangb, W., Li, S.: Assessment of deep recurrent neural network-based strategies for short-term building energy predictions. *Appl. Eenergy.* **236**, 700-710 (2018).
- [143] Chang, G.W., Lu, H.J., Chang, Y.R., Lee, Y.D.: An improved neural network-based approach for short-term wind speed and power forecast. *Renew. Energy.* **105**, 301-311 (2017).
- [144] Mijanur Rahman, M., Akter Setu T.: An implementation for combining neural networks and genetic algorithms. *Int. j. comput. sci. inf. technol.* **6**, 1-22 (2015).
- [145] Moreno, S.R., Coelho, S.: Wind speed forecasting approach based on Singular Spectrum Analysis and Adaptive Neuro Fuzzy Inference System. *Renew. Energy.* **126**, 736-754 (2018).
- [146] Chen, H., Wan, Q., Wang, Y.: Refined Diebold-Mariano Test methods for the evaluation of wind power forecasting models. *Energies.* **7**, 4185-4198 (2014).
- [147] Xiao, L., Shao, W., Yu, M., Ma, J., Jin, C.: Research and application of a hybrid wavelet neural network model with the improved cuckoo search algorithm for electrical power system forecasting. *Appl. Energy.* **198**, 203-222 (2017).
- [148] Wang, J., Heng, J., Xiao, L., Wang, C.: Research and application of a combined model based on multi-objective optimization for multi-step ahead wind speed forecasting. *Energy.* **125**, 591-613 (2017).

-
- [149] Fernandes, C.M.C.G., Marques, P.M.T., Martins, R.C., Seabr, J.H.O.: Film thickness and traction curves of wind turbine gear oils. *Tribology Int.* **86**, 1-9 (2015).
- [150] Mathew, S.: *Electric Renewable Energy Systems*. (2017).
- [151] Bakirci, M., Yilmaz, S.: Theoretical and computational investigations of the optimal tip-speed ratio of horizontal-axis wind turbines. *Int. J. Eng. Sci. Technol.* **21**, 1128-1142 (2018).
- [152] Kadhem, A.A., Izzri, N., Wahab, A., Aris, I., Jasni, J., Abdalla, A.N.: Advanced wind speed prediction model based on a combination of weibull distribution and an artificial neural network. *Energies.* **10**, 1-17 (2017).

List of Publications

1- **Hervice Roméo Fogno Fotso**, Claude Vidal Aloyem Kazé and Germaine Djuidje Kanmoé: Optimal input variables disposition of artificial neural networks models for enhancing time series forecasting accuracy. *Applied Artificial Intelligence* **34**, 1-24 (2020).

2- **Hervice Roméo Fogno Fotso**, Claude Vidal Aloyem Kazé and Germaine Djuidje Kanmoé: A novel hybrid model based on weather variables relationships improving applied for wind speed forecasting. *International Journal of Energy and Environmental Engineering* 1-14 (2021).

3- **Hervice Roméo Fogno Fotso**, Claude Vidal Aloyem Kazé and Germaine Djuidje Kanmoé: Real-time rolling bearing power loss in wind turbine gearbox modeling and prediction based on calculations and artificial neural network. *Tribology International* **163**, 1-10 (2021).

4- Germaine Djuidje Kanmoé, **Hervice Roméo Fogno Fotso** and Claude Vidal Aloyem Kazé: Comparative models for multi-step ahead wind speed forecasting applied for expected wind turbine power output prediction. *Wind Engineering* 1-16 (2021).



Optimal Input Variables Disposition of Artificial Neural Networks Models for Enhancing Time Series Forecasting Accuracy

Hervice Roméo Fogno Fotso , Claude Vidal Aloyem Kazé & Germaine Djuidje Kenmoe

To cite this article: Hervice Roméo Fogno Fotso , Claude Vidal Aloyem Kazé & Germaine Djuidje Kenmoe (2020): Optimal Input Variables Disposition of Artificial Neural Networks Models for Enhancing Time Series Forecasting Accuracy, Applied Artificial Intelligence, DOI: [10.1080/08839514.2020.1782003](https://doi.org/10.1080/08839514.2020.1782003)

To link to this article: <https://doi.org/10.1080/08839514.2020.1782003>



Published online: 24 Jun 2020.



Submit your article to this journal [↗](#)



View related articles [↗](#)



View Crossmark data [↗](#)



Optimal Input Variables Disposition of Artificial Neural Networks Models for Enhancing Time Series Forecasting Accuracy

Hervice Roméo Fogno Fotso^a, Claude Vidal Aloyem Kazé^b,
and Germaine Djuidje Kenmoe^a

^aLaboratory of Mechanics, Department of Physics, University of Yaoundé I, Yaoundé, Cameroon;

^bDepartment of Electrical and Power Engineering, HTTTC, University of Bamenda, Bamenda, Cameroon

ABSTRACT

Artificial Neural Networks (ANNs) models play an increasingly significant role in accurate time series prediction tools. However, an accurate time series forecasting using ANN requires an optimal model. Hence, great forecasting methods have been developed from optimized ANN models. Most of them focus more on input variables selection and preprocessing, topologies selection, optimum configuration and its associated parameters regardless of their input variables disposition. This paper provides an investigation of the effects of input variables disposition on ANNs models on training and forecasting performances. After investigation, a new ANNs optimization approach is proposed, consisting of finding optimal input variables disposition from the possible combinations. Therefore, a modified Back-Propagation neural networks training algorithm is presented in this paper. This proposed approach is applied to optimize the feed-forward and recurrent neural networks architectures; both built using traditional techniques, and pursuing to forecast the wind speed. Furthermore, the proposed approach is tested in a collaborative optimization method with single-objective optimization technique. Thus, Genetic Algorithm Back-Propagation neural networks aim to improve the forecasting accuracy relative to traditional methods was proposed. The experiment results demonstrate the requirement to take into consideration the input variables disposition to build a more optimal ANN model. They reveal that each proposed model is superior to its old considered model in terms of forecasting accuracy and thus show that the proposed optimization approach can be useful for time series forecasting accuracy improvement.

ARTICLE HISTORY

Introduction

In many domains of engineering (Feng, Zhou, and Dong 2019; Shahrul et al. 2018) climatology (Sher and Messori 2019), demography (Folorunso et al. 2010), Chemistry (Damir, Ricardo, and Aznarte 2019), finance (Soui

et al. 2019) (Wang, Huang, and Wang 2012), mechanics (Alevizakou, Siolas, and Pantazis 2018), energy (Kuo and Huang 2018a), and many more, there is the common necessity of accurate forecasting the future evolution of an activity through past measurements of it. Hence, several ideas of forecasts in order to improve the Time Series Forecasting (TSF) accuracy have been explored widely (Mendes Dantas and Cyrino Oliveira 2018). Artificial Intelligent (AI), especially the Artificial Neural Networks (ANNs) are widely used and demonstrated to have powerful for stochastic systems modeling and TSF, and easy implementation and combination with others in a different way compared with other existing forecasting tools (Kuo and Huang 2018a, 2018b). An accurate TSF requires an optimal ANN model based. These optimal models are commonly achieved by modifying the ANN learning paradigm and parameters such as nodes, weights, activation functions, and structures (Crone and Kourentzes 2009).

Nowadays, several efforts have been made in the development and applications of ANNs, mainly oriented toward the improvement of their optimization-based TSF. These existing optimization approaches are based on optimal parameters and minimum model structure of neural networks (Reza Loghmanian et al. 2012; Zongyan and Best 2015). The time-series input variables represent an external parameter of an ANN architecture. They are commonly collected at a different order of magnitude and relations with the target variable. Great publications have shown the adequate input variables as one of the most important parameters for an optimal ANN and accurate TSF (Crone and Kourentzes 2009). They influence the forecasting accuracy through the number of nodes, the length and the relation between them, and each of them and target (Wei, Yoshiteru, and Shouyang 2004). However, the optimal ANNs architectures have not been analyzed regarding their input variables disposition adequacy in TSF accuracy. Wei et al. (Wei, Yoshiteru, and Shouyang 2004) presented a general approach to determine the input variables of ANNs models for TSF. The proposed approach was based on autocorrelation criterion used to measure the degree of correlation between the neighboring time-series data used as input variables of feed-forward neural networks. Furthermore, Sovann et al. (Sovann, Nallagownden, and Baharudin 2014) proposed a method to determine the input variables for the ANN model; Autocorrelation, partial autocorrelation, and cross-correlation are used to measure the correlated input variables with target variable to increase the accuracy of Multilayer Perceptron neural networks architecture based on electrical load demand prediction. Yaïci et al. (Yaïci et al. 2017) studied the effect of reduced inputs of ANNs on the predictive performance of the solar energy system. The results of study show that the degree of feed forward predicting model accuracy would gradually decrease with reduced input variables number. Moreover, there is a great work proposed in the literature which used various types of optimization techniques and algorithm to determine the

optimal ANN models and combined models for accurate TSF improvement applied in many domains. Among the most prominent techniques is the Single-Objective optimization technique such as Evolutionary Algorithm, and Genetic Algorithm (Hassan and Hamada 2018; Loghmanian, Ahmad, and Jamaluddin 2009). Piazza et al. (Di Piazza, Di Piazza, and Vitale 2016) combined Genetic Algorithm (GA) and Optimal Brain Surgeon (OBS) strategy to determine the optimal nonlinear autoregression with exogenous input neural networks architecture to forecast wind speed and solar radiation. The optimization techniques of developed neural networks were based on optimal hidden neurons, biases, and weights determination. Therefore, it can be noticed that the optimization techniques of ANNs architectures based on accurate TSF presented in the literature have been limited on optimal input nodes, hidden nodes and weight, learning paradigm and so on, regardless of the input variables disposition. Unlike the traditional optimal input variables of an ANN determination method, the purpose of this study is to quantify the optimal disposition of input variables for an optimal ANN model based on accurate TSF.

The environmental problems, such as climate change, pollution, and global warming from the human activities reduce the development of sources of renewable energy in replacing the polluting sources as fossil fuels energy (Kuo and Huang 2018a, 2018b; Yaïci et al. 2017). Furthermore, the electricity demand and water pumping are steadily increasing as a consequence of world population growth throughout the world (Kuo and Huang 2018a). The sources of green energy such as wind energy potential are free and available in any part of the world, which give a great alternative in terms of electricity production and water pumping. As many sources of renewable energy, wind energy is an intermittent source of energy due to the random fluctuation of wind, since the generated power from a wind energy conversion system has an intimate relationship with the curve of wind speed. Wind speed could be easily influenced by obstacle and terrain (Jursa and Rohrig 2008; Kadhem et al. 2017; Sanchez 2006). Also, it varies from site to site and from height to height. Therefore, accurate wind speed forecasting is required for the wind energy integration (Kadhem et al. 2017; Shen, Wang, and Chen 2018). This will help the electrical production units decentralization and producers take decisions in order of energy production assessment, planning, and management. The recent researches have shown that the ANN model is good at nonlinear modeling and TSF of the stochastic nature of wind speed (Shen, Wang, and Chen 2018).

This work aims at investigating the effect of Input Variables Disposition (IVD) of two ANNs architectures in order to determine their optimal models pursuing to the horizontal TSF. Feed-forward and nonlinear autoregression with exogenous input neural networks were developed using the optimization method given in the literature: the Kolmogorov's theorem is used to determine

the number of hidden nodes and the autocorrelation method was used to select a large number of input nodes. The arrangement formula was applied to determine the number of models of each neural networks architecture through their IVD. A modified Back-Propagation neural networks (BPNN) training algorithm is proposed in this paper, by taking into consideration the IVD. This proposed optimization approach is able to be used in every method using ANN as an old Back-Propagation approach. Thus, it was tested in combining Genetic Algorithms with neural networks to the weighted update. The optimal IVD was provided through the better forecasting performance of the optimized ANN model. The paper is organized as follows: [Section 2](#) provides a description of both ANNs architectures designing, optimization, and models construction based on TSF. The framework of effects of the IVD on neural networks performances investigation is given in [Section 3](#). [Section 4](#) presents the details of the proposed neural networks optimization approach. The results of the study of the effects of the IVD investigation and the forecasting results of the proposed ANNs models and comparison models are presented and discussed in [Section 5](#). In [Section 6](#), relevant conclusions are drawn based on the results achieved from the study case.

Related Forecasting Methodology

Neural Networks and TSF

The TSF is a process which consists of estimating the future value of an activity over time (Alevizakou, Siolas, and Pantazis 2018). To handle TSF, broad methods have been developed. These methods can be broadly classified into physical, statistical, and hybrid (Jursa and Rohrig 2008; Kadhem et al. 2017). Physical method aims by physical consideration, in other words, this method uses the mathematical population modeling, while the statistical method process works by finding the relationship between the measured populations. A hybrid method combines two different methods in order to obtain a globally optimal forecasting performance (Zhang et al. 2017). In recent years, the statistical methods based on ANNs are catching researcher's attention. Nowadays, ANNs are the most TSF tools used in different fields due to their higher forecasting performance, capacity, flexibility, and robustness (Gogas, Papadimitriou, and Agrapetidou 2018; Kuo and Huang 2018b).

ANN is an information processing structure inspired by human nervous systems (Kuo and Huang 2018b). It consists of networks of many simple units, neurons, operating in parallel which the commonly used have three layers, one input layer, one or more hidden layers, and one output layer (Kuo and Huang 2018a; Yaïci et al. 2017). An ANN learns from given sample examples, by constructing the relationship between input and target variables (Cervone et al. 2017). This process helps to update the synaptic weights of the

connections between nodes. As the learning processes, the ANNs can differ through their structures, also called architectures (State, Uyo, and Offiong 2016). The widely ANNs architectures used in TSF can be classified into static and dynamic neural networks.

Static Neural Networks

The Feedforward Neural Networks (FFNN) also called static neural networks allow information to travel only from input to output. There is no feedback and memory. FFNN tend to be a straightforward network that associates inputs with outputs. The Multilayer Perceptron's with FFNN architecture is more used in many different types of applications (Kuo and Huang 2018a). Its greatest strength is in non-linear solutions to ill-defined problems (Crone and Kourentzes 2009). Figure 1 illustrates the architecture of an FFNN with one hidden layer, yellow, intended to the TSF.

From Figure 1, the input layer, black, is made of N nodes, $[x_1(t), x_2(t), \dots, x_N(t)]$, constituting the number of past data used as input variables of ANN, hidden layer has M nodes, yellow, and output layer have only one node, purple constructing the forecasting variable. t represents the sample time steps. The output of the hidden layer is calculated as follows:

$$h_i(t) = f\left(\sum_k^N w_{k,i} \cdot x_k(t) - b_i\right), k = 1, 2, \dots, N, i = 1, 2, \dots, M \quad (1)$$

where $h_i(t)$ is the output of the node of the hidden layer at a time step t , $w_{k,i}$ is the connection parameter, synaptic weight, between the k node of the input layer and the i node of the hidden layer, b_i is bias of the i node of the hidden

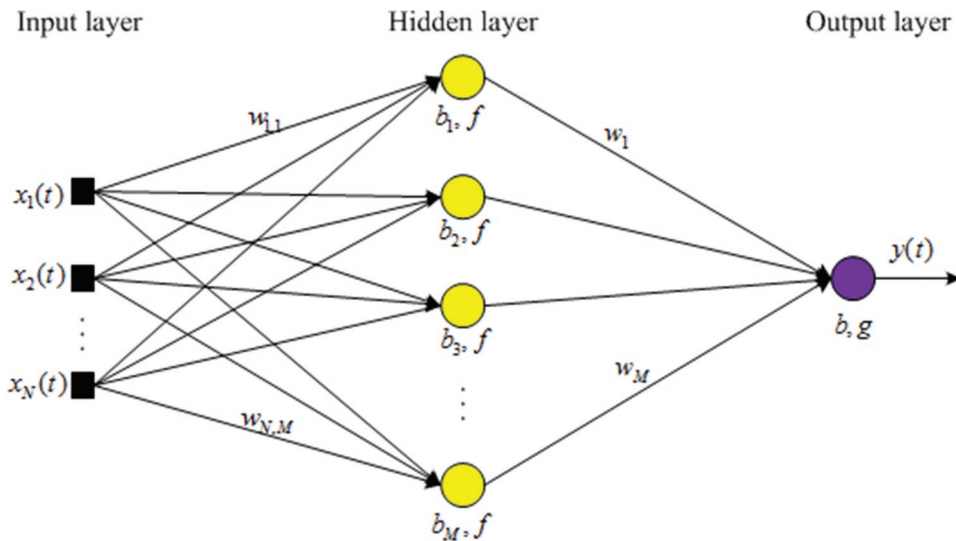


Figure 1. FFNN architecture intended to the TSF.

layer and f is the activation function used in each node of the hidden layer. The evaluation of the forecasting variable at the output layer is expressed as follows:

$$y(t) = g \left(\sum_i^M w_{i,y} \cdot h_i(t) - b_y \right), i = 1, 2, \dots, M \quad (2)$$

where $y(t)$ is the forecasting variable at a time step t at the output layer, $w_{i,y}$ is the synaptic weight which connects the i node of the hidden layer and the alone node of the output layer, b_y and g are the bias and activation function, respectively, of the output node.

Then, the forecasting variable from the developed FFNN is finally designed as

$$y(t) = g \left[\sum_i^M w_{i,y} \cdot f \left(\sum_k^N w_{k,i} \cdot x_k(t) - b_i \right) - b_y \right] \quad (3)$$

where the optimal N and M are set in [subsection 2.2](#), in response to the FFNN structure optimization.

Dynamic Neural Networks

Contrary to the previous FFNN structure, the second ANN architecture, Feedback neural networks also called Recurrent Neural Networks (RNN), or dynamic neural networks have signals traveling in both directions by introducing loops in the network (State, Uyo, and Offiong 2016). Consequently, an internal state of the RNN is created displaying a dynamic temporal behavior. The dynamic driven RNN called Nonlinear Autoregressive with exogenous inputs Neural Networks (NARX NN) is well suited to learn nonlinear dynamic systems or time-series relationships (Di Piazza, Di Piazza, and Vitale 2016). A NARX NN is a RNN with global feedback coming only from the output layer rather than by the hidden states. It consists of an FFNN which takes as inputs a window of past independent (exogenous inputs) and past outputs (endogenous inputs), and determines the current output (Zongyan and Best 2015). So, only the output of NARX NN is fed back to the FFNN. NARX NN architecture exists in open-loop and closed-loop (Di Piazza, Di Piazza, and Vitale 2016). [Figure 2](#) presents the NARX NN architectures aimed to the TSF.

NARX NN is designed as a class of discrete-time nonlinear systems and can be expressed mathematically as follows (Di Piazza, Di Piazza, and Vitale 2016):

$$\begin{aligned} y(t) &= \Gamma[y(t); x_1(t); x_2(t); \dots x_N(t)] \\ &= \Gamma[y(t-1), y(t-2), \dots, y(t-u_y); x_1(t), x_1(t-1), \dots, x_1(t-u_{x_1}); x_2(t), x_2(t-1), \dots, x_2(t) \\ &\quad x_N(t), x_N(t-1), \dots, x_N(t-u_{x_N})] \end{aligned} \quad (4)$$

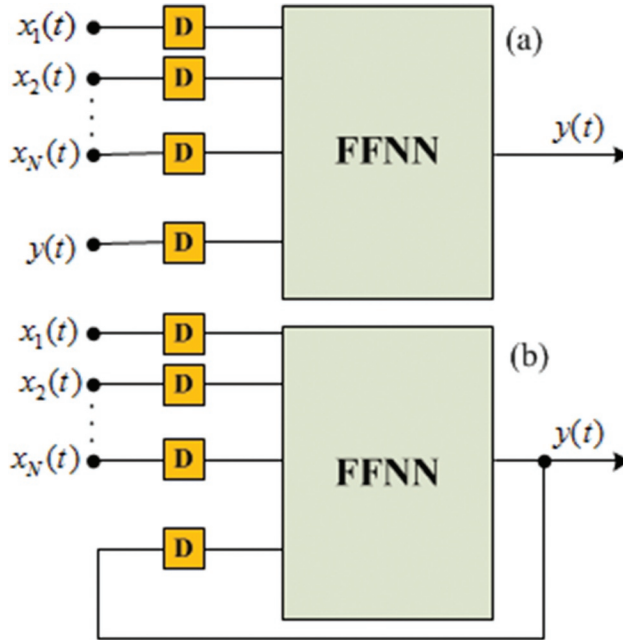


Figure 2. NARX NN architecture based on TSF: open-loop (a) and closed-loop (b).

where $y(t)$ is the current output, endogenous input, and $x_1(t), x_2(t), \dots, x_N(t)$ are the exogenous inputs at a time step t , D is the time delay line, f is an unknown mapping nonlinear function, and $u_y \geq 1, u_{x_1} = u_{x_2} = \dots = u_{x_N}$ are the inputs and output memory orders.

Neural Networks Models Optimization

Whatever ANN architecture, choosing an appropriate parameter is crucial to build an efficient forecasting model. In order to estimate the optimal FFNN and NARX NN architectures developed in the previous subsection 2.1 based on IVD investigation tested on more wind speed forecasting accuracy in this paper, the optimization methods presented in the literature by various authors were applied in each parameter of the networks. The method of autocorrelation was used to select the optimal input variables of neural networks. Therefore, the Spearman's rank correlation method was applied to determine the relation between past variables (see Table 1) (Upadhyay, Choudhary, and Tripathi 2011). After correlation determination, a maximum of four weather variables were chosen to be used as input variables of both neural networks, Since Yaïci et al. (Yaïci et al. 2017) provide that the forecasting performance of ANNs increases as the number of input nodes increases. Therefore, the past-selected input variables are air temperature (Ta), atmospheric pressure (Pa), relative humidity (RH), and the past wind speed (Ws) is the target of both ANNs. Also, the time step variation (T) is

Table 1. Relations between the actual variables.

	Ws	Ta	Pa	RH	T
Ws	1	0.3119	0.0432	-0.4859	-0.2631
Ta		1	0.2198	-0.5864	0.0175
Pa			1	-0.0761	0.0702
RH				1	-0.0457
T					1

used as the input variable of both ANNs architectures. Wei et al. (Wei, Yoshiteru, and Shouyang 2004) shown that the forecasting accuracy decreases as the training and forecasting data size increases. This criterion of ANNs optimization is not considered in this work. Therefore, a large size of the past data was recorded for 3 months with 10 minute intervals, 10573 datasets in the west region of Cameroon. The used variables for the present work and the results of the coefficient of correlation between them, obtained numerically are presented in Table 1.

Table 1 gives the values of the correlation coefficients between the output variable and each input variable as well as between the input variables themselves. Thus, we can see from Table 1 that there are smaller relations between the input variables and the target variable.

According to the Kolmogorov's theorem applied to determine the optimal number of hidden nodes of both ANNs architectures, for the three-layer neural networks as developed in this work, the number of hidden neurons is recommended as $M = 2N + 1$ (Peng, Liu, and Yang 2013). Therefore, each developed ANN architecture had nine hidden nodes, $M = 9$.

Neural Networks Models Building

We have chosen four variables to use as input variables of optimized static and dynamic neural networks architectures, aimed to better the accurate TSF. To study the influence of the IVD of each developed ANN on the training and TSF performances, we had used the mathematical formula of arrangement to determine the number of possible disposition of the chosen input variables. Thus, the way input variables were disposed defines the neural networks model. It can be expressed by Equation (5):

$$M_o = N! \quad (5)$$

where M_o is the possible number of ANNs models. Therefore, using the four chosen input variables, each of the developed ANNs structures had 24 models, $M_o = 25$ which were trained and tested to forecast one day-ahead of wind speed.

Forecasting Accuracy Evaluation

In order to investigate the performances of forecasting models, three errors criterion were taken into consideration. The Root Mean Square Error (RMSE), expressed as follows:

$$RMSE = \sqrt{\frac{1}{T} \sum_{t=1}^T \left(y(t)_m - y(t)_p \right)^2} \quad (6)$$

was used to measure the efficiency of the developed prediction tools in projecting future individual values. A smaller and more positive RMSE indicates a considerable convergence of the forecasted values and the real values. The Mean Absolute Error (MAE) is used to measure the long-term model forecasting, is defined as:

$$MAE = \frac{1}{T} \sum_{t=1}^T \left| y(t)_m - y(t)_p \right| \quad (7)$$

The Mean Absolute Percentage Error (MAPE) was used to establish the forecasting accuracy. It indicates in percentage the accuracy in fitting time series values in statistics in a particular trend. It is defined by the following equation:

$$MAPE = \frac{1}{T} \sum_{t=1}^T \left| \frac{y(t)_m - y(t)_p}{y(t)_m} \right| \times 100 \quad (8)$$

where $y(t)_m$ and $y(t)_p$ are the real and forecasted values, respectively, at the time step t , and T is the number of time step.

Effects of the IVD on Neural Networks Performances Investigation

Figure 3 indicates the steps followed to evaluate the influence of the IVD on both neural networks structures performances. All the developed ANNs models used the same common parameters. The tangent hyperbolic sigmoid and linear functions are used as activation functions of each hidden node and output node, respectively. The Lavenberg marquardt back-propagation algorithm is used to train the neural networks models following the error detection method. The NARX NN models were trained using its open-loop architecture and the multi-step forecasting was carried out with its closed-loop architecture. Several delays have been tried and the better results from NARX NN models had been achieved with four delays per variable, $D = 4$. Before the training process of neural networks models, the data sets are brought within the same order of magnitude. Thus, every data have been normalized between 0 and 1.

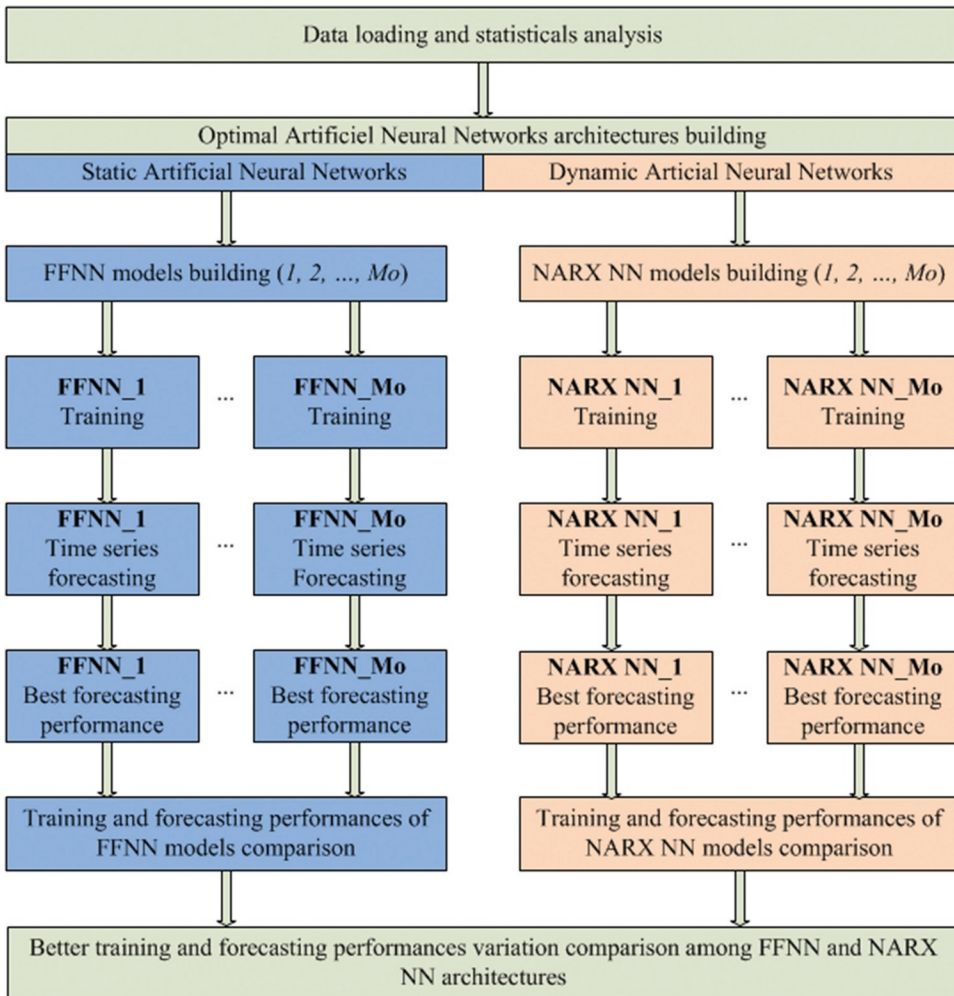


Figure 3. Flowchart of effects of input variables disposition of neural networks investigation.

Proposed Neural Networks Optimization Approach

Algorithm: Proposed neural networks based forecasting approach

Objective:

Minimize the forecasting errors through the optimal input variables of neural network disposition

Inputs:

X – Input variable

X_{tr} – Training input variable

X_s – Validation input variable

X_t – Testing input variable

Outputs:

Y – Forecasting variable

Y_{tr} – Training target variable

Y_s – Validation target variable

Parameters:

N – Number of input variables

(Continued)

Algorithm: Proposed neural networks based forecasting approach

Objective:

Minimize the forecasting errors through the optimal input variables of neural network disposition

Inputs:

X – Input variable

X_{tr} – Training input variable

X_s – Validation input variable

X_t – Testing input variable

Outputs:

Y – Forecasting variable

Y_{tr} – Training target variable

Y_s – Validation target variable

Parameters:

N – Number of input variables

E_{smin} – Minimum validation neural network performances

T_{max} – Maximum retraining iteration

1. $X = [x_1, x_2, \dots, x_N]$

2. Set target into Y_{tr} and Y_s

3. **for** $i = 1$ to $N!$ **do**

4. $X_i = \text{permute}(X_i)$

5. Set X_i into X_{tr} , X_s and X_t

6. Set neural network architecture and parameters

7. **for** $j = 1$ to T_{max} **do**

8. Randomly initialize neural network weights and biases

9. Train neural network model

10. $S_j^i = \text{Simulate}(\text{neural}_n \text{ etwork})$

11. $Es_j^i = \text{errors}(S_j^i, Y_s)$

12. **if** $Es_j^i < E_{smin}$ **then**

13. **break**

14. **end if**

15. **end for**

16. **for** $k = 1$ to $\text{length}(X_t)$ **do**

17. $O_i^k = \text{predict}(\text{neural}_n \text{ etwork}, X_{tr}^k)$

18. **end for**

19. $Ef_i = \text{errors}(O_i^k, Y_f)$

20. **if** $Ef_i < Ef_{i-1}$ **then**

21. $Ef = Ef_i$

22. $Y = O_i^k$

23. **else**

24. $Ef = Ef_{i-1}$

25. $Y = O_i^{k-1}$

26. **end if**

27. **end for**

28. **return** Ef

29. **return** Y

The goal of the proposed approach is to find the optimal IVD for a more optimal neural network solution. The neural networks are trained with modified Back-Propagation (BP) algorithm by introducing the IVD consideration. The traditional BP algorithm is used to update the neural networks weights with a random initial IVD. The IVD is permuted and the neural network is retrained to obtain an optimal solution. Figure 4 draws the flowchart of the proposed modified BPNN training algorithm. As shown in this Figure 4, the proposed modified BPNN have three main stages: Stage (I) is the traditional BPNN training algorithm constituted by a feed-forward pass, which consists to take an input variable to express the corresponding output through the synaptic weights, and a feedback pass which aims to update the neural network

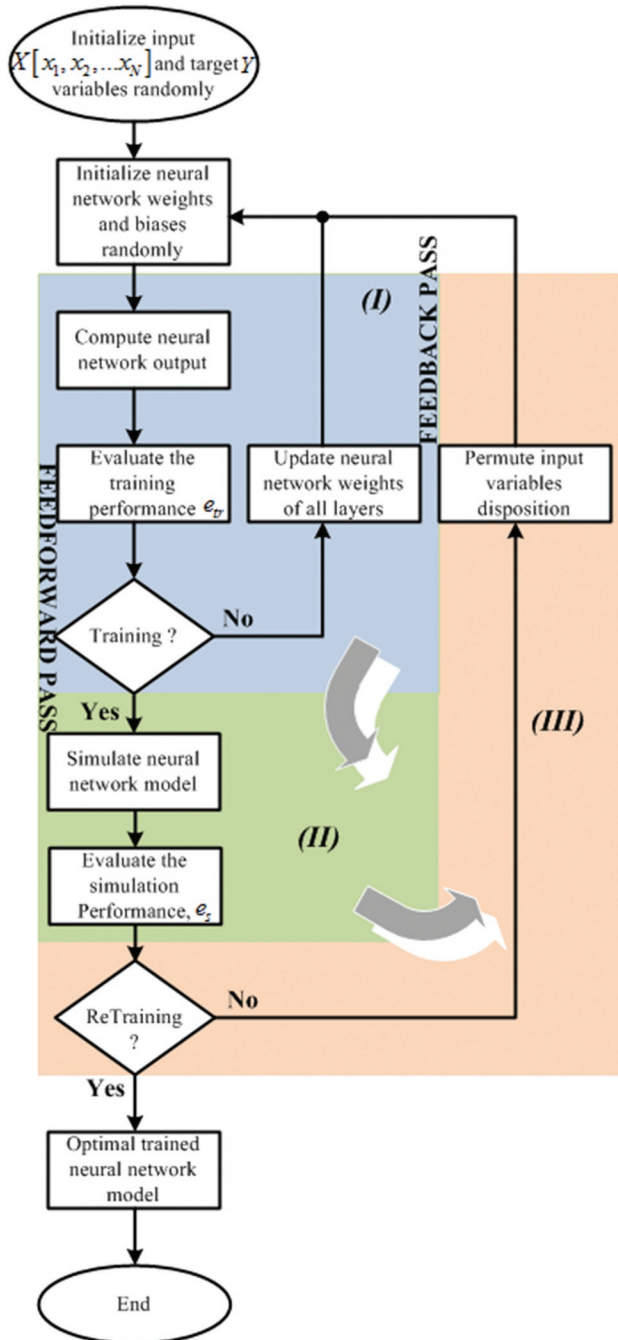


Figure 4. Flowchart of proposed BPNN with optimal IVD searching.

weights. At the end of this training process, the neural network is validated in the stage **(II)** by simulating its ability to generalize the desired output. This stage **(II)** allows to avoid the overlearning or overfitting, and to find the optimal model. Stage **(III)** is the added feedback pass, which allows to retrain

the neural network (back to stage (*I*)) for each IVD until the better solution is obtained.

The modified BPNN was proposed for improving TSF accuracy for 1 day ahead wind speed. The detail of the modified BPNN based on TSF is presented in *Algorithm*. As in the training process, the retraining process is controlled through the validation performances, e_s , and the number of retraining iteration, $T_{max} > Mo$.

The proposed modified BPNN are able to be used in combining model as the traditional BPNN. Then, this proposed optimization approach was evaluated in combining Genetic Algorithm (GA) and neural networks. Here, the GA was used to find the optimal weights of neural networks in the feedback pass of the stage (*I*). This for different possible IVD until an optimal solution is obtained. [Figure 5](#) indicates the whole process of BPNN optimization by GA and IVD consideration.

Experimental Results and Discussion

IVD and Neural Networks Performances

After both neural networks architectures setting and models are constructed in order to investigate the influence of IVD on forecasting accuracy, the sought of best training and forecasting performance of each model is required. Thus, there are 10 simulations each of them with 10430 datasets. Three months were used in the training process and tested to forecast the short-term wind speed. The better performances of these simulations are considered for each of the developed neural networks models. [Table 2](#) lists the different IVD, training, TrPerform, and forecasting performances of each of the models for FFNN and NARX NN architecture, respectively.

According to the results presented in [Table 2](#), all the models of both ANNs structures have different performances. In other words, the training and forecasting performances are varying according to the ANNs models. The difference between the minimum and maximum value of a performance criterion is evaluated in percentage using [Equation \(9\)](#). For the FFNN architecture, the training performance, TrPerform, varies from 0.0772 to 0.0819, 5.73%; the forecasting errors RMSE, MAE, and MAPE vary from 1.2934 to 1.9017, 31.98%, from 1.0183 to 1.6215, 37.20% and from 18.4749 to 20.9336, 11.74%, respectively. For the NARX NN architecture, the training performance, TrPerform, varies from 0.0289 to 0.0297, 2.69%; the forecasting errors RMSE, MAE, and MAPE vary from 1.0106 to 1.4272, 29.19%, from 0.8227 to 1.074, 23.39%, and from 14.1664 to 18.6297, 23.95%, respectively. These significant differences between each better and worse performance criterion indicate the high influence of the input variables disposition upon training and forecasting performances of neural networks models. Meanwhile, among both

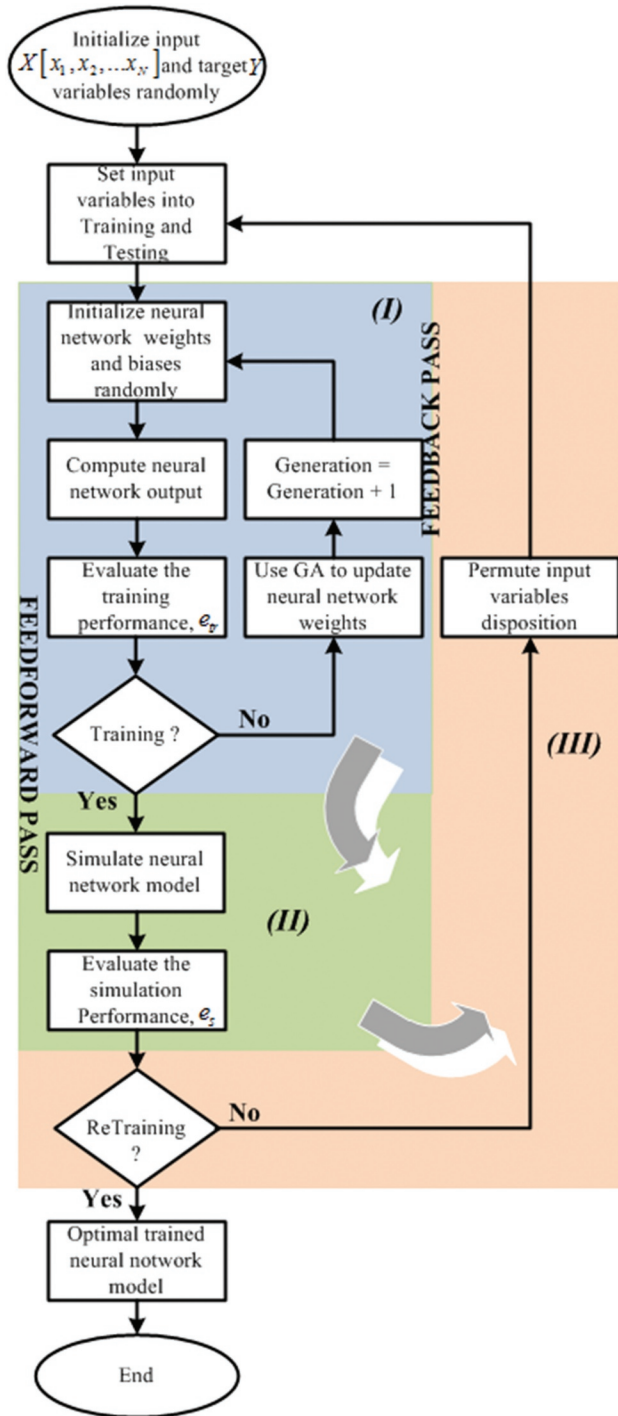


Figure 5. Proposed BPNN optimization by GA and IVD consideration.

neural networks, the FFNN structure has the more significant difference between the performance criteria. Therefore, we can conclude that the

Table 2. Statistical performances of ANNs models.

No	disposition	FFNN					NARX NN				
		TrPerform	RMSE	MAE	MAPE(%)	TrPerform	RMSE	MAE	MAPE(%)		
1	Ta-Pa-RH-T	0.0791	1.9017	1.6215	20.095	0.0294	1.113	0.883	16.4035		
2	Ta-Pa-T-RH	0.0803	1.3936	1.0975	20.185	0.0291	1.0973	0.859	16.1747		
3	Ta-T-Pa-RH	0.0785	1.4431	1.1681	20.934	0.0297	1.2409	0.963	16.7212		
4	Ta-T-RH-Pa	0.0791	1.395	1.1116	20.64	0.0294	1.2684	0.971	16.7102		
5	Ta-RH-T-Pa	0.0789	1.4144	1.0663	18.651	0.0293	1.4272	1.074	18.6297		
6	Ta-RH-Pa-T	0.0792	1.4026	1.0857	19.498	0.029	1.1854	0.917	17.3096		
7	Pa-Ta-RH-T	0.0782	1.4697	1.2028	20.893	0.0293	1.1796	0.949	18.1993		
8	Pa-Ta-T-RH	0.0788	1.4917	1.1592	19.115	0.0292	1.23	0.961	16.764		
9	Pa-T-RH-Ta	0.0772	1.3431	1.0619	19.349	0.0293	1.1973	0.946	17.4748		
10	Pa-RH-T-Ta	0.0787	1.326	1.0773	19.767	0.0295	1.1973	0.946	17.4748		
11	Pa-RH-Ta-T	0.0794	1.2934	1.0183	19.626	0.0291	1.1305	0.906	16.7442		
12	Pa-T-Ta-RH	0.0796	1.5071	1.0987	19.259	0.0295	1.0449	0.843	15.205		
13	RH-Pa-T-Ta	0.0798	1.3811	1.0525	18.485	0.0294	1.0685	0.852	16.01		
14	RH-Ta-Ta-T	0.0781	1.3726	1.0856	19.422	0.0292	1.1088	0.885	15.9322		
15	RH-T-Pa-Ta	0.0819	1.3763	1.0549	19.138	0.0289	1.1074	0.878	15.1771		
16	RH-Ta-Pa-T	0.0796	1.4609	1.1652	20.494	0.029	1.199	0.938	16.4563		
17	RH-T-Ta-Pa	0.0787	1.3763	1.0549	19.138	0.0293	1.0387	0.824	14.1664		
18	RH-Ta-T-Pa	0.0787	1.4118	1.1257	20.119	0.0289	1.3709	1.039	17.4982		
19	T-RH-Pa-Ta	0.0786	1.3433	1.0892	20.382	0.0293	1.0106	0.823	15.4901		
20	T-Pa-RH-Ta	0.0797	1.3584	1.0463	18.577	0.0292	1.1174	0.904	16.7915		
21	T-RH-Ta-Pa	0.0781	1.3128	1.0657	19.772	0.0293	1.2105	0.977	16.8154		
22	T-Ta-RH-Pa	0.0799	1.4297	1.1122	19.148	0.0293	1.0846	0.88	16.525		
23	T-Ta-Pa-RH	0.08	1.3492	1.0258	18.475	0.0292	1.0378	0.823	14.9924		
24	T-Pa-Ta-RH	0.0781	1.3489	1.0777	19.255	0.0292	1.0332	0.829	15.1903		

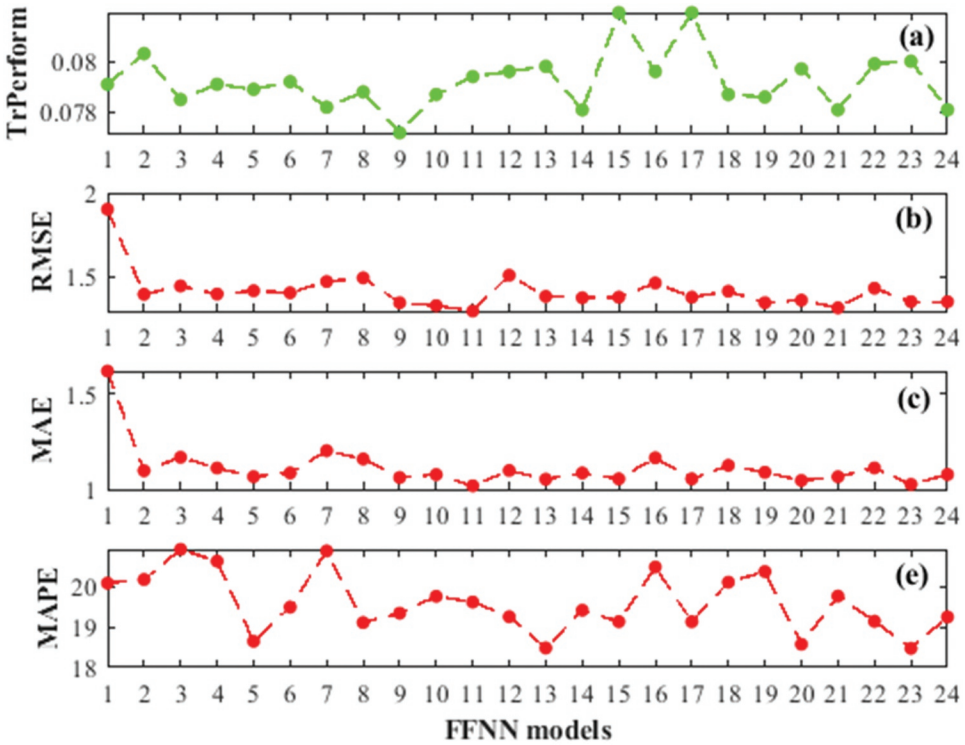


Figure 6. Training, (a), and forecasting, RMSE = (b), MAE = (c), MAPE (%) = (e), performances of FFNN models.

feedforward neural network is more sensible to IVD than recurrent neural networks. Figure 6 indicates the training and forecasting performances versus models of FFNN structure. Also, Figure 7 shows the training and forecasting performances versus models of NARX structure.

The fluctuations of performances of both developed ANNs architectures according to their models can be clearly observed in Figures 6–7. They clarify the influence of IVD upon static and dynamic neural networks models. Thus, the optimal IVD is required to build the optimal neural networks model based on more accurate TSF.

According to Table 2 and Figures 6–7, the first four most accurate forecasting models of the FFNN and NARX NN structure are the models 5, 20, 13, 23 and 12, 17, 15, 23, respectively. According to Wei, Yoshiteru, and Shouyang 2004 (Feng, Zhou, and Dong 2019), the input variables of an ANN need to have the high strength correlation between each of them and the target variable, but should not be correlated. According to the results presented in Tables 1 and 2, this is confirmed by the models 5 and 13 of the FFNN structure, but not for any NARX NN models. Therefore, based on the above experiments, it can be concluded that: (i) NARX NN structure obtains the most accurate results than FFNN structure. (ii) The way that the input

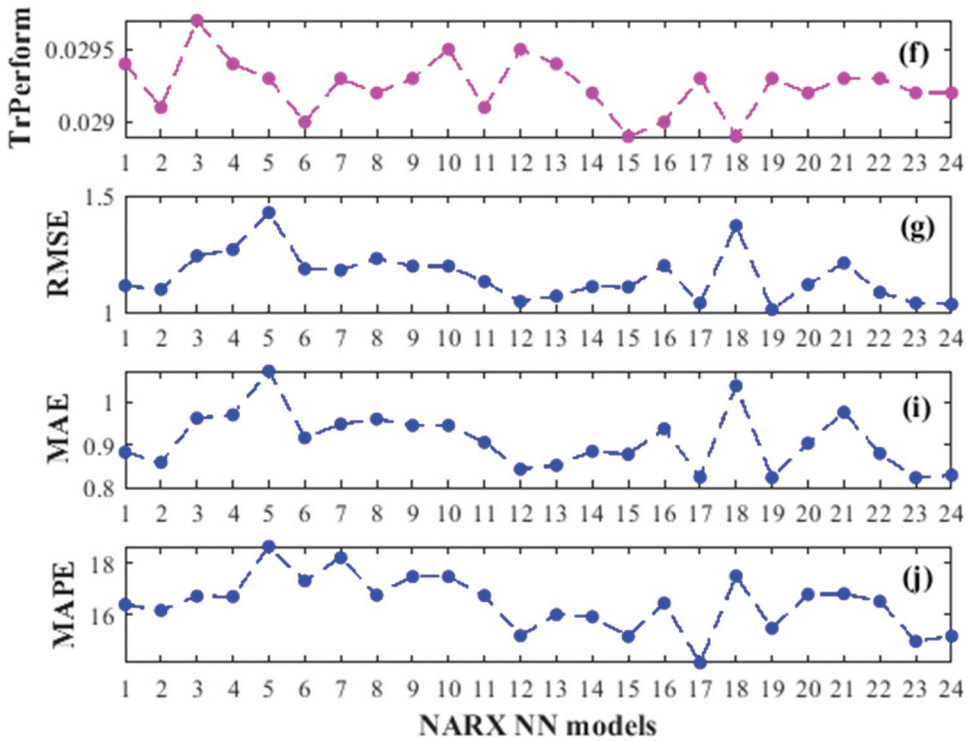


Figure 7. Training, (f), and forecasting, RMSE = (g), MAE = (i), MAPE (%) = (j), performances of NARX NN models.

variables disposition influence the neural networks performance is different according to their architectures. (iii) There is a tiny possibility of having an optimal FFNN model by arranging its input variables in such a way as to avoid the strength correlation between two neighboring input variables.

Also, we can see a real similarity in the variations of graphs 6(b), 6(c), and 6(e). This similarity is more considerable between graphs 7(g), 7(i), and 7(j). These similarities confirm the stability of the match of IVD with forecasting performances of the neural networks models. But these similarities are smaller between the training graph, 6(a), and the forecasting graphs, 6(b), 6(c), and 6(e). Event between 7(f) and 6(g), 6(i), and 6(j). Thus, these lack of concordance between the training performances and those of forecasting reflect the fact that some IVD are subject to overlearning or overfitting, e.g., models 12 and 18 of NARX NN and model 7 of FFNN. To further illustrate this, Table 3 gives the coefficients of correlation between the performances criteria from the two ANNs architectures.

The most remarkable observation in these results from Table 3 is the smaller relations between training and forecasting errors criteria. They also argue that there are strong relations between the forecasting errors from NARX NN models than FFNN. Therefore, we can conclude that the forecasting

Table 3. Relations between the performance criteria.

ANN	TrPrform	RMSE	MAE	MAPE	ANN
	TrPrform	-0.0651	-0.0317	0.0276	NARX NN
	RMSE	0.0073	0.9860	0.798	
	MAE	0.1369	0.9526	0.8450	
FFNN	MAPE	-0.3116	0.222	0.3989	

Table 4. Forecasting models parameter settings.

Models	Parameters	Values
FFNN	maximum iterations	1000
	validation check	500
	maximum retraining iterations	100
	layers	02
NARX NN	maximum iterations	1000
	validation check	500
	maximum retraining iterations	100
	delay	04
ANFIS	layers	02
	number of membership functions	02
	number of membership	Gaussian
	maximum epochs	1000
GA	layers	02
	maximum generations	2000
	fitness limit	10^{-5}
	convergence tolerance	10^{-10}

performance of NARX NN is less sensitive than that of FFNN to overlearning or overfitting that some IVD may cause.

Proposed Forecasting Models Evaluation

This section describes the experiments conducted to examine the performance of the proposed neural networks optimization approach, which was based on IVD pursuing to enhance TSF accuracy. The proposed forecasting models in this work were then based on this proposed optimization approach. Therefore, the FFNN, NARX NN, and GABPNN models were proposed. The proposed GABPNN model is based on the model proposed by Rahman et al. (Mijanur Rahman and Akter Setu 2015). To perform the evaluation of the forecasting ability of these proposed models, an another commonly used neural network forecasting model is used as the benchmark model, i.e., Adaptive Neuro-Fuzzy Inference System (ANFIS)(Cervone et al. 2017). Table 4 shows the experimental parameters of developed forecasting models.

To ensure that the final results are reliable and independent of the initial random weight and bias values of the proposed models, each developed model is repeated 10 times. It had been shown in the previous subsection 5.1 that the IVD influence the training and forecasting performance of neural networks. Therefore, we will take the better forecasting models of FFNN and NARX NN from Table 2 as comparison models of the proposed models, i.e., models 20

and 17, respectively. Equation (9) is used to describe the improvement percentage of the proposed models over the comparison models, it is defined as,

$$P_{Error} = \left(\frac{Error_2 - Error_1}{Error_2} \right) \times 100 \quad (9)$$

where *Error* represents each statistical error defined in Equations (6)–(8), subscript 1 indicates a proposed model, and the subscript 2 gives a comparison model. When a $P_{Error} > 0$, the proposed forecasting model is better than the comparison model and vice versa. The closer P_{Error} to 0, the smaller the difference between the two evaluation errors. The forecasting performance results of the proposed models and the comparing models of the study case are presented in Table 5.

According to Table 5 the GABPNN model forecasts well than the ANFIS model. Meanwhile, the proposed NARX NN model performs well the TSF than the proposed FFNN and GABPNN models, while ANFIS is the worse one. In Figure 8 the results of forecasting performances from the different proposed and comparing models are drawn. Table 6 gives the performances of forecasting improvement of the proposed models over the comparison models.

By observing Table 6, we can see that the proposed FFNN model leads to more accurate forecasting performance than the old FFNN model with a considerable difference, by up to 10% for every performance criteria. This shows the effectiveness of proposed FFNN model to perform TSF. Meanwhile, the proposed NARX NN model is being neutralized with the old model, but it obtains the most accurate results among all developed models. It is important to note that this comparison NAX NN model is built with optimal IVD as shown in subsection 5.1. Thus, the proposed NAX NN model can always work as a good forecasting model than the old model which is generally built with random IVD. The results presented in Table 6 show that the combining proposed model, GABPNN is the most accurate model than its old comparison model. The sensitivity of the GABPNN to the arrangement of input variables is clarified in Figure 9, which presents the fluctuation of best fitness values according to the neural networks models.

The research results of the proposed strategy to improve the multi-step TSF performance of ANNs show that the tested models for 24 hours-head wind speed forecasting have the following features: (1) Each proposed model always

Table 5. Forecasting performance evaluation of different models.

Models	RMSE	MAE	MAPE(%)
ANFIS	1.3456	1.0814	19.6528
GABPNN	1.2115	1.0231	18.3718
Proposed NARX NN	1.0289	0.8037	14.2817
Proposed FFNN	1.1617	0.9009	15.8855
Proposed GABPNN	1.2753	0.9901	16.5621

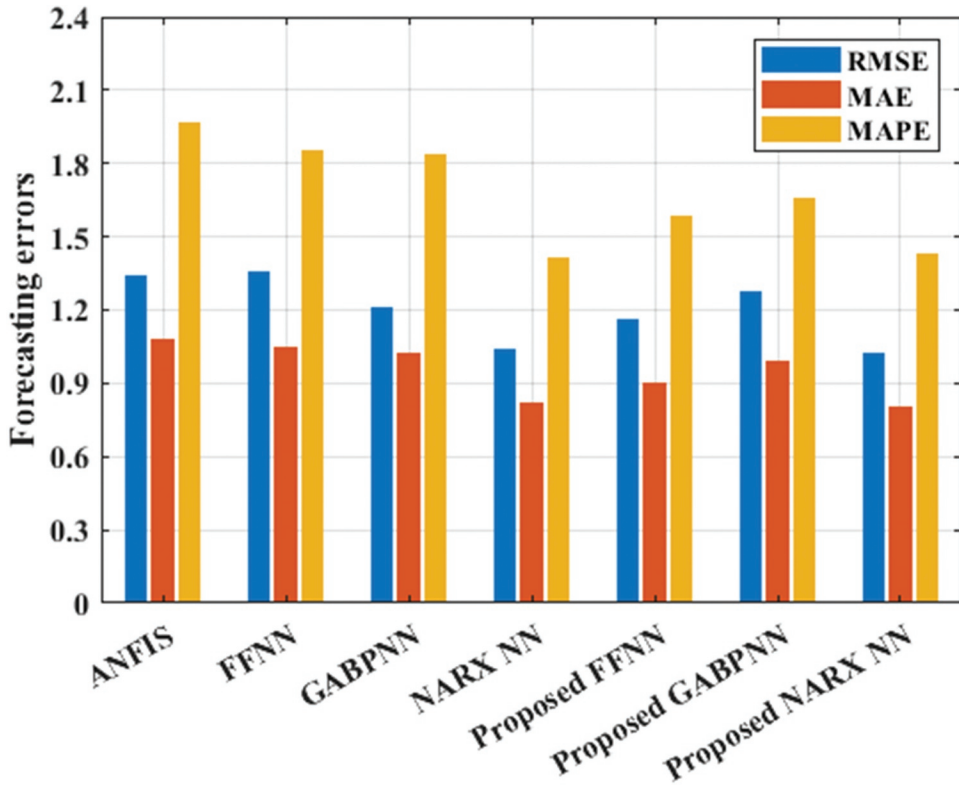


Figure 8. Bar chart showing the forecasting errors from the proposed and comparison models.

Table 6. Improvement percentages of the proposed models.

	Models	FFNN	NARX NN	GABPNN	ANFIS
RMSE	Proposed NARX NN	21.62%	0.940%	15.07%	23.53%
	Proposed FFNN	11.50%	-11.84%	4.110%	13.66%
	Proposed GABPNN	2.85%	-16.91%	-5.260%	5.220%
MAE	Proposed NARX NN	24.58%	2.220%	21.44%	25.67%
	Proposed FFNN	15.46%	-9.590%	11.94%	16.69%
	Proposed GABPNN	7.090%	-20.45%	3.220%	8.440%
MAPE	Proposed NARX NN	23.12%	-0.800%	22.26%	27.32%
	Proposed FFNN	14.48%	-12.13%	13.53%	19.16%
	Proposed GABPNN	10.84%	-22.77%	9.850%	15.72%

achieves more accurate value than old one. This shows the effectiveness of the proposed neural networks optimization approach to improve the multi-step head TSF accuracy. (2) Among all the proposed models, FFNN model is the most improved one with the highest improvement percentage values, by up to 10%. Thus, IVD is very important for static neural networks forecasting performances improvement than dynamic neural networks. (3) By using the worse neural networks models of Table 2 as comparison models, we will see that the difference between them and the proposed models will be more considerable.

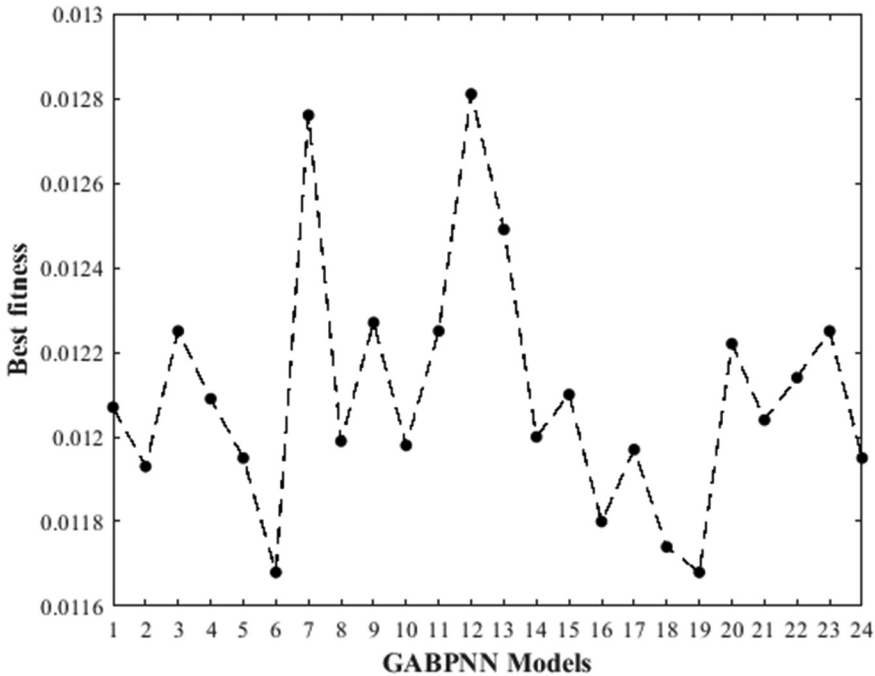


Figure 9. Best fitness values of GA along with neural networks models.

The presented experiments confirm the competitive forecasting performance of the proposed neural networks models and therefore, show that it will be important to take into consideration the IVD for the optimization of neural networks models. But it was complex to test step-by-step every possible IVD of neural networks aimed to find the optimal one. Thus, the key advantages of the proposed neural networks training and optimization approach are:

- It is possible to test all the possible IVD and the search of the optimal disposition is included in the neural networks training algorithm. Thus, the approach does not require any predisposition of the input variables and relations between them analysis stage.

- The complexity of the approach in terms of computation and speed is much less than step-by-step method used to find the optimal IVD, which facilitates the real-time application of the proposed neural networks optimization approach.

- The forecasting performance is better than that obtained by using other methods to search the optimal IVD such as step-by-step finding and non-correlated input variable methods.

- Possibility to be combined with other techniques to build the hybrid TSF models.

Conclusion

This paper introduces a new framework based on input variables disposition to construct optimal neural networks for more accurate time series forecasting. The investigation carries out on feed-forward and nonlinear autoregression with exogenous neural networks structures to forecast 24 hours ahead wind speed has shown that their training and forecasting performances change according to their input variables disposition. Meanwhile, the input variables disposition do not change the computational time of neural networks models. Thus, the optimal forecasting requires an optimal input variables disposition of ANN based. A new ANN training approach has been proposed; introducing the optimal input variables disposition into Back-Propagation algorithm. This proposed approach has been applied to develop the neural networks forecasting models including combining model using generic algorithm. The numerical results of the study case reveal the effectiveness of the proposed approach and neural networks models to improve accuracy of multi-step head time series forecasting, in which every proposed model improves the performance of its old model. Moreover, this proposed optimization approach could be also used together with the multi-objective algorithms for more time series forecasting models stability and errors minimizing such as bat algorithm, evolutionary algorithm, and firefly algorithm.

Conflicts Of Interest

The authors declare no conflict of interest.

References

- Alvezakou, E., G. Siolas, and G. Pantazis. 2018. Short-term and long-term forecasting for the 3D point position changing by using artificial neural networks. *International Journal of Geo-Information* 7:1–15.
- Cervone, G., L. Clemente-Harding, S. Alessandrini, and L. D. Monache. 2017. Short-term photovoltaic power forecasting using artificial neural networks and an analog ensemble. *Renewable Energy* 108:274–86.
- Crone, S. F., and N. Kourentzes, Input-variable specification for neural networks - an analysis of forecasting low and high time series frequency, Proceedings of International Joint Conference on Neural Networks, Atlanta, Georgia, USA, (2009), 619–26.
- Damir, V., N. Ricardo, and J. L. Aznarte. 2019. Forecasting hourly NO_2 concentrations by ensembling neural networks and mesoscale models. *Neurocomputing* 32:9331-9342.
- Di Piazza, A., M. C. Di Piazza, and G. Vitale. 2016. Solar and wind forecasting by NARX neural networks. *Renewable Energy Environmental Sustainability* 39:1–5.
- Feng, S., H. Zhou, and H. Dong. 2019. Using deep neural network with small dataset to predict material defects. *Materials & Design* 162:300–10.
- Folorunso, O., A. T. Akinwale, O. E. Asiribo, and A. Adeyemo. 2010. Population prediction using artificial neural network. *African Journal of Mathematics and Computer Science* 3:155–62.

- Gogas, P., T. Papadimitriou, and A. Agrapetidou. 2018. Forecasting bank failures and stress testing?: A machine learning approach. *International Journal of Forecasting* 34:40–456.
- Hassan, M., and M. Hamada. 2018. Genetic algorithm approaches for improving prediction accuracy of multi-criteria recommender systems. *International Journal of Computational Intelligence Systems* 11:146–62.
- Jursa, R., and K. Rohrig. 2008. Short-term wind power forecasting using evolutionary algorithms for the automated specification of artificial intelligence models. *International Journal of Forecasting* 24:694–709.
- Kadhem, A. A., N. I. Abdul Wahab, I. Aris, J. Jasni, and A. N. Abdalla. 2017. Advanced wind speed prediction model based on a combination of weibull distribution and an artificial neural network. *Energies* 10:1–17.
- Kuo, P., and C. Huang. 2018a. An electricity price forecasting model by hybrid structured deep neural networks. *Sustainability* 10:1–17.
- Kuo, P., and C. Huang. 2018b. A high precision artificial neural networks model for short-term energy load forecasting. *Energies* 11:1–13.
- Loghmanian, S. M. R., R. Ahmad, and H. Jamaluddin, Multi-objective optimization of NARX model for system identification using genetic algorithm, 2009 First International Conference on Computational Intelligence, Communication Systems and Networks, Indore, India (2009), 196–201.
- Mendes Dantas, T., and F. L. Cyrino Oliveira. 2018. Improving time series forecasting: An approach combining bootstrap aggregation. *Clusters and Exponential Smoothing, International Journal of Forecasting* 34:748–61.
- Mijanur Rahman, M., and T. Akter Setu. 2015. An implementation for combining neural networks and genetic algorithm. *International Journal of Computer Science and Technology* 6:218–22.
- Mohandes, M., S. Rehman, and S. M. Rahman. 2011. Estimation of wind speed profile using adaptive neuro-fuzzy inference system (ANFIS). *Applied Energy* 88:1–9.
- Peng, H., F. Liu, and X. Yang. 2013. A hybrid strategy of short term wind power prediction. *Renewable Energy* 50:590–95.
- Reza Loghmanian, S. M., H. Jamaluddin, R. Ahmad, R. Yusof, and M. Khalid. 2012. Structure optimization of neural network for dynamic system modeling using multi-objective genetic algorithm. *Neural Computing and Applications* 21:1281–95.
- Sanchez, I. 2006. Short-term prediction of wind energy production. *International Journal of Forecasting* 22:43–56.
- Shahrul, N. S., R. R. Muhammad, S. Sabrilhakim, and M. K. Mohd Shukry. 2018. Thumb-tip force prediction based on Hill's muscle model using electromyogram and ultrasound signal. *International Journal of Computational Intelligence Systems* 11:238–47.
- Shen, Y., X. Wang, and J. Chen. 2018. Wind power forecasting using multi-objective evolutionary algorithms for Wavelet neural network-optimized prediction intervals. *Applied Sciences* 8:1–13.
- Sher, S., and G. Messori. 2019. Weather and climate forecasting with neural networks: Using general circulation models (GCMs) with different complexity as a study ground. *Geoscientific Model Development* 12:2797–809.
- Soui, M., S. Smiti, M. W. Mkaouer, and R. Ejbali. 2019. Bankruptcy prediction using stacked auto-encoders. *Applied Artificial Intelligence* 34:1–21.
- Sovann, N., P. Nallagownden, and Z. Baharudin. 2014. A method to determine the input variable for the neural network model of the electrical system. 5th International Conference on Intelligent and Advanced Systems (ICIAS), Kuala Lumpur, Malaysia (2014), 3-5 .
- State, I., A. Uyo, and A. Offiong. 2016. Neural networks in materials science and engineering: A review of salient issues. *European Journal of Engineering and Technology* 3:40–54.

- Upadhyay, K. G., A. K. Choudhary, and M. M. Tripathi. 2011. Short-term wind speed forecasting using feed-forward back-propagation neural network. *International Journal of Engineering, Science and Technology* 3:107–12.
- Wang, B., H. Huang, and X. Wang. 2012. A novel text mining approach to financial time series forecasting. *Neurocomputing* 83:136–45.
- Wei, H., N. Yoshiteru, and W. Shouyang. 2004. A general approach based on autocorrelation to determine input variables of neural networks for time series forecasting. *Journal of Systems Science and Complexity* 17:297–305.
- Yaïci, W., M. Longo, E. Entchev, and F. Foiadelli. 2017. Simulation study on the effect of reduced inputs of artificial neural networks on the predictive performance of the solar energy system. *Sustainability* 9:1–14.
- Zhang, J., Y. Wei, Z. Tan, K. Wang, and W. Tian. 2017. A hybrid method for short-term wind speed forecasting. *sustainability* 9:1–10.
- Zongyan, L., and M. Best. 2015. Optimization of the input layer structure for feed-forward narx neural networks. *International Journal of Electrical and Computer Engineering* 9:673–67.



A novel hybrid model based on weather variables relationships improving applied for wind speed forecasting

Hervice Roméo Fogno Fotso¹ · Claude Vidal Aloyem Kazé² · Germaine Djuidje Kenmoé¹

Received: 7 May 2021 / Accepted: 26 June 2021
© Islamic Azad University 2021

Abstract

Accurate wind speed forecasting is imperative for producing wind power integration. Thus, this paper presents a novel combined ARIMA—artificial neural network (ANN) forecasting model based on improved relationships between the wind speed and other weather variables pursuing to forecast wind speed. The weather variables on which the wind speed depends are transformed for normalization and relationships improving by using a proposed approach. The ARIMA models are employed for each transformed variables modeling and the unknown values forecasting. The measured wind speed is normalized and used as the target variable and the transformed weather variables as input variables to train the ANN model. The predicted weather variables are employed as input variables of trained ANN to forecast the unknown wind speed values. The proposed forecasting model has been validated with five different ANN structures for multi-step ahead wind speed forecasting from two Datasets in Bapouh, Cameroon. The experimental results indicate that the proposed data preprocessing strategy is appropriate to enhance the relationships between two variables and decrease the seasonal variation. Furthermore, the proposed hybrid model in terms of forecasting accuracy outperforms other comparable models.

Keywords Wind speed forecasting · Weather variables relationships · Combined forecasting model · Multi-step ahead forecasting · Application

Introduction

Fossil fuels energy source constitutes a considerable cause of environmental problems. Moreover, the electrical energy demand growing rapidly as a result of industrialization and population growth all over the world [1, 2]. Therefore, electricity production while preserving the environment is one of the major challenges of this century. The use of wind energy will help to reduce greenhouse gas emission [3]. That is why the installed capacity worldwide of Wind Energy Conversion System (WTPG) has been increasing rapidly [3, 4].

Given the dependence of Wind Turbine Power Generation (WTPG) to the intermittent nature of wind speed, wind energy generation is nearly unpredictable and constitutes the most fluctuating renewable energy source [5]. Consequently,

an accurate wind speed forecasting model is crucial for the most efficient utilization of wind power [6, 7]. According to Krishnaveny R. Nair et al. [8], in order to increase the penetration of energy from wind, every producer has to predict their power production. For this reason, modeling of the wind speed through time series forecasting methods is becoming widespread. Many wind speed forecasting methods are been developed in the literature. They can be classified into the physical method, statistical method and hybrid method [9, 10]. The physical method forecasts the wind speed values by using the physical description of the atmosphere. The main physical method is the numerical weather prediction [11, 12], which requires solving complex mathematical equations of weather variables. It's not appropriate for short-term forecasting and performs well the wind speed forecasting when weather data are stable. The statistical method includes time series analysis (TSA) models, stochastic models, and Artificial Intelligence (AI) models. TSA models use mathematical statistics to construct the relationships from historical wind speed data pursuing for unknown values forecasting. The mostly used TSA models are autoregressive moving average [13], autoregressive

✉ Hervice Roméo Fogno Fotso
hervicefogno@yahoo.fr

¹ Laboratory of Mechanics, Department of Physics, University of Yaoundé I, P.O.Box 812, Yaoundé, Cameroon

² Department of Renewable Energy, HTTC Kumba, University of Buea, Buea, Cameroon



integrated moving average [14], grey prediction [15], and exponential smoothing [16]. The more accurate forecasting results are achieved from TSA models comparing with physical models [17]. But, they are suitable for linear time series and cannot capture the nonlinear patterns of wind speed very well. Stochastic models [18–20] use the mathematical models of stochastic equations to reproduce the wind speed behavior. They are based on wind speed historical data of a specific location to estimate its probability distributions. The AI models are based on the historical weather data sample process by learning the relationships between wind speed and other weather variables for desired values forecasting. The AI models such as artificial neural networks (ANNs) [21], support vector machines [22] and fuzzy logic [23] have been widely used and shown to have the ability in robust pattern modeling and nonlinear wind speed forecasting compared with other forecasting models. Erasmo Cadenas et al. [24] compared the ARIMA model and recurrent nonlinear autoregressive exogenous artificial neural network (NARXNN) model for wind speed forecasting. The achieved results showed that the NARXNN forecast well the wind speed than the ARIMA model. The hybrid method [25, 26] is combining different methods. The combined models have been shown to forecast wind speed accurately than single models. The mostly used hybrid models for wind speed forecasting are adaptive neuro-fuzzy inference system (ANFIS) [27], generic algorithm neural network [28], neural network and bat algorithm [29], neural network and particle swarm optimization [30] and ARIMA and neural network [31]. Saeed Samadianfard et al. [32] combined the multi-layer perceptron ANN and whale optimization algorithm for wind speed forecasting in Iran. The achieved results have demonstrated the superiority of the combined model among the individual multi-layer perceptron ANN model. Krishnaveny R. Nair et al. [8] compared single ANN models, ARIMA model, and hybrid ARIMA-ANN model for wind speed forecasting. To succeed in the hybrid ARIMA-ANN model, the forecasting variable is decomposed into linear and nonlinear parts. The achieved results showed that this hybrid forecasting model is accurate than the individual models. Also, other widely developed hybrid models are based on data preprocessing for AI models using techniques such as singular spectrum analysis [33], ensemble empirical mode decomposition [34] and wavelet transforms [9], to improve the wind speed forecasting accuracy. Unfortunately, no work is done to improve AI models forecasting performance based on the relationship between their variables improving.

Wind speed forecasting is not an easy task because it is affected by many parameters such as air temperature, atmospheric pressure, relative humidity, and wind direction [34]. The AI models proceed by capturing the natural relationships between those weather variables and wind speed. A forecasting model based on AI will be more accurate as

much as the relationship between each weather variable used as input and the wind speed is important. These relationships are intermittent over time as environmental changes and even almost non-existent in some cases. Thus, this paper presents a combined statistical model to ensure accurate wind speed forecasting everywhere and every moment. It's a novel hybrid neural network and ARIMA model to forecast wind speed with weather relationships improved. The traditional data normalization formula is reformulated and proposed to transform the training data set, increasing the relationships between the weather variables used as input of the ANN model and the wind speed variable used as the target. The ARIMA model is developed for each transformed weather variable modeling and pursuing unknown testing neural networks data set forecasting. The transformed data are used to forecast desired wind speed values. To test the proposed model, three single and two collaborative ANNs models are developed for multi-step wind speed forecasting for two Datasets from Cameroon. ARIMA model is used as benchmark model and the multi-step forecasting includes 1-step, 2-step, and 3-step ahead. To evaluate the efficiency of the proposed hybrid wind speed forecasting model, the traditional error criteria are used to measure the average spread, the average bias, and the percentage of the forecasting. Also, the Diebold-Mariano test is applied to evaluate the accuracy level of proposed forecasting models among the comparison models. Contributions of this paper can be summarized as follows:

- Proposed a novel data preprocessing for normalization and to enhance the relationships between the wind speed and dependent weather variables.
- Proposed a novel ensemble ARIMA neural network model to forecast the complex wind speed.
- The proposed model outperforms comparison forecasting models in multi-step forecasting accuracy.

The remainder of the paper is subdivided into four sections: "Proposed wind speed forecasting scheme" section draws the scheme of the proposed hybrid wind speed forecasting model, the study case for the experiment is presented in "Case study in Cameroon" section, the experiment results and application are presented, and discussed in "Experiments results" section and the final "Conclusion" section draws a conclusion of this paper.

Proposed wind speed forecasting scheme

In order to contribute to deciding on wind energy integration, we proposed, in this paper, a novel model to forecast wind speed as shown in Fig. 1. To achieve the most accurate

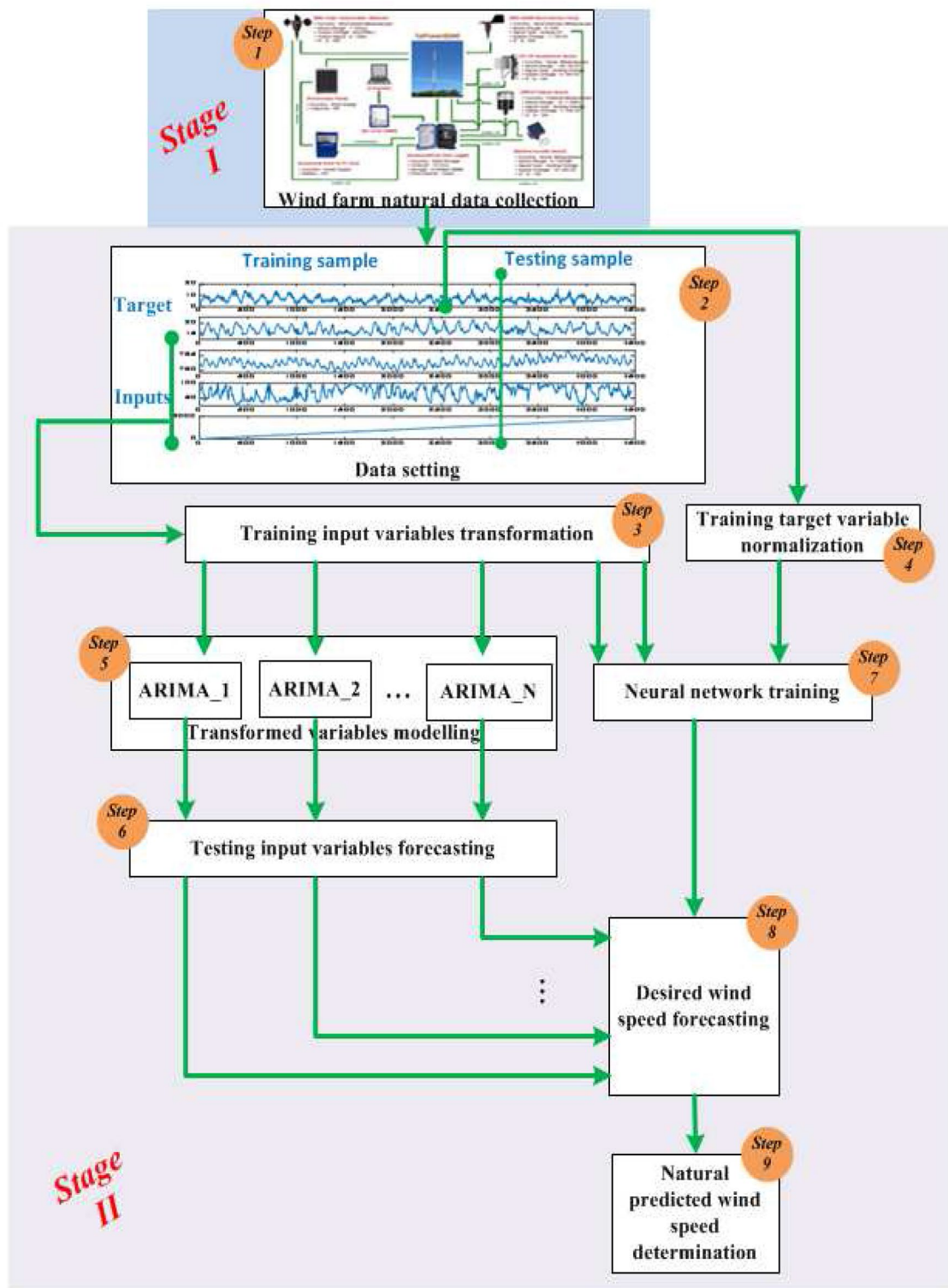


Fig. 1 Flowchart of proposed hybrid wind speed forecasting model

wind speed forecasting, the proposed hybrid forecasting model combines ANN and ARIMA models.

The neural networks models process by learning the relationships between its input variables and its target variables. Therefore, the proposed wind speed forecasting model consists to improve the relationship between the weather variables used as input variables and the wind speed used as output variables, respectively, of neural network models pursuing to get more accurate desired wind speed forecasting values. As shown in Fig. 1, it's carried out following nine steps (in two stages) sequentially from step 1 (*stage I*) to step 9. The historical data sample of the weather variables is collected in step 1 and subdivided into the training set and testing set in the second step. Since these input and target weather variables of the prediction tools are collected at a different order of magnitude, to minimize the noise and so that the ANN can learn relevant patterns, they are transformed (or normalized) during the data preprocessing step. Traditionally, Eq. (1) allows normalizing the data between 0 and 1. Therefore, in the proposed forecasting model, Eq. (1) is used to normalize the training target variable (wind speed) in step 4, before the training process of the neural network model. Before it, to normalize the training input variables of the neural network model by increasing the relationship between each of them and the wind speed variable, we have proposed a novel form of time series data normalization given in Eq. (2) to transform them in step 3. Therefore, the expression of the Eq. (2) allows each input variable to fit the target variable by normalizing it between 0 and 1,

$$y_n^N = \frac{y_n - y_{\min}}{y_{\max} - y_{\min}}, \tag{1}$$

$$x_n^N = \frac{x_n \cdot y_n - x_{\min} \cdot y_{\min}}{x_{\max} \cdot y_{\max} - x_{\min} \cdot y_{\min}}, \tag{2}$$

where y_n and y_n^N denote, respectively, the natural measured and normalized wind speed variable, x_n and x_n^N denote, respectively, a natural measured and transformed weather variables used as input variables of neural network model, at a given time step n ; y_{\max} , y_{\min} , x_{\max} and x_{\min} are, respectively, the maximum and minimum value of the natural measured output and input variables.

An optimal ARIMA model is developed for each transformed input variable modeling (step 5) and used to forecast (step 6) the testing input data. The ANN model is trained by using the transformed input variables and normalized target variable in step 7. By using the predicted testing input variables from the ARIMA model, the trained ANN model is used to forecast the unknown wind speed values in step 8. At the end of the forecasting process, the natural values of the forecasting wind speed variable are gotten in step 9 by transforming the normalized forecasting values using Eq. (3) given as following,

$$y_n^p = y_n^{N \cdot p} (y_{\max} - y_{\min}) + y_{\min}, \tag{3}$$

where y_n^p and $y_n^{N \cdot p}$ are the natural, and normalized forecasting wind speed variable, respectively, at a given time step n ; y_{\max} and y_{\min} are, respectively, the maximum and minimum value of the natural target variable used in the training process. The ARIMA model is built following the procedure given in Fig. 2.

To ensure the effectiveness of this proposed wind speed forecasting model, we had applied it in three single neural networks structures including Back-Propagation Neural Network (BPNN) [35], Radial Basis Function Neural Network (RBFNN) [21], Nonlinear AutoRegression with eXogenous input Neural Network (NARXNN) [24, 35]. Also, the collaborative Genetic Algorithm Back-Propagation Neural Network (GABPNN) [28, 36] and Adaptive Neuro-Fuzzy Inference System (ANFIS) [33] are applied to evaluate the ability of the proposed hybrid wind speed forecasting model and the ARIMA [24] model is employed as the benchmark model.

Case study in Cameroon

Experiment data

The commercial energy is from hydropower and thermal sources in Cameroon. According to Asan Vernyuy Wirba et al., [37], the development of new renewable energy sources such as wind energy is required for Cameroon electrification, necessary to reinforce its economic development. Until 2020, no wind energy farm has been constructed in Cameroon. But, many systems are installed in many places in the better to collect weather data which can be used to evaluate and analyze the renewable energy potential by locality before further WECS installation. It's in this

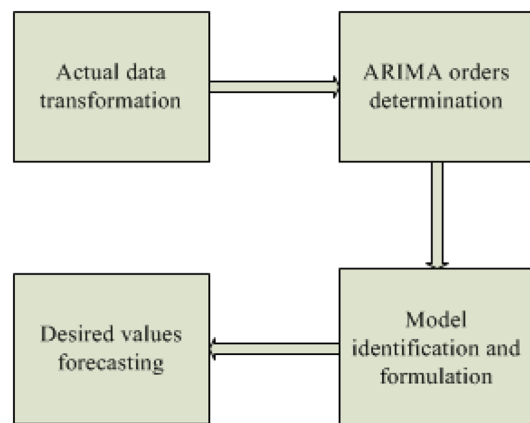


Fig. 2 Flowchart of ARIMA model development for time series forecasting



Fig. 3 Specific location of the study site

perspective that the present work was applied in the site of Bapouh in Cameroon to support decision-making for wind energy exploitation.

Bapouh is a village located near the town of Bafang, in the Western Region of Cameroon as shown in Fig. 3. The geographical coordinates of the site are N 05°09'35.52" and E 10°19'21.90". The data are collected from the meteorological sensor readings and stored in the SymphonyPlus3 data logger.

The weather data including natural wind speed (W_s), air temperature (T_a), relative humidity (RH), and atmospheric pressure (Pa) for two years were recorded at an interval of 10 minutes from 2016 to 2017. The height of measurement is 70 m and the scanning frequency is 144 times per day from 00:00 to 24:00. In order to ascertain the applicability and the performances of the proposed hybrid model, wind speed data from two Datasets in Bapouh were employed for multi-step ahead forecasting. These Datasets, involving Dataset1

and Dataset2 are made up of two months of real measured wind speed data from 1st to 30th December 2016 and from 1st to 30th January 2017, respectively. Each Dataset has 4320 points, these actual data are split into two subsets, which are the training set and testing set. The characteristics of the wind speed in both Datasets are given in Table 1.

From the Table 1, the large gap between minimum and maximum wind speed values of both Datasets shows the very fluctuation of wind speed amplitude and frequency between series. Moreover, the Standard Deviation (S_d) of the wind speed observations for Dataset1 and Dataset2 is 3.01 m/s and 2.54 m/s, respectively, which demonstrate significant fluctuations of the wind speed of these Datasets. Also, by using the Spearman rank correlation method, the relationships (R^2) between the natural W_s and each other weather variable are evaluated. The results presented in Table 2 show that the relation between W_s and the other variables is weak. As shown in

Table 1 Statistical information of the considered wind speed Datasets

Datasets	Samples	Numbers	Characteristics			
			Mean(m/s)	Max(m/s)	Min(m/s)	Sd(m/s)
Dataset1	Observations	4320	8.52	20.80	1	3.01
	Training	4176	8.56	20.80	1	3.04
	Testing	144	7.31	11.00	3.30	1.59
Dataset2	Observations	4320	6.69	16.80	1	2.54
	Training	4176	6.70	16.80	1	2.56
	Testing	144	6.24	10.10	2.50	1.67

Table 2 Normalized and transformed weather variables characteristics

Variables	Dataset1				Dataset2			
	Normalized		Transformed		Normalized		Transformed	
	R^2	Sd	R^2	Sd	R^2	Sd	R^2	Sd
Temperature (Ta)	0.25	0.19	0.97	0.13	0.39	0.15	0.96	0.13
Time (T)	0.07	0.15	0.57	0.15	-0.13	0.17	0.39	0.16
Relative humidity (RH)	-0.47	0.23	0.63	0.08	-0.53	0.26	0.55	0.08
Pressure (Pa)	-0.12	0.28	0.99	0.14	0.17	0.28	0.99	0.13

Table 1, the testing samples represent the data of the 30th day and the training samples remain of the days of both Datasets.

The multi-step ahead is a step-by-step process which consists in using previous forecasting wind speed values to forecast the next value [29]. The applied multi-step ahead wind speed forecasting in this work consists 1-step, 2-step and 3-step. With the 1-step ahead forecasting, the desired value \hat{y}_{N+1} is achieved only through the actual values $\{y_1, y_2, \dots, y_{N-1}, y_N\}$. In the 2-step ahead forecasting, the desired value \hat{y}_{N+2} is achieved by using the actual measured values $\{y_2, y_3, \dots, y_{N-1}, y_N\}$ and the previously forecasting value \hat{y}_{N+1} . While the unknown value \hat{y}_{N+3} in 3-step ahead is obtained based on the historical $\{y_3, y_4, \dots, y_{N-1}, y_N\}$ and the two previously forecasting values $\{\hat{y}_{N+1}, \hat{y}_{N+2}\}$, with N the total number of wind speed training samples.

Forecasting model evaluation

The traditional evaluation criteria are employed to evaluate the accuracy of the proposed forecasting models. Furthermore, Diebold-Mariano (DM) test is used to evaluate their significance level in comparison with traditional models.

Traditional forecasting accuracy criterion

Three traditional error criteria are used in the forecasting experiments to measure the average spread, the average bias, and the percentage of the error of the forecasting models, including the Root Mean Square Error (RMSE), the Mean Absolute Error (MAE), and the Mean Absolute Percentage Error (MAPE), respectively. They are expressed as,

$$RMSE = \sqrt{\frac{1}{N} \sum_{n=1}^N (y_n - \hat{y}_n)^2}, \tag{4}$$

$$MAE = \frac{1}{N} \sum_{n=1}^N |y_n - \hat{y}_n|, \tag{5}$$

$$MAPE = \frac{1}{N} \sum_{n=1}^N \left| \frac{y_n - \hat{y}_n}{y_n} \right| \times 100, \tag{6}$$

where y_n and \hat{y}_n are the measured and predicted wind speed values, respectively, at the time step n , and N is the total number of the forecasting time steps. The forecasting model is better as its RMSE, MAE, and MAPE values are the lowest. To compare the forecasting performance of the proposed models among the comparison models, the improvement percentage of three errors criteria are evaluated as follows:

$$P_{RMSE} = \left| \frac{RMSE_1 - RMSE_2}{RMSE_2} \right| \times 100, \tag{7}$$

$$P_{MAE} = \left| \frac{MAE_1 - MAE_2}{MAE_2} \right| \times 100, \tag{8}$$

$$P_{MAPE} = \left| \frac{MAPE_1 - MAPE_2}{MAPE_2} \right| \times 100, \tag{9}$$

where subscript 1 indicates a proposed model, and subscript 2 gives a comparison model.

Diebold-Mariano test

The traditional forecast evaluation criteria have limitations in application to some degree [38]. Then, to further analyze the forecasting performance, the significant differences in forecasting accuracy between the proposed models and comparison models are evaluated by using Diebold-Mariano (DM) test. DM is a hypothesis test used to quantify the level of confidence of the difference between two forecasting models [17, 39]. It's defined as follows:

let the observed value be defined by

$$y_n, n = 1, \dots, t + k, \tag{10}$$

and

$$\hat{y}_n^{(1)}, n = 1, \dots, t + k, \tag{11}$$

$$\hat{y}_n^{(2)}, n = 1, \dots, t + k, \tag{12}$$

defines the forecasting values from two competing models. The forecasting errors of the two models are

$$\varepsilon_{n+h}^{(1)} = y_{n+h,m} + y_{n+h,p}^{(1)}, h = 1, \dots, k, \quad (13)$$

$$\varepsilon_{n+h}^{(2)} = y_{n+h,m} + y_{n+h,p}^{(2)}, h = 1, \dots, k. \quad (14)$$

The precision of each forecasting model is measured by a proper loss function $L(\varepsilon_{n+h}^{(i)})$, $i = 1, 2$.

Two popular loss functions involve the square error loss defined by

$$L(\varepsilon_{n+h}^{(i)}) = (\varepsilon_{n+h}^{(i)})^2, \quad (15)$$

and the absolute deviation loss defined by

$$L(\varepsilon_{n+h}^{(i)}) = |\varepsilon_{n+h}^{(i)}|. \quad (16)$$

The Diebold-Mariano test statistic can be defined as

$$DM = \frac{\frac{1}{T} \sum_{n=1}^T (L(\varepsilon_{n+h}^{(1)}) - L(\varepsilon_{n+h}^{(2)}))}{\sqrt{S^2/k}}, \quad (17)$$

where S^2 is an estimator of the variance of $d_h = L(\varepsilon_{n+h}^{(1)}) - L(\varepsilon_{n+h}^{(2)})$ [17].

To determine whether one model is more accurate than another, we test the equal accuracy hypothesis. The null hypothesis is defined by

$$H_0 : L(\varepsilon_{n+h}^{(1)}) - L(\varepsilon_{n+h}^{(2)}) = 0, \forall n. \quad (18)$$

The null hypothesis is that the two forecasting models have the same accuracy. The alternative hypothesis is that the two forecasting models have different levels of accuracy. The DM test statistics converge to a standard normal distribution, the null hypothesis at 10% level of significance is rejected if $|DM| \leq 1.96$. If $2.8 \leq |DM| > 1.96$ the null hypothesis is rejected at the 5% significance level and is rejected at 1% when $|DM| > 2.8$ [17, 29, 38, 39].

Experiments results

As presented in "Case study in Cameroon" section, the proposed approach is applied for one day ahead wind speed forecasting in the Bapouh locality. Thus, data from two Datasets are used to ensure the effectiveness of this hybrid model through multi-step ahead forecasting.

Data preprocessing and input weather variables forecasting

The relationships between wind speed and other weather variables are shown in Table 2 for both Datasets. From

the results of Table 2, it can be observed that the values of R^2 between the natural wind speed and the other natural weather variables are too weak in both Datasets. While it can be seen that the relationships between the normalized wind speed and the transformed weather variables are greatly improved in comparison with that obtained with natural data in both Datasets, both on strength (absolute values of R^2) and on the sense (signs of R^2). Also, results of Sd are given in table 2, which is employed to evaluate the dispersion degree of series of the natural and transformed weather variables. Thus, it is clear that the Sd of all transformed weather variables is improved for both Datasets comparing with the same normalized variables. This means that the degree of linearity of these variables is improved.

In addition to elucidating the relationships between the weather variables, Fig. 4 draws the transformed and normalized data versus time for all the recorded weather variables. It can be observed in Fig. 4a and c the very strong non-compliance between the normalized pace of wind speed and those of other weather variables. This shows more the disparity between the natural weather variables of both Datasets. While Fig. 4b and d show that the transformed variables try to copy the pace of the normalized wind speed over time. In Fig. 4b and d, the curves of pressure are confused with that of wind speed in both cases, reflecting high strength of correction coefficient achieved in Table 2.

Furthermore, how the relationships between the actual normalized wind speed variable and each actual transformed other weather variables, the scatter plots are visualized as shown in Fig. 5. The advantages of the scatter plot between the desired variable versus dependent variable allow to see the direction, forms, strength, and outliers of their relations. It can be observed in Fig. 5 that the disparity between normalized variables is considered in each case. However, it can be confirmed that all the transformed variables have a positive dependency on the actual normalized wind speed. It's thus clear that all the actual transformed have shown a strong linear dependency with the actual wind speed. Therefore, we can affirm that the proposed data preprocessing formula perform well the data normalization while improving the degree of dependency between two variables and decrease the degree of nonlinearity of the second variable. This dependency between the variables which we will use as input and the target variable, respectively, of the neural networks models is crucial for their performance, because it will help them to better learn and convergence. Also, the weak nonlinearity of the transformed variables is a capital requirement for ARIMA model modeling.

As shown in Fig. 2, based on autocorrelation function and partial autocorrelation function, an optimal ARIMA model was developed for each transformed weather variable modeling and pursuing to forecast the desired values.



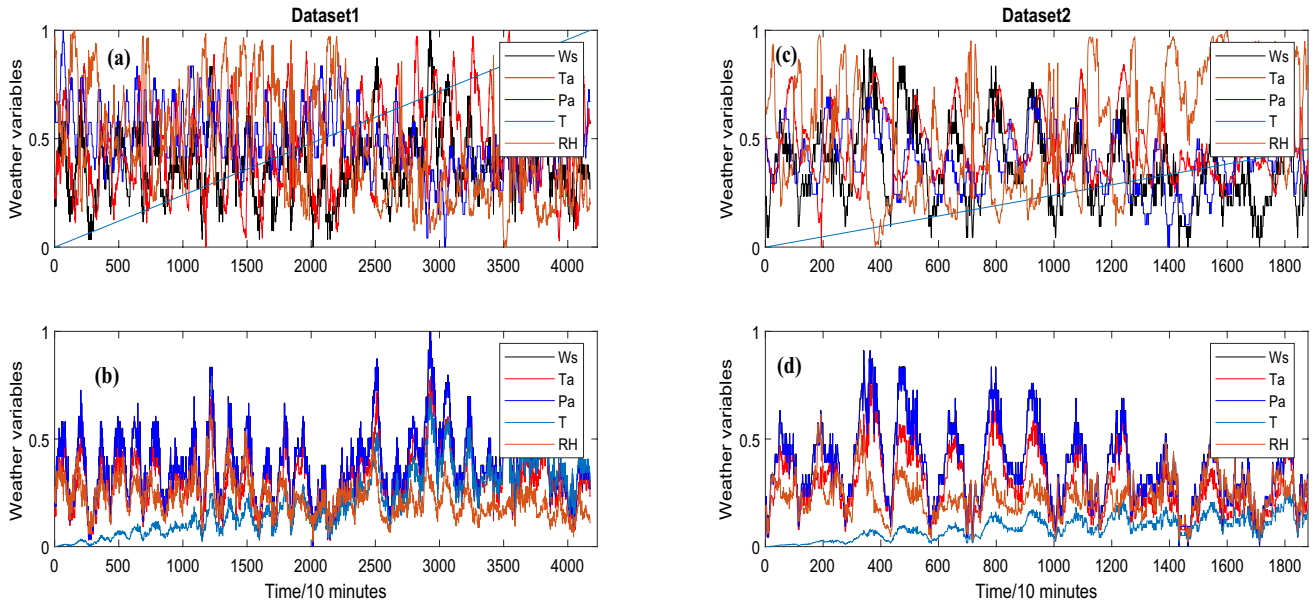


Fig. 4 Concordance between the weather variables. All normalized: (a) and (b). Transformed Ta, Pa, T, RH and normalized Ws: (b) and (d)

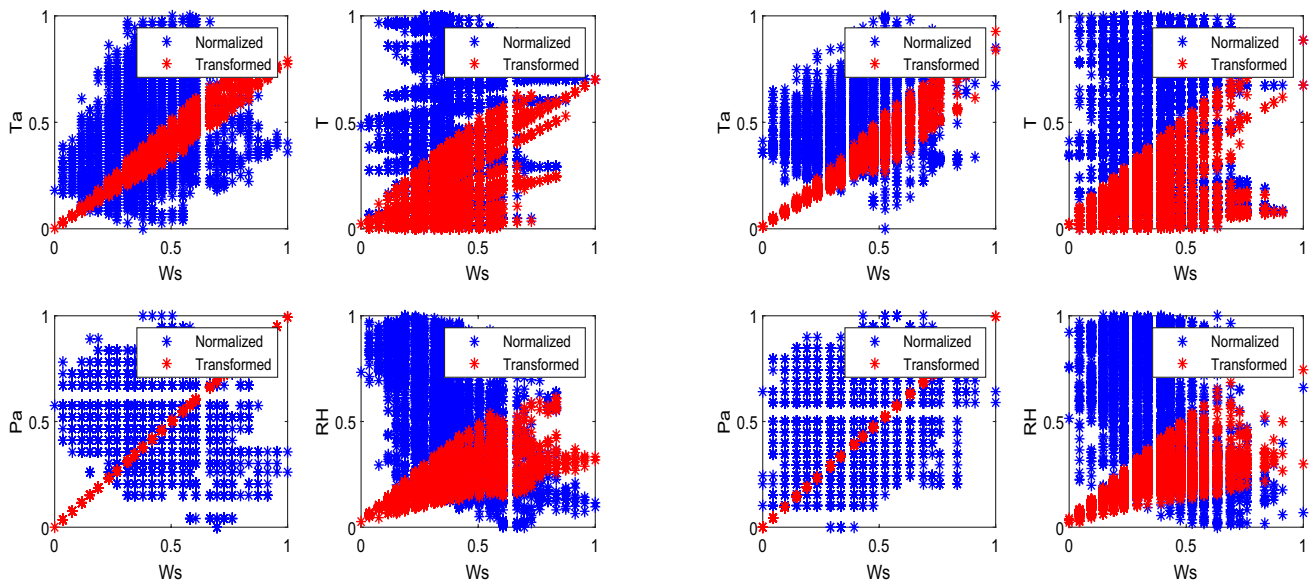


Fig. 5 Concordance between normalized wind speed and other transformed weather variables

Multi-step forecasting is applied for each variable involving 1-step, 2-step, and 3-step ahead in both Datasets.

Multi-step wind speed forecasting

To evaluate the applicability of the proposed hybrid wind speed forecasting method, the BPNN, ANFIS, RBFNN, NARXNN, and GABNN models are trained using the transformed T, Ta, Pa, and RH as input variables and normalized Ws as the target variable. By using the previous

input variables forecasting, these trained neural network models are applied to forecast one day ahead of unknown wind speed values in two Datasets. The ARIMA model is employed as the benchmark model. Every combined model is also compared with the developed traditional ANN model. The forecasting models are developed according to the parameters giving in Table 3. Moreover, all experiments are operated in MATLAB R2018a on Windows 7 with 2.27 GHz Intel Core i3-6700HQ CPU, 64-bit, and 2 GB RAM.

All developed neural networks models have two layers. The number of hidden nodes is determined by using Kolmogorov’s method [40], such as $H = 2M + 1$, where H is the number of hidden nodes and M is the number of the input nodes. Thus, with four selected input variables we have used nine hidden neurons for each neural network model with a linear output node. The tangent hyperbolic function is used in hidden nodes of BPNN and NARXNN models, and Gaussian is used as MF (Membership Function) of the ANFIS model.

The transformation of weather variables used as input of neural networks models increases the relationship between them as shown in Table 4. Thus, in order to minimize the impact of relationships between the input variables on the neural networks forecasting performance, they are arranged

so as avoid to the higher strength relation between the neighboring variables [41]. Therefore, we disposed of the input variables of neural networks models in both Datasets as $Pa - Ta - RH - T$.

First experiment: models evaluation based on traditional criteria

Tables 4 and 5 present the multi-step forecasting results from the Dataset1 and Dataset2, respectively, using MAPE, MAE and RMSE error criteria. From Tables 4 and 5, it can obviously be seen that the MAPE, MAE, and MSE values show that the performance is different according to the forecasting step, Datasets, and forecasting model. Also, it can be seen that the proposed hybrid models, CBPNN, CNARXNN,

Table 3 Experiment parameters of developed forecasting tools

Indexes	Parameters	Values	Indexes	Parameters	Values
BPNN	Maximum iterations	1000	RBFNN	Spread	0.5
	Validation check	1000		Maximum number of training	1000
NARXNN	Maximum iterations	1000	GA	Training requirement precision	0.00002
	Validation check	1000		Maximum generations	200
	Delay	04		Fitness limit	10^{-5}
ANFIS	Number of MF	02			
	Maximum epochs	1000			

Table 4 Relation between the weather variables used as input variables of neural networks models

	Transformed								
	Dataset1				Dataset2				
	Pa	Ta	T	RH	Pa	Ta	T	RH	
Natural	Pa		0.97	0.56	0.63		0.96	0.32	0.58
	Ta	0.05		0.52	0.57	0.30		0.33	0.44
	T	-0.38	0.16		0.59	0.39	0.07		0.34
	RH	0.15	-0.59	-0.57		-0.22	-0.65	0.07	

Table 5 Forecasting results from Dataset1

Models	1-step			2-step			3-step		
	RMSE	MAE	MAPE (%)	RMSE	MAE	MAPE (%)	RMSE	MAE	MAPE (%)
BPNN	1.61	1.27	17.78	1.52	1.24	18.37	1.48	1.21	19.18
AMFIS	2.37	1.88	26.28	2.43	1.95	28.23	2.35	1.89	27.40
NARXNN	0.97	0.73	11.94	1.16	0.84	15.22	1.35	1.04	15.26
RBFNN	1.31	1.04	17.34	1.43	1.18	18.36	1.43	1.18	18.36
GABPNN	1.25	1.01	15.38	1.60	1.30	21.44	1.69	1.44	22.95
ARIMA	1.23	1.03	14.90	1.26	1.01	14.86	1.31	1.07	15.47
CBPNN	0.82	0.64	9.29	0.75	0.58	8.27	0.68	0.55	8.13
CAMFIS	0.83	0.64	9.31	0.76	0.59	8.44	0.69	0.55	8.15
CNARXNN	0.77	0.59	8.99	0.85	0.66	9.37	0.82	0.64	9.11
CRBFNN	0.83	0.64	9.35	0.76	0.60	8.46	0.68	0.55	8.13
CGABPNN	0.82	0.64	9.57	0.81	0.65	9.26	0.84	0.65	9.76

CANFIS, CRBFNN, and CGABPNN give the most forecasting performance among other models used in the comparison. Moreover, according to *Athraa Ali Kadhem et al.*, [7], by considering MAPE criterion, each proposed model has a high forecasting accuracy from both Datasets in all forecasting steps, which is not the case for any traditional model and benchmark model (Table 6).

The percentage of improvement of each combined model versus its based neural network traditional model and ARIMA model is evaluated and presented in Table 7 and Table 8 for the Dataset1 and Dataset2, respectively. Thus, Table 7 and Table 8 show that the forecasting errors are highest improved in each combined model among the single and benchmark models, for the three forecasting steps:

Table 6 Forecasting results from Dataset2

Models	1-step			2-step			3-step		
	RMSE	MAE	MAPE (%)	RMSE	MAE	MAPE (%)	RMSE	MAE	MAPE (%)
BPNN	1.74	1.33	21.33	1.62	1.25	21.12	1.62	1.26	21.15
AMFIS	2.34	1.58	24.69	3.10	2.30	37.02	2.41	1.66	25.86
NARXNN	1.03	1.03	17.33	1.48	1.23	19.20	1.47	1.22	19.51
RBFNN	1.36	1.17	20.83	1.32	1.12	21.21	1.33	1.15	20.72
GABPNN	1.19	1.00	18.96	1.55	1.31	23.70	1.20	1.02	18.99
ARIMA	1.24	0.98	17.50	1.22	0.98	16.92	1.30	1.00	17.21
CBPNN	0.85	0.65	9.53	0.86	0.66	9.76	0.81	0.65	9.09
CAMFIS	0.86	0.65	9.95	0.83	0.65	9.55	0.82	0.65	9.24
CNARXNN	0.82	0.65	9.64	0.83	0.65	9.74	0.87	0.67	9.95
CRBFNN	0.81	0.65	9.26	0.82	0.65	9.58	0.80	0.65	9.00
CGABPNN	0.87	0.66	9.98	0.87	0.66	9.99	0.85	0.65	9.56

Table 7 Improving percentage of forecasting performance from Dataset1

Models	Proposed	Comparisons	1-step			2-step			3-step		
			P_{RMSE}	P_{MAE}	P_{MAPE}	P_{RMSE}	P_{MAE}	P_{MAPE}	P_{RMSE}	P_{MAE}	P_{MAPE}
CBPNN	BPNN	ARIMA	48.82	49.69	47.76	50.72	52.69	54.94	46.67	44.55	49.40
		ARIMA	32.89	37.73	37.68	40.81	42.14	44.29	47.69	48.27	47.47
CANFIS	ANFIS	ARIMA	64.79	65.82	64.57	68.46	69.29	70.08	70.66	70.64	70.24
		ARIMA	32.29	37.46	37.55	39.33	41.15	43.17	47.47	48.20	47.32
CNARXNN	NARXNN	ARIMA	20.27	18.64	24.69	26.85	65.91	38.43	61.23	47.84	56.48
		ARIMA	37.02	42.34	39.67	32.64	34.67	36.93	37.52	40.19	41.12
CRBFNN	RBFNN	ARIMA	37.28	46.12	48.56	56.62	60.51	63.66	56.51	59.04	61.88
		ARIMA	32.29	37.28	50.44	39.29	40.96	43.02	47.73	48.30	47.44
CGABPNN	GABPNN	ARIMA	34.61	36.44	37.78	49.10	49.42	56.78	48.58	41.07	44.96
		ARIMA	33.30	37.36	35.80	35.38	35.36	37.64	47.81	38.89	36.89

Table 8 Improving percentage of forecasting performance from Dataset2

Models	Proposed	Comparisons	1-step			2-step			3-step		
			P_{RMSE}	P_{MAE}	P_{MAPE}	P_{RMSE}	P_{MAE}	P_{MAPE}	P_{RMSE}	P_{MAE}	P_{MAPE}
CBPNN	BPNN	ARIMA	51.22	50.67	55.29	46.69	47.09	53.76	50.00	48.29	57.01
		ARIMA	31.30	33.12	45.52	29.22	32.21	42.29	37.96	34.98	47.18
CANFIS	ANFIS	ARIMA	62.98	58.60	59.68	73.15	71.67	74.18	66.00	60.63	64.25
		ARIMA	30.02	33.02	43.13	31.69	33.43	43.53	37.15	34.86	46.27
CNARXNN	NARXNN	ARIMA	19.80	36.49	44.36	43.60	47.24	49.25	44.49	40.51	48.97
		ARIMA	33.26	33.12	44.90	31.48	33.74	42.42	33.08	32.29	42.13
CRBFNN	RBFNN	ARIMA	39.37	44.21	54.80	37.56	41.52	54.80	39.32	43.31	56.53
		ARIMA	33.26	33.12	45.21	32.48	32.82	43.34	38.23	35.03	47.65
CGABPNN	GABPNN	ARIMA	26.80	34.00	47.31	43.59	49.65	57.83	29.63	36.11	49.65
		ARIMA	29.80	32.72	42.93	28.25	32.41	40.95	35.04	34.88	44.42

- From Dataset1, the percentage of improvement of forecasting errors among the corresponding traditional model range from about 20.27%, 18.64%, and 24.69% to 70.66%, 70.64%, and 70.24% for RMSE, MAE and MAPE, respectively. Among the ARIMA models, they are improved at 32.64%, 34.67%, 36.93% to 47.69%, 48.27%, and 47.47% for RMSE, MAE, and MAPE, respectively.
- From Dataset2, the improvements of forecasting errors are greatest at about 18.80%, 35.49%, 44.36% to 73.15%, 71.67%, 74.98%, for RMSE, MAE, and MAPE, respectively, among the respective traditional model. Comparing with the ARIMA models, they are improved at about 28.85%, 32.41% and 38.23% to 38.23%, 35.50%, and 47.68% for RMSE, MAE, and MAPE, respectively.

Second experiment: models evaluation based on DM test

The results of absolute values of DM test of each proposed forecasting model among the based neural network traditional model are given in Table 9, for each forecasting step of both Datasets. The average of absolute values of the DM test of the proposed forecasting models among the ARIMA model is calculated for each forecasting step. Also, Table 9 shows the average of absolute values of the DM test of forecasting steps. It can be observed that the forecasting errors of proposed models comparing with the based neural networks models and benchmark model are at least rejected at 10% of significance level for all the forecasting steps and Datasets. Moreover, it can be seen that the smallest value of the mean DM test from the three forecasting steps in Table 9 is 2.01, which is larger than the critical value of the 5% significance level. This result means that the proposed forecasting models are significantly superior to the other compared models.

Table 9 DM test results of different models

Models	DM test							
	Dataset1				Dataset2			
	1-step	2-step	3-step	Mean	1-step	2-step	3-step	Mean
BPNN	5.18***	4.50***	3.34***	4.34***	11.69***	0.97*	1.02*	4.56***
ANFIS	4.26***	4.41***	5.19***	4.57***	3.86***	3.31***	2.38**	3.18***
NARXNN	2.12**	9.29***	2.67***	5.51***	3.86***	12.61***	5.65***	7.37***
RBFNN	4.83***	5.55***	1.06*	3.81***	4.30***	2.98***	3.48***	3.58***
GABPNN	3.05***	1.17*	1.82**	2.01**	1.11*	6.17***	3.71***	3.66***
ARIMA	6.94***	10.54***	2.09***	6.52***	3.93***	1.08*	4.22***	2.99***

*, **, and *** denote the significance level at 10%, 5% and 1%, respectively

Discussions on the proposed wind speed forecasting model

The experiments results of the five combined ARIMA-ANN models are proposed based on three single and two collaborative neural networks models for 1-step, 2-step, and 3-step 24-hours ahead wind speed forecasting from two different Datasets. Considering the ANN model as the main forecasting tool, the input variables of the training set are transformed by trying to fit the shape of wind speed by using a proposed formula.

- To verify the effectiveness of characteristics and relationships improvement of transformed weather variables by using the proposed approach, R^2 and Sd are employed. The achieved results from both Datasets shown that every transformed weather variable has the data normalized between 0 and 1, the same direction of variation with wind speed, a very large improvement in the Sd and the decrease in the value of Sd . This revealed that all the transformed weather variables have a strong linear dependency with the actual wind speed and the degree of linearity improved. Then, the proposed data transformation approach is effective to normalize, to improve the data characteristics and the relationships between them.
- The ARIMA models have more ability for wind speed dependent transformed weather variables modeling to forecast the unknown values. Since the degree of non-linearity of these variables is decreased in comparison with that of natural values for both Datasets. This implies that accurate multi-step forecasting is guaranteed for any transformed weather variables using the proposed approach, regardless of its unpredictable initial characteristic.
- Based on five ANN models structures, five combined models are developed involving CBPNN, CANFIS, CNARXNN, CRBFNN, and CGABPNN to forecast the trend of wind speed by using the forecasting values of transformed weather variables as input variables. The achieved results from two Datasets shown that all the

proposed models have a high forecasting accuracy, with the RMSE, MAE, and MAPE error evaluation criteria smaller than that of the comparison and benchmark models. The percentage of improvement as shown in Tables 7 and 8 is range at about 19% to 73%, 18% to 71%, and 24% to 74% for RMSE, MAE, and MAPE, respectively, for both Datasets and all forecasting steps. Also, the results presented in Table 9 have shown high DM test values where very few are rejected at 10% of significance level with the majority rejected at 1% for all the forecasting steps. Based on the above analysis, the proposed forecasting model has superior performance in wind speed forecasting among all comparison models.

Applications of proposed forecasting model

We found that by using the transformed data as input variables, all the neural networks models typically converge much faster and generalize better-forecasting performance than these other, which used the traditional data normalization. Thus, the proposed hybrid wind speed forecasting method has not only superior forecasting ability, but also several real applications, as shown below:

1. The success of the proposed weather variables transformation allows to apply our combined model anywhere and under all conditions regardless the meteorological and environmental condition for accurate wind speed forecasting. Therefore, the unpredictable character of weather variables will not affect the performance of the forecasting model event over time and wind farm conditions.
2. An accurate wind speed forecasting induces an accurate WTPG forecasting. Then, by using the power curve of a wind turbine, the power output values are estimated proportionally to the forecasting wind speed values without worrying about other wind farm characteristics. An accurate WTPG is crucial for electrify grid planning, which helps to plan and promote real-time balance of system power. Also, it allows to timely adjust the adverse effects of wind farm operation avoid large-scale power failure accidents, thus reducing the uncontrollable nature of electricity production and improving its penetration. In addition, effective WTPG forecasting will help to construct control strategies, greatly reduce the rotating reserve capacity, and thus reduce the overall cost of wind energy production [34].
3. Wind speed forecasting may also be used for solar power, wave power, and hydropower sources management.
4. Traditionally, the WTPG forecasting approaches based on ANN models use the actual wind speed-dependent weather variables to forecast the desired values. But the

proposed hybrid wind speed forecasting in this paper can be carried out without actual dependent weather variables. Since these actual variables are predicted individually through the ARIMA model. Therefore, this presents a real step forward for the real-time application of WTPG forecasting.

Conclusion

The accurate Wind Turbine Power Generation (WTPG) forecasting model is crucial to guarantee the wind power integration into the electricity grid. But WTPG forecasting is not an easy task because affected by the unpredictable character of wind speed, too, affected by many weather factors, including air temperature, relative humidity, atmospheric pressure, time, etc. Then, in order to contribute to accurate wind speed forecasting models development for WTPG forecasting, this paper has proposed a new strategy to stabilize the variations of dependent actual weather variables around the wind speed to ensure its accurate forecasting using a novel hybrid ARIMA-ANN model. Thus, the main contribution of this paper is the proposed hybrid wind speed forecasting model, which combines the ARIMA model and ANN model based on relationships between wind speed and other dependent weather variables improving. The ARIMA models are built to forecast transformed input for testing ANN forecasting. Three neural network structures involving BPNN, RBFNN, and NARXNN and hybrid GABPNN, and ANFIS are employed to experiment with the proposed hybrid model for 24-hour multi-step wind speed forecasting. The multi-step forecasting involves 1-step, 2-step, and 3-step based on data from two Datasets in Cameroon. The series of achieved results revealed the effectiveness of the proposed approach for data transformation improving the relationships between two weather variables. Also, the Standard Deviation results have shown that the transformed data have a low level of dispersion compared to real series. This facilitated the high forecasting of actual values of each transformed weather variable. This transformation has been shown ideal to facilitate the neural network model learning and unknown wind speed values forecasting. Thus, results of RMSE, MAE, and MAPE employed to evaluate the forecasting accuracy have shown the higher superiority of all the proposed models among the comparison models with the percentage of improvement up to 77%, 76%, and 74%, respectively. Meanwhile, the experiment results of the Diebold-Mariano test employed to evaluate the significance level of forecasting accuracy of each combined model among the based neural network and benchmark models proved the ability of the proposed hybrid wind speed forecasting model. Then, based on the reported experiments, it can be concluded that the proposed hybrid wind speed forecasting model is a promising

model with high accuracy. This implies that the proposed forecasting models can be used at all times and in all situations, regardless of the weather variables characteristics, especially that of the wind speed. We have also seen that the proposed hybrid model is ideal for real-time WTPG applications. Moreover, outside the field of wind speed and WTPG forecasting, the proposed hybrid model could be used to forecast energy demand, electrical load, and another renewable energy potential such as solar, hydropower, and so on.

Declaration

Conflict of interest The authors declare that there is no known conflict of interests that could have appeared to influence the work reported in this paper.

References

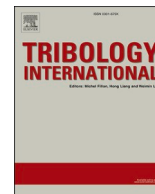
- Guo, Z., Zhao, W., Lu, H., Wang, J.: Multi-step forecasting for wind speed using a modified EMD-based artificial neural network model. *Renew. Energy* **37**, 241–249 (2012)
- Didane, D.H., Rosly, N., Zulkaffi, M.F., Shamsudin, S.S.: Evaluation of wind energy potential as a power generation source in Chad. *Int. J. Rotat. Mach.* (2017). <https://doi.org/10.1155/2017/3121875>
- Zhang, J., Wei, Y., Tan, Z., Wang, K., Tian, W.: A hybrid method for short-term wind speed forecasting. *Sustainability* **9**, 1–10 (2017). <https://doi.org/10.3390/su9040596>
- Aoife, M., Paul, G., Eamon, J.: Current methods and advances in forecasting of wind power generation. *Renew. Energy* **37**, 1–8 (2012). <https://doi.org/10.1016/j.renene.2011.05.033>
- Lei, M., Shiyan, L., Chuanwen, J., Hongling, L., Yan, Z.: A review on the forecasting of wind speed and generated power. *Renew. Sustain. Energy Rev.* **13**, 915–920 (2009). <https://doi.org/10.1016/j.rser.2008.02.002>
- Chang, W.: A literature review of wind forecasting methods. *J. Power Energy Eng.* **2**, 161–168 (2014). <https://doi.org/10.4236/jpee.2014.24023>
- Kadhem, A.A., Izzri, N., Wahab, A., Aris, I., Jasni, J., Abdalla, A.N.: Advanced wind speed prediction model based on a combination of weibull distribution and an artificial neural network. *Sustainability* **9**, 1–17 (2017). <https://doi.org/10.3390/en10111744>
- Nair, K.R.: Forecasting of wind speed using ANN, ARIMA and hybrid models, International Conference on Intelligent Computing, Instrumentation and Control Technologies. **9**, 170–175 (2017)
- Liu, D., Niu, D., Wang, H., Fan, L.: Short-term wind speed forecasting using wavelet transform and support vector machines optimized by genetic algorithm. *Renew. Energy* **62**, 592–597 (2014). <https://doi.org/10.1016/j.renene.2013.08.011>
- Yan, X., Liu, Y., Xu, Y., Jia, M.: Multistep forecasting for diurnal wind speed based on hybrid deep learning model with improved singular spectrum decomposition. *Energy Convers. Manag.* **225**, 113456 (2020). <https://doi.org/10.1016/j.enconman.2020.113456>
- Alonzo, B., Plougonven, R., Mougeot, M., Fischer, A.: From numerical weather prediction outputs to accurate local surface wind speed: statistical modeling and forecasts **1–22**, (2017)
- Hai, Z., Xiang, Z., Lawan, S.M., Azlan, W., Abidin, W.Z., Abubakar, U., Datasets, D.D., Near, P.S.: Multi-step-ahead method for wind speed prediction correction based on numerical weather prediction and historical measurement data multi-step-ahead method for wind speed prediction correction based on numerical weather prediction and historical measurement data. *J. Phys. Conf. Ser.* **926**, 1–11 (2017). <https://doi.org/10.1088/1742-6596/926/1/012007>
- Torres, J.L., De Blas, M., De Francisco, A., Garc, A.: Forecast of hourly average wind speed with ARMA models in Navarre (Spain). *Sol. Energy* **79**, 65–77 (2005). <https://doi.org/10.1016/j.solener.2004.09.013>
- Kavasseri, E.B.R.G., Seetharaman, K.: Day-ahead wind speed forecasting using f-ARIMA models. *Renew. Energy* **34**, 1388–1393 (2009). <https://doi.org/10.1016/j.renene.2008.09.006>
- Salama, M.M.A.: Grey predictor for wind energy conversion systems output power prediction. *IEEE Trans. Power Syst.* **21**, 1450–1452 (2006). <https://doi.org/10.1109/TPWRS.2006.879246>
- Cadenas, E., Jaramillo, O.A., Rivera, W.: Analysis and forecasting of wind velocity in chetumal, quintana roo, using the single exponential smoothing method. *Renew. Energy* **35**, 925–930 (2010). <https://doi.org/10.1016/j.renene.2009.10.037>
- Zhang, W., Qu, Z., Zhang, K., Mao, W., Ma, Y., Fan, X.: A combined model based on CEEMDAN and modified flower pollination algorithm for wind speed forecasting. *Energy Convers. Manag.* **136**, 439–451 (2017). <https://doi.org/10.1016/j.enconman.2017.01.022>
- Iversen, E.B., Morales, J.M., Møller, J.K., Madsen, H.: Short-term probabilistic forecasting of wind speed using stochastic differential equations. *Int. J. Forecast.* (2015). <https://doi.org/10.1016/j.ijforecast.2015.03.001>
- Loukatou, A., Howell, S., Johnson, P., Duck, P.: Stochastic wind speed modelling for estimation of expected wind power output. *Appl. Energy* **228**, 1328–1340 (2018). <https://doi.org/10.1016/j.apenergy.2018.06.117>
- Zárate-miñano, R., Anghel, M., Milano, F.: Continuous wind speed models based on stochastic differential equations. *Appl. Energy* **104**, 42–49 (2013). <https://doi.org/10.1016/j.apenergy.2012.10.064>
- Fazelpour, F., Tarashkar, N., Rosen, M.A.: Short-term wind speed forecasting using artificial neural networks for Tehran. *Iran. Int. J. Energy Environ. Eng.* (2016). <https://doi.org/10.1007/s40095-016-0220-6>
- Mohandes, M.A., Halawani, T.O., Rehman, S., Hussain, A.A.: Support vector machines for wind speed prediction. *Renew. Energy* **29**, 939–947 (2004). <https://doi.org/10.1016/j.renene.2003.11.009>
- Damousis, I.G., Alexiadis, M.C., Theocharis, J.B., Dokopoulos, P.S.: A fuzzy omel for wind speed prediction and power generation in wind parks using spatial correlation. *IEEE Trans. Power Syst.* **19**, 352–361 (2004)
- Cadenas, E., Rivera, W., Campos-amezcua, R., Heard, C.: Wind speed prediction using a univariate ARIMA model and a multivariate NARX model. *Energies* **9**, 1–15 (2016). <https://doi.org/10.3390/en9020109>
- Samadianfard, S., Hashemi, S., Kargar, K., Izadyar, M.: Wind speed prediction using a hybrid model of the multi-layer perceptron and whale optimization algorithm. *Energy Rep.* **6**, 1147–1159 (2020). <https://doi.org/10.1016/j.egy.2020.05.001>
- Wang, J., Hu, J.: A robust combination approach for short-term wind speed forecasting and analysis e Combination of the ARIMA (Autoregressive Integrated Moving Average), ELM (Extreme Learning Machine), SVM (Support Vector Machine) and LSSVM (Least Square SVM) forecasts using a GPR (Gaussian Process Regression) model. *Energy* **93**, 41–56 (2015). <https://doi.org/10.1016/j.energy.2015.08.045>
- Badrul, N., Mat, L., Shamshirband, S., Petkovic, D.: Sensorless estimation of wind speed by adaptive neuro-fuzzy methodology. *Electr. Power Energy Syst.* **62**, 490–495 (2014). <https://doi.org/10.1016/j.jepes.2014.04.065>



28. Wang, S., Zhang, N., Wu, L., Wang, Y.: Wind speed forecasting based on the hybrid ensemble empirical mode decomposition and GA-BP neural network method. *Renew. Energy* **94**, 629–636 (2016). <https://doi.org/10.1016/j.renene.2016.03.103>
29. Wang, J., Heng, J., Xiao, L., Wang, C.: Research and application of a combined model based on multi-objective optimization for multi-step ahead wind speed forecasting. *Energy* (2017). <https://doi.org/10.1016/j.energy.2017.02.150>
30. Wang, J., Dong, Y., Zhang, K., Guo, Z.: A numerical model based on prior distribution fuzzy inference and neural networks. *Renew. Energy* (2017). <https://doi.org/10.1016/j.renene.2017.05.053>
31. Jian, J.: A hybrid forecasting method for wind speed. *MATEC Web Conf.* **232**, 1–5 (2018). <https://doi.org/10.1051/mateconf/201823203013>
32. Pearre, N.S., Swan, L.G.: Statistical approach for improved wind speed forecasting for wind power production. *Sustain. Energy Technol. Assess* **27**, 180–191 (2018). <https://doi.org/10.1016/j.seta.2018.04.010>
33. Moreno, S.R., Coelho, S.: Wind speed forecasting approach based on singular spectrum analysis and adaptive neuro fuzzy inference system. *Renew. Energy* (2018). <https://doi.org/10.1016/j.renene.2017.11.089>
34. Hao, Y., Tian, C.: A novel two-stage forecasting model based on error factor and ensemble method for multi-step wind power forecasting. *Appl. Energy* **238**, 368–383 (2019). <https://doi.org/10.1016/j.apenergy.2019.01.063>
35. Fogno Fotso, H.R., Aloyem Kazé, C.V., Djuidje Kanmoe, G.: Optimal input variables disposition of artificial neural networks models for enhancing time series forecasting accuracy. *Appl. Artif. Intell.* **31**, 1–24 (2020). <https://doi.org/10.1080/08839514.2020.1782003>
36. Profile, S.E.E.: An implementation for combining neural networks and genetic algorithms. *Int. J. Comput. Sci. Technol.* **6**, 218–222 (2015)
37. Vernyuy, A., Abubakar, A., Muhammad-sukki, F., Karim, E.: Renewable energy potentials in Cameroon: Prospects and challenges. *Renew. Energy* **76**, 560–565 (2015). <https://doi.org/10.1016/j.renene.2014.11.083>
38. Chen, H., Wan, Q., Wang, Y.: Refined Diebold-Mariano test methods for the evaluation of wind power forecasting models. *Energies* **7**, 4185–4198 (2014). <https://doi.org/10.3390/en7074185>
39. Xiao, L., Shao, W., Yu, M., Ma, J., Jin, C.: Research and application of a hybrid wavelet neural network model with the improved cuckoo search algorithm for electrical power system forecasting. *Appl. Energy* **198**, 203–222 (2017). <https://doi.org/10.1016/j.apenergy.2017.04.039>
40. Peng, H., Liu, F., Yang, X.: A hybrid strategy of short term wind power prediction. *Renew. Energy* **50**, 590–595 (2013). <https://doi.org/10.1016/j.renene.2012.07.022>
41. Wei, H., Yoshiteru, N., Shouyang, W.: A general approach based on autocorrelation to determine input variables of neural networks for time series forecasting. *J. Syst. Sci. Complex.* **17**, 297–305 (2004)

Publisher's Note Springer Nature remains neutral with regard to jurisdictional claims in published maps and institutional affiliations.





Real-time rolling bearing power loss in wind turbine gearbox modeling and prediction based on calculations and artificial neural network

Hervice Roméo Fogno Fotso^a, Claude Vidal Aloyem Kazé^b, Germaine Djuidje Kenmoé^{a,*}

^a *Laboratory of Mechanics, Department of physics, University of Yaoundé I, P.O.Box 812, Yaoundé, Cameroon*

^b *Department of Renewable Energy, HTTTC Kumba, University of Buea, Cameroon*

ARTICLE INFO

Key words:

Wind turbine
Gearbox
Rolling bearing
Real-time power loss prediction

ABSTRACT

This paper investigates the bearing power loss in gearbox for wind turbines under actual operating wind speed. Actual power loss values are calculated using calibrated SKF model for three different wind turbine gearbox oils. The gearbox applied load at each operating step is determined by using the wind turbine power curve. Wind data from experiments in Cameroon are used for validation. The back-propagation neural network is designed for actual power loss modeling and predicting desired values. The achieved results revealed that the bearing power loss is highly influenced by the wind turbine operating parameters, capacity, and oil. The difference between actual and neural network predicted bearing power loss values under real-time operating parameters showed the effectiveness of the proposed approach.

1. Introduction

Wind energy generated by Wind Turbine (WT) technology is one of the fastest developing sustainable power sources due to its promising potential [1]. The blades of WT must capture the power from the wind required to turn a generator for the production of electrical energy. But, the generators used require a very high drive speed, of the order of 1000 revolutions per minute (rpm), while the turbine blades rotate at the wind speed, which is very low, typically 20 rpm. Thus, to accommodate the rotational speed of the main rotor blades to the needs of the generator, a multiplying gearbox is inserted between the hub and the electrical generator [2]. The WT gearboxes have many configuration technologies involving planetary and parallel gear. Planetary gearing systems exhibit higher power densities than parallel axis gears, and are able to offer a multitude of gearing options, and a large change in rpm within a small volume [3]. The main gearbox used in WT consists of three stages, with planetary gear for each of the first two stages and helical gear for the output stage [4].

The generated power by WTs already exceeds 5.0 MW. This means that the power to be handled by the gearboxes increases [2]. The WT gearboxes are subjected to inevitable power losses during operation, which greatly depends on the amount of power transmitted [5]. The reduction of these power losses will increase the gearbox efficiency. Even a small efficiency increase can save energy useful for several more

households [6]. Studies about the gearboxes power loss has subsequently attracted the attention of several researchers and have been the subject of several publications. Several calculation models have been implemented and experimentally calibrated to study this power loss [7–10]. They have shown that the load-dependent gear and rolling bearing are main sources of power loss in gearbox [11].

The rolling bearing loss can be divided into load dependent and load independent power losses [12]. The load dependent bearing losses depend on bearing type and size, load and sliding conditions in the bearing and on the lubricant type. While load independent bearing losses depend on bearing type and size, bearing arrangement, lubricant viscosity and supply [13–16]. To contribute to rolling bearing prediction, Carlos M.C.G. Fernandes et al. [4] calibrated a rolling bearing torque loss model using the experimental results for ball bearings and roller bearings lubricated with several WT gear oils under different formulations. Based on the model presented in [4], Carlos MCG Fernandes et al. [6] predicted the power loss for a 2.5 MW WT gearbox by calculations based on an analytical model. This prediction is carried out under rated operating conditions involving input rotational speed, input torque and transmitted power.

It is very difficult to develop a simple and general formulation to evaluate these power losses in WT gearbox [17]. The calculations based on existing analytical models remain complex and robust, and require the experimental parameters according to the systems for effective

* Corresponding author.

E-mail address: kjdjuidje@yahoo.fr (G.D. Kenmoé).

<https://doi.org/10.1016/j.triboint.2021.107171>

Received 11 March 2021; Received in revised form 29 June 2021; Accepted 2 July 2021

Available online 5 July 2021

0301-679X/© 2021 Elsevier Ltd. All rights reserved.

power loss prediction. Wind speed is one of the most critical characteristics in wind power generation. It varies in both time and space, and influenced by many factors such as geographic and weather conditions. The stochastic nature of WT operating wind speed induces the transmitted power intermittent. Each modern WT has a unique power curve, which displays the power output as a function of the wind speed. The power curve shows that a WT transmits the power in two typical regions: (1) the nonlinear region; the WT power output increases with the increase of the wind speed until reaching a saturated point (rated speed), e.g. the transmitted power remains intermittent as wind speed increases; (2) the rated region; the power output is at its maximum value and is constant (rated power), e.g. increasing the wind speed will not increase the transmitted power. For a comprehensive review of the WT power curve, we suggest to refer to the work reported in Refs. [18–21].

Most of the WTs operate in the nonlinear region, because the rated

speed is reached very rarely. Due to WT working conditions under variable load and its operating environment, it is imperative to predict the power loss in the gearbox under real-time operating conditions. Previous works have limited their studies on rated operating parameters with fixed rotational speed. Furthermore, artificial intelligence, particularly artificial neural networks (ANN) models, have been shown to be capable of dealing with the uncertainties that arise when solving real-world problems, providing robust solutions and easy implementation in a different way [22]. Therefore, this work aims to predict the rolling bearing power loss in the gearbox for a modern WT under real-time operating conditions by using an ANN model. The related gearbox has three stages, including two planetary and one parallel gear. Due to lack of a historical dataset of experimental data, the bearing power loss model was developed by using the previous experimental calibrated analytical model. The relations between the real-time wind speed and

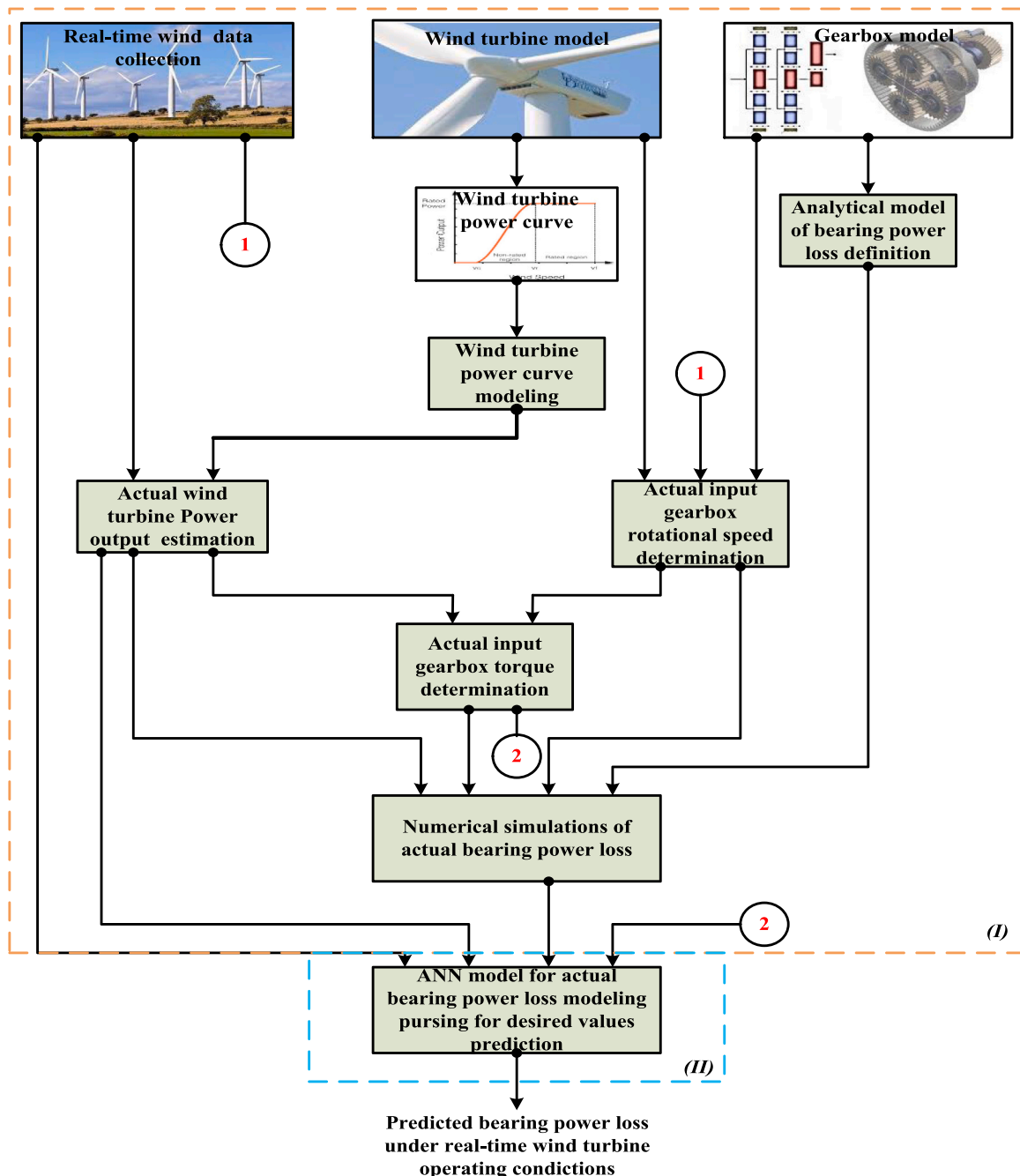


Fig. 1. Flowchart of proposed rolling bearing power loss prediction in wind turbine gearbox approach.

gearbox load, and rotational speed are established. Based on calibrated analytical models, calculations were carried out to determine the actual bearing power loss data. An ANN model is developed for actual values of power loss modelling, to predict the unknown values. This proposed approach is validated for 2.0 MW and 2.5 MW WTs using the wind data recorded in Cameroon.

The remainder of the paper is organized as follows: Section 2 sets out the methodology from the description of the gearbox to the analytical bearing power loss model and application context. Section 3 provides calculations, while the ANN model building is presented in Section 4. The results are presented and discussed in Section 5. Finally, Section 6 concludes the paper based on achieved results.

2. Related methodology

Fig. 1 shows the flowchart of the proposed rolling bearing power loss in wind turbine gearbox under real-time operating conditions prediction scheme. It consists of two main phases, the experimental stage (I) and modelling and prediction stage (II). The experimental stage consists of collecting wind data for actual WT operating parameters and bearing power loss calculation. Then, actual bearing power loss data in the

gearbox are estimated by using the calibrated SKF model with actual WT operating conditions. Stage (II) consists of designing and training of an ANN model using the actual data of bearing power loss and WT operating parameters for predicting the desired bearing power loss values.

In this study, the Backpropagation neural network (BPNN) model was employed. BPNN is a type of Feedforward Neural Network (FFNN) model based on a gradient descent method that minimizes the sum of the squared errors between the output values and the actual values [23]. It is many applications and is considered as a base ANN model; since several other models of ANN are derived from it. BPNN is widely used and is powerful in robust pattern modelling and time series prediction.

2.1. Model definition

2.1.1. Gearbox description

The considered gearbox model in this study is presented in Ref [6]. It consists of three stages gear configurations with planetary gear at stage 1 (low-speed stage) and stage 2 (intermediate speed stage), and a helical gear at stage 3 (high-speed stage) as shown in Fig. 2.a. The planetary gears have the fixed ring, the Low Speed Shaft (LSS) of the first stage would be connected to the rotor hub to receive the input speed and

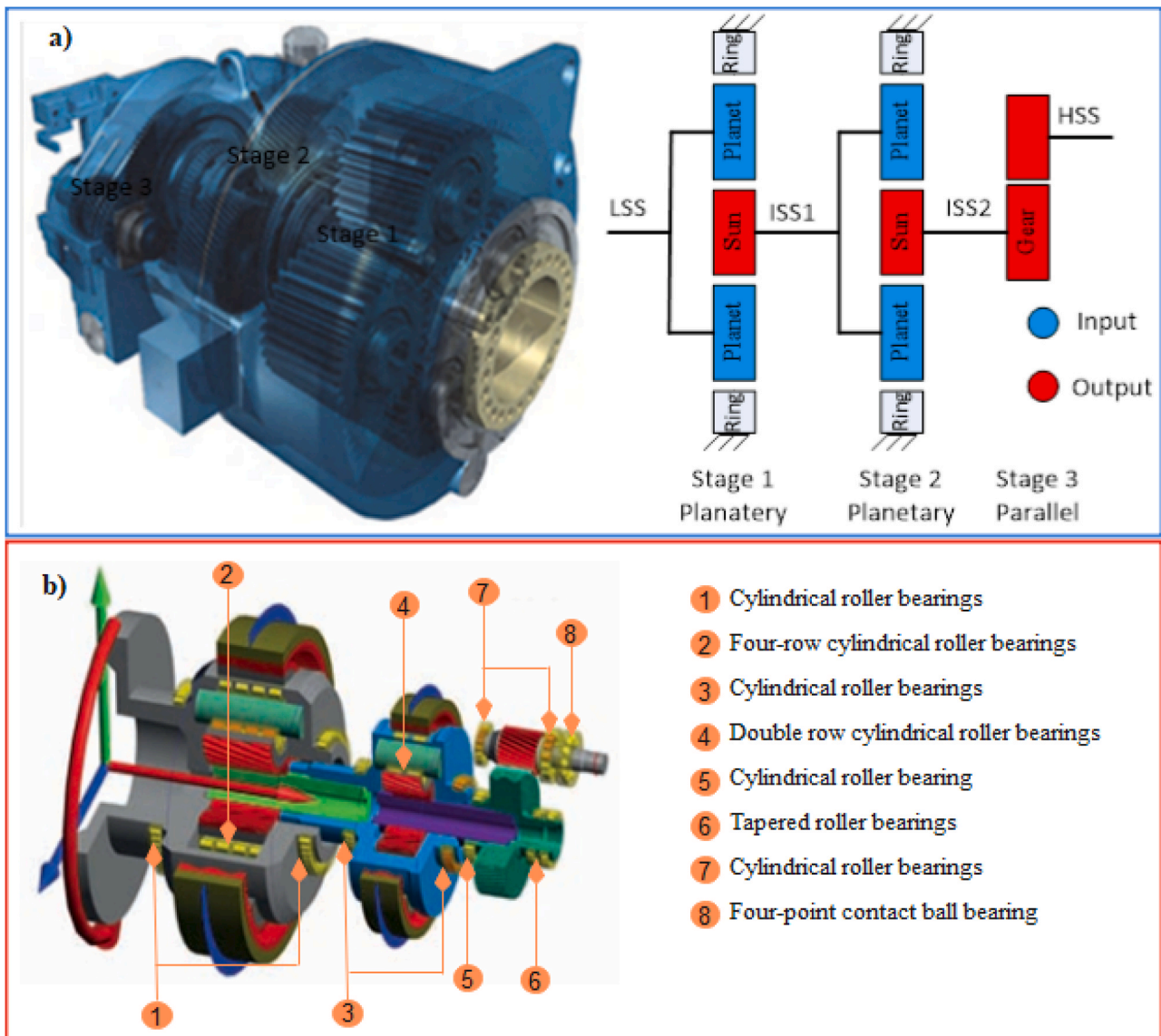


Fig. 2. WT Gearbox: a) two-stage planetary and one-stage parallel [3] and b) bearings setup.

torque, while its sun gear would be connected to the first Intermediate Speed Shaft (ISS1) of the carrier of second stage. The torque from the sun of the second stage would be transferred in third stage through the second Intermediate Speed Shaft (ISS2). The High Speed Shaft (HSS) would make the gearbox output torque available to the electrical generator. The total transmission ratio of gearbox is 102. Fig. 2.b shows the gearbox bearings setup. The basic properties for the gears in the gearbox are shown in Table 1. The parameters of rolling bearings that supported the shafts are listed in Table 2. Where Z is the gear number of teeth, i is the gear ratio, β is the gear helix angle in degree, α is gear pressure angle in degree, and m is the gear module in mm.

Three fully formulated ISO VG 320 gear oils are been considered, involving mineral (MINR), polyalpholephin (PAOR), and polyalkylene glycol (PAGD) oils. Their physical properties are displayed in Table 3. Where ρ is the oil density in g/cm^3 , α_t is the thermal expansion coefficient and VI is the viscosity index. More chemical structure such as infrared spectra which allows to identify some of the characteristic peaks of the investigated WT gear oils are shown in Refs [4,24].

2.2. Bearing power loss model

SKF model [25] was used for analytical bearing power loss formulation. The power loss is expressed through the torque loss. Therefore, the total bearing friction torque T_t accounts for rolling frictional torque T_{rr} , sliding frictional torque T_{sl} , viscous drag T_{drag} , and the seal torque loss T_{seal} as given in Eq. (1),

$$T_t = T_{rr} + T_{sl} + T_{drag} + T_{seal}. \tag{1}$$

The seal loss (T_{seal}) was disregarded in this study, because we assumed that the system does not have seal. The rolling torque is defined by Eq. (2) as follow,

$$T_{rr} = \phi_{ish} \cdot \phi_{rs} \cdot [G_{rr}(n \cdot v)^{0.6}], \tag{2}$$

where ϕ_{ish} defines the inlet shear heating given in Eq. (3), while ϕ_{rs} given in Eq. (4), defines the replenishment/starvation reduction factor, both for rolling element raceway contact,

$$\phi_{ish} = \frac{1}{1 + 1.84 \times 10^{-9} \cdot (n \cdot d_m)^{1.28} \cdot v^{0.64}}, \tag{3}$$

$$\phi_{rs} = \frac{1}{e^{K_{rs} \cdot v \cdot n \cdot (d+D)} \sqrt{K_Z / 2 \cdot (D-d)}}, \tag{4}$$

with n the rotational speed in rpm, v the kinematic viscosity in mm^2/s of the lubricant at the operating temperature, d_m the bearing mean diameter in mm, K_{rs} the replenishment/starvation constant for oil lubrication, K_Z geometric factor of related bearing, D and d are the bearing outside and bearing bore in mm, respectively. The bearing load constant G_{rr} represents the influence of applied load and geometrical parameters on the rolling friction torque. Then, it is defined according to the bearing type, as given in Eqs. (5) and (6) for Cylindrical Roller Bearing (CRB) and Tapered Roller Bearing (TRB), and Eq. (7) for Contact Ball Bearing

(CBB), respectively,

$$G_{rr} = R_1 \cdot d_m^{2.41} \cdot F_a^{0.31}, \tag{5}$$

$$G_{rr} = R_1 \cdot d_m^{2.38} (F_r + R_2 \cdot Y \cdot F_a)^{0.31}, \tag{6}$$

$$G_{rr} = R_1 \cdot d_m^{1.97} (F_r + F_{Mg} + R_2 \cdot F_a)^{0.54}, \tag{7}$$

with

$$F_{Mg} = R_3 \cdot d_m^4 \cdot n^2, \tag{8}$$

where F_a and F_r represent the axial and radial load in N respectively, while Y is the axial load factor. R_1 , R_2 and R_3 are the geometric constants for rolling frictional moments, where their values depend on bearing series. Both loads, F_r and F_a are always considered as positive.

The sliding torque is expressed by Eq. (9) as,

$$T_{sl} = G_{sl} \cdot \mu_{sl}, \tag{9}$$

where G_{sl} is the sliding friction parameter, Which represents the influence of the bearing load on the sliding resistance. It is defined according to the bearing type as given in Eqs. (10) and (11) for CRB and TRB, respectively. It is expressed for CBB in Eq. (12),

$$G_{sl} = S_1 \cdot d_m^{0.9} \cdot F_a + S_2 \cdot d_m \cdot F_r, \tag{10}$$

$$G_{sl} = S_1 \cdot d_m^{0.82} (F_r + S_2 \cdot Y \cdot F_a), \tag{11}$$

$$G_{sl} = S_1 \cdot d_m^{0.26} ((F_r + F_{Gg})^{4/3} + S_2 \cdot F_a^{4/3}), \tag{12}$$

with

$$F_{Gg} = S_3 \cdot d_m^4 \cdot n^2, \tag{13}$$

where S_1 , S_2 , and S_3 are the geometric constants, depending on bearing series.

The global coefficient of friction, μ_{sl} permits the study of the effect of lubrication on sliding friction of the rolling bearing. It strongly depends on the lubrication regime and is defined as given in Eq. (13),

$$\mu_{sl} = \phi_{bl} \cdot \mu_{bl} + (1 - \phi_{bl}) \cdot \mu_{EHL}, \tag{13}$$

where μ_{bl} and μ_{EHL} are the boundary film coefficient of friction and the full film friction coefficient respectively. Their recommended values are $\mu_{bl} = 0.15$ and $\mu_{EHL} = 0.05$ for mineral oils and $\mu_{EHL} = 0.04$ for synthetic oils. The weighting factor, ϕ_{bl} materializes the influence of asperity contact and lubricant shearing mechanisms. It is expressed as given in Eq. (14),

$$\phi_{bl} = \frac{1}{e^{2.6 \times 10^{-8} (n \cdot v)^{1.4} \cdot d_m}}. \tag{14}$$

The bearing drag losses are defined for ball bearings and roller bearings by Eqs. (15) and (16), respectively,

Table 1
Parameters of the related gearbox rolling bearings.

Stage	Type	Reference	Location	Number	d(mm)	D(mm)	B(mm)
Stage 1	CRB	SKF NU 20/800 ECMA	Carrier	1	800	1150	200
Stage 2	CRB	SKF NU 1080 MA	Carrier	1	400	600	90
Stage 3	CRB	SKF NNUD 6056 ECMAS/P53	Planets	3	280	420	250
	CRB	SKF NU 244 ECMA	Carrier	1	200	400	65
	CRB	SKF NU 1060 MA	Carrier	1	300	460	74
	CRB	SKF NNCF 4930 CV	Planets	3	150	210	60
	CRB	SKF NU 1060 MA	Wheel shaft	1	300	460	74
	TRB	SKF 32960	Wheel shaft	2	300	420	76
	CRB	SKF NU 1036 ML	Pinion shaft	1	180	280	46
	CRB	SKF NU 236 ECMA	Pinion shaft	1	180	320	52
	CBB	NSK QJ1036	Pinion shaft	1	180	280	46

Table 2
Gear geometric parameters of the gearbox.

Parameter	Stage 1			Stage 2			Stage 3	
	Sun	Planet	Ring	Sun	Planet	Ring	Pinion	Wheel
Z	21	35	-96	23	38	-103	117	35
i	5.587			5.464			3.343	
β	20			20			20	
α	10			10			10	
m	16			9			7	

Table 3
Physical properties of gear oils.

Parameter	Unit	MINR	PAOR	PAGD
ρ at 15 °C	g/cm ³	0.902	0.859	1.059
$\alpha_t \times 10^{-4}$	cSt	5.8	5.5	7.1
ν at 40 °C	cSt	319.22	313.52	290.26
ν at 70 °C	cSt	65.81	84.99	102.33
ν at 100 °C	cSt	22.33	33.33	51.06
VI		85	153	252

$$T_{drag} = 0.4V_M \cdot K_{ball} \cdot d_m^5 \cdot n^2 + 1.093 \times 10^{-7} n^2 \cdot d_m^3 \left(\frac{n \cdot d_m^2 \cdot f_t}{\nu} \right)^{-1.379} R_s, \quad (15)$$

$$T_{drag} = 4V_M \cdot K_{roll} \cdot C_w \cdot B \cdot d_m^4 \cdot n^2 + 1.093 \times 10^{-7} n^2 \cdot d_m^3 \left(\frac{n \cdot d_m^2 \cdot f_t}{\nu} \right)^{-1.379} R_s, \quad (16)$$

with

$$K_{ball} = \frac{i_{rw} \cdot K_Z (d + D)}{d - D} \times 10^{-12}, \quad (17)$$

and

$$K_{roll} = \frac{K_L \cdot K_Z (d + D)}{d - D} \times 10^{-12}, \quad (18)$$

where i_{rw} is the number of ball rows. The C_w factor is given by Eq. (19),

$$C_w = 2.789 \times 10^{-10} l_D^3 - 2.786 \times 10^{-4} l_D^2 + 0.0195 l_D + 0.6439, \quad (19)$$

with

$$l_D = \frac{5 \cdot K_L \cdot B}{d_m}, \quad (20)$$

$$f_t = \begin{cases} f_t = \sin(0.5t), & \text{if } 0 \leq t \leq \pi \\ f_t = 1, & \text{if } \pi \leq t \leq 2\pi \end{cases} \quad (21)$$

$$R_s = 0.36 d_m^2 (t - \sin t) f_A,$$

were

$$t = 2\cos^{-1} \left(\frac{0.6d_m - H}{0.6d_m} \right), \quad (22)$$

and

$$f_A = \frac{0.005 \cdot K_Z \cdot (D + d)}{D - d}. \quad (23)$$

The total bearing power loss (P_{LV} in kW) in WT gearbox was calculated using Eq. (24) as follow [11],

$$P_{LV} = \frac{n \cdot T_i}{9550} \quad (24)$$

2.3. Wind turbine and application context

The transmitted power of a WT significantly varies with wind speed.

Hence, every controlled WT has a unique power performance curve which aids in generating power prediction without the technical details of the components of the WT generating system. In order to investigate the power loss in the WT gearbox under real conditions, ENERCON 2.0 MW (E-82 2000 kW) WT was chosen as the application. Its manufacturer's power curve is shown in Table 4. Table 4 shows WT power output as a function of the hub height wind speed. It can be observed that this WT starts with the useful power transmission from 2 m/s (cut-in speed) and stops with power generation at 25 m/s (cut-out speed), while from 13 m/s (rated speed) the transmitted power stays constant. Its rotor diameter is equal to 82 m with 3 blades.

In order to predict the bearing power loss under real conditions, Eq. (25) was used to estimate WT transmitted power [20],

$$P_r(V) = \begin{cases} 0 & V < V_{ci} \\ P_f(V) & V_{ci} \leq V < V_r \\ P_r & V_r \leq V < V_{co} \\ 0 & V_{co} < V \end{cases} \quad (25)$$

where P_r is the rated power, V_{ci} is the cut-in speed, V_r is the rated speed, and V_{co} is the cut-out speed, $P_f(V)$ is the nonlinear part of the transmitted power defined in Eq. (26) [21],

$$P_f(v) = P_r \left(\frac{V^a - V_{ci}^a}{V_r^a - V_{ci}^a} \right), \quad (26)$$

With a , being the order of power output curve, and its value for this work is 2.9, obtained by fitting the wind curve provided by the manufacturer of the interested WT.

The input gearbox rotational speed and torque at LSS were determined using Eqs. (27) and (28), respectively [26],

$$n = \frac{60 \times TSR}{2\pi \cdot R} V, \quad (27)$$

$$T_{in} = \frac{9550 \times P_{tr}}{n}, \quad (28)$$

where TSR is the tip speed ratio [27], which depends on the number of blades and R is the rotor radius in m. TSR was considered equal to 6 for three blades. The Willis formula expressed in Eq. (29) was used to determine the different transmission ratios in gearbox stages as follows,

$$n_p \cdot Z_p = Z_c \cdot (Z_p + Z_s) - n_s \cdot Z_s, \quad (29)$$

Table 4
Manufacturer's power curve of E-82 2000 kW WT.

Wind speed (m/s)	Output power (kW)	Wind speed (m/s)	Output power (kW)	Wind speed (m/s)	Output power (kW)
1	0	10	1 580	19	2 050
2	3	11	1 810	20	2 050
3	25	12	1 980	21	2 050
4	82	13	2 050	22	2 050
5	174	14	2 050	23	2 050
6	321	15	2 050	24	2 050
7	532	16	2 050	25	2 050
8	815	17	2 050		
9	1 180	18	2 050		

where n_p, n_c, n_s are the planet, carrier and sun rotational speeds respectively; while Z_p, Z_c, Z_s are the planet, carrier and sun number of teeth, respectively.

The wind speed data collected in Bapou in the Western Region of Cameroon, was used to validate the proposed approach. The geographical coordinates of the site are N 05°09'35.52" and E 10°19'21.90". Data collected for two months at an interval of 10 min from 20th November 2016–31st January 2017 was available. The scanning frequency is 144 times per day from 00:00–24:00, with 10512 samples for 73 days. Their values range from 0.2 m/s to 17.1 m/s. 523 samples (4.98%) appearing on certain days between 6 p.m. and 2 a.m. are less than 2 m/s. 72 samples (0.68%) appearing on three days between 5 a.m. and 4 p.m. are greater than or equal to 13 m/s. This means that the WT will mainly operate at the nonlinear part of the power curve in this site, since the rated value is reached very rarely.

3. Power loss calculations

The calculations were carried out using the experimental calibrated parameters of the bearing power loss model presented in Subsection 2.2. The usual operating temperature of the gearbox ranges between 60 °C and 80 °C. Carlos MCG Fernandes et al. [6] showed that the difference between the power loss at 60 °C and 80 °C is very weak. Therefore, the bearing power loss was predicted at 80 °C in the present study. The calibrated coefficients of friction μ_{bl} and μ_{EHD} in Ref [4], at the operating temperature of 80 °C for $3262.5 < n.d_m < 52200$ for Thrust Ball Bearing (TBB) and RTB as given in Table 5 were used. Table 6 gives the SKF bearings constants used on the calculations, $K_{rs} = 3 \times 10^{-8}$.

In order to validate the effectiveness of the developed model and calculations, the power loss of 2.5 MW WT with two planetary and one helical gearbox under rated rotational speed and transmitted power reported in Ref. [6] was used as the benchmark (see Fig. 4).

4. Neural network prediction

4.1. ANN Prediction model designing

BPNN model was built for bearing power loss modelling and prediction by using the gearbox operating parameters as input variables and P_{LV} as output variable, as given in Fig. 3. The gearbox operating parameters include V, P_{tr}, T_{in} , and operating time step (t_s). The ANN model was built using the Lavenberg Marquardt (LM) learning algorithm with hyperbolic tangent sigmoid and linear functions as activation function in the hidden and output layers, respectively, 1000 epochs, and 500 validation checks. The magnitude of the input and target variables were normalized in the range of [0 1]. The number of hidden node was determined using Kolmogorov method [23,28], so that nine neurons were used. All experiments were operated in MATLAB R2018a on Windows 7 with 2.27 GHz Intel Core i3-6700HQ CPU, 64-bit and 2 GB RAM with a developed code. Wind data for four days was used for validation. Their values range from 2.15 m/s to 11.2 m/s. Three days (from 28th to 30th January 2017) of actual power loss data were used to train the ANN model for predicting the unknown values of the fourth day (31st January 2017).

Table 5
Coefficient of friction at 80 °C [4].

Oil Parameter		Bearing type	
		TBB	RTB
MINR	μ_{bl}	0.058	0.035
PAOR	μ_{EHD}	0.056	0.018
PAGD	μ_{bl}	0.049	0.039
	μ_{EHD}	0.044	0.010
	μ_{bl}	0.054	0.025
	μ_{EHD}	0.044	0.010

4.2. Prediction model evaluation criteria

To check the prediction capacity of the developed ANN model, three statistical evaluation criteria were considered to assess performance, involving Mean Absolute Error (MAE), Root Mean Square Error (RMSE), and Mean Absolute Percentage Error (MAPE), as defined in Eqs. (30), (31) and (32) respectively,

$$MAE = \frac{1}{N} \sum_{j=1}^N |y_j - \hat{y}_j|, \tag{30}$$

$$RMSE = \sqrt{\frac{1}{N} \sum_{j=1}^N (y_j - \hat{y}_j)^2}, \tag{31}$$

$$MAPE = \frac{1}{N} \sum_{j=1}^N \left| \frac{y_j - \hat{y}_j}{y_j} \right| \times 100, \tag{32}$$

where y_j and \hat{y}_j are the actual and predicted values, respectively at the time step j , and N is the number of prediction time step. Smaller values of MAE, RMSE and MAPE reflect better prediction performance.

5. Results and discussion

This section describes the experiments conducted to examine the effectiveness of the proposed scheme. Fig. 4.a and 4.b show the bearing power loss at different stages of gearboxes at rated parameters of 2.0 MW (WT1) and 2.5 MW (WT2) WTs respectively. As mentioned in Section 3, the bearing power loss results shown in Fig. 4b were presented in Ref. [6], which are used in the present study as comparison and validation model. The calculations are done for three oil formulations, MINR, PAOR and PAGD. The input rotational speed of the gearboxes is 20 rpm, and the transmitted power is 2.0 MW and 2.5 MW for WT1 and WT2, respectively. From Fig. 4, it can be observed that the power loss is very low in the first stage, while stage 3 constitutes the main source of bearing power loss in both gearboxes. The total losses are 39 kW, 40 kW and 43 kW for WT1 with MINR, POAR and PAGD oil, respectively. They are 43 kW, 44 kW and 47 kW for WT2 with MINR, POAR and PAGD oil, respectively. The above results show that, by using MINR oil with respect to PAGD, it is possible to save 4 kW in both WTs, which increases the gearboxes efficiency. These are consistent with the results of other researchers [6].

Fig. 5 shows the P_{LV} for each considered oil and 1.5% of P_{tr} for WT1 power curve. The results presented in Fig. 5 were used to predict the P_{LV} around the WT1 power curve. Therefore, it can be observed that the P_{LV} increases as the P_{tr} and V increase in the nonlinear part of the power curve. In the rated zone, despite the fact that the P_{tr} remains constant, the P_{LV} increases with increasing V . For instance, with MINR oil, the power loss is 35 kW at 13 m/s and 133 kW at 25 m/s. To ensure the safety of the gearbox, its input rotational speed must be stopped at a certain value of V .

The results presented in Figs. 4 and 5 show that the P_{LV} greatly depends on V and P_{tr} . To experiment the P_{LV} under actual operation conditions, the experiment's actual wind speed data presented in Fig. 6a is used to estimate the P_{tr}, T_{in} and then P_{LV} as given in Fig. 6b, c and d, respectively. P_{LV} is calculated for three days at intervals of 10 min. We observe that V, P_{tr}, T_{in} and P_{LV} all have the same shape over time, which reflects strong relationships between them. This relationship introduced by V through P_{tr} , confirms the dependence of P_{LV} on V and P_{tr} .

From Fig. 6, V range from 2.2 m/s to 11.9 m/s, P_{tr} range from 18 kW to 1766.7 kW, and P_{LV} range from 0.46 kW to 29 kW for MINR oil, from 0.53 kW to 30 kW for PAOR oil, from 0.62 kW to 32 kW for PAGD oil. Therefore, the influence of lubricant type is observed in real-time operation. We also confirmed that the WT associated with experimental data of this study only operates in the nonlinear zone of the

Table 6
Constants of the SKF bearings.

Reference	K_L	K_Z	S_1	S_2	S_3	R_1	R_2	R_3
NU 20/800 ECMA	0.65	5.1	0.16	0.0015	-	1.23×10^{-6}	-	-
NU 1080 MA	0.65	5.1	0.16	0.0015	-	1.23×10^{-6}	-	-
NNUD 6056 ECMAS/P53	0.7	6.2	0.16	0.0015	-	2.13×10^{-6}	-	-
NU 244 ECMA	0.65	5.1	0.16	0.0015	-	1.23×10^{-6}	-	-
NU 1060 MA	0.65	5.1	0.16	0.0015	-	1.23×10^{-6}	-	-
NNCF 4930 CV	0.7	6.2	0.16	0.0015	-	2.13×10^{-6}	-	-
NU 1036 ML	0.65	5.1	0.16	0.0015	-	1.23×10^{-6}	-	-
NU 236 ECMA	0.65	5.1	0.16	0.0015	-	1.23×10^{-6}	-	-
SKF 32960	0.7	6	0.009	2	-	$1.23 \times 10^{-6-6}$	10.9	-
NSK QJ1036	-	3.1	1.2×10^{-2}	0.9	1.4×10^{-12}	4.78×10^{-6}	2.42	1.40×10^{-12}

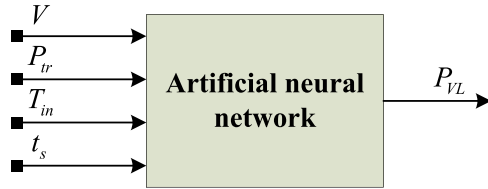


Fig. 3. ANN for power loss prediction flowchart.

power curve. The intermittent nature of the WT operating environment, such as wind speed, causes the bearing power loss to vary over time. This means that the gearbox efficiency will be intermittent as wind speed of WT operation over time.

To further investigate the influence of oil and WTs capacity on P_{LV} , Eq. (30) was used to assess the percentage difference (IP_{LV}) of one result of P_{LV} over another,

$$IP_{LV} = \left| \frac{P_{LV_2} - P_{LV_1}}{P_{LV_1}} \right| \times 100, \quad (33)$$

where subscript 1 indicates a referential P_{LV} result and subscript 2 gives a compared P_{LV} result, both achieved with two different gearbox oils or WT capacity.

The percentage difference of the P_{LV} of WT1 compared to WT2 are

10.25%, 10%, and 9.3% for MINR, POAR, and PAGD oils, respectively. Thus, the above results show that P_{LV} is more important in WT1 than in WT2 at the same gearbox input rotational speed. It is clear that the bearing power loss depends also on WT capacity. Also, it can be seen that IP_{LV} between WT1 and WT2 is more important when MINR oil is used compared to POAR and PAGD oils. Table 7 displays the IP_{LV} for different oils. The MINR is taken as reference oil. At the rated parameters, it can be seen from Table 7 that PAGD oil produces high bearing P_{LV} in the gearbox in comparison with MINR and POAR oils, with the IP_{LV} equal to 9.3% and 6.81% in WT1, and 10.25% and 7.69% in WT2. Compared to POAR oil, MINR oil produces P_{LV} , the IP_{LV} in this case is 2.32% and 2.25% in WT1 and WT2, respectively. The mean values of IP_{LV} under WTPC and real operating conditions for different oils are also presented in Table 7 for WT1. It can be observed that under both WTPC and real WT operating conditions, the P_{LV} is lower when using MINR oil and POAR oil than when PAGD oil is used. Comparing MINR oil to PAGD, IP_{LV} are 7.67% and 12.63% under power curve and actual WT operating conditions, respectively. Also, MINR oil reduces the P_{LV} by 2.79% and 4.16% compared to POAR oil. Comparing POAR oil to PAGD oil under power curve and real-time WT operating conditions, P_{LV} is reduced by 2.79% and 4.16%, respectively. Therefore, MINR oil produces less P_{LV} than MINR oil and PAGD oil whatever the exogenous conditions in which the WT operates.

To avoid complex and robust calculations in the future, we use the ANN and historical bearing power loss values to predict the desired

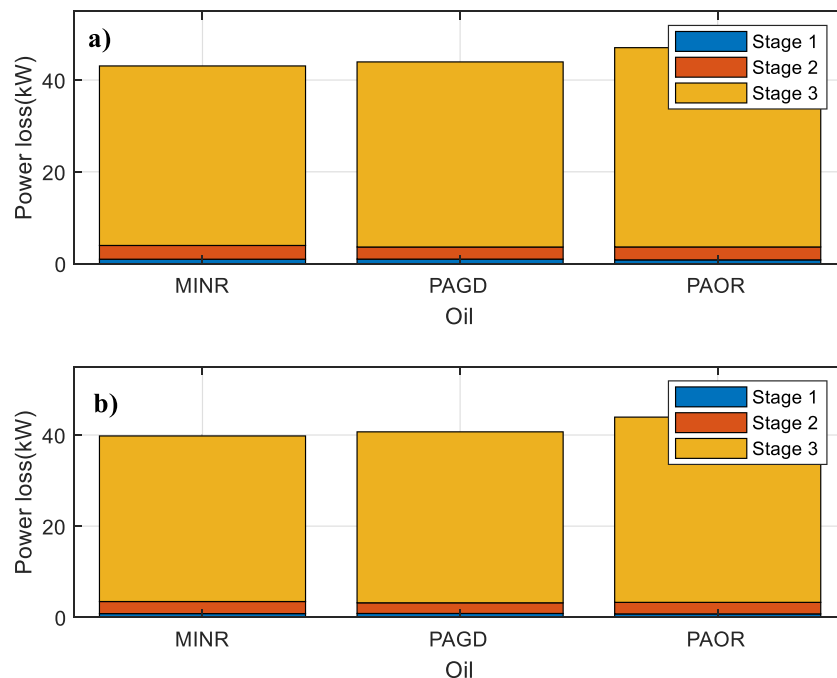


Fig. 4. Bearing power loss at each stage of gearboxes under rated parameters: a) WT1 and b) WT2 from Ref. [6].

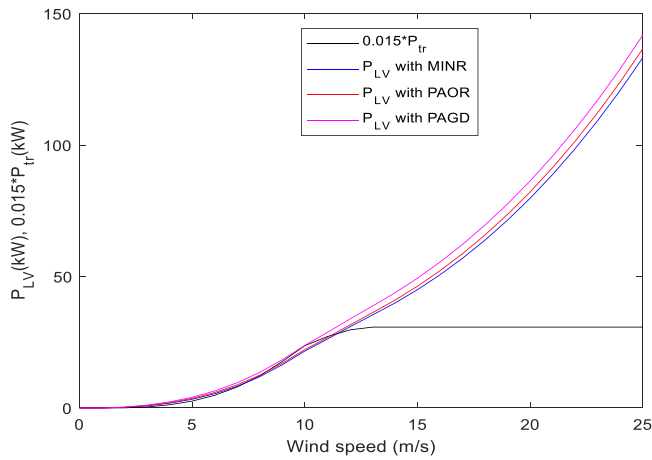


Fig. 5. Bearing power loss around power curve of WT1.

values under real operating conditions. The previous calculated power loss values are used as actual values to validate the proposed neural network model. Thus, data for 3 days, providing a total of 672 samples, was selected to train the ANN model by using t_s , P_{tr} , T_{in} and V as input variables and P_{LV} as target variable. The following 144 samples from one day of WT operating parameters, t_s , P_{tr} , T_{in} , and V , were fed into a trained neural network model to predict the corresponding P_{LV} samples. Fig. 7a,

b, and c shows the prediction results after comparison between the actual and predicted P_{LV} for MINR, PAOR, and PAGD oils, respectively. The approximations of the curves of the actual and predicted values of P_{LV} reflect a high prediction efficiency for all three cases.

Furthermore, Table 8 shows the statistical performance of the ANN prediction results of each gearbox oil. From Table 8, RMSE and MAE are below 0.02 kW, and MAPE are below 0.3% for all oil formations. These very low values of RMSE, MAE and MAPE reflect a very high prediction performance of bearing power loss based on BPNN.

6. Conclusion

Several previous publications experimentally calibrated the analytical models for rolling bearing power losses in WT gearboxes evaluation; but the complete calculation stays robust because it requires complex mathematical equations solving. Furthermore, the WT operation is influenced by many factors, such as geographical context. As a result, it is critical to predict rolling bearing power loss in real-time WT operating conditions. This, this paper combined analytical and artificial neural network models for bearing power loss under real-time WT operating conditions estimation. The calibrated SKF model is implemented at 80 °C for bearing power loss in a gearbox with two planetary and one helical gear modeling under three oil formulations, involving MINR oil, PAOR oil and PAGD oil. The calculations results at the rated parameters have shown that the bearing power loss is higher for 2.5 MW WT than for 2.0 MW WT with a percentage difference of 10.25%, 10%, and 9.3%

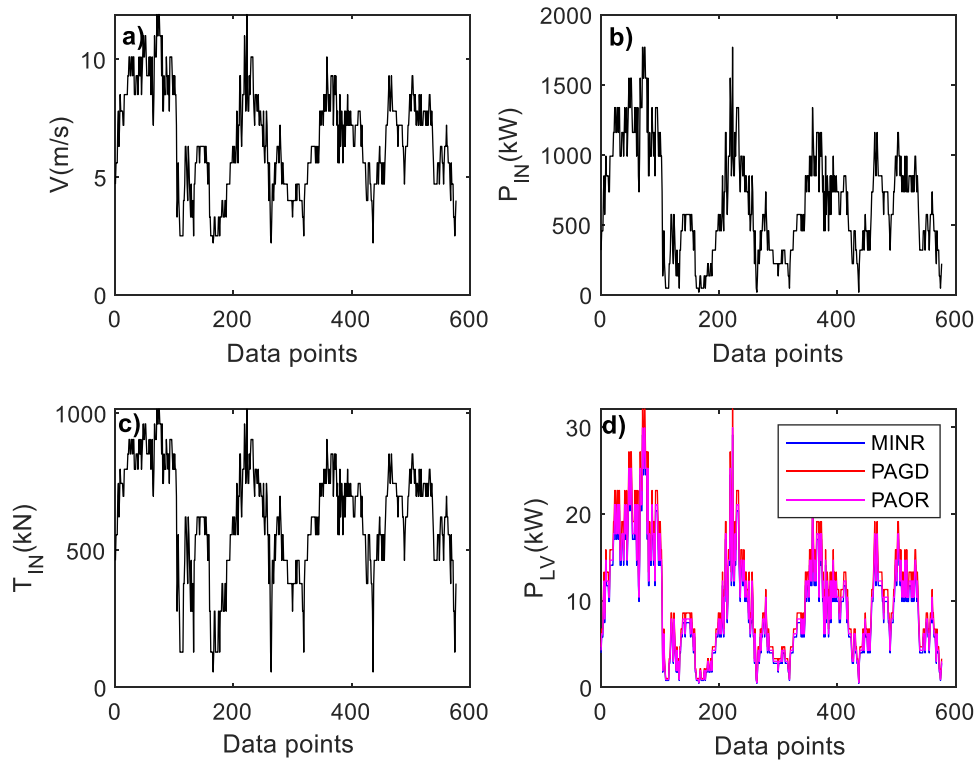


Fig. 6. Gearbox operating parameters and bearing power loss of WT1.

Table 7
Percentage difference of P_{LV} for different oils.

Oil	WT1				WT2			
	Rated		WTPC		Actual		Rated	
	POAR	PAGD	POAR	PAGD	POAR	PAGD	POAR	PAGD
MINR	2.32%	9.3%	2.79%	7.67%	4.16%	12.63%	2.25%	10.25%
POAR	-	6.81%	-	4.75	-	8.13%	-	7.69%

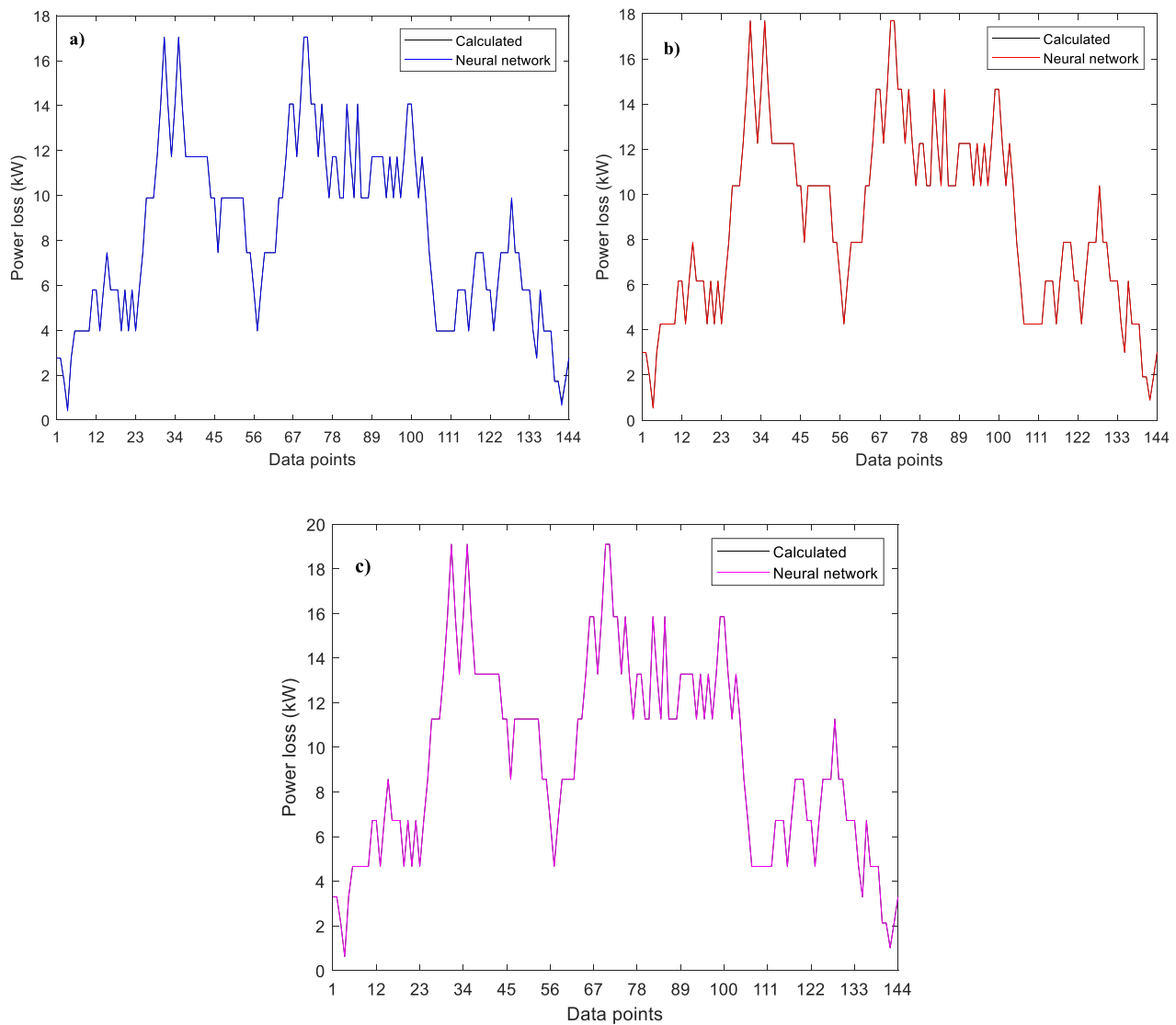


Fig. 7. Comparing actual and ANN predicted bearing power loss with different oils: a) MINR, b) POAR, c) PAGD.

Table 8
Prediction performance of bearing power loss.

	MINR	PAOR	PAGD
RMSE (kW)	0.0142	9.1717e-04	4.4080e-04
MAE (kW)	0.0040	6.7458e-04	2.3080e-04
MAPE (%)	0.2921	0.0201	0.0088

for MINR, POAR and PAGD oils, respectively. In both WTs, the main source of power loss is stage 3, higher than 30 kW. Stage 1 has the lowest loss, less than 1 kW. The bearing loss in stage 2 is slightly higher than that of stage 1.

The achieved results under power curve characteristics of 2.0 MW WT showed that the power loss varies with the variation of the wind speed and the transmitted power in the nonlinear region. While in the rated zone, the power loss increases with the wind speed despite the constant transmitted power. The real wind speed recorded in a wind farm in Cameroon is employed for real-time rolling bearing power loss calculation. The results for four days for 2.0 MW WT showed that the random nature of wind speed makes bearing power loss intermittent. At rated, power curve and real-time 2.0 MW WT operating parameters, the bearing power losses are on average reduced by 9.86% when MINR oil is

used and by 5.56% when PAOR oil is used compared to PAGD oil. They are reduced by 3.09% when MINR oil is used compared to PAOR oil.

The back-propagation neural network is built for three days bearing power loss modelling for predicting desired one day ahead values by using the real wind speed, input torque, transmitted power and time step as exogenous input variables. The achieved results of RMSE, MAE, and MAPE employed to compare the calculated and the ANN predicted bearing power loss values are 0.0142, 0.0040 and 0.2921 for MINR oil, 9.1717e-04, 6.7458e-04 and 0.0201 for PAOR, 4.4080e-04, 2.3080e-04 and 0.0088 for PAGD oil, respectively.

Therefore, the following conclusions were made:

- The increase in the WT capacity induces an increase in bearing power losses and vice versa.
- The high rotational speed of stage 3 of WT gearbox causes significant bearing power losses at this level. Bearing power losses are less important in stages 1 and 2 because of their low rotational speed.
- The bearing power losses are more significant when PAGD oil is used compared to MINR and PAOR oils whatever the WT operating conditions. At the same time, the bearing power loss is less significant when MINR oil is used compared to PAOR oil.

- The back-propagation neural network performs very well the real-time bearing power loss prediction by generating very high performance.
- The effectiveness of bearing power loss prediction in WT gearbox models using an artificial neural network model under real-time operating conditions makes a significant contribution to WT gearbox efficiency prediction.

CRedit authorship contribution statement

Fogno Fotso: Provided the gearbox model and the analytical rolling bearing power loss calculation model, designed the artificial neural network model and its implementation, performed the computations, and participated in the interpretation and discussion of results, the writing of the original manuscript and the revised version. **Aloyem Kazé:** collected and provided the wind data used, developed the model for the wind turbine power transmitted calculation and participated in the interpretation and discussion of results and in the revision of the manuscript. **Djujide Kenmoé:** Provided the project idea and methodology, and participated in the interpretation and discussion of results and in the writing of the original manuscript and the revision version.

Declaration of Competing Interest

The authors declare that they have no known competing financial interests or personal relationships that could have appeared to influence the work reported in this paper.

References

- [1] Li G, Liu W, Su X. The sun and planetary gear design of a 1.5 MW wind turbine. *J Vib Eng Technol* 2018;6:495–501. <https://doi.org/10.1007/s42417-018-0066-8>.
- [2] Fernandes CMCG, Blazquez L, Martins RC, Seabra JHO. Energy efficiency tests in a full scale wind turbine gearbox. *Tribology Int* 2016;101:375–82. <https://doi.org/10.1016/j.triboint.2016.05.001>.
- [3] Ragheb AM, Ragheb M. Wind turbine gearbox technologies. In: proceedings of INREC10, Amman, Jordan, March 21–24, 2010:1–8.
- [4] Fernandes CMCG, Marques PMT, Martins RC. Gearbox power loss. Part I: losses in rolling bearings. *Tribology Int* 2015;88:298–308. <https://doi.org/10.1016/j.triboint.2014.11.017>.
- [5] Nutakor C, Klodowski A, Sopian J, Mikkola A, Pedrero JI. Planetary gear sets power loss modeling: application to wind turbines. *Tribology Int* 2017;105:42–54. <https://doi.org/10.1016/j.triboint.2016.09.029>.
- [6] Fernandes CMCG, Hammami M. Power loss prediction: application to a 2.5 MW wind turbine gearbox. *J Eng Tribology* 2015;0:1–13. <https://doi.org/10.1177/1350650115622362>.
- [7] Michaelis K, Michael BH, Hinterstoßer M. Influence factors on gearbox power loss! Purpose!Design/methodology/approach!Findings!Originality/value. *Ind Lubr Tribology* 2011;63:46–55. <https://doi.org/10.1108/00368791111101830>.
- [8] Fernandes CMCG, Marques PMT, Martins RC, Seabra JHO. Influence of gear loss factor on the power loss prediction 2015:81–8. doi:10.5194/ms-6-81-2015.
- [9] Marques PMT, Fernandes CMCG, Martins RC, Seabra JHO. Efficiency of a gearbox lubricated with wind turbine gear oils. *Tribology Int* 2014;71:7–16. <https://doi.org/10.1016/j.triboint.2013.10.017>.
- [10] Marques PMT, Fernandes CMCG, Martins RC, Seabra JHO. Tribology International Power losses at low speed in a gearbox lubricated with wind turbine gear oils with special focus on churning losses. *Tribology Int* 2013;62:186–97. <https://doi.org/10.1016/j.triboint.2013.02.026>.
- [11] Fernandes CMCG, Marques PMT, Martins RC, Seabra JHO. Gearbox power loss. Part III: application to a parallel axis and a planetary gearbox. *Tribology Int* 2015;88:317–26. <https://doi.org/10.1016/j.triboint.2015.03.029>.
- [12] Li X, Olofsson U. FZG gear efficiency and pin-on-disc frictional study of sintered and wrought steel gear materials. *Tribol Lett* 2015;60:9. <https://doi.org/10.1007/s11249-015-0582-6>.
- [13] Fernandes CMCG, Amaro PMP, Martins RC, Seabra JHO. Torque loss in cylindrical roller thrust bearings lubricated with wind turbine gear oils at constant temperature. *Tribology Int* 2013;67:72–80. <https://doi.org/10.1016/j.triboint.2013.06.016>.
- [14] Fernandes CMCG, Martins RC, Seabra JHO. Friction torque of thrust ball bearings lubricated with wind turbine gear oils. *Tribology Int* 2013;58:47–54. <https://doi.org/10.1016/j.triboint.2012.09.005>.
- [15] Fernandes CMCG, Martins RC, Seabra JHO. Friction torque of cylindrical roller thrust bearings lubricated with wind turbine gear oils. *Tribology Int* 2013;59:121–8. <https://doi.org/10.1016/j.triboint.2012.05.030>.
- [16] Singh H. Investigation of microstructural alterations in low-and high-speed intermediate-stage Wind turbine gearbox bearings. *Tribol Lett* 2017;65:81. <https://doi.org/10.1007/s11249-017-0861-5>.
- [17] Fernandes CMCG, Marques PMT, Martins RC, Seabra JHO. Gearbox power loss. Part II: friction losses in gears. *Tribology Int* 2015;88:309–16. <https://doi.org/10.1016/j.triboint.2014.12.004>.
- [18] Di E, Cidra J, Carrillo C, Montan AFO. Review of power curve modelling for wind turbines. *Renew Sustain Energy Rev* 2013;21:572–81. <https://doi.org/10.1016/j.rser.2013.01.012>.
- [19] Pelletier F, Masson C, Tahan A. Wind turbine power curve modelling using artificial neural network. *Renew Energy* 2016;89:207–14. <https://doi.org/10.1016/j.renene.2015.11.065>.
- [20] Lydia M, Kumar SS, Selvakumar AI, Prem GE. A comprehensive review on wind turbine power curve modeling techniques. *Renew Sustain Energy Rev* 2014;30:452–60. <https://doi.org/10.1016/j.rser.2013.10.030>.
- [21] Teyabean AA, Jwaid AE. Power curve modelling for wind turbines. In: International Conference on Modelling & Simulation. 2017;179–184. doi:10.1109/UKSim.2017.30.
- [22] Roméo H, Fotso F, Vidal C, Kazé A, Djujide G. Optimal input variables disposition of artificial neural networks models for enhancing time series forecasting accuracy. *Appl Artif Intell* 2020;00:1–24. <https://doi.org/10.1080/08839514.2020.1782003>.
- [23] Zhang W, Qu Z, Zhang K, Mao W, Ma Y, Fan X. A combined model based on CEEMDAN and modified flower pollination algorithm for wind speed forecasting. *Energy Convers Manag* 2017;136:439–51. <https://doi.org/10.1016/j.enconman.2017.01.022>.
- [24] Fernandes CMCG, Marques PMT, Martins RC, Seabra JHO. Film thickness and traction curves of wind turbine gear oils. *Tribology Int* 2015;86:1–9. <https://doi.org/10.1016/j.triboint.2015.01.014>.
- [25] SKF General Catalogue 6000 EN, SKF, November 2005.
- [26] Beig AR, Muyeen SM. Wind energy. *Electr Renew Energy Syst* 2017. <https://doi.org/10.1016/B978-0-12-804448-3/00004-9>.
- [27] Bakurci M, Yilmaz S. Theoretical and computational investigations of the optimal tip-speed ratio of horizontal-axis wind turbines. *Eng Sci Technol Int J* 2018;21:1128–42. <https://doi.org/10.1016/j.jestch.2018.05.006>.
- [28] Peng H, Liu F, Yang X. A hybrid strategy of short term wind power prediction. *Renew Energy* 2013;50:590–5. <https://doi.org/10.1016/j.renene.2012.07.022>.

Comparative models for multi-step ahead wind speed forecasting applied for expected wind turbine power output prediction

Wind Engineering

1–16

© The Author(s) 2021

Article reuse guidelines:

sagepub.com/journals-permissions

DOI: 10.1177/0309524X211052015

journals.sagepub.com/home/wie

Germaine Djuidje Kenmoé¹, Hervice Roméo Fogno Fotso¹ 
and Claude Vidal Aloyem Kazé²

Abstract

This paper investigates six of the most widely used wind speed forecasting models for a combination of statistical and physical methods for the purpose of Wind Turbine Power Generation (WTPG) prediction in Cameroon. Statistical method based on both single static and dynamic neural networks architectures and two hybrid neural networks architectures in comparison to ARIMA model are employed for multi-step ahead wind speed forecasting in two Datasets in Bapouh, Cameroon. The physical method is used to estimate 1 day ahead expected WTPG for each Dataset using the previous predicted wind speed from better forecasting models. The obtained results of multi-step ahead forecasting showed that the ARIMA and nonlinear autoregression with exogenous input neural network (NARXNN) models perform well the wind speed forecasting than other forecasting models in both Datasets. The better performances of ARIMA are achieved with one-step ahead and two-step ahead forecasting, while NARXNN is better with one-step ahead forecasting. But NARXNN models have more computational time than other models such as ARIMA models. Furthermore, the effectiveness of employed hybrid method for WTPG prediction is proven.

Keywords

Artificial intelligence, ARIMA, forecasting methods, multi-step forecasting, wind speed, wind turbine power generation, Cameroon

Introduction

The main sources of commercial energy in Cameroon are from hydropower (73%) and thermal power (10%; Veezee et al., 2021). According to Wirba et al. (2015), the development of new renewable energy sources such as wind energy is required for Cameroon electrification, necessary to jeopardize its economic development. Given the dependence of Wind Turbine Power Generation (WTPG) to the intermittent nature of wind speed, wind energy generation is highly fluctuating and uncertain (Chitsazan et al., 2019; Loukatou et al., 2018). Due to its uncertainty, the WTPG integration into electric grid produces great challenges for power system management and operations (Hao and Tian, 2019). Accurate short-term WTPG prediction is useful in power system operations planning and for electricity trading in power markets where wind power and energy storage can be traded or hedged (Hao and Tian, 2019; Loukatou et al., 2018). Also, accurate short-term wind speed is also crucial to the operation of wind turbines so that dynamic controls can be accomplished to increase the energy conversion efficiency and reduce the risk of overloading (Chang et al., 2017). Therefore, under such circumstances, several methods for wind speed and WTPG forecasting have been proposed in recent years. The hybrid method combining wind speed forecasting method and WTPG forecasting method is suitable and more used compared to other method (Chang et al.,

¹Laboratory of Mechanics, Department of Physics, University of Yaoundé I, Yaoundé, Cameroon

²Department of Renewable Energy, Higher Technical Teachers Training College Kumba, University of Buea, Buea, Cameroon

Corresponding author:

Germaine Djuidje, Laboratory of Mechanics, Department of Physics, University of Yaoundé I, P.O. Box 812, Yaoundé, Cameroon.

Email: hervicefogno@yahoo.fr

2017; Peng et al., 2013). It allows to forecast both wind speed and WTPG. The WTPG forecasting method commonly used is based on Wind Turbine Power Curve (WTPC) modeling and wind speed forecasting. The accuracy of WTPG prediction depends on wind speed forecasting accuracy. Thus, the accurate forecasting of wind speed is a great necessity for the exploitation of wind energy (Salfate et al., 2018).

To handle wind speed forecasting, many methods have been proposed involving physical method, statistical method, and hybrid method (Hao and Tian, 2019; Zhang et al., 2017b). Physical method uses a physical and meteorological variables, including numerical weather prediction (NWP) and environmental temperature for wind speed prediction. It usually requires solving complex mathematical equations and do not appraise for short-term forecasting (Fogno Fotso et al., 2021a). The statistical method includes time series analysis (TSA) method and Artificial Intelligence (AI) method. TSA models such as AutoRegressive Moving Average (ARMA) and AutoRegressive Integrated Moving Average (ARIMA) models draw the relationship between the historical data of wind speed based on mathematical statistics to forecast the unknown values (Jain, 2018). Artificial Intelligence (AI) models such as Artificial Neural Networks (ANN) models, Support Vector Machine (SVM) model, and Adaptive Neuro-Fuzzy Inference System (ANFIS) model learn the available historical data of wind speed pursuing to forecast the unknown values (Hur, 2021). The hybrid method combines two different methods (Yan et al., 2020). AI models have been proved to have the higher precision than other models for nonlinear wind speed forecasting (Wang et al., 2017; Zhang et al., 2017a). Also, ARIMA model have been showed to be better for linear wind speed forecasting than other statistical models (Jiao, 2018; Nair, 2017). Nowadays, several works have been conducted on wind speed forecasting aim to WTPG prediction over the world using AI and ARIMA models. Cadenas and Rivera (2009) used multi-layers Perceptron neural network for short-term wind speed forecasting in La Venta, Oaxaca, México. Peng et al. (2013) combined statistical and physical methods based on single feedforward ANN model and WTPC, respectively for shorn-term wind speed forecasting applied for WTPG estimation. Cadenas et al. (2016) presented an ARIMA model and recurrent neural network model comparison for one-step ahead wind speed forecasting. The forecasting step plays an important role in term of forecasting accuracy. Therefore, the multi-step forecasting ahead is required to find the more accurate models. But most of the previous work are done with a specific forecasting step and model.

Until January 2021, none wind energy conversion system is constructed in Cameroon for commercial energy production. But, several works are done which will help the decision maker to give the best orientation on the development of the wind energy systems. Kisito et al. (2015) assessed wind energy in Bafoussam, Cameroon, by using power density and Weibull approach. Arreyndip et al. (2016) carried the wind energy potential assessment of Cameroon's coastal regions for the installation of an onshore wind farm. Flora et al. (2021) carried out the wind farm sites selection in Cameroon based on GIS using a Boolean method.

To guide in decision-making for future wind energy projects in Cameroon on the one hand and to suggest the better model and forecasting step on the other hand, this work investigates the mostly used of existing wind speed forecasting models with application for hybrid wind turbine power output prediction. Prediction tools are developed though three single ANN models, Genetic Algorithm Back-propagation ANN model, ANFIS model, and ARIMA model for multi-step wind speed forecasting. The multi-step forecasting involves one-step, two-step, and three-step ahead. Physical method based on manufacturer's WTPC modeling is used to predict the expected WTPG using the previous predicted wind speed. Two Datasets from Bapouh, Cameroon are employed for validation. The remainder of the paper is organized as follows: Section 2, provides the related methodology; the context of the case study is presented in Section 3; the forecasting models designing scheme is given in Section 4; the achieved results are presented and discussed in Section 5; and finally, a conclusion summarizes the work.

Related methodology

Hybrid method combining statistical and physical methods is developed to predict the expected WTPG in Cameroon. The schematic illustration of the followed methodology is depicted in Figure 1. It consists of three main stages. The historical wind data are collected in *stage (I)*. In *stage (II)*, the statistical method is used to forecast the wind speed events. To find the best way of wind speed forecasting, the mostly used statistical prediction tools are investigated on different step ahead forecasting. Therefore, four AI models and ARIMA model (Zhang et al., 2017b) are developed for multi-step ahead wind speed forecasting. There are the single ANN models involving Backpropagation neural network (BPNN; Fogno Fotso et al., 2020), Radial Basis Function neural network (RBFNN; Liu et al., 2018), and Nonlinear AutoRegression with eXogenous input (NARXNN; Di Piazza et al., 2016) and the hybrid models involving Generic Algorithm Backpropagation neural network (GABPNN; Wang et al., 2016) and Adaptive Neuro-Fuzzy Inference System (ANFIS; Damousis et al., 2004; Moreno and Dos

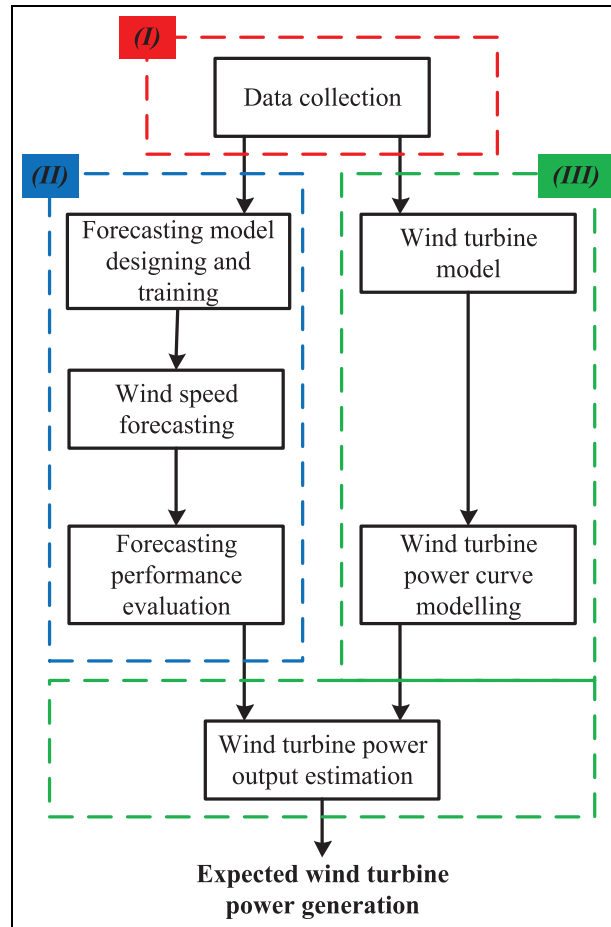


Figure 1. Methodology flowchart.

Santos Coelho, 2018). Each model is developed and trained using historical wind data pursuing for desired wind speed values forecasting. The forecasting performance of each model at each step is measured using statistical criteria. *Stage (III)* consists of using the physical method for estimating the WTPG. Firstly, the characteristics of the related wind turbine are determined. And, its power curve is modeled and used with the previously predicted wind speed values to estimate the corresponding expected WTPG.

Multi-step ahead forecasting

Multi-step ahead forecasting is the task of forecasting a sequence of values step-by-step, by using the predicted value of the current time step to determine its value in the next time step (Wang et al., 2017). The multi-step ahead applied in this study involves one-step, two-step, and three-step ahead forecasting as given in Figure 2. With the one-step ahead forecasting, the forecasting value $\hat{y}(N+1)$ is achieved only through the past observation values $\{y(1), y(2), \dots, y(N-1), y(N)\}$, with N the total number of wind speed training samples. In the two-step ahead forecasting, the forecasting value $\hat{y}(N+2)$ is achieved by using the past values $\{y(2), y(3), \dots, y(N-1), y(N)\}$ and the previously forecasting value $\hat{y}(N+1)$. While the forecasting value $\hat{y}(N+3)$ in three-step ahead is obtained based on the historical $\{y(3), y(4), \dots, y(N-1), y(N)\}$ and the two previously forecasting values $\{y(3), y(4), \dots, y(N-1), y(N)\}$.

Expected WTPG estimation

Expected WTPG was estimate based on WTPC as follow. The maximum power available that crosses the rotor of an installed wind turbine in a wind farm can be estimated by the following,

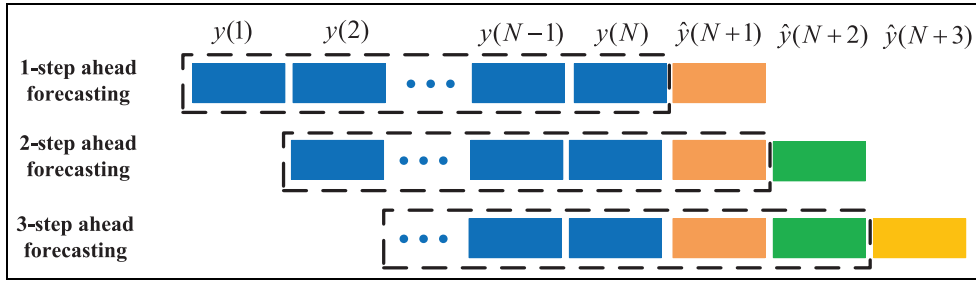


Figure 2. Multi-step ahead forecasting scheme.

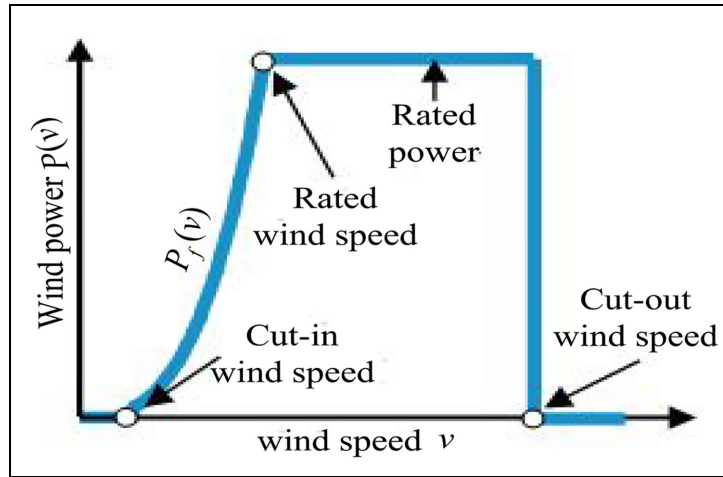


Figure 3. General model of wind power curve.

$$P_w = \frac{1}{2} \cdot \rho \cdot A \cdot v^3, \quad (1)$$

where P_w is the total wind power delivered to the turbine, A is the area swept by the turbine blades, and ρ is the air density.

The electrical power that can be generated by the wind turbine by conversion of the previous available wind power (P_w) is usually represented by its WTPC (Carrillo et al., 2013). The WTPC establishes the relationship between the wind speed and the power generation of a wind turbine (Teyabean and Jwaid, 2017). Each wind turbine has one power curve which is calibrated and provided by its manufacturer (Lydia et al., 2014). Therefore, WTPC is one of most important tools commonly used to forecast the WTPG under given wind condition of a wind farm (Bandi and Apt, 2016; Lydia et al., 2014). The typical power curve of a pitch controlled wind turbine is mathematically modeled as shown in equation (2),

$$P(v) = \begin{cases} 0 & v < v_{ci} \\ P_f(v) & v_{ci} \leq v < v_r \\ P_r & v_r \leq v < v_{co} \\ 0 & v_{co} < v \end{cases}, \quad (2)$$

where $P(v)$ is the wind turbine power output at a given wind speed v , $P_f(v)$ is the nonlinear part of wind power generation, P_r is the *rated power*, v_{ci} is the *cut-in speed*, v_r is the *rated speed*, and v_{co} is the *cut-out speed* (Bandi and Apt, 2016; Lydia et al., 2014; Pelletier et al., 2016). These distinct regions of a controlled wind turbine is shown in Figure 3.

In this study, equation (2) was used for WTPG representation with the general model developed by Teyabean and Jwaid (2017) used for the nonlinear part of the WTPC modeling as shown in equation (3),

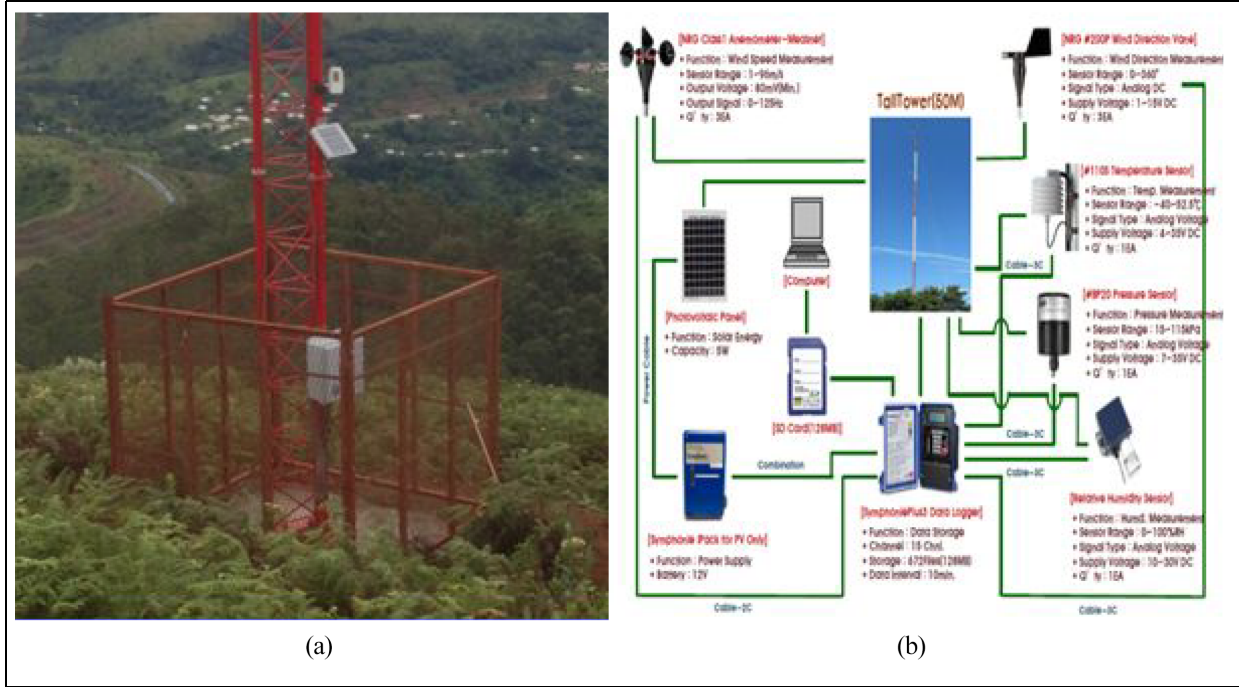


Figure 4. Bapouh experiment: (a) site and (b) data recording system configuration.

$$P_f(v) = P_r \left(\frac{v^a - v_{ci}^a}{v_r^a - v_{ci}^a} \right), \quad (3)$$

where a , being the order of power output curve, and its value for this work is 2.9 obtained by fitting the manufacturer's WTPC of the interested wind turbine.

Geographical context and experimental detail

To validate the developed WTPG prediction approach in Cameroon, the recording of data on the measurement of wind speed (v), ambient temperature (T_a), air pressure (P_a), and relative humidity (RH) is provided by equipment installed in Bapouh in the Western Region. The geographical coordinates of the site are N05°09'35.52" and E10°19'21.90". The data are collected from the meteorological sensor readings and stored in the SymphonyPlus3 data logger. The site and the configuration of the measuring system as well as the characteristics of the different components are shown in Figure 4.

The weather data were recorded for 2 years after every 10 minutes from 2016 to 2017. The height of measurement is 70 m and the scanning frequency is 144 times per day from 00:00 to 24:00. Therefore, data from two Datasets in Bapouh were employed for multi-step ahead forecasting. These Datasets, involving Dataset1 and Dataset2 are made up of 2 months of real measured wind speed data from 1st to 30th December 2016 and from 1st to 30th January 2017 respectively. Each Dataset has 4320 data points, these observations are split into two subsets, which are training set and testing set.

In this study, according to the application wind characteristics, the wind turbine model E-82 2000 kW of ENERCON manufacturer, have been chosen for application. Its power curve is shown in Table 1.

Wind speed forecasting models designing

Designing a forecasting model requires several distinct steps, because it involves the selection of many variables and parameters. However, a successful design can be achieved if the accurate forecasting result is achieved. In this work, five neural networks models and ARIMA model are designed, trained, and tested for multi-step ahead wind speed forecasting by using the errors detector method.

Table 1. Manufacturer power curve of E-82 2000 kW wind turbine.

Wind speed (m/s)	Output power (kW)	Wind speed (m/s)	Output power (kW)	Wind speed (m/s)	Output power (kW)
1	0	10	1.580	19	2.050
2	3	11	1.810	20	2.050
3	25	12	1.980	21	2.050
4	82	13	2.050	22	2.050
5	174	14	2.050	23	2.050
6	321	15	2.050	24	2.050
7	532	16	2.050	25	2.050
8	815	17	2.050		
9	1180	18	2.050		

Data preprocessing

Time (t), air temperature (T_a), atmospheric pressure (P_a), and relative humidity (RH) are employed as input variables of neural networks models, while wind speed is used as target variable. The input and target variables of the prediction tools have been collected at difference unity. There are several methods to transform it in order to minimize noise and so that the ANNs can learn relevant patterns as defined in Kugiumtzis and Tsimpiris (2010). Therefore, in this study, every used variables are transformed by normalizing it between 0 and 1 using equation (4) before the training process of ANN models. At the end of the forecasting process, the natural values of the forecasting variables are achieved by transforming its normalized values using equation (5) given as following,

$$y_N(t) = \frac{y(t) - y_{\min}}{y_{\max} - y_{\min}}, \quad (4)$$

$$y(t) = y_p(t)(y_{\max} - y_{\min}) + y_{\min}, \quad (5)$$

where $y(t)$, $y_p(t)$, and $y_N(t)$ are natural, predicted, and normalized variable respectively, at a given time step t ; y_{\max} and y_{\min} are respectively the maximum and minimum value of the natural measured variables.

Forecasting accuracy evaluation

There is a wide range of functions which can be used to evaluate the forecasting accuracy. In this paper, the Root Mean Square Error (RMSE), the Mean Absolute Error (MAE), and the Mean Absolute Percentage Error (MAPE) are used to measure the difference between the measured and forecasting variables (Fogno Fotso et al., 2021b). They are expressed respectively as:

$$RMSE = \sqrt{\frac{1}{K} \sum_{t=1}^K (y(t) - \hat{y}(t))^2}, \quad (6)$$

$$MAE = \frac{1}{K} \sum_{t=1}^K |y(t) - \hat{y}(t)|, \quad (7)$$

$$MAPE = \frac{1}{K} \sum_{t=1}^K \left| \frac{y(t) - \hat{y}(t)}{y(t)} \right| \times 100, \quad (8)$$

where $y(t)$ and $\hat{y}(t)$ are the measured and predicted values respectively at the time step t , and K is the number of time step. The forecasting model is better as its RMSE, MAE, and MAPE values are lowest. To compare the forecasting performance of the proposed models among the comparison models, the improvement percentage of three errors criterion are evaluated as follow,

$$P_{Error} = \left| \frac{Error_2 - Error_1}{Error_2} \right| \times 100, \quad (9)$$

Table 2. Experiment parameters of developed forecasting tools.

Indexes	Parameters	Values
BPNN	Maximum iterations	1000
	Validation check	1000
NARXNN	Maximum iterations	1000
	Validation check	1000
	Delay	04
ANFIS	Number of MF	02
	Maximum epochs	1000
RBFNN	Spread	0.5
	Maximum number of training	1000
GA	Training requirement precision	0.00002
	Maximum generations	200
	Fitness limit	10^{-5}

where subscript 1 indicates the main model, and the subscript 2 gives a comparison model.

Experiment results and discussions

The prediction tools are built according to the parameters giving in Table 2. The experiments are operated in MATLAB R2018a on Windows 7 with 2.27 GHz Intel Core i3-6700HQ CPU, 64-bit and 2 GB RAM. All developed neural models have two layers. The number of hidden node is determined by using Hecht–Nelson method (Xiao et al., 2017), such as $H = 2M + 1$. Where H is the number of hidden node and M is the number of input node. Thus, with four selected input variables we have used nine hidden neuron for each neural network model with a linear output node. The tangent hyperbolic function is used in hidden nodes of BPNN and NARXNN models, and Gaussian is used as membership function of ANFIS model. For NARXNN model, the open-loop architecture is used in training process and closed-loop architecture is used in forecasting stage. Unlike other types of neural networks, in NARXNN architectures, the output depends not only on the current input but on the current and previous inputs, outputs, or states of the network, as well. In open loop NARXNN architecture, the true output is available while the network is being trained, it is efficient to use it instead of feeding back the estimated output. The advantage of this architecture during training is that the input to the ANN is more accurate. In the closed-loop architecture, the output is fed back to the input in a feed forward setup and then inputs and the initial values of the outputs, are used to predict the outputs at future time steps (see Figure 5).

The data from 01st to 30th December 2016 and from 01st to 30th January 2017 are modeled to forecast wind speed of the day of 1st December 2016 and 31st January 2017, respectively. Tables 3 and 4 present the multi-step forecasting results from the Dataset1 and Dataset2 respectively, using MAPE, MAE, and RMSE error criteria. From Tables 3 and 4, it can be obviously seen that the MAPE, MAE, and MSE values show that the performance are different according to forecasting step, Datasets and forecasting models :

- According to forecasting models, the ARIMA models perform the wind speed forecasting in all steps and Datasets than neural networks models. The average forecasting errors, RMSE, MAE, and MAPE from ARIMA models are 1.1938, 1.04, and 15.0837, respectively in Dataset1. Their values in Datasets2 are 1.25, 0.98, and 17.21, respectively. While the NARXNN models are the best among the neural networks models for all forecasting steps and in both Datasets. The ANFIS models presents the worst wind speed multi-step ahead forecasting performances.
- According to forecasting steps, one-step ahead forecasting globally presents the better results in both Datasets. The average one-step ahead forecasting errors, RMSE, MAE, and MAPE are 1.46, 1.16, and 17.27 in Dataset1 and 1.53, 1.18, and 20.11 in Dataset2, respectively. While the three-step ahead forecasting has the worst performance in both Datasets. The average RMSE, MAE, and MAPE for three-step ahead forecasting are 1.60, 1.30, and 19.77 in Dataset1 and 1.5606, 1.2210, and 20.5793 in Dataset2, respectively.
- Globally, NARXNN models under one-step ahead forecasting have the better wind speed forecasting performance among the other AI models from both Datasets. While the better wind speed forecasting performance from ARIMA models for both Datasets are achieved under one-step ahead and two-step ahead forecasting.

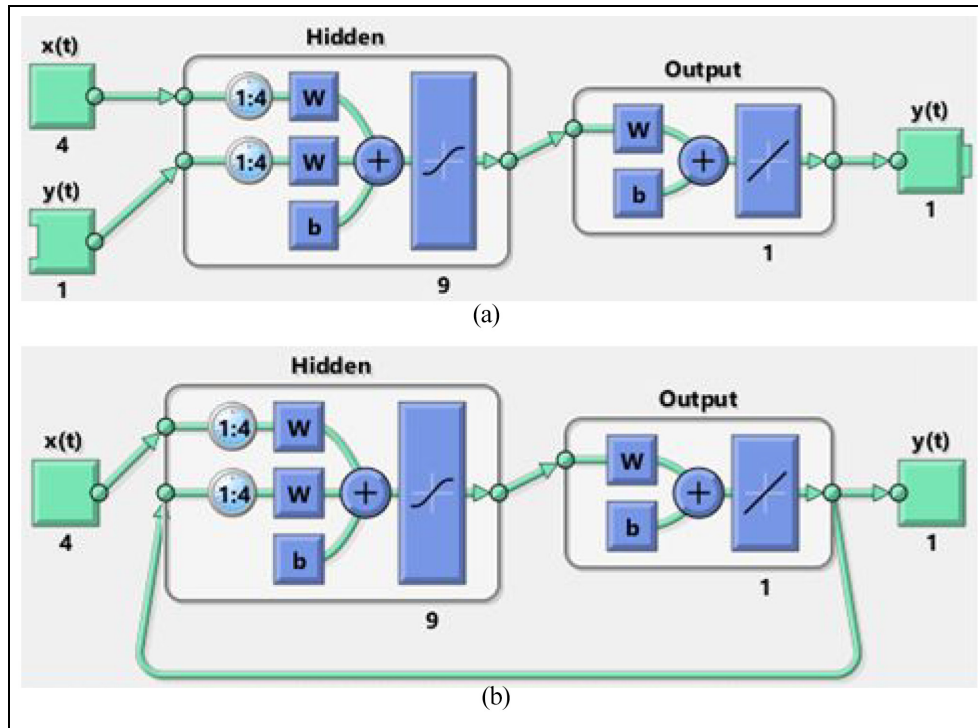


Figure 5. Open-loop NARNN architecture (a) and closed loop NARNN architecture (b).

Table 3. Wind speed forecasting results from Dataset 1.

Models	One-step			Two-step			Three-step		
	RMSE	MAE	MAPE (%)	RMSE	MAE	MAPE (%)	RMSE	MAE	MAPE (%)
BPNN	1.6180	1.277	17.7854	1.5229	1.245	18.3758	1.4819	1.2131	19.1811
NARXNN	0.9747	0.731	11.9438	1.1676	0.849	15.2240	1.3537	1.0465	15.2608
RBFNN	1.3180	1.046	17.3428	1.4373	1.183	18.3653	1.4373	1.1839	19.3653
GABPNN	1.2585	1.017	15.3856	1.6099	1.301	21.4453	1.6913	1.4429	22.9588
AMFIS	2.3729	1.889	26.2847	2.4394	1.951	28.2338	2.3558	1.8928	27.4045
ARIMA	1.2339	1.032	14.9098	1.2679	1.018	14.8628	1.3155	1.0726	15.4784

Table 4. Wind speed forecasting results from Dataset 2.

Models	One-step			Two-step			Three-step		
	RMSE	MAE	MAPE (%)	RMSE	MAE	MAPE (%)	RMSE	MAE	MAPE (%)
BPNN	1.7485	1.330	21.3338	1.6209	1.257	21.1243	1.6238	1.2623	21.1507
NARXNN	1.0331	1.033	17.3378	1.4831	1.232	19.2052	1.4721	1.2246	19.5185
RBFNN	1.3667	1.176	20.8394	1.3200	1.127	21.2186	1.3320	1.1505	20.7264
GABPNN	1.1905	1.000	18.9608	1.5528	1.317	23.7008	1.2080	1.0233	18.9994
AMFIS	2.3471	1.587	24.6921	3.1063	2.305	37.0238	2.4190	1.6612	25.8695
ARIMA	1.2414	0.981	17.5050	1.2208	0.981	16.9266	1.3086	1.0039	17.2114

Figures 6 and 7 plot the comparison between actual and forecasting wind speed values versus time in Dataset1 and Dataset2, respectively. Based on the proximity of the curves of the predicted values to those of the measured

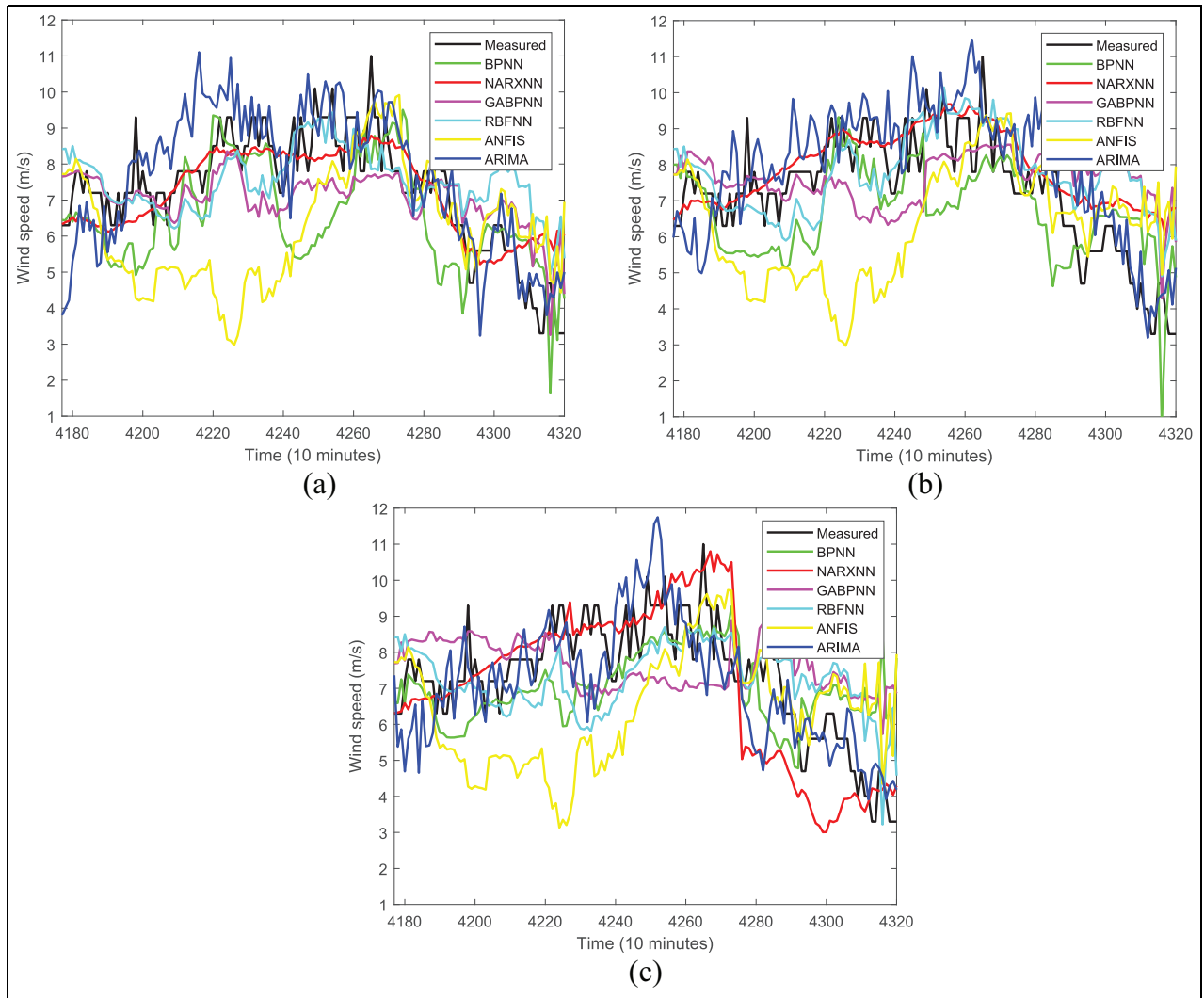


Figure 6. Comparing wind speed forecasting results from Dataset 1: (a) one-step, (b) two-step, and (c) three-step.

values, we can confirm that NARXNN models under one-step ahead forecasting and ARIMA models under one-step and two-step ahead forecasting perform well the wind speed forecasting in both Datasets in Bapouh, Cameroon.

To measure the degree of difference in wind speed forecasting performance between the NARXNN and ARIMA models and the other models, Tables 5 and 6 give the results of the improvement percentages for each criteria of the error and for the Dataset1 and the Dataset2 respectively. Overall we observe that these improvement percentages are considerable with values reaching 61% for Dataset1 and 60% for Dataset2. The higher the improvement percentage, the better the main model is compared to the other models. We can observe from Tables 5 and 6 that the improvement percentages are higher for the NARXNN model under one-step ahead forecasting and for the ARIMA model under one-step ahead and two-step ahead forecasting. This further demonstrates the superiority of the NARXNN and ARIMA models over the developed models in terms of wind speed forecasting performance. Also, it further demonstrates the influence of the forecasting step on the different models. Thus, NARXNN is better for one-step ahead while ARIMA is better for one-step ahead and two-step ahead forecasting.

Table 7 gives the computational time of each model developed for multi-step ahead wind speed forecasting in this study for the two Datasets involved. From Table 7 it can be seen that the models that take more computational time to produce the results obtained in both Datasets are GABPNN, NARXNN, and ANFIS respectively. The RBFNN model has the lowest computational time followed by the ARIMA models. It can also be observed that the computational time of each model is a function of the Datasets and the forecasting step. This

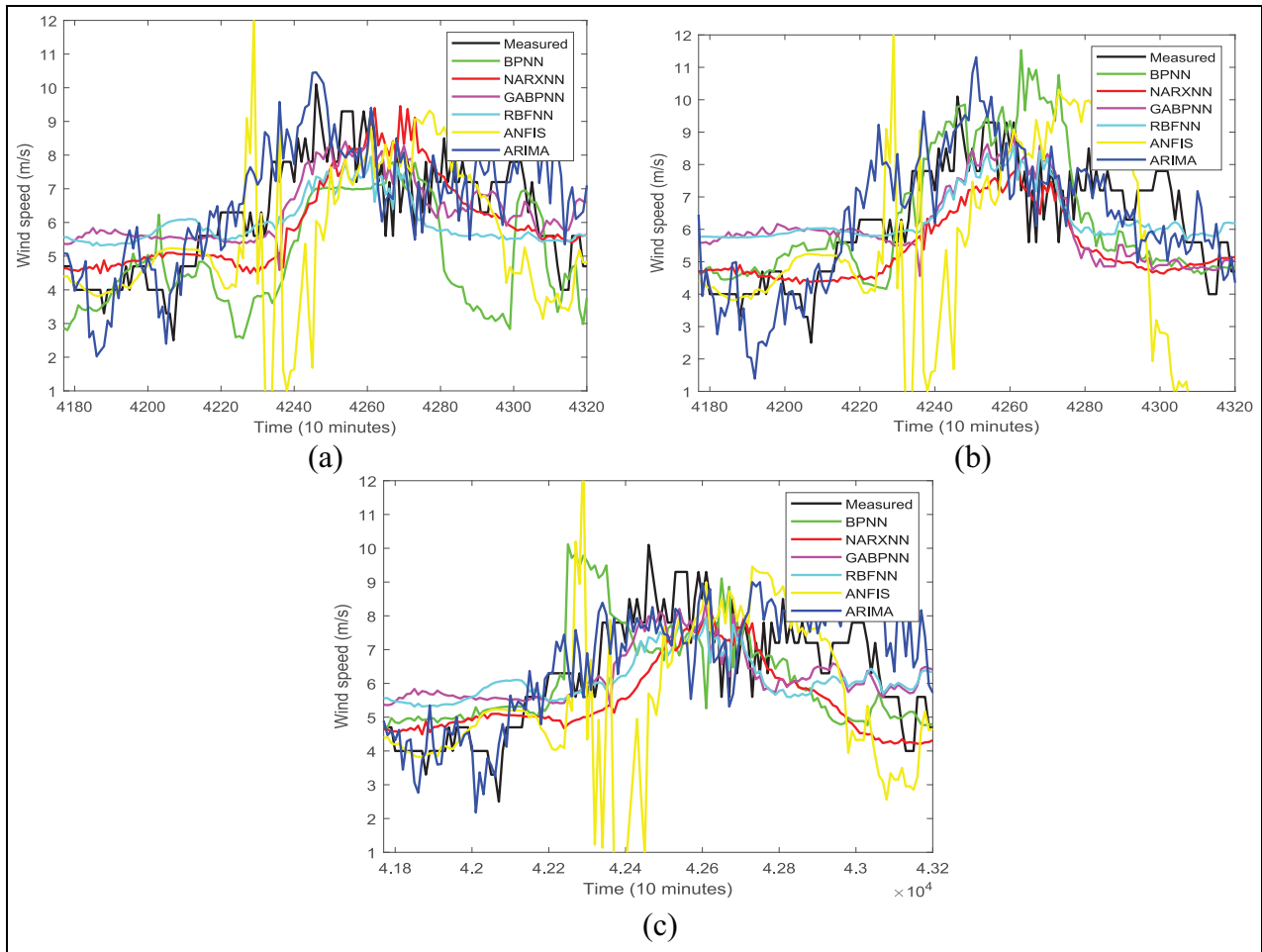


Figure 7. Comparing wind speed forecasting results from Dataset2: (a) one-step, (b) two-step, and (c) three-step.

Table 5. Improving percentage of forecasting performance from Dataset 1.

Comparison models		One-step			Two-step			Three-step		
		P_{RMSE} (%)	P_{MAE} (%)	P_{MAPE} (%)	P_{RMSE} (%)	P_{MAE} (%)	P_{MAPE} (%)	P_{RMSE} (%)	P_{MAE} (%)	P_{MAPE} (%)
NARXNN	BPNN	44	45	44	23	31	17	8	13	20
	RBFNN	26	30	31	18	28	17	25	11	5
	GABPNN	22	28	22	27	34	29	33	27	19
	AMFIS	58.9	61	54	52	56	46	42	44	44
ARIMA	BPNN	29	22	30	16	18	19	11	11	19
	RBFNN	6	1	14	11	13	19	24	9	8
	GABPNN	1.9	1	3	30	21	21	32	25	22
	AMFIS	48	45	43	48	47	47	43	43	44

computational time increases with the forecasting step; one-step ahead forecasting has a lower computational time than two-step ahead forecasting which in turn has a lower computational time than two-step ahead forecasting.

To compare the results from this study, Table 8 gives the research articles referred in the review, describing some models for wind speed forecasting. We have in the first part of this Table 8 the one-step ahead forecasting articles and in the second part an article on multi-step ahead wind speed forecasting. The forecasting models

Table 6. Improving percentage of forecasting performance from Dataset 2.

Comparison models		One-step			Two-step			Three-step		
		P_{RMSE} (%)	P_{MAE} (%)	P_{MAPE} (%)	P_{RMSE} (%)	P_{MAE} (%)	P_{MAPE} (%)	P_{RMSE} (%)	P_{MAE} (%)	P_{MAPE} (%)
NARXNN	BPNN	40	22	18	8	1.9	9	9	2.9	7
	RBFNN	24	12	16	12	9	9	10	6	5
	GABPNN	13	3	8	4	6	18	4	0.1	2
ARIMA	AMFIS	55	34	29	52	46	48	39	26	24
	BPNN	29	26	17	24	21	19	19	20	18
	RBFNN	9	16	16	7	12	20	1.7	12	16.9
	GABPNN	4	1.9	7	21	25	28	7	17.9	13.9
	AMFIS	47	38	29	60	57	54	45.9	39	33

Table 7. Computation time of wind speed forecasting models.

Models	Time in second (Dataset1)			Time in second (Dataset2)		
	One-step	Two-step	Three-step	One-step	Two-step	Three-step
BPNN	66	114	195	59	108	172
NARXNN	595	803	1021	813	1469	1984
RBFNN	34	52	86	18	49	76
GABPNN	1514	3111	4758	2049	3361	4087
ANFIS	512	952	1366	472	787	1345
ARIMA	39	97	142	85	157	185

involved are ARIMA, ANFIS, BPNN, RBFNN, Persistent, SVM (Support Vector Machine), SVM-GA (hybrid Support Vector Machine and Generic Algorithm), and LSTM (Long Short Term Memory). Firstly, the results in Table 8 show that the forecasting performance is a function of the forecasting period (number of forecasting samples). The lower the number of samples the better the forecasting performance. The comparison of the forecasting models of this review with the NARXNN and ARIMA models presented in Tables 3 and 4 in terms of forecasting performance proves the superiority of the latter. The multi-step ahead wind speed forecasting given in Table 8 shows that the one-step ahead forecasting is better, and the forecasting performance decreases with increasing forecasting step.

Usually, the ultimate goal of wind prediction is to predict wind power to be generated with a specific wind turbine or wind farm. Therefore, by using the previous WTPC modeling in Subsection 2.2, each better result of predicted wind speed achieved from neural networks models and from ARIMA models are applied for 24 hours expected WTPG from E-82 2000 kW wind turbine prediction in both Datasets. Then, the results from NARXNN models under one-step ahead forecasting and from ARIMA models under two-step ahead forecasting are employed. The measured wind speed data are used to estimate the actual WTPG values, which are used to compare the predicted values from hybrid models. Figures 8 and 9 give the WTPG comparisons, between the actual values (P_m) and predicted values from hybrid NARXNN models (P_{NARXNN}) and hybrid ARIMA models (P_{ARIMA}) for Dataset1 and Dataset2, respectively. Figures 8(a) and 9(a) give the P_m , P_{NARXNN} , and P_{ARIMA} versus time for Dataset1 and Dataset2 respectively. From Figure 8(a) it can be observed that P_{NARXNN} follows the form of P_m more than P_{ARIMA} ; while from Figure 9(a) we see that P_{ARIMA} follows the form of P_m more than P_{NARXNN} . Figures 8(b) and 9(b) give the difference between P_m and P_{NARXNN} on the one hand, and between P_m and P_{ARIMA} on the other hand versus time for Dataset1 and Dataset2, respectively. These are the absolute values of errors $P_m - P_{NARXNN}$ and $P_m - P_{ARIMA}$. From Figure 8(b), $P_m - P_{NARXNN}$ is range from 0.28 to 567 kW; while $P_m - P_{ARIMA}$ is range from 1.7 to 822 kW. From Figure 9(b), $P_m - P_{NARXNN}$ is range from 0.99 to 707 kW; while $P_m - P_{ARIMA}$ is range from 1.3 to 783 kW. The average values of $P_m - P_{NARXNN}$ and $P_m - P_{ARIMA}$ are 132 and 197 kW in Dataset1 and 175 and 165 kW in Dataset2. From the previous results, it is clear that the wind speed

Table 8. Research articles referred in the review.

Articles	Forecasting periods	Models	Forecasting performance								
			RMSE (m/s)		MAE (m/s)		MAPE (%)				
Tekta (2010)	6 months with 1 hour intervals	ARIMA	1.70		1.17						
Liu et al. (2014)	7 days with 30 minutes intervals	ANFIS	1.71		1.32						
		Persistent SVM-GA	1.22		0.83			22.64			
Kumar (2019)	3 days with 15 minutes intervals	BPNN	1.21		0.78					14.79	
		RBFNN	1.48		1.11						
Huang and Kuo (2018)	3 days with 1 hour interval	SVM	1.29		1.03						
		RFNN	1.19		0.96						
		BPNN	1.03		0.83						
Liu et al. (2018)	4 days with 1 hour interval	BPNN	One-step	1.02		0.83					
			Two-step	1.51		1.19					
		ARIMA	One-step	1.19		0.90					
			Two-step	1.33		1.10					
		LSTM	One-step	1.20		1.02					
			Two-step	1.44		0.71					
			Three-step	2.00		1.59					
			Three-step	1.60		1.28					
			Three-step	1.75		1.32					
			One-step	1.47		10.47					
			One-step	10.74		11.54					
			One-step	9.39		14.59					
			Two-step	13.85		18.53					
			Two-step	11.54		13.51					
			Two-step	14.59		17.40					

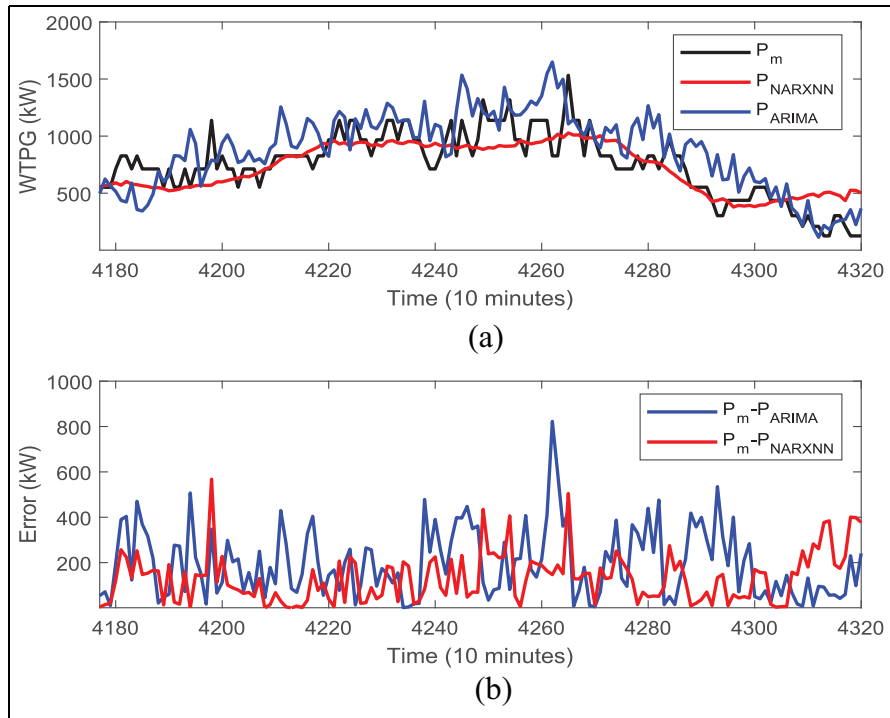


Figure 8. Predicted WTPG from Dataset 1 comparison: (a) power and (b) error.

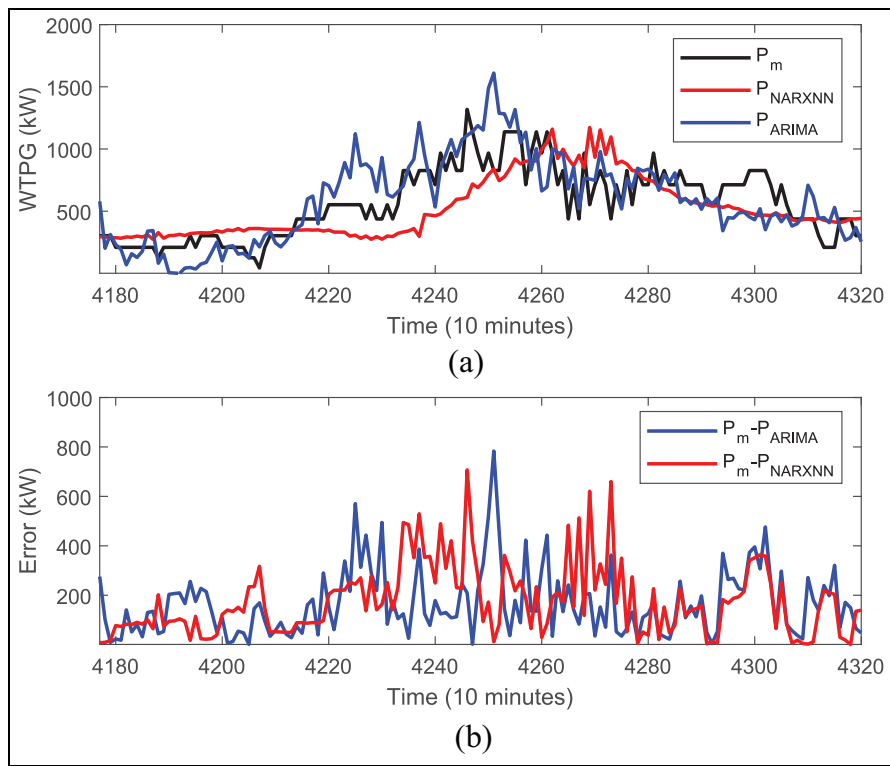


Figure 9. Predicted WTPG from Dataset 2 comparison: (a) power and (b) error.

forecasting accuracy is crucial for effective WTPG prediction. The hybrid method based on one-step ahead wind speed forecasting using NARXNN model and WTPC modeling is more efficient for WTPG prediction.

Conclusion

Cameroon is a developing country in Central Africa. The lack and insufficiency of electrical energy, and drinking water still affect more than 40% of its population, despite its aspiration to emergence by 2035. In order to contribute to the orientation in the decision-making for the development of wind farm in Cameroon, on the one hand, and to the development of accurate models for predicting the wind speed and Wind Turbine Power Generation (WTPG) on the other hand, this paper has presented an investigation of six wind speed forecasting models applied to predict the expected WTPG in Bapouh, Cameroon. Multi-step ahead forecasting involving one-step, two-step, and three-step are investigated with those forecasting models. Thus, three single Artificial Neural Networks (ANNs) models involving BPNN, NARXNN, and RBFNN, two collaborative neural networks models involving GABPNN and ANFIS, and ARIMA model are built for 1 day ahead wind speed forecasting in two Datasets. The power curve of E-82 2000 kW wind turbine is modeled and employed for WTPG prediction in both Datasets based on predicted wind speed. The wind speed forecasting results are shown that the NARXNN models and ARIMA models perform better than other models. The ANFIS models are the worst wind speed forecasting models. Also, it was shown that the one-step ahead is better for wind speed forecasting, while the three-step ahead forecasting is the worst in both Datasets. Furthermore, the computational time is according to the models, Dataset and forecasting step. One-step ahead forecasting has less computational time than two-step and three-step for all models and Datasets. NARXNN, ANFIS, and GABPNN models have more computational time than the other models. The achieved WTPG prediction are revealed that its result is good as well as the wind speed forecasting result is accurate. This has proved that the accurate wind speed forecasting is crucial for WTPG prediction.


Declaration of conflicting interests

The author(s) declared no potential conflicts of interest with respect to the research, authorship, and/or publication of this article.

Funding

The author(s) received no financial support for the research, authorship, and/or publication of this article.

ORCID iD

Hervice Roméo Fogno Fotso  <https://orcid.org/0000-0003-2994-629X>

References

- Arreyndip NA, Joseph E and David A (2016) Wind energy potential assessment of Cameroon's coastal regions for the installation of an onshore wind farm. *Heliyon* 2(11): e00187.
- Bandi M and Apt J (2016) Variability of the wind turbine power curve. *Applied Sciences* 6(9): 262–269.
- Cadenas E and Rivera W (2009) Short term wind speed forecasting in La Venta, Oaxaca, México, using artificial neural networks. *Renewable Energy* 34: 274–278.
- Cadenas E, Rivera W, Campos-Amezcuea R, et al. (2016) Wind speed prediction using a univariate ARIMA model and a multivariate NARX model. *Energies* 9(2): 109–115.
- Carrillo C, Obando Montaña AF, Cidrás J, et al. (2013) Review of power curve modelling for wind turbines. *Renewable and Sustainable Energy Reviews* 21: 572–581.
- Chang GW, Lu HJ, Chang YR, et al. (2017) An improved neural network-based approach for short-term wind speed and power forecast. *Renewable Energy* 105: 301–311.
- Chitsazan MA, Sami Fadali M and Trzynadlowski AM (2019) Wind speed and wind direction forecasting using echo state network with nonlinear functions. *Renewable Energy* 131: 879–889.
- Damousis IG, Alexiadis MC, Theocharis JB, et al. (2004) A fuzzy model for wind speed prediction and power generation in wind parks using spatial correlation. *IEEE Transactions on Energy Conversion* 19(2): 352–361.
- Di Piazza A, Di Piazza MC and Vitale G (2016) Solar and wind forecasting by NARX neural networks. *Renewable Energy and Environmental Sustainability* 1: 39–45.
- Flora FMI, Donatien N, Tchinda R, et al. (2021) Selection wind farm sites based on GIS using a Boolean method: Evaluation of the case of Cameroon. *Journal of Power and Energy Engineering* 9: 1–24.

- Fogno Fotso HR, Aloyem Kazé CV and Kenmoé GD (2020) Optimal input variables disposition of artificial neural networks models for enhancing time series forecasting accuracy. *Applied Artificial Intelligence* 34: 792–815.
- Fogno Fotso HR, Aloyem Kazé CV and Djuidge Kenmoé G (2021a) A novel hybrid model based on weather variables relationships improving applied for wind speed forecasting. *International Journal of Energy and Environmental Engineering*. Epub ahead of print 1 July 2021. DOI: 10.1007/s40095-021-00408-x.
- Fogno Fotso HR, Aloyem Kazé CV and Djuidge Kenmoé G (2021b) Real-time rolling bearing power loss in wind turbine gearbox modeling and prediction based on calculations and artificial neural network. *Tribology International* 163: 1–10.
- Hao Y and Tian C (2019) A novel two-stage forecasting model based on error factor and ensemble method for multi-step wind power forecasting. *Applied Energy* 238: 368–383.
- Huang CJ and Kuo PH (2018) A short-term wind speed forecasting model by using artificial neural networks with stochastic optimization for renewable energy systems. *Energies* 11: 2777–2820.
- Hur SH (2021) Short-term wind speed prediction using extended Kalman filter and machine learning. *Energy Reports* 7: 1046–1054.
- Jain G (2018) Time-Series analysis for wind speed forecasting. *Malaya Journal of Matematik* 1: 55–61.
- Jiao J (2018) A hybrid forecasting method for wind speed. *MATEC Web of Conferences* 232: 1–5.
- Kisito TP, Nfor BG Jr, David Y, et al. (2015) Wind energy assessment at Bafoussam, Cameroon. *Journal of Sustainable Development* 8(9): 106–120.
- Kugiumtzis D and Tsimpiris A (2010) Measures of analysis of time series (MATS): AMATLABToolkit for computation of multiple measures on time series data bases. *Journal of Statistical Software* 33: 1–30.
- Kumar PS, (2019) Improved prediction of wind speed using machine learning. *EAI Endorsed Transactions on Energy Web* 6(23): 1–7.
- Liu D, Niu D, Wang H, et al. (2014) Short-term wind speed forecasting using wavelet transform and support vector machines optimized by genetic algorithm. *Renewable Energy* 62: 592–597.
- Liu H, Mi XW and Li YF (2018) Wind speed forecasting method based on deep learning strategy using empirical wavelet transform, long short term memory neural network and Elman neural network. *Energy Conversion and Management* 156: 498–514.
- Loukatou A, Howell S, Johnson P, et al. (2018) Stochastic wind speed modelling for estimation of expected wind power output. *Applied Energy* 228: 1328–1340.
- Lydia M, Kumar SS, Selvakumar AI, et al. (2014) A comprehensive review on wind turbine power curve modeling techniques. *Renewable and Sustainable Energy Reviews* 30: 452–460.
- Moreno SR and Dos Santos Coelho L (2018) Wind speed forecasting approach based on singular spectrum analysis and adaptive neuro fuzzy inference system. *Renewable Energy* 126: 736–754.
- Nair KR (2017) Forecasting of wind speed using ANN, ARIMA and hybrid models. In: *International conference on intelligent computing, instrumentation and control technologies*, Kerala, India, 6–7 July 2017, pp.170–175. New York, NY: IEEE.
- Pelletier F, Masson C and Tahan A (2016) Wind turbine power curve modelling using artificial neural network. *Renewable Energy* 89: 207–214.
- Peng H, Liu F and Yang X (2013) A hybrid strategy of short term wind power prediction. *Renewable Energy* 50: 590–595.
- Salfate I, López-Caraballo CH, Sabin-Sanjulián C, et al. (2018) 24-hours wind speed forecasting and wind power generation in La Serena (Chile). *Wind Engineering* 42: 607–623.
- Tekta M (2010) Weather forecasting using ANFIS and ARIMA models. A case study for Istanbul. *Environmental Research Engineering and Management* 1(51): 5–10.
- Teyabean AA and Jwaide AE (2017) Power curve modelling for wind turbines. In: *19th international conference on modelling & simulation*, Cambridge, 5–7 April 2017, pp.179–184. <https://doi.org/10.1109/UKSim.2017.30>
- Veeyee KF, Bup ND, Boldor D, et al. (2021) Potentials of sustainable electricity production from sawdust by small-scale wood transformation units: A case study in Cameroon. *International Journal of Energy and Environmental Engineering* 12(1): 101–114.
- Wang J, Heng J, Xiao L, et al. (2017) Research and application of a combined model based on multi-objective optimization for multi-step ahead wind speed forecasting. *Energy* 125: 591–613.
- Wang S, Zhang N, Wu L, et al. (2016) Wind speed forecasting based on the hybrid ensemble empirical mode decomposition and GA-BP neural network method. *Renewable Energy* 94: 629–636.
- Wirba AV, Abubakar Mas'ud A, Muhammad-Sukki F, et al. (2015) Renewable energy potentials in Cameroon: Prospects and challenges. *Renewable Energy* 76: 560–565.
- Xiao L, Shao W, Yu M, et al. (2017) Research and application of a hybrid wavelet neural network model with the improved cuckoo search algorithm for electrical power system forecasting. *Applied Energy* 198: 203–222.
- Yan X, Liu Y, Xu Y, et al. (2020) Multistep forecasting for diurnal wind speed based on hybrid deep learning model with improved singular spectrum decomposition. *Energy Conversion and Management* 225: 1–22.
- Zhang J, Wei Y, Tan ZF, et al. (2017a) A hybrid method for short-term wind speed forecasting. *Sustainability* 9: 596–610.
- Zhang W, Qu Z, Zhang K, et al. (2017b) A combined model based on CEEMDAN and modified flower pollination algorithm for wind speed forecasting. *Energy Conversion and Management* 136: 439–451.

Author biographies

Germaine Djuidje Kenmoé is a Professor of Physics at the University of Yaoundé I, Yaoundé, Cameroon, where she offers courses and supervises the research work in the Laboratory of Mechanics of the same University. Her research interests relate to friction and wear processes on the molecular scale (Nanotribology), stochastic processes and machine learning. She is the author and coauthor of many publications in these fields.

Hervice Roméo Fogno Fotso is a PhD student in the Laboratory of Mechanics, Department of Physics, University of Yaoundé I, Yaoundé, Cameroon. He is interested in renewable energy and machine learning. He is the author and coauthor of many publications in these fields.

Claude Vidal Aloyem Kazé received his PhD from the University of Dschang, Cameroon in 2012. He is interested in renewable energy and is the author and coauthor of many publications in this field. He is the head of Department of Renewable Energy at the Higher Technical Teacher's Training College, University of Buea and a Trainer of Trainers at the National Institute of Vocational Trainers and Program Development, Cameroun.